

UC Irvine

UC Irvine Electronic Theses and Dissertations

Title

Copper-Catalyzed Hydroamination: Enantioselective Addition of Pyrazoles to Cyclopropenes

Permalink

<https://escholarship.org/uc/item/77k9j8vs>

Author

Simon, Julie Christine

Publication Date

2024

Copyright Information

This work is made available under the terms of a Creative Commons Attribution License, available at <https://creativecommons.org/licenses/by/4.0/>

Peer reviewed|Thesis/dissertation

UNIVERSITY OF CALIFORNIA, IRVINE

Copper-Catalyzed Hydroamination: Enantioselective Addition of Pyrazoles to Cyclopropenes

THESIS

submitted in partial satisfaction of the requirements for the degree of

MASTER OF SCIENCE

In

Chemistry

By

Julie Christine Simon

Thesis Committee:

Professor Vy Dong, Chair

Professor Elizabeth Jarvo

Professor Scott Rychnovsky

2024

© 2024 Julie Christine Simon

DEDICATION

To

my parents, John and Linda Simon,

for their continuous love and support

and my dog, Delphi,

for bringing joy to every day.

TABLE OF CONTENTS

	Page
LIST OF FIGURES	v
LIST OF SCHEMES	vii
LIST OF TABLES	viii
LIST OF ABBREVIATIONS	ix
ACKNOWLEDGEMENTS	xii
ABSTRACT OF THE THESIS	xiii
CHAPTER 1: Introduction and Background	1
1.1 Introduction	1
1.2 Background	2
1.3 Proposal	4
1.4 References	5
CHAPTER 2: Results and Conclusions	14
2.1 Results	14
2.2 Conclusions and Future Work	31
2.3 References	32
CHAPTER 3: Supporting Information	40

3.1 General Methods	40
3.2 Optimization of the Hydroamination of Cyclopropenes with Pyrazoles	41
3.3 Asymmetric Hydroamination	42
3.4 Synthesis of Cyclopropenes	59
3.5 Rate Studies	61
3.6 Deuterium Labeling Studies	68
3.7 NMR Studies	69
3.8 Kinetic Isotope Effect Study	72
3.9 Synthesis and Reactivity of Copper–Trimer VI	74
3.10 Electrospray Ionization Mass Spectrometer Analysis	75
3.11 Density Functional Theory Calculations	76
3.12 X-ray Crystallography	76
3.13 References	79
APPENDIX A: ^1H and ^{13}C NMR Spectral Data	83
APPENDIX B: SFC Traces	124
APPENDIX C: X-Ray Crystallographic Data	157

LIST OF FIGURES

	Page
Figure 1 Bioactive Molecules with Pyrazole Motifs	1
Figure 2 Bioactive Molecules with Cyclopropyl Motifs	2
Figure 3 First Cu–Amido Complex Isolation – Gunnoe (2003 & 2005)	3
Figure 4 Reactivity of NHC Ligands	15
Figure 5 Effect of Bulky Electron-Rich Chiral Ligands	16
Figure 6 Optimization of Reaction Conditions	17
Figure 7 N-Heterocycle Scope	19
Figure 8 Cyclopropene Scope	21
Figure 9 Effect of Copper Loading on Reaction Order	23
Figure 10 ^{31}P NMR Titrations	24
Figure 11 Calculated KIE Values	25
Figure 12 Potential <i>cis</i> -Aminocupration Pathways	26
Figure 13 Relative Transition State Energies of Aminocupration Proposals	27
Figure 14 Relative 4- and 5-Centered <i>cis</i> -Aminocupration Transition State Energies	29
Figure 15 Proposed Catalytic Cycle	31
Figure 16 Synthesized Cyclopropenes	59
Figure 17 VTNA Graphs for Cyclopropene 1a	62
Figure 18 VTNA Graphs for Pyrazole 2a	63
Figure 19 VTNA Graphs for DBU	64
Figure 20 VTNA Graphs for Copper at Low Loading	66

	Page
Figure 21 VTNA Graphs for Copper at High Loading	67
Figure 22 GCMS of Cyclopropene 1a and d-1a	68
Figure 23 ^{31}P NMR with Varied Copper Loadings	72
Figure 24 ESI-MS Spectrum for Cu + L3 + MeCN	75

LIST OF SCHEMES

	Page
Scheme 1 Previous Hydroamination with Pyrazoles	3
Scheme 2 Rare Earth Metal Catalyzed Cyclopropene Hydroamination – Hou (2016)	4
Scheme 3 This Work: Enantioselective Cu–Amido Catalyzed Hydroamination	4
Scheme 4 Undesired Reactivity of Achiral Phosphine Ligands	14
Scheme 5 Deuterium Labelling Study	25
Scheme 6 Experimentation of Copper–Trimer VI	30

LIST OF TABLES

		Page
Table 1	Data from Competition KIE Study	73

LIST OF ABBREVIATIONS

Å	angstrom
Bpin	boronic pinacol ester
CI	chemical ionization
cm	centimeter(s)
<i>d</i>	deuterated
DBU	diazabicycloundecene
DPPF	1,1'ferrocenediyl-bis(diphenylphosphine)
<i>dr</i>	diastereomeric ratio
EI	electron ionization
equiv.	equivalents
<i>er</i>	enantiomeric ratio
ESI	electrospray ionization
FDA	Food and Drug Administration
FID	flame ionization detection
FT-IR	Fourier-transform – infrared
g	gram(s)
GC	gas chromatography
GC-MS	gas chromatography – mass spectrometry
HIV	human immunodeficiency virus
HPLC	high-performance liquid chromatography

HRMS	high-resolution mass spectrometry
Hz	Hertz
IPA	isopropyl alcohol
ⁱ Pr	isopropyl
KIE	kinetic isotope effect
mL	milliliter(s)
mm	millimeter(s)
mmol	millimole
MS	molecular sieve
NHC	N-heterocyclic carbene
nm	nanometer(s)
NMR	nuclear magnetic resonance
NOE	nuclear Overhauser effect
NOESY	nuclear Overhauser effect spectroscopy
PCM	polarized continuum solvation model
Ph	phenyl
PPM	parts per million
Py	pyridine
QRRHO	quasi-rigid rotor harmonic oscillator
<i>rr</i>	regioisomeric ratio
SFC	supercritical fluid chromatography
^t Bu	tert-butyl

TLC thin-layer chromatography

TS transition structure

UV ultraviolet

ACKNOWLEDGEMENTS

I would like to thank Professor Vy Dong for accepting me into her group at the University of California, Irvine and giving me the opportunity to study catalysis in her lab. I greatly appreciate how supportive and encouraging Vy has been during my time in graduate school.

I would also like to thank my committee members, Professor Elizabeth Jarvo and Professor Scott Rychnovsky, for taking time to read my thesis and offering their guidance. In addition, I would like to thank Phil Dennison in the NMR facility, as well as Dr. Felix Grün and the rest of the faculty in the mass spectrometry facility for their assistance in my research.

I would like to thank the members of the Dong lab for all of the help, ideas, and enthusiasm they have shared with me. In particular, I would like to thank Minghao Wang and Sophia Xu, who worked with me on this project and without whom it would not have been possible. I would furthermore like to thank Professor Jennifer Hirschi, as well as Stephanie Corio from the Hirschi lab, who collaborated with us on this project.

I would also like to thank Professor Silas Cook at Indiana University for providing me with the opportunity to do research in his lab as an undergraduate, as well as Dr. Paul Marcyk, the graduate student that took me under his wing in the Cook lab. You played a crucial role in helping me grow as an organic chemist.

Acknowledgement to the National Institutes of Health (R35GM127071) and National Science Foundation (CHE-2751956457) for providing funding for this work.

ABSTRACT OF THE THESIS

Copper-Catalyzed Hydroamination: Enantioselective Addition of Pyrazoles to Cyclopropenes

By

Julie Christine Simon

Master of Science in Chemistry

University of California, Irvine, 2024

Professor Vy Dong, Chair

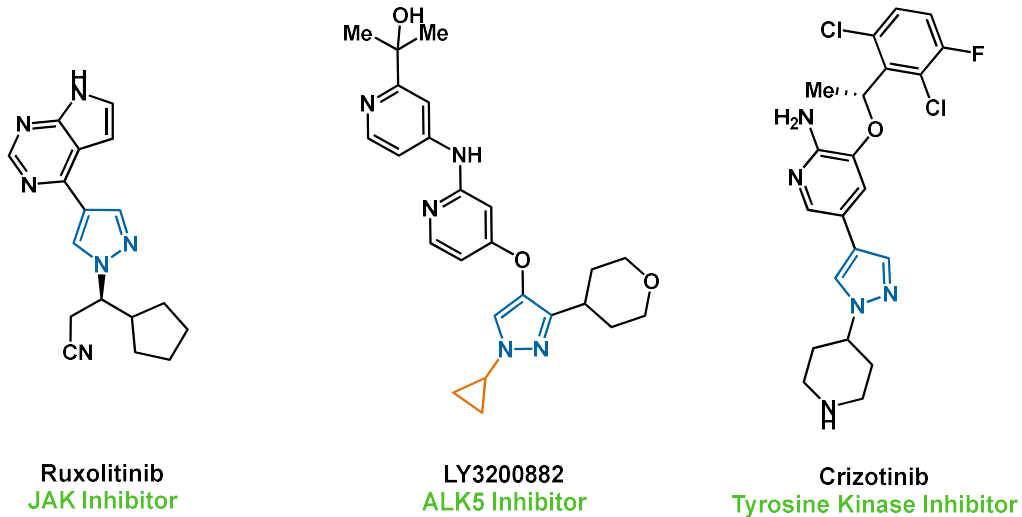
Hydroamination of cyclopropenes presents an appealing approach to increase molecular complexity. In this study we explore an earth-abundant copper-catalyzed hydroamination of cyclopropenes with pyrazoles and structurally related heterocycles under mild conditions with high regio-, diastereo-, and enantiocontrol. The observed regioselectivity favors the more hindered nitrogen of the pyrazole. Experimental and DFT studies support a unique mechanism featuring a five-centered aminocupration.

CHAPTER 1: Introduction and Background

1.1 Introduction

Nitrogen-containing heterocycles play an increasingly significant role in drug discovery. They appear in a significant percentage of natural products¹ and a majority of small molecule drugs approved by the FDA.²⁻⁴ Among these, pyrazoles have been found to have a diverse range of biological activity. Pyrazoles are the fourth most common nitrogen-containing heterocycle in recently approved pharmaceuticals,⁵ contributing to the antibacterial, antiviral, and anticancer capabilities of various drug candidates (**Figure 1**).⁶ Efficient catalytic functionalization of these nitrogen-containing heterocycles therefore represents an important and exciting area of study to further expand their utility and facilitate new drug development.

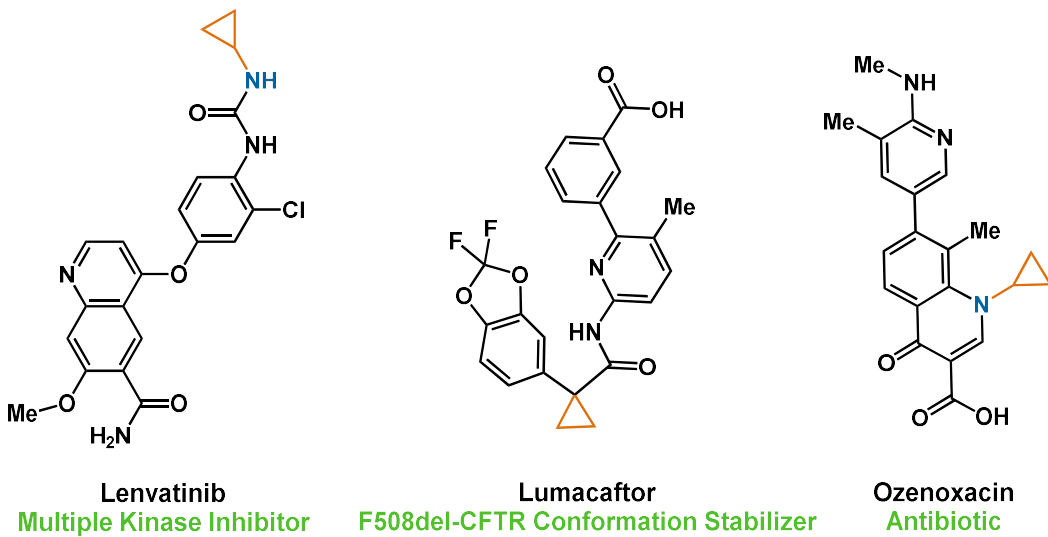
Figure 1 : Bioactive Molecules with Pyrazole Motifs



Cyclopropyl rings are another motif increasingly represented in FDA approved drugs (**Figure 2**)^{5,7} and other bioactive molecules,⁸ due to their ability to impose steric rigidity, enhance target specificity, and limit off-target activity.⁹ Many groups including ours have examined the

synthesis of such biologically significant chiral cyclopropanes^{9,10} by developing methods for direct hydrofunctionalization of cyclopropenes.¹¹⁻²¹

Figure 2 : Bioactive Molecules with Cyclopropyl Motifs

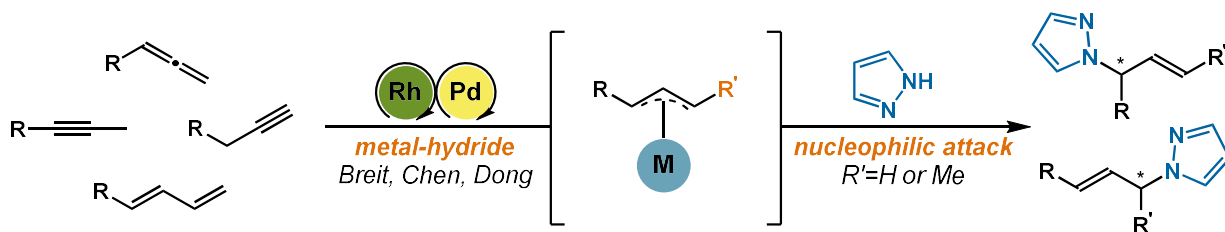


1.2 Background

1.2.1 Hydroamination

To this end, hydroamination presents an attractive and atom-economical²² approach to C–N bond formation.²³⁻³¹ However, current methods for hydroamination involving N-heterocycles such as pyrazole are underdeveloped. Precedent methods require the use of precious metal catalysts to couple pyrazoles with allenes,^{32,33} dienes,^{34,35} or alkynes (**Scheme 1**).³⁶ This work represents an advancement of previous hydroamination methods through the use of earth abundant catalysts to facilitate the enantioselective addition of pyrazoles and related N-heterocycles into cyclopropenes.

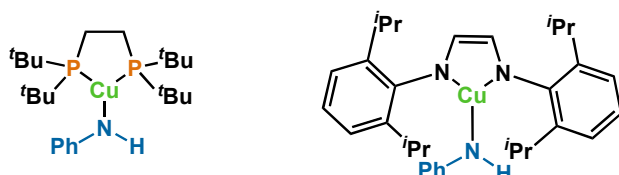
Scheme 1 : Previous Hydroamination with Pyrazoles



1.2.2 Copper Amido Catalysis

Furthermore, this study features an exciting application of copper amido catalysis. The first isolation and characterization of a copper amido complex was achieved by Gunnoe and coauthors (**Figure 3**),³⁷ though many cross-couplings are thought to have involved copper amido complexes.³⁸⁻⁴² Their work demonstrated that copper amido species add into electron-deficient alkenes.^{43,44} This reactivity has subsequently been extended to other electrophiles, such as allenes,⁴⁵ nitrostyrenes,⁴⁶ and azabenzonorbornadienes,⁴⁷ but to date no asymmetric hydroamination using copper amido catalysis are known.

Figure 3 : First Cu-Amido Complex Isolation - Gunnoe (2003 & 2005)

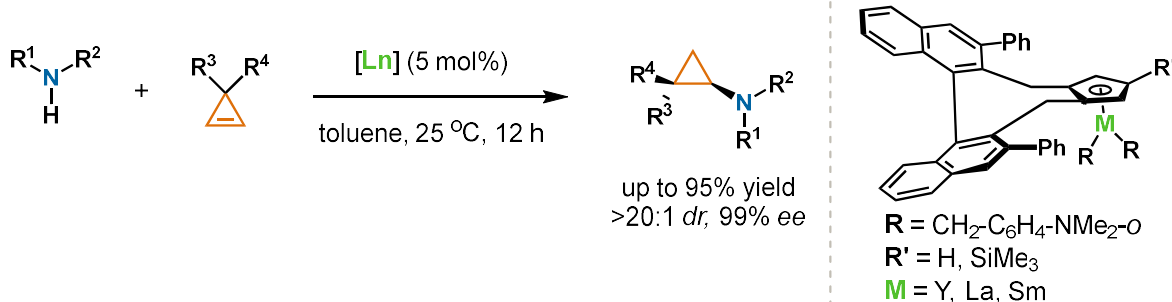


1.2.3 Cyclopropene Hydrofunctionalization

Cyclopropene hydrofunctionalization represents a versatile strategy for synthesizing chiral cyclopropanes.^{9-21,48-51} Of particular note is the work of Hou and coworkers on the asymmetric coupling of cyclopropenes with secondary amines, including morpholine, pyrrolidine, and

dibenzylamines, by rare earth metal catalysts, including samarium, yttrium, and lanthanum (**Scheme 2**).¹⁵ Furthermore, the Buchwald group developed an enantioselective hydroamination of 1-silyl- or 1-aryl-substituted cyclopropenes using copper-hydride catalysis,¹⁷ with *O*-benzoylhydroxylamines as oxidants^{52,53} and silanes as a stoichiometric reductant.⁵⁴⁻⁵⁶

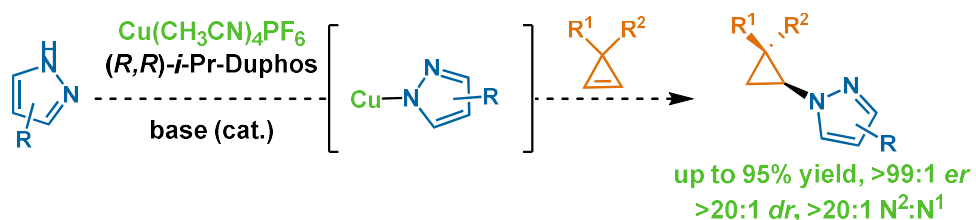
Scheme 2 : Rare Earth Metal Catalyzed Cyclopropene Hydroamination - Hou (2016)



1.3 Proposal

With all of this in mind, our strategy aims to access late-stage construction of cyclopropyl pyrazole derivatives regio-, diastereo-, and enantioselectively by using copper amido catalysis. We hypothesized that the deprotonation of pyrazole with a catalytic amount of base would generate a copper-pyrazolate catalyst, which would undergo aminocupration to cyclopropenes (**Scheme 3**).⁵⁷ Subsequent protodemetalation would produce cyclopropyl pyrazoles. If successful, this method would enable a novel and late-stage⁵⁸⁻⁶⁷ cyclopropylation of pyrazoles with high atom economy.²²

Scheme 3 : This Work: Enantioselective Cu-Amido Catalyzed Hydroamination



1.4 References

1. Ertl, P.; Schuhmann, T. A Systematic Cheminformatics Analysis of Functional Groups Occurring in Natural Products. *J. Nat. Prod.* **2019**, *82*, 1258–1263.
2. Vitaku, E.; Smith, D. T.; Njardarson, J. T. Analysis of the Structural Diversity, Substitution Patterns, and Frequency of Nitrogen Heterocycles among U.S. FDA Approved Pharmaceuticals: Miniperspective. *J. Med. Chem.* **2014**, *57*, 10257–10274.
3. Kalaria, P. N.; Karad, S. C.; Raval, D. K. A Review on Diverse Heterocyclic Compounds as the Privileged Scaffolds in Antimalarial Drug Discovery. *Eur. J. Med. Chem.* **2018**, *158*, 917–936.
4. Kerru, N.; Gummidi, L.; Maddila, S.; Gangu, K. K.; Jonnalagadda, S. B. A Review on Recent Advances in Nitrogen-Containing Molecules and Their Biological Applications. *Molecules* **2020**, *25*, 1909.
5. Bhutani, P.; Joshi, G.; Raja, N.; Bachhav, N.; Rajanna, P. K.; Bhutani, H.; Paul, A. T.; Kumar, R. U.S. FDA Approved Drugs from 2015–June 2020: A Perspective. *J. Med. Chem.* **2021**, *64*, 2339–2381.
6. Karrouchi, K.; Radi, S.; Ramli, Y.; Taoufik, J.; Mabkhot, Y.; Al-aizari, F.; Ansar, M. Synthesis and Pharmacological Activities of Pyrazole Derivatives: A Review. *Molecules* **2018**, *23*, 134.
7. Yap, T. A.; Vieito, M.; Baldini, C.; Sepúlveda-Sánchez, J. M.; Kondo, S.; Simonelli, M.; Cosman, R.; van der Westhuizen, A.; Atkinson, V.; Carpentier, A. F.; Löhr, M.; Redman, R.; Mason, W.; Man, M.; Gandhi, L.; Avsar, E.; Melisi, D. First-In-Human Phase I Study of a Next-Generation, Oral, TGF β Receptor 1 Inhibitor, LY3200882, in Patients with Advanced Cancer. *Clin. Cancer Res.* **2021**, *27*, 6666–6676.

8. Vianello, P.; Botrugno, O. A.; Cappa, A.; Ciossani, G.; Dessanti, P.; Mai, A.; Mattevi, A.; Meroni, G.; Minucci, S.; Thaler, F.; Tortorici, M.; Trifiró, P.; Valente, S.; Villa, M.; Varasi, M.; Mercurio, C. Synthesis, biological activity and mechanistic insights of 1-substituted cyclopropylamine derivatives: A novel class of irreversible inhibitors of histone demethylase KDM1A. *Eur. J. Med. Chem.* **2014**, *86*, 352–363.
9. Talele, T. T. The “Cyclopropyl Fragment” Is a Versatile Player That Frequently Appears in Preclinical/Clinical Drug Molecules. *J. Med. Chem.* **2016**, *59*, 8712–8756.
10. Shearer, J.; Castro, J. L.; Lawson, A. D. G.; MacCoss, M.; Taylor, R. D. Rings in Clinical Trials and Drugs: Present and Future. *J. Med. Chem.* **2022**, *65*, 8699–8712.
11. Dian, L.; Marek, I. Asymmetric Preparation of Polysubstituted Cyclopropanes Based on Direct Functionalization of Achiral Three-Membered Carbocycles: Focus Review. *Chem. Rev.* **2018**, *118*, 8415–8434.
12. Tarwade, V.; Liu, X.; Yan, N.; Fox, J. M. Directed Carbozincation Reactions of Cyclopropene Derivatives. *J. Am. Chem. Soc.* **2009**, *131*, 5382–5383.
13. Phan, D. H. T.; Kou, K. G. M.; Dong, V. M. Enantioselective Desymmetrization of Cyclopropenes by Hydroacylation. *J. Am. Chem. Soc.* **2010**, *132*, 16354–16355.
14. Parra, A.; Amenós, L.; Guisán-Ceinos, M.; López, A.; García Ruano, J. L.; Tortosa, M. Copper-Catalyzed Diastereo- and Enantioselective Desymmetrization of Cyclopropenes: Synthesis of Cyclopropylboronates. *J. Am. Chem. Soc.* **2014**, *136*, 15833–15836.
15. Teng, H.-L.; Luo, Y.; Wang, B.; Zhang, L.; Nishiura, M.; Hou, Z. Synthesis of Chiral Aminocyclopropanes by Rare-Earth-Metal-Catalyzed Cyclopropene Hydroamination. *Angew. Chem. Int. Ed.* **2016**, *55*, 15406–15410.

16. Li, Z.; Zhao, J.; Sun, B.; Zhou, T.; Liu, M.; Liu, S.; Zhang, M.; Zhang, Q. Asymmetric Nitrone Synthesis via Ligand-Enabled Copper-Catalyzed Cope-Type Hydroamination of Cyclopropene with Oxime. *J. Am. Chem. Soc.* **2017**, *139*, 11702–11705.
17. Feng, S.; Hao, H.; Liu, P.; Buchwald, S. L. Diastereo- and Enantioselective CuH-Catalyzed Hydroamination of Strained Trisubstituted Alkenes. *ACS Catal.* **2020**, *10*, 282–291.
18. Nie, S.; Lu, A.; Kuker, E. L.; Dong, V. M. Enantioselective Hydrothiolation: Diverging Cyclopropenes through Ligand Control. *J. Am. Chem. Soc.* **2021**, *143*, 6176–6184.
19. Huang, M.-Y.; Zhao, Y.-T.; Chai, H.; Zhang, C.-D.; Zhu, S.-F. Copper-Catalyzed Ring-Opening/Borylation of Cyclopropenes. *CCS Chem* **2022**, *4*, 1232–1237.
20. Yu, R.; Cai, S.; Li, C.; Fang, X. Nickel-Catalyzed Asymmetric Hydroaryloxy- and Hydroalkoxycarbonylation of Cyclopropenes. *Angew. Chem. Int. Ed.* **2022**, *61* (36), e202200733.
21. Huang, Q.; Chen, Y.; Zhou, X.; Dai, L.; Lu, Y. Nickel-Hydride-Catalyzed Diastereo- and Enantioselective Hydroalkylation of Cyclopropenes. *Angew. Chem. Int. Ed.* **2022**, *61* (46), e202210560.
22. Trost, B. The Atom Economy—A Search for Synthetic Efficiency. *Science* **1991**, *254*, 1471–1477.
23. Beller, M.; Seayad, J.; Tillack, A.; Jiao, H. Catalytic Markovnikov and Anti-Markovnikov Functionalization of Alkenes and Alkynes: Recent Developments and Trends. *Angew. Chem. Int. Ed.* **2004**, *43*, 3368–3398.
24. Severin, R.; Doye, S. The Catalytic Hydroamination of Alkynes. *Chem. Soc. Rev.* **2007**, *36*, 1407–1420.

25. Müller, T. E.; Hultsch, K. C.; Yus, M.; Foubelo, F.; Tada, M. Hydroamination: Direct Addition of Amines to Alkenes and Alkynes. *Chem. Rev.* **2008**, *108*, 3795–3892.
26. Nishina, N.; Yamamoto, Y. Late Transition Metal-Catalyzed Hydroamination. In *Hydrofunctionalization*; Ananikov, V. P., Tanaka, M., Eds. Top. Organomet. Chem.; Springer Berlin Heidelberg: Berlin, Heidelberg, 2012; Vol. 43, pp 115–143.
27. Reznichenko, A. L.; Nawara-Hultsch, A. J.; Hultsch, K. C. Asymmetric Hydroamination. In *Stereoselective Formation of Amines*; Li, W., Zhang, X., Eds.; Topics in Current Chemistry; Springer Berlin Heidelberg: Berlin, Heidelberg, 2013; Vol. 343, pp 191–260.
28. Huang, L.; Arndt, M.; Gooßen, K.; Heydt, H.; Gooßen, L. J. Late Transition Metal-Catalyzed Hydroamination and Hydroamidation. *Chem. Rev.* **2015**, *115*, 2596–2697.
29. Michon, C.; Abadie, M.-A.; Medina, F.; Agbossou-Niedercorn, F. Recent Metal-Catalysed Asymmetric Hydroaminations of Alkenes. *J. Organomet. Chem.* **2017**, *847*, 13–27.
30. Chen, J.; Lu, Z. Asymmetric Hydrofunctionalization of Minimally Functionalized Alkenes via Earth Abundant Transition Metal Catalysis. *Org. Chem. Front.* **2018**, *5*, 260–272.
31. Colonna, P.; Bezzanine, S.; Gil, R.; Hannoudache, J. Alkene Hydroamination via Earth-Abundant Transition Metal (Iron, Cobalt, Copper and Zinc) Catalysis: A Mechanistic Overview. *Adv. Synth. Catal.* **2020**, *362*, 1550–1563.
32. Haydl, A. M.; Xu, K.; Breit, B. Regio- and Enantioselective Synthesis of N-Substituted Pyrazoles by Rhodium-Catalyzed Asymmetric Addition to Allenes. *Angew. Chem. Int. Ed.* **2015**, *54*, 7149–7153.
33. Hilpert, L. J.; Sieger, S. V.; Haydl, A. M.; Breit, B. Palladium-and Rhodium-Catalyzed Dynamic Kinetic Resolution of Racemic Internal Allenes Towards Chiral Pyrazoles. *Angew. Chem. Int. Ed.* **2019**, *58*, 3378–3381.

34. Jiang, W.; Ji, D.; Zhang, W.; Zhang, G.; Min, X.; Hu, Y.; Jiang, X.; Chen, Q. Orthogonal Regulation of Nucleophilic and Electrophilic Sites in Pd-Catalyzed Regiodivergent Couplings between Indazoles and Isoprene. *Angew. Chem. Int. Ed.* **2021**, *60*, 8321–8328.
35. Jiu, A. Y.; Slocumb, H. S.; Yeung, C. S.; Yang, X.; Dong, V. M. Enantioselective Addition of Pyrazoles to Dienes. *Angew. Chem. Int. Ed.* **2021**, *60*, 19660–19664.
36. Haydl, A. M.; Hilpert, L. J.; Breit, B. Regioconvergent and Enantioselective Rhodium-Catalyzed Hydroamination of Internal and Terminal Alkynes: A Highly Flexible Access to Chiral Pyrazoles. *Chem. Eur. J.* **2016**, *22*, 6547–6551.
37. Blue, E. D.; Davis, A.; Conner, D.; Gunnoe, T. B.; Boyle, P. D.; White, P. S. Synthesis, Solid-State Crystal Structure, and Reactivity of a Monomeric Copper(I) Anilido Complex. *J. Am. Chem. Soc.* **2003**, *125*, 9435–9441.
38. Strieter, E. R.; Bhayana, B.; Buchwald, S. L. Mechanistic Studies on the Copper-Catalyzed *N*-Arylation of Amides. *J. Am. Chem. Soc.* **2009**, *131*, 78–88.
39. Mankad, N. P.; Antholine, W. E.; Szilagyi, R. K.; Peters, J. C. Three-Coordinate Copper(I) Amido and Aminyl Radical Complexes. *J. Am. Chem. Soc.* **2009**, *131*, 3878–3880.
40. Harry, N. A.; Jagadeesh, R. V. Copper-Catalyzed Aminations. In *Copper Catalysis in Organic Synthesis*; Anilkumar, G., Saranya, S., Eds.; Wiley, 2020; pp 239–259.
41. Ziegler, D. T.; Choi, J.; Muñoz-Molina, J. M.; Bissember, A. C.; Peters, J. C.; Fu, G. C. A Versatile Approach to Ullmann C–N Couplings at Room Temperature: New Families of Nucleophiles and Electrophiles for Photoinduced, Copper-Catalyzed Processes. *J. Am. Chem. Soc.* **2013**, *135*, 13107–13112.

42. Giri, R.; Hartwig, J. F. Cu(I)–Amido Complexes in the Ullmann Reaction: Reactions of Cu(I)–Amido Complexes with Iodoarenes with and without Autocatalysis by CuI. *J. Am. Chem. Soc.* **2010**, *132*, 15860–15863.
43. Munro-Leighton, C.; Blue, E. D.; Gunnoe, T. B. Anti-Markovnikov N–H and O–H Additions to Electron-Deficient Olefins Catalyzed by Well-Defined Cu(I) Anilido, Ethoxide, and Phenoxide Systems. *J. Am. Chem. Soc.* **2006**, *128*, 1446–1447.
44. Goj, L. A.; Blue, E. D.; Delp, S. A.; Gunnoe, T. B.; Cundari, T. R.; Pierpont, A. W.; Petersen, J. L.; Boyle, P. D. Chemistry Surrounding Monomeric Copper(I) Methyl, Phenyl, Anilido, Ethoxide, and Phenoxide Complexes Supported by N -Heterocyclic Carbene Ligands: Reactivity Consistent with Both Early and Late Transition Metal Systems. *Inorg. Chem.* **2006**, *45*, 9032–9045.
45. Perego, L. A.; Blieck, R.; Groué, A.; Monnier, F.; Taillefer, M.; Ciofini, I.; Grimaud, L. Copper-Catalyzed Hydroamination of Allenes: From Mechanistic Understanding to Methodology Development. *ACS Catal.* **2017**, *7*, 4253–4264.
46. Park, S.; Kang, S.; Lee, Y. Copper-Catalyzed Intermolecular Hydroamination of Arylamines or Aza-Heterocycles with Nitrostyrene Derivatives. *Adv. Synth. Catal.* **2019**, *361*, 1071–1083.
47. Kim, K.; Lee, Y. Copper-Catalyzed Hydroamination of Oxa- and Azabenzonorbornadienes with Pyrazoles. *J. Org. Chem.* **2022**, *87*, 569–578.
48. Dian, L.; Marek, I. Rhodium-Catalyzed Arylation of Cyclopropenes Based on Asymmetric Direct Functionalization of Three Membered Carbocycles. *Angew. Chem., Int. Ed.* **2018**, *57*, 3682–3686.

49. Zhang, H.; Huang, W.; Wang, T.; Meng, F. Cobalt-Catalyzed Diastereo- and Enantioselective Hydroalkenylation of Cyclopropenes with Alkenylboronic Acids. *Angew. Chem., Int. Ed.* **2019**, *58*, 11049–11053.
50. Dian, L.; Marek, I. Pd-Catalyzed Enantioselective Hydroalkynylation of Cyclopropenes. *ACS Catal.* **2020**, *10*, 1289–1293.
51. Huang, W.; Meng, F. Cobalt-Catalyzed Diastereo- and Enantioselective Hydroalkylation of Cyclopropenes with Cobalt Homoenolates. *Angew. Chem., Int. Ed.* **2021**, *60*, 2694–2698.
52. Hirano, K.; Miura, M. Hydroamination, Aminoboration, and Carboamination with Electrophilic Amination Reagents: Umpolung-Enabled Regio- and Stereoselective Synthesis of N -Containing Molecules from Alkenes and Alkynes. *J. Am. Chem. Soc.* **2022**, *144*, 648–661.
53. Mohite, S. B.; Bera, M.; Kumar, V.; Karpoormath, R.; Baba, S. B.; Kumbhar, A. S. O-Benzoylhydroxylamines: A Versatile Electrophilic Aminating Reagent for Transition Metal-Catalyzed C–N Bond-Forming Reactions. *Top. Curr. Chem.* **2023**, *381*, 4.
54. Zhu, S.; Niljianskul, N.; Buchwald, S. L. Enantio- and Regioselective CuH-Catalyzed Hydroamination of Alkenes. *J. Am. Chem. Soc.* **2013**, *135*, 15746–15749.
55. Miki, Y.; Hirano, K.; Satoh, T.; Miura, M. Copper-Catalyzed Intermolecular Regioselective Hydroamination of Styrenes with Polymethylhydrosiloxane and Hydroxylamines. *Angew. Chem., Int. Ed.* **2013**, *52*, 10830–10834.
56. Liu, R. Y.; Buchwald, S. L. CuH-Catalyzed Olefin Functionalization: From Hydroamination to Carbonyl Addition. *Acc. Chem. Res.* **2020**, *53*, 1229–1243.

57. Paderes, M. C.; Belding, L.; Fanovic, B.; Dudding, T.; Keister, J. B.; Chemler, S. R. Evidence for Alkene Cis-Aminocupration, an Aminoxygénéation Case Study: Kinetics, EPR Spectroscopy, and DFT Calculations. *Chem. - Eur. J.* **2012**, *18*, 1711–1726.
58. Wencel-Delord, J.; Glorius, F. C–H Bond Activation Enables the Rapid Construction and Late-Stage Diversification of Functional Molecules. *Nat. Chem.* **2013**, *5*, 369–375.
59. DiRocco, D. A.; Dykstra, K.; Krska, S.; Vachal, P.; Conway, D. V.; Tudge, M. Late-Stage Functionalization of Biologically Active Heterocycles Through Photoredox Catalysis. *Angew. Chem., Int. Ed.* **2014**, *53*, 4802–4806.
60. Sharma, A.; Hartwig, J. F. Metal-Catalyzed Azidation of Tertiary C–H Bonds Suitable for Late-Stage Functionalization. *Nature* **2015**, *517*, 600–604.
61. Cernak, T.; Dykstra, K. D.; Tyagarajan, S.; Vachal, P.; Krska, S. W. The Medicinal Chemist’s Toolbox for Late-Stage Functionalization of Drug-like Molecules. *Chem. Soc. Rev.* **2016**, *45*, 546–576.
62. Gianatassio, R.; Lopchuk, J. M.; Wang, J.; Pan, C.-M.; Malins, L. R.; Prieto, L.; Brandt, T. A.; Collins, M. R.; Gallego, G. M.; Sach, N. W.; Spangler, J. E.; Zhu, H.; Zhu, J.; Baran, P. S. Strain-Release Amination. *Science* **2016**, *351*, 241–246.
63. Shang, M.; Wang, M.; Saint-Denis, T. G.; Li, M.; Dai, H.; Yu, J. Copper-Mediated Late-Stage Functionalization of Heterocycle-Containing Molecules. *Angew. Chem., Int. Ed.* **2017**, *56*, 5317–5321.
64. Le, C.; Liang, Y.; Evans, R. W.; Li, X.; MacMillan, D. W. C. Selective sp^3 C–H Alkylation via Polarity-Match-Based Cross-Coupling. *Nature* **2017**, *547*, 79–83.
65. Uehling, M. R.; King, R. P.; Krska, S. W.; Cernak, T.; Buchwald, S. L. Pharmaceutical Diversification via Palladium Oxidative Addition Complexes. *Science* **2019**, *363*, 405–408.

66. Feng, K.; Quevedo, R. E.; Kohrt, J. T.; Oderinde, M. S.; Reilly, U.; White, M. C. Late-Stage Oxidative C(sp³)-H Methylation. *Nature* **2020**, *580*, 621–627.
67. Zhang, L.; Ritter, T. A Perspective on Late-Stage Aromatic C–H Bond Functionalization. *J. Am. Chem. Soc.* **2022**, *144*, 2399–2414.

CHAPTER 2: Results and Conclusions

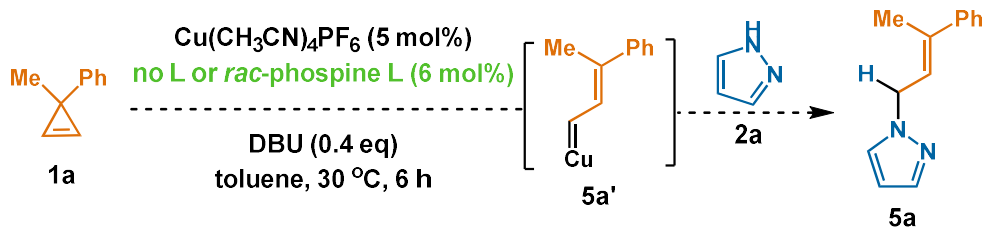
2.1 Results

2.1.1 Development of Reaction Conditions

2.1.1.1 Ligand Selection

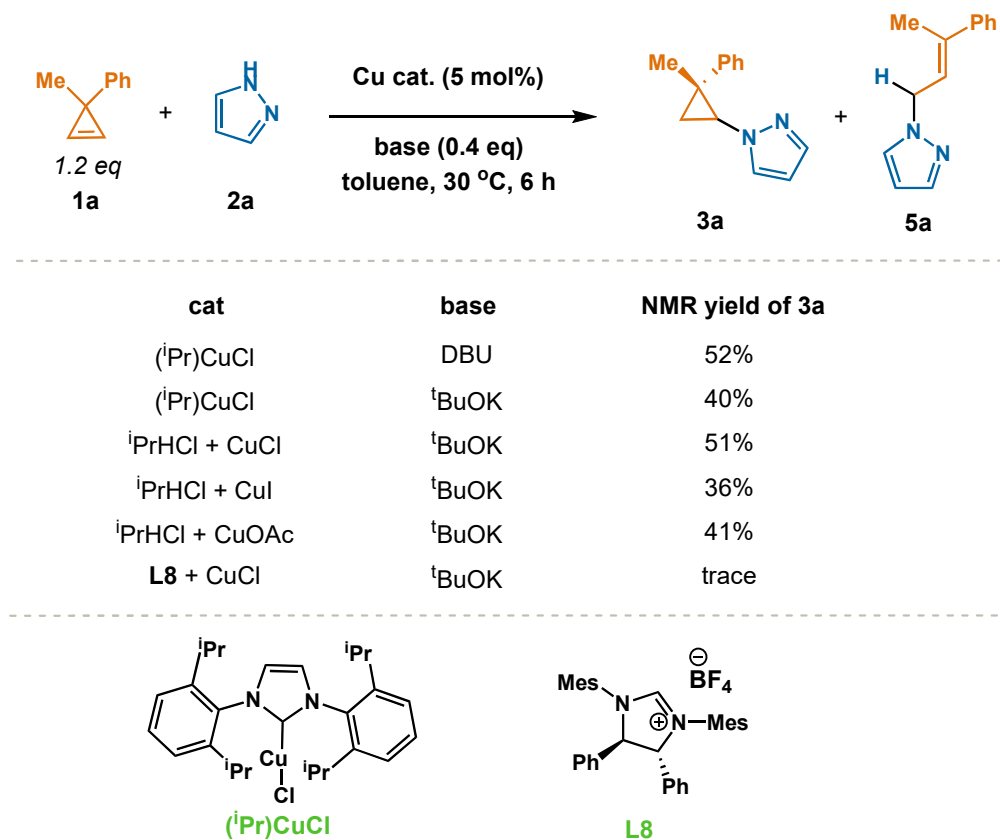
To begin this study, we selected the coupling of achiral cyclopropene **1a** with pyrazole **2a** as the model reaction on which to develop our methodology. If successful, the resulting cyclopropyl pyrazole **3a** would contain two stereocenters, allowing us to probe the enantioselectivity of this hydroamination. Initial tests using copper with no ligands gave an undesired allylic pyrazole **5a** with none of the desired product observed (**Scheme 4**). A number of experiments conducted with achiral ligands, including *rac*-BINAP, DPPF, and Xantphos, all resulted in exclusive formation of the undesired allylic pyrazole **5a**. We believe this product is formed through a ring-opening pathway¹⁻³ involving N–H bond insertion into allylic carbene intermediate **5a'**.⁴⁻⁹

Scheme 4 : Undesired Reactivity of Achiral Phosphine Ligands



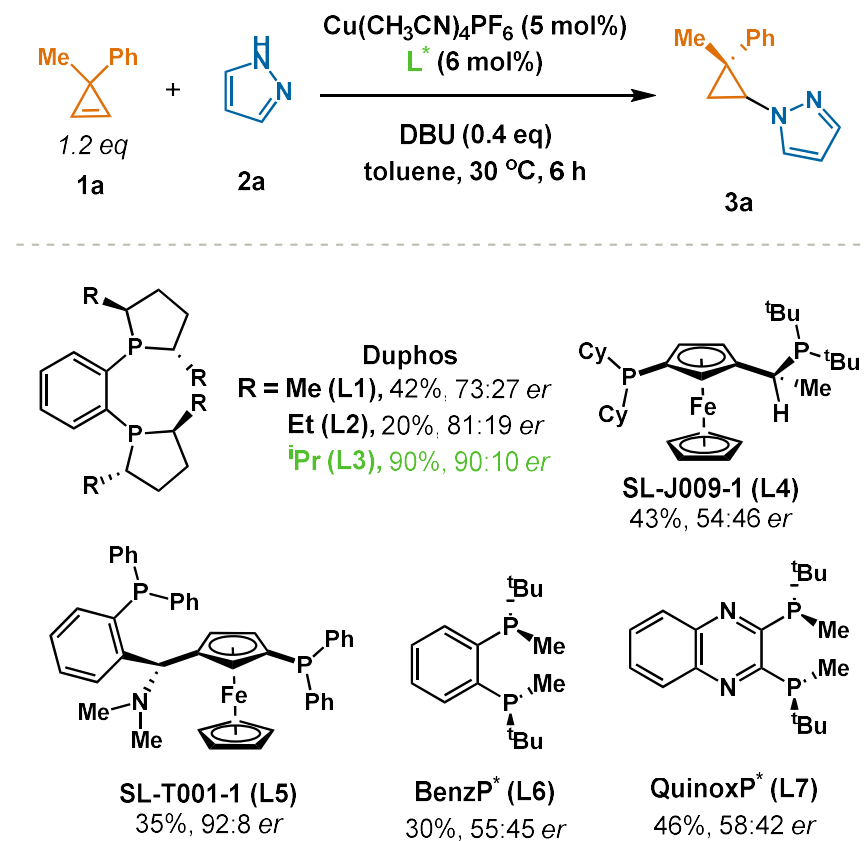
We then turned our attention to examining NHC ligands. Using the commercial (*i*Pr) CuCl complex, we conducted a series of experiments which produced relatively high chemoselective preference for the desired closed-ring product **3a** (**Figure 4**).¹⁰ However, when we attempted to generate chiral NHC-copper complexes *in situ*, the allylic **5a** product was favored. We propose

Figure 4 : Reactivity of NHC Ligands



the ring opening pathway with the copper chloride complex outcompetes NHC carbene formation and ligation. Gunnoe and coworkers observed greater copper–nitrogen nucleophilicity with bulky electron-rich phosphine ligands than with NHC ligands.^{9,11} Drawing from this, we chose to examine bulky electron-rich chiral phosphine ligands, as we believed they may favor copper-amido insertion over a ring-opening mechanism. A series of experiments were conducted (**Figure 5**), and the tested ligands (**L1-L7**) all strongly favored the desired cyclopropyl pyrazole **3a** product. The best results were obtained with (*R,R*)-*i*-Pr-Duphos **L3**, which afforded high yield (90%) and enatioselectivity (90:10 *er*).

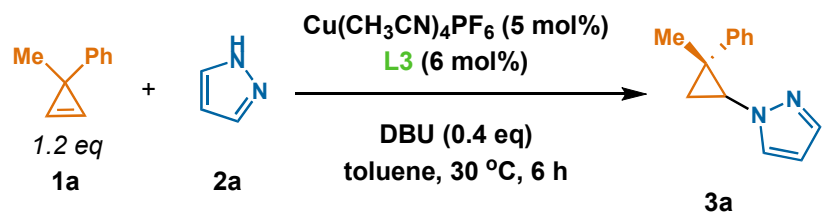
Figure 5 : Effects of Bulky Electron-Rich Chiral Ligands



2.1.1.2 Optimization

We examined a number of experimental parameters to optimize our reaction conditions (**Figure 6**). Intriguingly, doubling the equivalents of pyrazole **2a** resulted in a substantial decrease in yield (40%), an observation that was supported by our later kinetics studies (see section 2.1.3.1). Increasing the temperature to 60 °C was found to have a small detrimental effect on yield (85%). Interestingly, decreasing the temperature to 0 °C improved the enantiomeric ratio (95:5 *er*), but resulted in a small decrease in yield (90%), and significantly required a reaction time of four days. We therefore elected to use 30 °C for the standard conditions.

Figure 6 : Optimization of Reaction Conditions



derivations	NMR yield	er
none	>95%	90:10
no base	n.r.	/
2 eq pyrazole	40%	90:10
60 °C	85%	90:10
0 °C	90% (4 days)	95:5
LiO <i>i</i> Pr	48%	90:10
KO <i>t</i> Bu	63%	88:12
Cs ₂ CO ₃	94%	87:13
K ₃ PO ₄	83%	86:14
NaHMDS	42%	90:10
THF	46%	90:10
Dioxane	55%	90:10
CPME	60%	83:17
DCM	21%	92:8
DMSO	63%	92:8
DMF	71%	91:9
CH₃CN	>95%	94:6

Several bases were tested with promising results obtained from cesium carbonate with yield (94%) and both lithium isoproperoxide and sodium bis(trimethylsilyl)amide for enantioselectivity (90:10 *er*), but DBU showed the best combination results for both factors. A number of polar aprotic solvents were also examined. Our initial experiments were done in toluene, but we found reactions in acetonitrile to afford superior yields (>95%) and enantioselectivity (94:6 *er*).

2.1.2 Substrate Scope

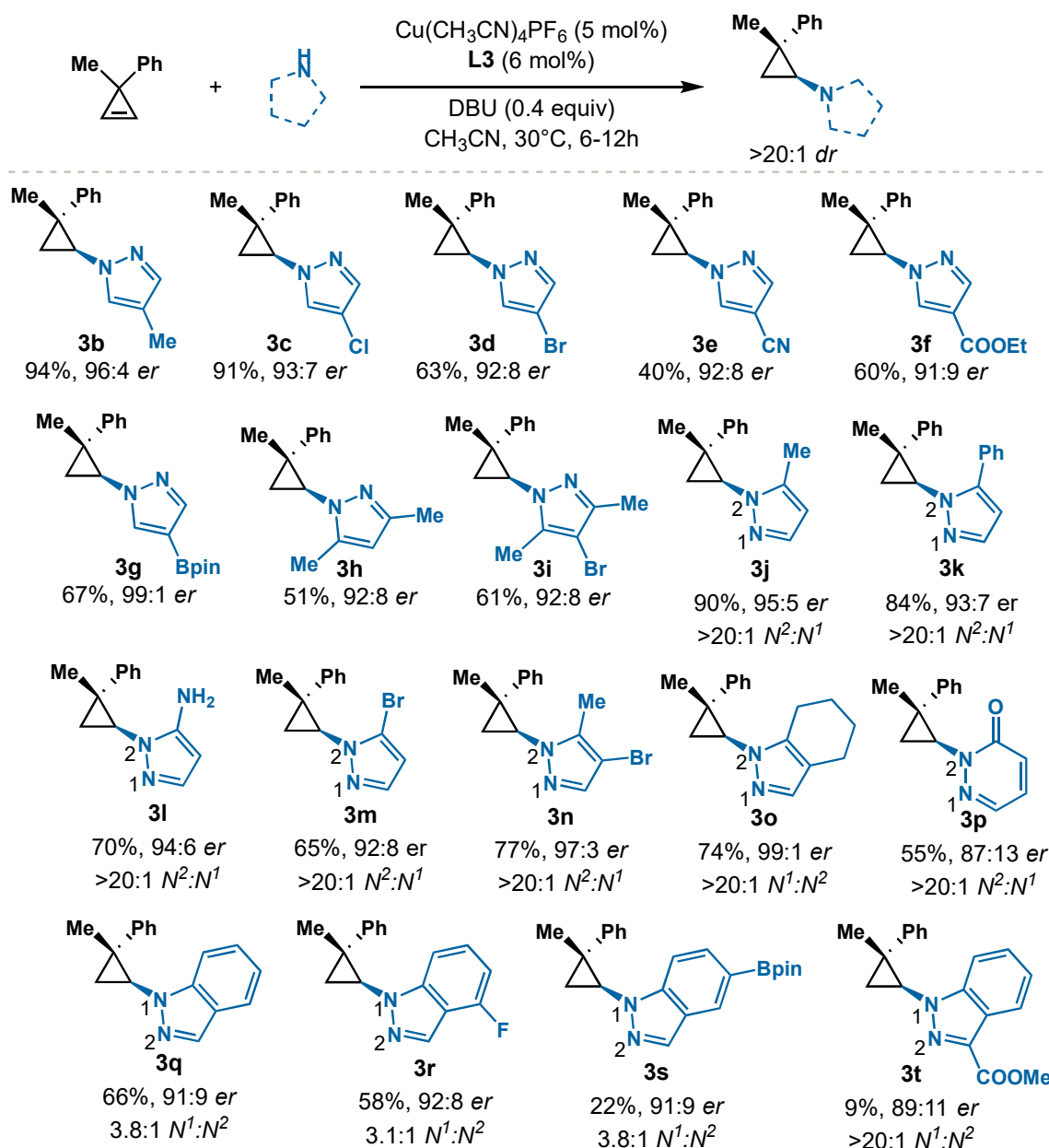
2.1.2.1 Pyrazoles and other N-Heterocycles

With our protocol optimized, we next endeavored to probe the scope of this hydroamination. We began by examining the enantioselective coupling of a variety of pyrazoles to cyclopropene **1a** (**Figure 7**). High diastereoselectivity of >20:1 was consistently observed, which we attributed to the significant steric difference between the phenyl and methyl substituents on the cyclopropyl ring.¹² Reactions involving symmetric pyrazoles **2b-2i**, producing cyclopropyl pyrazoles **3b-3i**, resulted in a wide disparity in yield (40-94%), but consistently high enantioselectivity (91:9-99:1 *er*). The variance in yield appears to be in part a result of sterics, as pyrazole with a single methyl substituent (**2b**) affording the same yield as pyrazole **2a** (94%), while the more hindered demethylated pyrazoles (**2h**, **2i**) gave notably lower yields (51% and 61% respectively). Electron-deficient pyrazoles (**2c-2f**) were tolerated, with yields ranging from 40% to 60%. The lowest yield was observed for cyano-substituted pyrazole **2e**, caused by a significant formation of the undesired allylic pyrazole side product.

For unsymmetric pyrazoles (**2j-2o**), yields of the resulting cyclopropyl pyrazole products (**3j-3o**) ranging from 65% to 90% with 92:8-99:1 *er* were observed. Interestingly, nitrogen regioselectivity consistently and strongly favored the more sterically hindered N² (N²:N¹ > 20:1). This observation was verified by NOE experiments on cyclopropyl pyrazole products **3k**, **3n**, and **3o**. Further confirmation was obtained by X-ray crystallographic analysis of cyclopropyl pyrazole **3j**. All of these studies indicated the coupling of the cyclopropene to the more hindered nitrogen. This finding is notable due to the rarity of this regioselectivity in pyrazole functionalization.^{10,13-20} Another noteworthy observation is the high chemoselective cyclopropylation for pyrazole

nitrogens seen in the coupling with pyrazole **2l**. The desired cyclopropyl pyrazole **3l** was isolated exclusively, with no side reactivity at the amino substituent observed.

Figure 7 : N-Heterocycle Scope



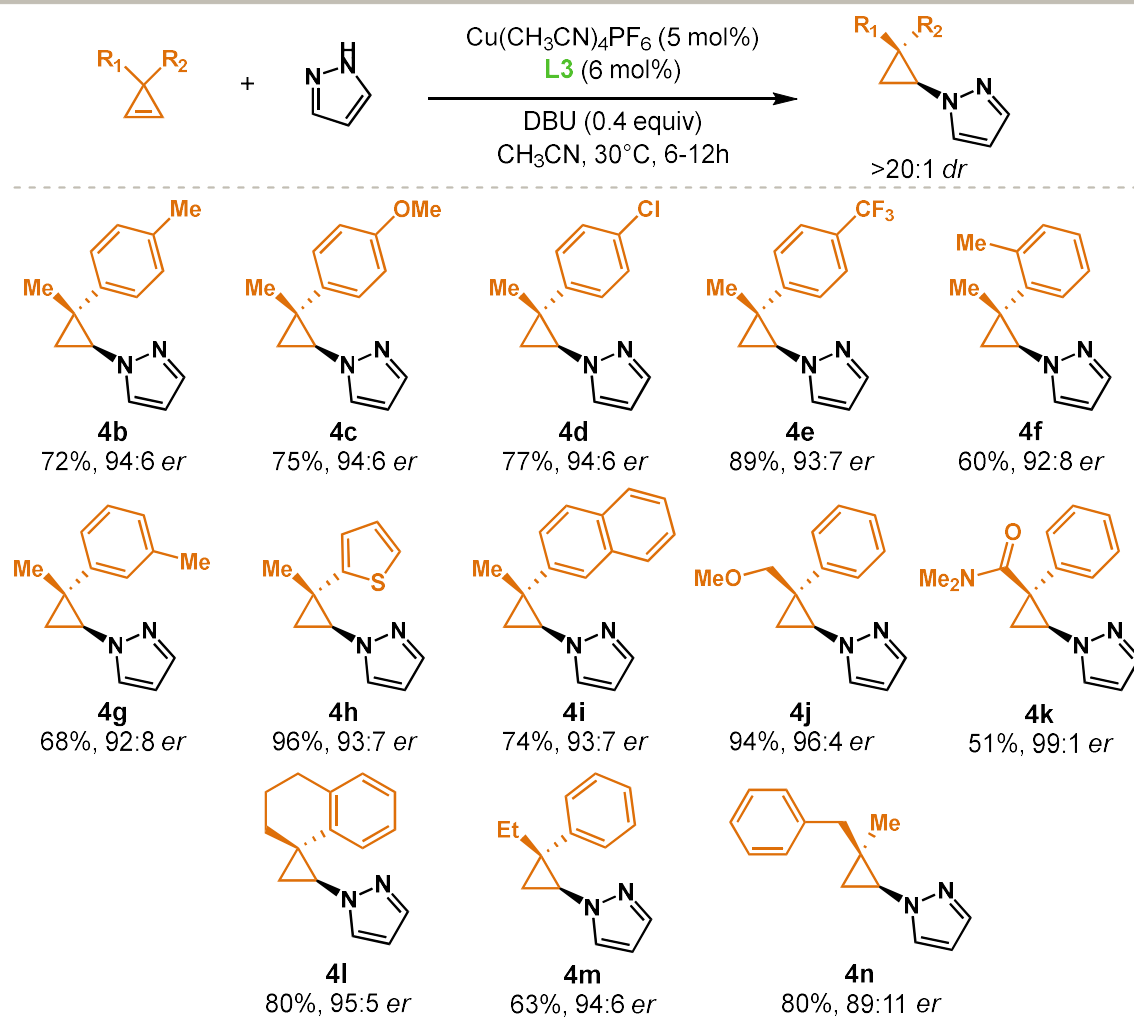
We then expanded our investigation into using other nitrogen-containing heterocycles. First, pyridazone **2p** was selected for study, as it is a nitrogen-rich heterocycle with potential implications as a drug discovery target due to its noted analgesic and anti-inflammatory properties.^{21,22} This afforded cyclopropyl pyridazinone **3p** in 55% yield, 87:13 *er*, and >20:1 N² regioselectivity. We next turned our attention to indazoles. Indazole derivatives have been found to possess anti-inflammatory, anti-HIV, and anticancer properties, and are a growing area of interest in new pharmaceutical development.²³ Chiral cyclopropyl indazoles (**3q-3t**) were successfully prepared in yields ranging from 9% to 60%, but required higher temperatures than the standard conditions (60 °C). The low yields of cyclopropyl indazoles **3s** and **3t** (22% and 9% respectively) are theorized to be a result of the profound electron deficiency of indazoles **2s** and **2t**. The cyclopropyl indazoles (**3q-3t**) were prepared with decent enantioselectivity (89:11-92:8 *er*), but notably, with the exception of ester-substituted **3t** (>20:1 *rr*), a substantial decrease in nitrogen regioselectivity was observed (3.1:1-3.8:1 *rr* for **3q-3s**). Other nitrogen nucleophiles, including a number of imidazoles, triazoles, and aniline, were examined but exhibited no desired reactivity under our standard conditions, and present an interesting avenue for further development of this methodology.²⁴

2.1.2.2 Cyclopropenes

We further looked to expand the scope by examining the enantioselective hydroamination of pyrazole **2a** with a variety of cyclopropenes **1** (Figure 8). We first examined the effects that altering the electronics of the phenyl ring substituent on cyclopropenes **1** may have on the reactivity and enantioselectivity of the hydroamination. Products with electron-rich phenyl rings (**4b**, **4c**, **4f**, and **4g**) were obtained with good yields (60-75%) and enantioselectivity (92:8-94:6 *er*). Comparable results were observed for cyclopropyl pyrazoles with electron-poor phenyl rings

(**4d** and **4e**), with yields ranging from 77% to 89% and 93:7-94:6 *er*, indicating a negligible impact of the electronics of the phenyl ring on the outcome of the reaction.

Figure 8 : Cyclopropene Scope



We next explored replacing the phenyl ring with alternative aromatic rings. Both thiophenyl- (**1h**) and naphthyl-substituted (**1i**) cyclopropenes were successful, affording high yields (74 and 96%, respectively) and enantioselectivities (93:7 *er*). X-ray crystallographic analysis of naphthyl-substituted cyclopropyl pyrazole **4i** was conducted to verify its absolute configuration.

Alternatives for the methyl substituent for cyclopropenes **1** were also studied. Methoxy- (**1j**) and amide-substituted (**1k**) cyclopropene resulted in substantially disparate yields (94% and 51% respectively), but enhanced enantioselectivity was observed for both (96:4 and 99:1 *er* respectively). X-ray crystallographic analysis conducted on amide-substituted cyclopropyl pyrazole **4k** confirmed addition of pyrazole *cis* to the amide substituent, suggesting the group may have directing group functionality.²⁵ Test with spirocycle- (**1l**) and ethyl-substituted (**1m**) cyclopropenes resulted in good yields (80% and 63% respectively) and enantioselectivity (95:5 and 94:6 *er* respectively). Finally, a dialkyl-substituted cyclopropene (**1n**) afforded cyclopropyl pyrazole **4n** in 80% yield with 89:11 *er*. However, no diastereoselectivity was observed, and the product was collected as a 1:1 mixture of diastereomers.²⁶⁻²⁸ Difluoro-substituted cyclopropene was examined but showed no reactivity under standard conditions.²⁹

2.1.3 Mechanistic Studies

2.1.3.1 Rate Studies

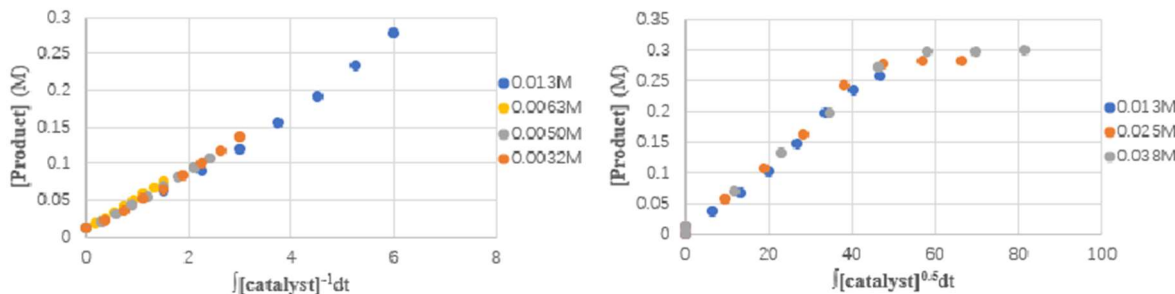
Our next goal was to explore the mechanism of the catalytic cycle. To this end, we began our inquiry by employing variable-time normalization analysis (VTNA) to probe the kinetic profile of the hydroamination.³⁰ The addition of pyrazole **2a** into cyclopropene **1a** was selected as the model reaction for this study. A first-order dependence was observed both on cyclopropene **1a** and the copper catalyst, while an inverse-first-order dependence was observed on pyrazole **2a**. Interestingly, there was found to be a fractional order of 0.5 on DBU.

These results are reminiscent of previous studies conducted by the Dong lab on rhodium-catalyzed hydrothiolation, in which inverse fractional orders in thiols were observed.³¹⁻³³ We attributed these kinetics to the coordination of multiple thiol groups to rhodium in an off-cycle resting state. Given this, and the known coordinating ability of pyrazoles, we propose the

formation of an off-cycle catalyst resting state consisting of a 2:1 relative ratio of pyrazole **2a** to copper.

We wished to test this hypothesis further, and drew inspiration from an experiment conducted by the Blackmond group, in which they observed a variance in the order of palladium in the Heck reaction between first-order and a fractional order of 0.5 depending on the amount of catalyst monomer released from an off-cycle dimer.^{34,35} We therefore conducted the VTNA study again at higher copper loading and observed a fractional order dependence of 0.5 on copper (**Figure 9**). These data further support the proposal regarding the off-cycle resting state, and suggest the possibility that it may be a dimeric copper species.³⁶⁻³⁸

Figure 9 : Effect of Copper Loading on Reaction Order

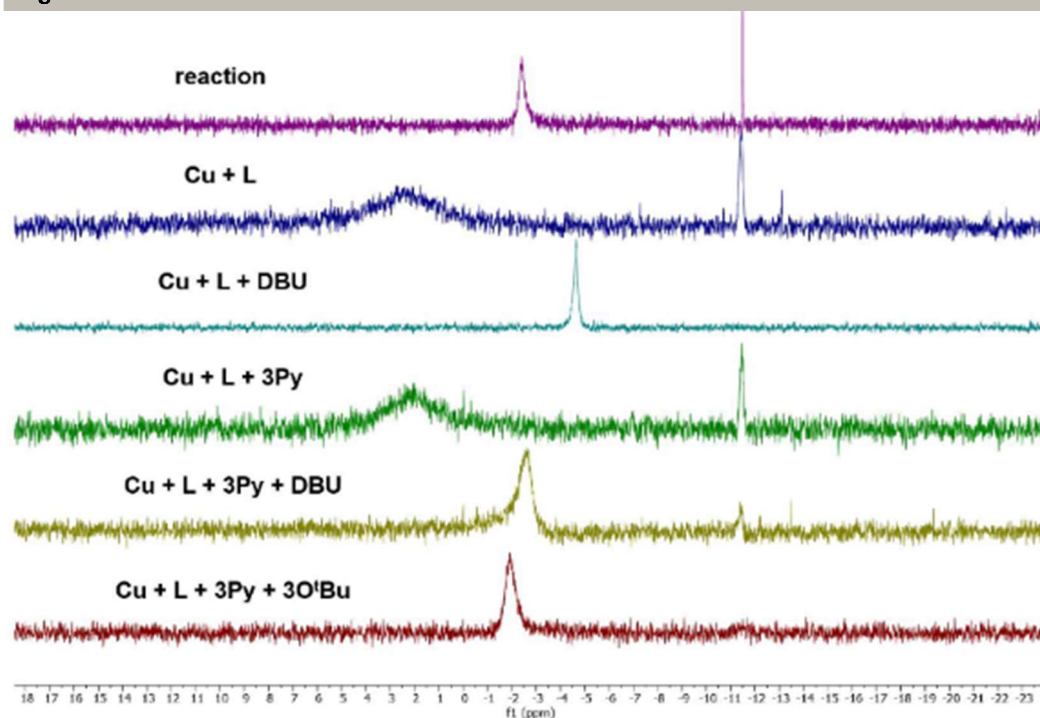


2.1.3.2 NMR Studies

We then turned our attention to studying the catalyst resting state. To this end, we performed ³¹P NMR studies, monitoring the chemical shift of **L3**. The coupling of cyclopropene **1a** with pyrazole **2a** was selected as the model reaction for this study. We observed a signal at -2.4 ppm, which we propose as a plausible catalyst resting state. Over the course of the reaction this signal disappeared as a singlet at -4.7 ppm grew in.

NMR titrations³⁹ using stoichiometric quantities of copper, pyrazole, and DBU were conducted to further elucidate these data. Results indicated that the -2.4 ppm signal was from a copper-Duphos-pyrazolate complex,^{40,41} while the -4.7 ppm resonance was a copper-Duphos-DBU complex (**Figure 10**). These studies suggest an interesting dual role of DBU in the reaction, serving as both a base to deprotonate pyrazole and as a copper ligand.⁴² This multiple functionality may contribute to the fractional order in DBU we observed in our rate studies.

Figure 10 : ^{31}P NMR Titrations

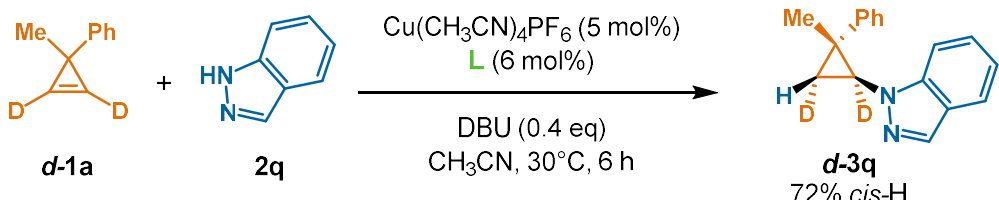


2.1.3.3 Deuterium Labeling Study

We conducted a deuterium labeling study, coupling deuterated cyclopropene **d-1a** and indazole **2q** under standard conditions (**Scheme 5**). NOE analysis of the resulting deuterated cyclopropyl indazole **d-3q** product exclusive *syn* proton incorporation relative to indazole. These

results suggest C–N bond is formed by inner-sphere *cis*-aminocupration followed by retentive protodemetalation, rather than through outer outer-sphere nucleophilic addition.⁴³

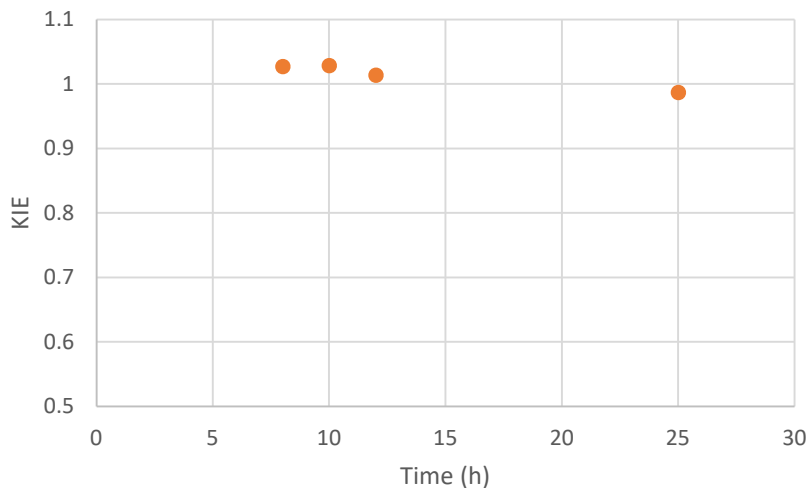
Scheme 5 : Deuterium Labelling Study



2.1.3.4 Kinetic Isotope Effect Study

In order to gain a more complete understanding of the catalytic cycle, we conducted a competitive kinetic isotope effect (KIE) study to probe to turnover-limiting step.⁴⁴ A calculated KIE of 1.0 was determined (**Figure 11**). These results indicate the rehybridization of the cyclopropene double bond does not occur during the turnover-limiting step. This suggests the protodemetalation step as the most probable turnover-limiting step. Further experimentation is warranted to strengthen this proposal.

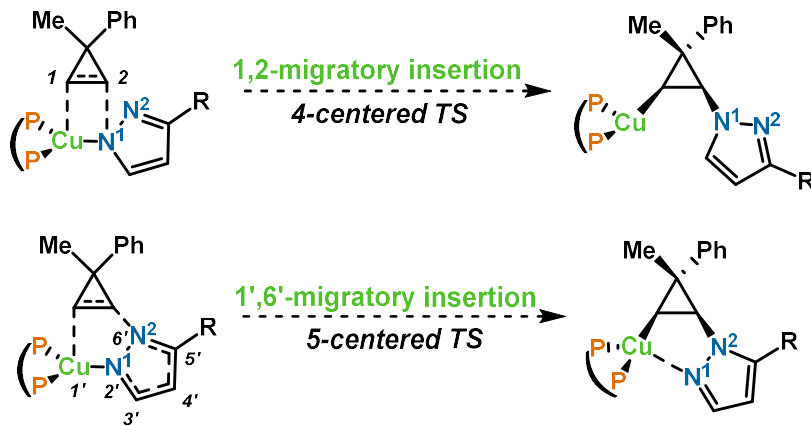
Figure 11 : Calculated KIE Values



2.1.3.5 Density Functional Theory Calculations

We initially envisioned a 1,2-migratory insertion of cyclopropene into the Cu–N bond with a four-centered transition state. However, the observed N²:N¹ regioselectivity is inconsistent with this mechanism. We therefore proposed a 1',6'-migratory insertion for the aminocupration (**Figure 12**). In this model, the less hindered nitrogen N¹ coordinates with copper in the five-centered transition state,⁴⁵ with the more-hindered nitrogen N² forging the C–N bond with the cyclopropane. This mechanistic proposal is consistent with that suggested by Lee, who observed similar nitrogen regioselectivity in her work involving pyrazole hydroamination.¹⁰

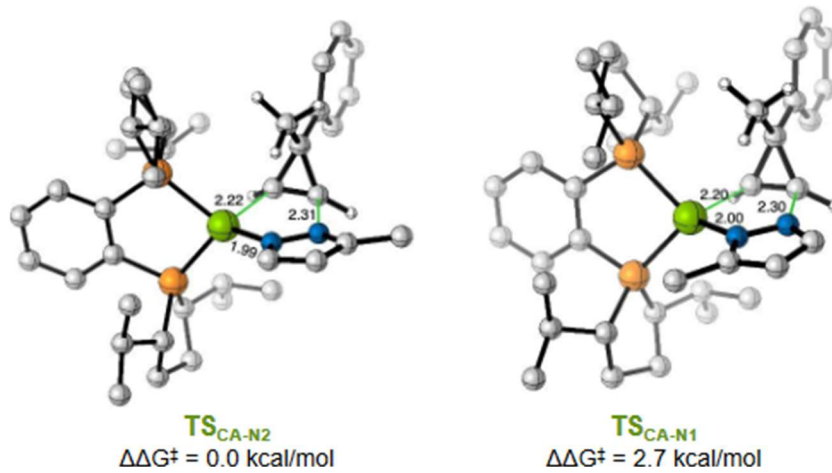
Figure 12 : Potential *cis*-Aminocupration Pathways



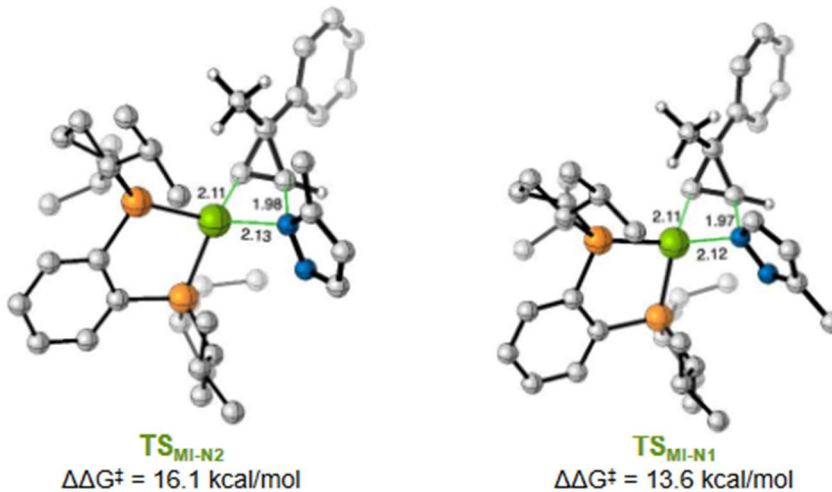
In order to more fully test this mechanistic proposal, we coordinated with our collaborators in the Hirschi group to perform density functional theory (DFT) analysis. We selected the copper-**L3**-catalyzed coupling of cyclopropene **1a** and pyrazole **2j** yielding 3-methyl cyclopropyl pyrazole **3j**. Initial DFT calculations were performed at the M06-2X/6-311+G** PCM(MeCN)//M06-2X/6-31G* level of theory,^{46,47} as implemented in Gaussian 16.⁴⁸ We explored the two most probable migratory insertion pathways for the addition of pyrazole **2j** to cyclopropene **1a**: the 1,2-migratory insertion and the 1',6'-migratory insertion.

Figure 13 : Relative Transition State Energies of Aminocupration Proposals

A. Aminocupration via 1'6'-migratory insertion pathway



B. Aminocupration via 1,2-migratory insertion pathway

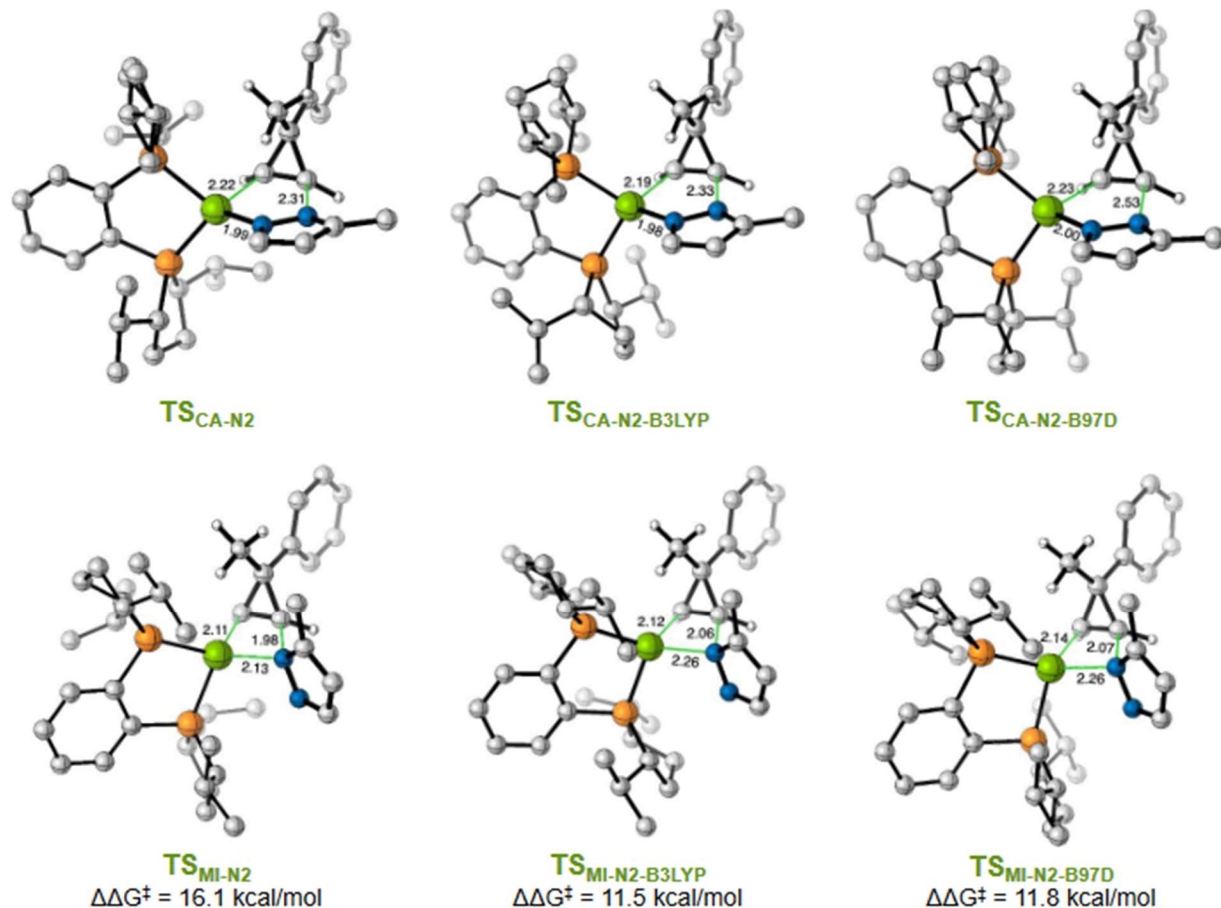


The 1,2-migratory insertion pathway can be described as a 4-centered transition state in which cyclopropene inserts into and breaks the Cu–N bond, thereby forming new C–Cu and C–N bonds. In this transition state, the same pyrazole nitrogen coordinated to the copper catalyst is inserted into cyclopropene. This was explored for the addition of both the less sterically hindered N¹ and the more hindered N² (TS_{MI-N1} and TS_{MI-N2}, respectively). It was found that the insertion of N¹ into cyclopropene via this 1,2-migratory insertion pathway (TS_{MI-N1}) was favored by 2.5 kcal/mol compared to TS_{MI-N2} (Figure 13).

However, we determined this 1,2-migratory insertion is overall higher in energy and is therefore disfavored as the means of achieving aminocupration compared to a 1',6'-migratory insertion pathway. The 1',6'-migratory insertion can be described as a 5-centered transition state, in which the copper catalyst remains bound to one of the pyrazole nitrogen heteroatoms, while the other adds onto the cyclopropene substrate. Transition states were located for both the coordination of N¹ to copper and C–N bond formation from N² (**TSCA-N2**), as well as for the coordination of N² to copper and C–N bond formation from N¹ (**TSCA-N1**). **TSCA-N1**, resulting in the minor N¹ regioisomer, was found to be 2.7 kcal/mol higher in energy than **TSCA-N2**, which resulted in the major N² regioisomer. This is consistent with the experimentally observed N¹:N² regioselectivity of the reaction. Overall, **TSCA-N2** represents the lowest energy transition state for the aminocupration of cyclopropene with the 1',6'-migratory insertion pathway being favored over the 1,2-migratory pathway for both regioisomers (**TSMI-N1** and **TSMI-N2**) by 13.6 and 16.1 kcal/mol respectively.

To further verify these results in identifying the most favorable aminocupration pathway, we located **TSCA-N2** and **TSMI-N2** at two other levels of theory: B3LYP-D3BJ/6-311+G** PCM(MeCN) // B3LYP-D3BJ/6-31G*^{49,50} and ωB97XD/def2-TZVP PCM(MeCN) // B97D/def2-SVP.⁵¹⁻⁵⁴ Across all three levels of theory employed, similar geometries were achieved for each transition state, and the 5-centered aminocupration **TSCA-N2** was consistently lower in energy than **TSMI-N2** by 11.5-16.1 kcal/mol (**Figure 14**).

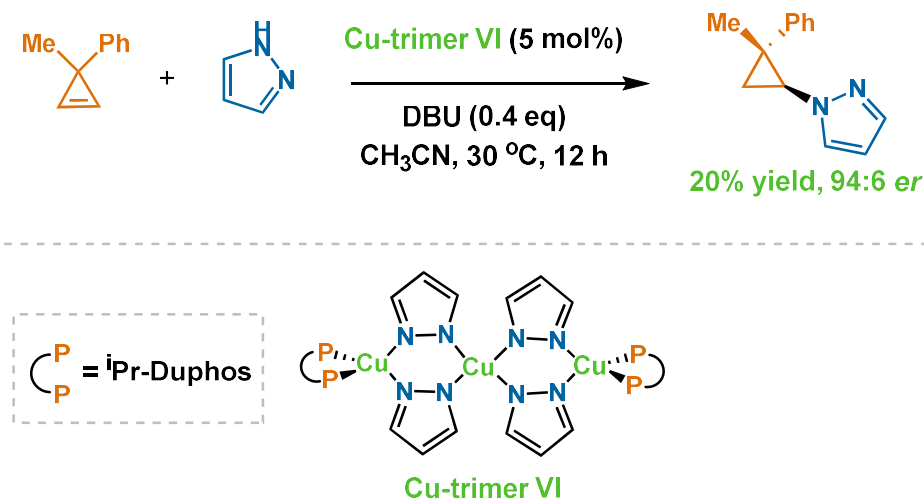
Figure 14 : Relative 4- and 5-Centered *cis*-Aminocupration Transition State Energies



2.1.3.6 Efforts to Characterize the Catalyst Resting State

In an attempt to isolate and characterize the catalyst resting state, a solution of copper (1 equiv.), **L3** (1.2 equiv.), pyrazole **2a** (12 equiv.), and DBU (6 equiv.) in deuterated acetonitrile was allowed to crystallize. To our surprise, X-ray crystallographic analysis of the resulting crystal instead revealed a trimeric copper species, named Copper-trimer **VI**. The unusual structure consisted of a central copper bringing two neighboring copper-Duphos complexes through four pyrazolates (**Scheme 6**). These structure observations lend support to the feasibility of copper-pyrazolate complexes.^{40,41}

Scheme 6 : Experimentation with Copper-Trimer VI

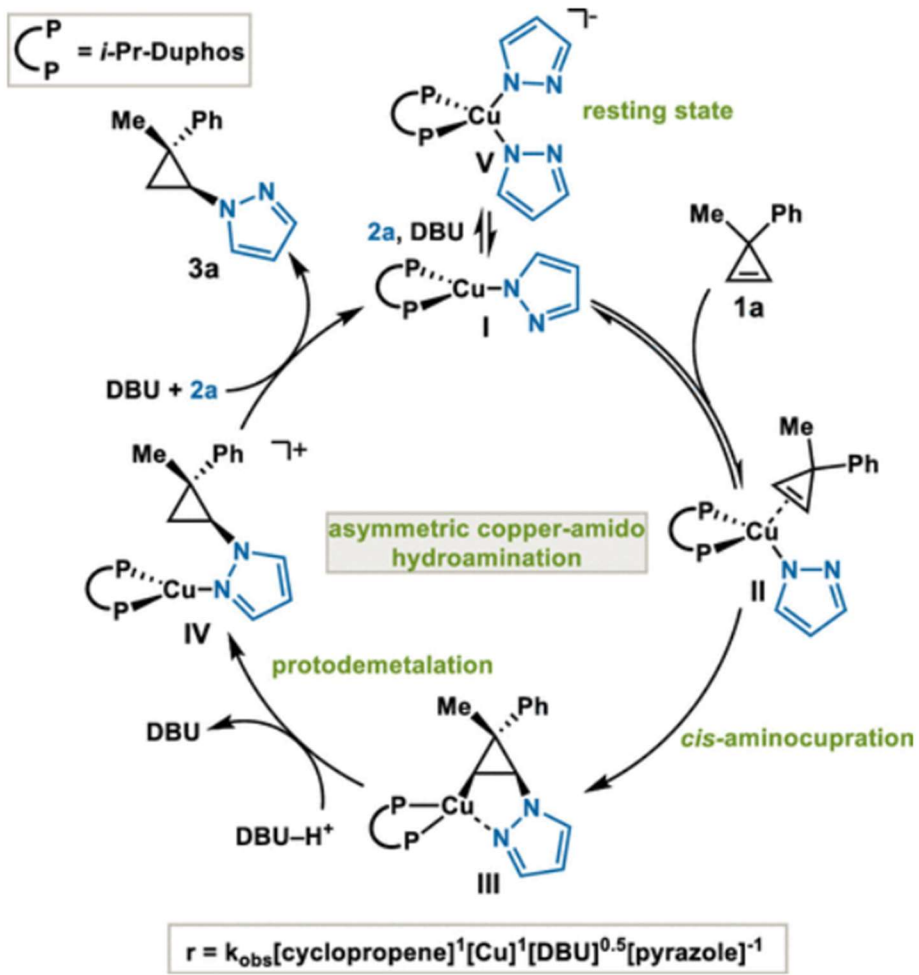


We then subjected this crystal to our standard conditions to test its reactivity, resulting in 20% yield of the desired product with 94:6 *er*. This lowered reactivity is believed to be the result of partial oxidation during crystallization.

2.1.3.7 Proposed Catalytic Cycle

Based on these experimental results and literature precedent, we developed a proposal for the catalytic cycle for this hydroamination (**Figure 15**). We believe the inactive off-cycle catalyst resting state is copper dipyrzolate **V**. From this species, the dissociation of one of the pyrazolates releases the active copper-amido catalyst **I**. The active catalytic compound subsequently binds to cyclopropene **1a**, beginning the catalytic cycle. This is followed by the *cis*-aminocupration of π complex **II**, forging the key C–N bond in the resulting cyclopropyl copper intermediate **III**.^{55,56} Protodemetalation of intermediate **III** protonated DBU then produces copper complex **IV**.⁴² Ligand exchange between copper complex **IV** and pyrazole **2a** releases the cyclopropyl pyrazole **3a** product and restarts the catalytic cycle.

Figure 15 : Proposed Catalytic Cycle



2.2 Conclusions and Future Work

In summary, hydroamination has been found to be an attractive approach for the enantioselective coupling of cyclopropenes with pyrazoles. A number of chiral *N*-cyclopropyl pyrazoles and N-heterocycles were successfully prepared using an earth-abundant copper catalyst under mild conditions with high regio-, diastereo-, and enantiocontrol. The more hindered pyrazole nitrogen was favored for coupling, and mechanistic studies suggest this observation may arise from a unique 1',6'-migratory insertion. Further exploration of this mechanism is warranted.

This copper-amido approach provides a complement to the more common copper-hydride method for hydroamination and will guide further studies into functionalization of N-heterocycles.

This work has been published in the *Journal of the American Chemical Society*.⁵⁷

2.3 References

1. Feng, S.; Hao, H.; Liu, P.; Buchwald, S. L. Diastereo- and Enantioselective CuH-Catalyzed Hydroamination of Strained Trisubstituted Alkenes. *ACS Catal.* **2020**, *10*, 282–291.
2. Vicente, R. C–C Bond Cleavages of Cyclopropenes: Operating for Selective Ring-Opening Reactions. *Chem. Rev.* **2021**, *121*, 162–226.
3. Huo, H.; Gong, Y. Construction of Heterocyclic Rings from Cyclopropenes. *Org. Biomol. Chem.* **2022**, *20*, 3847–3869.
4. Lee, E. C.; Fu, G. C. Copper-Catalyzed Asymmetric N–H Insertion Reactions: Couplings of Diazo Compounds with Carbamates to Generate α -Amino Acids. *J. Am. Chem. Soc.* **2007**, *129*, 12066–12067.
5. Phan, D. T. H.; Dong, V. M. Silver-Catalyzed Ring-Opening of Cyclopropenes: Preparation of Tertiary α -Branched Allylic Amines. *Tetrahedron* **2013**, *69*, 5726–5731.
6. Hyde, S.; Veliks, J.; Liégault, B.; Grassi, D.; Taillefer, M.; Gouverneur, V. Copper-Catalyzed Insertion into Heteroatom-Hydrogen Bonds with Trifluorodiazooalkanes. *Angew. Chem., Int. Ed.* **2016**, *55*, 3785–3789.
7. Arredondo, V.; Hiew, S. C.; Gutman, E. S.; Premachandra, I. D. U. A.; Van Vranken, D. L. Enantioselective Palladium-Catalyzed Carbene Insertion into the N–H Bonds of Aromatic Heterocycles. *Angew. Chem., Int. Ed.* **2017**, *56*, 4156–4159.
8. Li, M.-L.; Yu, J.-H.; Li, Y.-H.; Zhu, S.-F.; Zhou, Q.-L. Highly Enantioselective Carbene Insertion into N–H Bonds of Aliphatic Amines. *Science* **2019**, *366*, 990–994.

9. Goj, L. A.; Blue, E. D.; Munro-Leighton, C.; Gunnoe, T. B.; Petersen, J. L. Cleavage of X-H Bonds (X = N, O, or C) by Copper(I) Alkyl Complexes To Form Monomeric Two-Coordinate Copper(I) Systems. *Inorg. Chem.* **2005**, *44*, 8647–8649.
10. Kim, K.; Lee, Y. Copper-Catalyzed Hydroamination of Oxa- and Azabenzonorbornadienes with Pyrazoles. *J. Org. Chem.* **2022**, *87*, 569–578.
11. Goj, L. A.; Blue, E. D.; Delp, S. A.; Gunnoe, T. B.; Cundari, T. R.; Pierpont, A. W.; Petersen, J. L.; Boyle, P. D. Chemistry Surrounding Monomeric Copper(I) Methyl, Phenyl, Anilido, Ethoxide, and Phenoxy Complexes Supported by N -Heterocyclic Carbene Ligands: Reactivity Consistent with Both Early and Late Transition Metal Systems. *Inorg. Chem.* **2006**, *45*, 9032–9045.
12. Muller, P. Glossary of Terms Used in Physical Organic Chemistry (IUPAC Recommendations 1994). *Pure Appl. Chem.* **1994**, *66*, 1077–1184.
13. Xu, D.; Frank, L.; Nguyen, T.; Stumpf, A.; Russell, D.; Angelaud, R.; Gosselin, F. Magnesium-Catalyzed N2-Regioselective Alkylation of 3-Substituted Pyrazoles. *Synlett* **2020**, *31*, 595–599.
14. Bengel, L. L.; Aberle, B.; Egler-Kemmerer, A.; Kienzle, S.; Hauer, B.; Hammer, S. C. Engineered Enzymes Enable Selective N-Alkylation of Pyrazoles with Simple Haloalkanes. *Angew. Chem., Int. Ed.* **2021**, *60*, 5554–5560.
15. Chen, S.-J.; Golden, D. L.; Krska, S. W.; Stahl, S. S. Copper-Catalyzed Cross-Coupling of Benzylic C–H Bonds and Azoles with Controlled N-Site Selectivity. *J. Am. Chem. Soc.* **2021**, *143*, 14438–14444.

16. Antilla, J. C.; Baskin, J. M.; Barder, T. E.; Buchwald, S. L. Copper-Diamine-Catalyzed N -Arylation of Pyrroles, Pyrazoles, Indazoles, Imidazoles, and Triazoles. *J. Org. Chem.* **2004**, *69*, 5578–5587.
17. Goikhman, R.; Jacques, T. L.; Sames, D. C–H Bonds as Ubiquitous Functionality: A General Approach to Complex Arylated Pyrazoles via Sequential Regioselective C - Arylation and N -Alkylation Enabled by SEM-Group Transposition. *J. Am. Chem. Soc.* **2009**, *131*, 3042–3048.
18. Ye, Y.; Kevlishvili, I.; Feng, S.; Liu, P.; Buchwald, S. L. Highly Enantioselective Synthesis of Indazoles with a C3-Quaternary Chiral Center Using CuH Catalysis. *J. Am. Chem. Soc.* **2020**, *142*, 10550–10556.
19. Dow, N. W.; Cabré, A.; MacMillan, D. W. C. A General N-Alkylation Platform via Copper Metallaphotoredox and Silyl Radical Activation of Alkyl Halides. *Chem* **2021**, *7*, 1827–1842.
20. Das, M.; Zamani, L.; Bratcher, C.; Musacchio, P. Z. Azolation of Benzylic C–H Bonds via Photoredox-Catalyzed Carbocation Generation. *J. Am. Chem. Soc.* **2023**, *145*, 3861–3868.
21. Singh, J.; Sharma, D.; Bansal, R. Pyridazinone: An Attractive Lead for Anti-Inflammatory and Analgesic Drug Discovery. *Future Med. Chem.* **2017**, *9*, 95–127.
22. Dubey, S.; Bhosle, P. A. Pyridazinone: An Important Element of Pharmacophore Possessing Broad Spectrum of Activity. *Med. Chem. Res.* **2015**, *24*, 3579–3598.
23. Mal, S.; Malik, U.; Mahapatra, M.; Mishra, A.; Pal, D.; Paidesetty, S. K. A Review on Synthetic Strategy, Molecular Pharmacology of Indazole Derivatives, and Their Future Perspective. *Drug Dev. Res.* **2022**, *83*, 1469–1504.

24. Kim, S.; Kang, S.; Kim, G.; Lee, Y. Copper-Catalyzed Aza-Michael Addition of Aromatic Amines or Aromatic Aza-Heterocycles to α,β -Unsaturated Olefins. *J. Org. Chem.* **2016**, *81*, 4048–4057.
25. Tarwade, V.; Liu, X.; Yan, N.; Fox, J. M. Directed Carbozincation Reactions of Cyclopropene Derivatives. *J. Am. Chem. Soc.* **2009**, *131*, 5382–5383.
26. Parra, A.; Amenós, L.; Guisán-Ceinos, M.; López, A.; García Ruano, J. L.; Tortosa, M. Copper-Catalyzed Diastereo- and Enantioselective Desymmetrization of Cyclopropenes: Synthesis of Cyclopropylboronates. *J. Am. Chem. Soc.* **2014**, *136*, 15833–15836.
27. Teng, H.-L.; Luo, Y.; Wang, B.; Zhang, L.; Nishiura, M.; Hou, Z. Synthesis of Chiral Aminocyclopropanes by Rare-Earth-Metal-Catalyzed Cyclopropene Hydroamination. *Angew. Chem. Int. Ed.* **2016**, *55*, 15406–15410.
28. Dian, L.; Marek, I. Pd-Catalyzed Enantioselective Hydroalkynylation of Cyclopropenes. *ACS Catal.* **2020**, *10*, 1289–1293.
29. Nosik, P.; Pashko, M.; Poturai, A.; Kvasha, D.; Pashenko, A.; Rozhenko, A.; Suikov, S.; Volochnyuk, D.; Ryabukhin, S.; Yagupolskii, Y. Monosubstituted 3,3-Difluorocyclopropenes as Bench-Stable Reagents: Scope and Limitations. *Eur. J. Org. Chem.* **2021**, *47*, 6604–6615.
30. Burés, J. Variable Time Normalization Analysis: General Graphical Elucidation of Reaction Orders from Concentration Profiles. *Angew. Chem. Int. Ed.* **2016**, *55*, 16084–16087.
31. Zhang, H.; Huang, W.; Wang, T.; Meng, F. Cobalt-Catalyzed Diastereo-and Enantioselective Hydroalkenylation of Cyclopropenes with Alkenylboronic Acids. *Angew. Chem., Int. Ed.* **2019**, *58*, 11049–11053.

32. Yang, X.-H.; Davison, R. T.; Dong, V. M. Catalytic Hydrothiolation: Regio- and Enantioselective Coupling of Thiols and Dienes. *J. Am. Chem. Soc.* **2018**, *140*, 10443–10446.
33. Yang, X.-H.; Davison, R. T.; Nie, S.-Z.; Cruz, F. A.; McGinnis, T. M.; Dong, V. M. Catalytic Hydrothiolation: Counterion-Controlled Regioselectivity. *J. Am. Chem. Soc.* **2019**, *141*, 3006–3013.
34. Rosner, T.; Le Bars, J.; Pfaltz, A.; Blackmond, D. G. Kinetic Studies of Heck Coupling Reactions Using Palladacycle Catalysts: Experimental and Kinetic Modeling of the Role of Dimer Species. *J. Am. Chem. Soc.* **2001**, *123*, 1848–1855.
35. Burés, J. A Simple Graphical Method to Determine the Order in Catalyst. *Angew. Chem., Int. Ed.* **2016**, *55*, 2028–2031.
36. Hein, J. E.; Armstrong, A.; Blackmond, D. G. Kinetic Profiling of Prolinate-Catalyzed α -Amination of Aldehydes. *Org. Lett.* **2011**, *13*, 4300–4303.
37. Bandar, J. S.; Pirnot, M. T.; Buchwald, S. L. Mechanistic Studies Lead to Dramatically Improved Reaction Conditions for the Cu-Catalyzed Asymmetric Hydroamination of Olefins. *J. Am. Chem. Soc.* **2015**, *137*, 14812–14818.
38. Blackmond, D. G. Kinetic Profiling of Catalytic Organic Reactions as a Mechanistic Tool. *J. Am. Chem. Soc.* **2015**, *137*, 10852–10866.
39. Gibbons, S. K.; Valleau, C. R. D.; Peltier, J. L.; Cain, M. F.; Hughes, R. P.; Glueck, D. S.; Golen, J. A.; Rheingold, A. L. Diastereoselective Coordination of P-Stereogenic Secondary Phosphines in Copper(I) Chiral Bis(Phosphine) Complexes: Structure, Dynamics, and Generation of Phosphido Complexes. *Inorg. Chem.* **2019**, *58*, 8854–8865.

40. Titov, A. A.; Filippov, O. A.; Smol'yakov, A. F.; Baranova, K. F.; Titova, E. M.; Averin, A. A.; Shubina, E. S. Dinuclear Cu^I and Ag^I Pyrazolates Supported with Tertiary Phosphines: Synthesis, Structures, and Photophysical Properties. *Eur. J. Inorg. Chem.* **2019**, *2019*, 821–827.
41. Watanabe, Y.; Washer, B. M.; Zeller, M.; Savikhin, S.; Slipchenko, L. V.; Wei, A. Copper(I)-Pyrazolate Complexes as Solid-State Phosphors: Deep-Blue Emission through a Remote Steric Effect. *J. Am. Chem. Soc.* **2022**, *144*, 10186–10192.
42. Zall, C. M.; Linehan, J. C.; Appel, A. M. Triphosphine-Ligated Copper Hydrides for CO₂ Hydrogenation: Structure, Reactivity, and Thermodynamic Studies. *J. Am. Chem. Soc.* **2016**, *138*, 9968–9977.
43. Kainz, Q. M.; Matier, C. D.; Bartoszewicz, A.; Zultanski, S. L.; Peters, J. C.; Fu, G. C. Asymmetric Copper-Catalyzed C–N Cross-Couplings Induced by Visible Light. *Science* **2016**, *351*, 681–684.
44. Dale, H. J. A.; Leach, A. G.; Lloyd-Jones, G. C. Heavy-Atom Kinetic Isotope Effects: Primary Interest or Zero Point? *J. Am. Chem. Soc.* **2021**, *143*, 21079–21099.
45. Luo, Y.; Hou, Z. A Five-Center Rather than a Four-Center Transition State for Alkene Insertion into the Metal-Alkyl Bond of a Cationic Binuclear Yttrium Complex. *Organometallics* **2006**, *25*, 6162–6165.
46. Zhao, Y.; Truhlar, D. G. The M06 suite of density functionals for main group thermochemistry, thermochemical kinetics, noncovalent interactions, excited states, and transition elements: two new functionals and systematic testing of four M06-class functionals and 12 other functionals. *Theor. Chem. Acc.* **2008**, *120*, 215–241.

47. Hehre, W. J.; Stewart, R. F.; Pople, J. A. Self-Consistent Molecular-Orbital Methods. I. Use of Gaussian Expansions of Slater-Type Atomic Orbitals. *J. Chem. Phys.* **1969**, *51*, 2657–2664.
48. Frisch, M. J.; Trucks, G. W.; Schlegel, H. B.; Scuseria, G. E.; Robb, M. A.; Cheeseman, J. R.; Scalmani, G.; Barone, V.; Petersson, G. A.; Nakatsuji, H.; Li, X.; Caricato, M.; Marenich, A. V.; Bloino, J.; Janesko, B. G.; Gomperts, R.; Mennucci, B.; Hratchian, H. P.; Ortiz, J. V.; Izmaylov, A. F.; Sonnenberg, J. L.; Williams; Ding, F.; Lipparini, F.; Egidi, F.; Goings, J.; Peng, B.; Petrone, A.; Henderson, T.; Ranasinghe, D.; Zakrzewski, V. G.; Gao, J.; Rega, N.; Zheng, G.; Liang, W.; Hada, M.; Ehara, M.; Toyota, K.; Fukuda, R.; Hasegawa, J.; Ishida, M.; Nakajima, T.; Honda, Y.; Kitao, O.; Nakai, H.; Vreven, T.; Throssell, K.; Montgomery, J. A., Jr.; Peralta, J. E.; Ogliaro, F.; Bearpark, M. J.; Heyd, J. J.; Brothers, E. N.; Kudin, K. N.; Staroverov, V. N.; Keith, T. A.; Kobayashi, R.; Normand, J.; Raghavachari, K.; Rendell, A. P.; Burant, J. C.; Iyengar, S. S.; Tomasi, J.; Cossi, M.; Millam, J. M.; Klene, M.; Adamo, C.; Cammi, R.; Ochterski, J. W.; Martin, R. L.; Morokuma, K.; Farkas, O.; Foresman, J. B.; Fox, D. J. *Gaussian 16*; rev. C.01; Gaussian, Inc.: Wallingford, CT, 2016.
49. Becke, A. D. Density-functional thermochemistry. III. The role of exact exchange. *J. Chem. Phys.* **1993**, *98*, 5648–5652.
50. Grimme, S.; Ehrlich, S.; Goerigk, L. Effect of the damping function in dispersion corrected density functional theory. *J. Comput. Chem.* **2011**, *32*, 1456–1465.
51. Grimme, S. Semiempirical GGA-type density functional constructed with a long-range dispersion correction. *J. Comput. Chem.* **2006**, *27*, 1787–1799.

52. Becke, A. Density-Functional Thermochemistry. V. Systematic Optimization of Exchange-Correlation Functionals. *J. Chem. Phys.* **1997**, *107*, 8554–8560.
53. Chai, J. D.; Head-Gordon, M. Long-range corrected hybrid density functionals with damped atom-atom dispersion corrections. *Phys. Chem. Chem. Phys.* **2008**, *10*, 6615–6620.
54. Weigend, F.; Ahlrichs, R. Balanced basis sets of split valence, triple zeta valence and quadruple zeta valence quality for H to Rn: Design and assessment of accuracy. *Phys. Chem. Chem. Phys.* **2005**, *7*, 3297–3305.
55. Li, Z.; Zhao, J.; Sun, B.; Zhou, T.; Liu, M.; Liu, S.; Zhang, M.; Zhang, Q. Asymmetric Nitrone Synthesis via Ligand-Enabled Copper-Catalyzed Cope-Type Hydroamination of Cyclopropene with Oxime. *J. Am. Chem. Soc.* **2017**, *139*, 11702–11705.
56. Paderes, M. C.; Belding, L.; Fanovic, B.; Dudding, T.; Keister, J. B.; Chemler, S. R. Evidence for Alkene Cis-Aminocupration, an Aminoxygénéation Case Study: Kinetics, EPR Spectroscopy, and DFT Calculations. *Chem. Eur. J.* **2012**, *18*, 1711–1726.
57. Wang, M.; Simon, J. C.; Xu, M.; Corio, S. A.; Hirschi, J. S.; Dong, V. M. Copper-Catalyzed Hydroamination: Enantioselective Addition of Pyrazoles to Cyclopropenes. *J. Am. Chem. Soc.* **2023**, *145*, 14573–14580.

CHAPTER 3: Supporting Information

3.1 General Methods

Commercial reagents were purchased from Sigma Aldrich, Strem, Alfa Aesar, Acros Organics or TCI and used without further purification. Acetonitrile was purchased from Sigma Aldrich, degassed by three freeze-pump-thaw cycles, and stored over 3Å MS within a N₂ filled glove box. All experiments were performed in oven-dried or flame-dried glassware under an atmosphere of N₂ or in a glove box with a N₂ atmosphere. Reactions were monitored using either thin-layer chromatography (TLC; EMD Silica Gel 60 F254 plates) or gas chromatography using an Agilent Technologies 7890A GC system equipped with an Agilent Technologies 5975C inert XL EI/CI MSD. Visualization of the developed plates was performed under UV light (254 nm) or KMnO₄ stain. Organic solutions were concentrated under reduced pressure on a Büchi rotary evaporator. Purification and isolation of products were performed via silica gel chromatography (both column and preparative thin-layer chromatography). Column chromatography was performed with Silicycle Silica-P Flash Silica Gel using glass columns. Solvents were purchased from Sigma Aldrich. ¹H, ²H, ¹³C, and ³¹P NMR spectra were recorded on Bruker AVANCE-600, CRYO-500 or DRX-400 spectrometer. ¹H NMR spectra were internally referenced to the residual solvent signal or TMS. ¹³C NMR spectra were internally referenced to the residual solvent signal. Data for ¹H NMR are reported as follows: chemical shift (δ ppm), multiplicity (s = singlet, d = doublet, t = triplet, q = quartet, m = multiplet), coupling constant (Hz), integration. Data for ¹³C NMR are reported in terms of chemical shift (δ ppm). Infrared (IR) spectra were obtained on a Nicolet iS5 FT-IR spectrometer with an iD5 ATR and are reported in terms of frequency of absorption (cm⁻¹). High resolution mass spectra (HRMS) were obtained on a micromass 70S-250 spectrometer (EI) or an ABI/Sciex QStar Mass Spectrometer (ESI). Enantiomeric ratio (*er*) for

enantioselective reactions were determined by chiral SFC analysis using an Agilent Technologies HPLC (1200 series) system and Aurora A5 Fusion. Cyclopropenes **1a-1n** used here were known compounds and synthesized according to reported methods.¹⁻³

3.2 Optimization of the Hydroamination of Cyclopropenes with Pyrazoles

3.2.1 General Procedure for Determination of Copper Catalyst Reactivity

In a N₂-filled glove box, (ⁱPr)CuCl (2.8 mg, 0.0050 mmol, 5 mol%) and toluene (0.30 mL) were added to a 1-dram vial containing a stir bar. The resulting mixture was stirred for 10 min. **Base** (0.040 mmol, 0.4 equiv.) and pyrazole **2a** (0.10 mmol, 1.0 equiv.) were added sequentially, followed by cyclopropene **1a** (0.10 mL, 1.2 M solution in toluene, 0.12 mmol) to initiate the reaction. The mixture was held at 30 °C until no starting material was observed by TLC or GC-MS. Yields were determined by ¹H NMR analysis of the unpurified reaction mixture using trimethoxybenzene as an internal standard.

3.2.2 General Procedure for Optimization of Hydroamination Reaction Parameters

In a N₂-filled glove box, Cu(CH₃CN)₄PF₆ (1.9 mg, 0.0050 mmol, 5 mol%), **L3** (2.5 mg, 0.0060 mmol, 6 mol%), and solvent (0.30 mL) were added to a 1-dram vial containing a stir bar. The resulting mixture was stirred for 10 min. **Base** (0.040 mmol, 0.4 equiv.) and pyrazole **2a** (0.10 mmol, 1.0 equiv.) were added sequentially, followed by cyclopropene **1a** (0.10 mL, 1.2 M solution in solvent, 0.12 mmol) to initiate the reaction. The mixture was held at 30 °C until no starting material was observed by TLC or GC-MS. Yields were determined by ¹H NMR analysis of the unpurified reaction mixture using trimethoxybenzene as an internal standard. Chiral SFC analysis was used for enantioselectivity ratios (*er*).

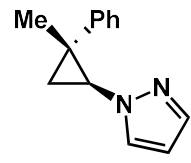
3.3 Asymmetric Hydroamination

3.3.1 General Procedure for Asymmetric Hydroamination

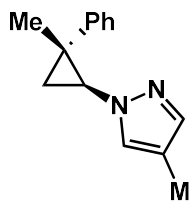
In a N₂-filled glove box, Cu(CH₃CN)₄PF₆ (1.9 mg, 0.0050 mmol, 5 mol%), **L3** (2.5 mg, 0.0060 mmol, 6 mol%), and MeCN (0.30 mL) were added to a 1-dram vial containing a stir bar. The resulting mixture was stirred for 10 min. DBU (6.0 μ L, 0.040 mmol, 0.4 equiv.) and pyrazole **2** (0.10 mmol, 1.0 equiv.) were added sequentially, followed by cyclopropene **1** (0.10 mL, 1.2 M solution in MeCN, 0.12 mmol) to initiate the reaction. The mixture was held at 30 °C until no starting material was observed by TLC or GC-MS. Regioisomeric and diastereomeric ratios (*rr* and *dr*, respectively) were determined by ¹H NMR analysis of the unpurified reaction mixture. Isolated yields (obtained by column chromatography on silica gel or preparative thin-layer chromatography) of the title compound are reported.

3.3.2 Characterization of Unknown Compounds

1-((1*S*,2*R*)-2-methyl-2-phenylcyclopropyl)-1*H*-pyrazole (3a)

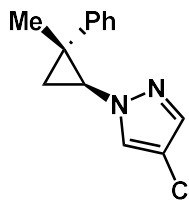
 Colorless oil, 91% yield, 94:6 *er*, >20:1 *dr*, $[\alpha]^{24}_D = +29.9^\circ$ (*c* 0.088, CHCl₃). **¹H NMR** (600 MHz, CDCl₃) δ 7.56 (d, *J* = 1.8 Hz, 1H), 7.51 (d, *J* = 2.3 Hz, 1H), 7.42-7.32 (m, 4H), 7.25 (t, *J* = 7.2 Hz, 1H), 6.30 (t, *J* = 2.1 Hz, 1H), 3.78 (dd, *J* = 8.0, 4.7 Hz, 1H), 1.69-1.61 (m, 2H), 1.17 (s, 3H). **¹³C NMR** (151 MHz, CDCl₃) δ 144.69, 139.67, 130.39, 128.73, 127.56, 126.68, 105.64, 44.41, 28.32, 20.27, 19.33. **IR** (ATR): 2925, 1513, 1496, 1445, 1396, 1027, 952, 749, 698, 615 cm⁻¹. **HRMS** calculated for C₁₃H₁₄N₂ [M]⁺ 198.1157, found 198.1156. **Chiral SFC:** 100 mm CHIRALCEL OD-H, 5% iPrOH, 2.5 mL/min, 254 nm, 44 °C, nozzle pressure = 200 bar CO₂, t_{R1} (major) = 1.8 min, t_{R2} (minor) = 2.3 min.

4-methyl-1-((1*S*,2*R*)-2-methyl-2-phenylcyclopropyl)-1*H*-pyrazole (3b)



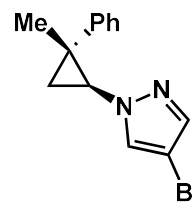
Colorless oil, 94% yield, 96:4 *er*, >20:1 *dr*, $[\alpha]^{24}_D = +62.1^\circ$ (*c* 0.10, CHCl₃). **¹H NMR** (600 MHz, CDCl₃) δ 7.40-7.31 (m, 5H), 7.28 (s, 1H), 7.25-7.21 (m, 1H), 3.71 (dd, *J* = 7.9, 4.8 Hz, 1H), 2.10 (s, 3H), 1.65-1.58 (m, 2H), 1.18 (s, 3H). **¹³C NMR** (151 MHz, CDCl₃) δ 144.80, 139.99, 129.27, 128.70, 127.54, 126.61, 116.16, 44.36, 28.25, 20.25, 19.26, 9.07. **IR** (ATR): 2925, 1603, 1496, 1445, 1379, 980, 845, 763, 699, 610 cm⁻¹. **HRMS** calculated for C₁₄H₁₆N₂ [M+H]⁺ 213.1392, found 231.1397. **Chiral SFC**: 100 mm CHIRALCEL OJ-H, 1% iPrOH, 2.5 mL/min, 220.2 nm, 44 °C, nozzle pressure = 200 bar CO₂, t_{R1} (major) = 3.0 min, t_{R2} (minor) = 3.2 min.

4-chloro-1-((1*S*,2*R*)-2-methyl-2-phenylcyclopropyl)-1*H*-pyrazole (3c)

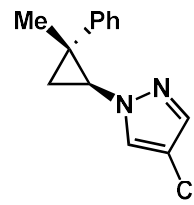


White solid, 91% yield, 93:7 *er*, >20:1 *dr*, $[\alpha]^{24}_D = +57.2^\circ$ (*c* 0.214, CHCl₃). **¹H NMR** (600 MHz, CDCl₃) δ 7.49 (d, *J* = 14.1 Hz, 2H), 7.39-7.32 (m, 4H), 7.26-7.23 (m, 1H), 3.73 (dd, *J* = 8.2, 4.4 Hz, 1H), 1.65 (dd, *J* = 8.2, 6.2 Hz, 1H), 1.61 (dd, *J* = 6.2, 4.4 Hz, 1H), 1.19 (s, 3H). **¹³C NMR** (151 MHz, CDCl₃) δ 144.22, 138.13, 128.80, 128.54, 127.51, 126.85, 110.03, 44.99, 28.51, 20.34, 19.13. **IR** (ATR): 3103, 1497, 1446, 1322, 1055, 967, 847, 755, 696, 616 cm⁻¹. **HRMS** calculated for C₁₃H₁₃ClN₂ [M+H]⁺ 233.0845, found 233.0853. **Chiral SFC**: 250 mm CHIRALCEL OD-H, 2.5% iPrOH, 2.0 mL/min, 230.4 nm, 44 °C, nozzle pressure = 200 bar CO₂, t_{R1} (major) = 8.8 min, t_{R2} (minor) = 7.9 min.

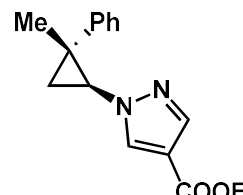
4-bromo-1-((1*S*,2*R*)-2-methyl-2-phenylcyclopropyl)-1*H*-pyrazole (3d)


 White solid, 63% yield, 92:8 *er*, >20:1 *dr*, $[\alpha]^{24}\text{D} = +4.2^\circ$ (*c* 0.90, CHCl_3). **^1H NMR** (400 MHz, CDCl_3) δ 7.52 (dt, *J* = 7.8, 1.2 Hz, 2H), 7.41-7.30 (m, 4H), 7.25 (ddt, *J* = 7.0, 5.8, 3.0 Hz, 1H), 3.75 (ddd, *J* = 8.3, 4.5, 1.6 Hz, 1H), 1.66 (ddd, *J* = 8.0, 6.2, 1.6 Hz, 1H), 1.62-1.58 (m, 1H), 1.18 (s, 3H). **^{13}C NMR** (101 MHz, CDCl_3) δ 144.19, 140.25, 130.68, 128.80, 127.53, 126.86, 93.12, 44.90, 28.54, 20.38, 19.16. **IR** (ATR): 3101, 2923, 1598, 1496, 1443, 1394, 1112, 982, 947, 847, 757, 696, 613 cm^{-1} . **HRMS** calculated for $\text{C}_{13}\text{H}_{13}\text{BrN}_2$ $[\text{M}+\text{H}]^+$ 277.0340, found 277.0327. **Chiral SFC:** 250 mm CHIRALCEL OD-H, 5% $^3\text{PrOH}$, 2.5 mL/min, 230.4 nm, 44 °C, nozzle pressure = 200 bar CO_2 , t_{R1} (major) = 5.2 min, t_{R2} (minor) = 4.3 min.

1-((1*S*,2*R*)-2-methyl-2-phenylcyclopropyl)-1*H*-pyrazole-4-carbonitrile (3e)


 Colorless oil, 40% yield, 92:8 *er*, >20:1 *dr*, $[\alpha]^{24}\text{D} = +10.0^\circ$ (*c* 0.020, CHCl_3). **^1H NMR** (600 MHz, CDCl_3) δ 7.92 (s, 1H), 7.85 (s, 1H), 7.40-7.34 (m, 4H), 7.28 (dq, *J* = 5.8, 3.0 Hz, 1H), 3.81 (dd, *J* = 8.1, 4.4 Hz, 1H), 1.73 (dd, *J* = 8.1, 6.4 Hz, 1H), 1.62 (dd, *J* = 6.4, 4.4 Hz, 1H), 1.17 (s, 3H). **^{13}C NMR** (151 MHz, CDCl_3) δ 143.57, 142.51, 135.52, 128.93, 127.54, 127.16, 113.43, 92.55, 44.96, 28.75, 20.50, 19.33. **IR** (ATR): 2924, 2233, 1543, 1446, 1010, 864, 763, 699, 630 cm^{-1} . **HRMS** calculated for $\text{C}_{14}\text{H}_{13}\text{N}_3$ $[\text{M}+\text{Na}]^+$ 246.1007, found 246.1168. **Chiral SFC:** 100 mm CHIRALPAK AD-H, 5% $^3\text{PrOH}$, 2.5 mL/min, 220.2 nm, 44 °C, nozzle pressure = 200 bar CO_2 , t_{R1} (major) = 1.9 min, t_{R2} (minor) = 2.2 min.

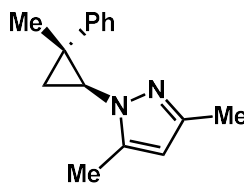
Ethyl 1-((1*S*,2*R*)-2-methyl-2-phenylcyclopropyl)-1*H*-pyrazole-4-carboxylate (3f)


 Colorless oil, 60% yield, 91:9 *er*, >20:1 *dr*, $[\alpha]^{24}_D = +43.3^\circ$ (*c* 0.094, CHCl₃).
¹**H NMR** (600 MHz, CDCl₃) δ 8.00 (s, 1H), 7.96 (s, 1H), 7.41-7.32 (m, 4H), 7.27-7.24 (m, 1H), 4.31 (q, *J* = 7.1 Hz, 2H), 3.79 (dd, *J* = 8.1, 4.4 Hz, 1H), 1.69 (dd, *J* = 8.2, 6.2 Hz, 1H), 1.62 (dd, *J* = 6.3, 4.4 Hz, 1H), 1.36 (t, *J* = 7.1 Hz, 3H), 1.18 (s, 3H).
¹³**C NMR** (151 MHz, CDCl₃) δ 163.15, 144.08, 141.37, 133.86, 128.83, 127.63, 126.95, 115.24, 60.40, 44.78, 28.63, 20.45, 19.21, 14.55. **IR** (ATR): 2977, 1712, 1553, 1446, 1247, 1220, 1126, 1024, 996, 763, 699, 612 cm⁻¹. **HRMS** calculated for C₁₆H₁₈N₂O₂ [M+H]⁺ 271.1447, found 271.1438. **Chiral SFC**: 250 mm CHIRALCEL OD-H, 5% iPrOH, 2.5 mL/min, 230.4 nm, 44 °C, nozzle pressure = 200 bar CO₂, t_{R1} (major) = 6.7 min, t_{R2} (minor) = 5.7 min.

1-((1*S*,2*R*)-2-methyl-2-phenylcyclopropyl)-4-(4,4,5,5-tetramethyl-1,3,2-dioxaborolan-2-yl)-1*H*-pyrazole (3g)

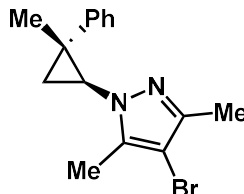
Colorless oil, 67% yield, 99:1 *er*, >20:1 *dr*, $[\alpha]^{24}_D = +45.9^\circ$ (*c* 0.09, CHCl₃). ¹**H NMR** (600 MHz, CDCl₃) δ 7.83 (d, *J* = 13.8 Hz, 2H), 7.42-7.37 (m, 2H), 7.33 (t, *J* = 7.7 Hz, 2H), 7.26-7.21 (m, 1H), 3.77 (dd, *J* = 8.2, 4.5 Hz, 1H), 1.65 (dd, *J* = 8.2, 6.1 Hz, 1H), 1.61 (dd, *J* = 6.1, 4.5 Hz, 1H), 1.33 (s, 11H), 1.16 (s, 3H). ¹³**C NMR** (151 MHz, CDCl₃) δ 145.81, 144.58, 137.43, 128.74, 127.75, 126.75, 83.50, 44.20, 28.51, 24.99, 24.93, 20.51, 19.11. **IR** (ATR): 2976, 1556, 1371, 1297, 1261, 1143, 1123, 984, 856, 762, 690 cm⁻¹. **HRMS** calculated for C₁₉H₂₅BN₂O₂ [M+Na]⁺ 347.1910, found 347.1914. **Chiral SFC**: 250 mm CHIRALCEL OD-H, 5% iPrOH, 2.5 mL/min, 230.4 nm, 44 °C, nozzle pressure = 200 bar CO₂, t_{R1} (major) = 5.3 min, t_{R2} (minor) = 3.9 min.

3,5-dimethyl-1-((1*S*,2*R*)-2-methyl-2-phenylcyclopropyl)-1*H*-pyrazole (3h)



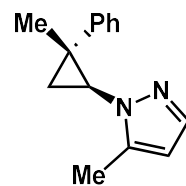
Colorless oil, 51% yield, 92:8 *er*, >20:1 *dr*, $[\alpha]^{24}_D = -39.1^\circ$ (*c* 0.052, CHCl₃). **¹H NMR** (600 MHz, CDCl₃) δ 7.35 (d, *J* = 4.4 Hz, 4H), 7.24 (dt, *J* = 8.7, 4.2 Hz, 2H), 5.87 (s, 1H), 3.46 (dd, *J* = 8.4, 4.4 Hz, 1H), 2.32 (s, 3H), 2.25 (s, 3H), 1.95 (t, *J* = 5.3 Hz, 1H), 1.70 (dd, *J* = 8.4, 6.1 Hz, 1H), 1.16 (s, 3H). **¹³C NMR** (151 MHz, CDCl₃) δ 146.97, 144.65, 128.76, 126.70, 126.64, 126.49, 105.77, 42.98, 27.67, 19.53, 19.07, 13.66, 11.65. **IR** (ATR): 2925, 1603, 1557, 1497, 1463, 1383, 1260, 1023, 779, 762, 697 cm⁻¹. **HRMS** calculated for C₁₅H₁₈N₂ [M+H]⁺ 227.1548, found 227.1538. **Chiral SFC:** 250 mm CHIRALCEL OD-H, 2% iPrOH, 2.5 mL/min, 230.4 nm, 44 °C, nozzle pressure = 200 bar CO₂, t_{R1} (major) = 6.9 min, t_{R2} (minor) = 7.6 min.

4-bromo-3,5-dimethyl-1-((1*S*,2*R*)-2-methyl-2-phenylcyclopropyl)-1*H*-pyrazole (3i)

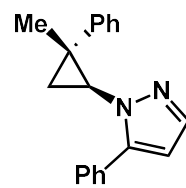


White solid, 61% yield, 92:8 *er*, >20:1 *dr*, $[\alpha]^{24}_D = +53.4^\circ$ (*c* 0.20, CHCl₃). **¹H NMR** (400 MHz, CDCl₃) δ 7.40-7.30 (m, 4H), 7.27-7.23 (m, 1H), 3.49 (ddd, *J* = 8.4, 4.4, 1.7 Hz, 1H), 2.32 (s, 3H), 2.23 (s, 3H), 1.91 (ddd, *J* = 6.3, 4.4, 1.8 Hz, 1H), 1.69 (td, *J* = 6.2, 3.2 Hz, 1H), 1.14 (s, 3H). **¹³C NMR** (101 MHz, CDCl₃) δ 145.65, 144.29, 139.26, 128.81, 126.67, 126.63, 94.49, 68.63, 43.84, 27.77, 19.15, 19.08, 12.50, 10.88. **IR** (ATR): 2922, 1498, 1449, 1379, 1074, 1040, 828, 753, 699 cm⁻¹. **HRMS** calculated for C₁₅H₁₇BrN₂ [M+H]⁺ 305.0653, found 305.0638. **Chiral SFC:** 250 mm CHIRALCEL OD-H, 2% iPrOH, 2.5 mL/min, 230.4 nm, 44 °C, nozzle pressure = 200 bar CO₂, t_{R1} (major) = 8.1 min, t_{R2} (minor) = 8.9 min.

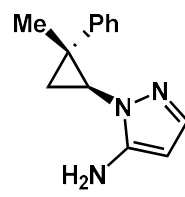
3-methyl-1-((1*S*,2*R*)-2-methyl-2-phenylcyclopropyl)-1*H*-pyrazole (3j)


 White solid, 90% yield, 95:5 *er*, >20:1 *rr*, >20:1 *dr*, $[\alpha]^{24}_D = +67.7^\circ$ (*c* 0.20, CHCl₃). **¹H NMR** (600 MHz, CDCl₃) δ 7.40 (s, 1H), 7.38-7.34 (m, 4H), 7.25 (ddt, *J*=8.5, 5.6, 2.5 Hz, 1H), 6.09 (s, 1H), 3.53 (dd, *J*=8.4, 4.3 Hz, 1H), 2.38 (s, 3H), 1.97 (t, *J*=5.3 Hz, 1H), 1.71 (dd, *J*=8.4, 6.0 Hz, 1H), 1.13 (s, 3H). **¹³C NMR** (151 MHz, CDCl₃) δ 144.64, 140.39, 137.96, 128.77, 126.76, 126.54, 105.93, 43.15, 27.80, 19.29, 19.07, 11.65. IR (ATR): 2924, 1500, 1450, 1402, 925, 785, 764, 699 cm⁻¹. **HRMS** calculated for C₁₄H₁₆N₂ [M+H]⁺ 213.1392, found 213.1383. **Chiral SFC**: 250 mm CHIRALCEL OD-H, 5% iPrOH, 2.5 mL/min, 230.4 nm, 44 °C, nozzle pressure = 200 bar CO₂, t_{R1} (major) = 3.9 min, t_{R2} (minor) = 4.5 min.

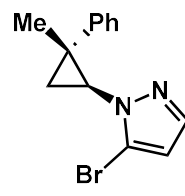
1-((1*S*,2*R*)-2-methyl-2-phenylcyclopropyl)-3-phenyl-1*H*-pyrazole (3k)


 White solid, 84% yield, 93:7 *er*, >20:1 *rr*, >20:1 *dr*, $[\alpha]^{24}_D = +5.4^\circ$ (*c* 0.70, CHCl₃). **¹H NMR** (600 MHz, CDCl₃) δ 7.54 (d, *J*=1.8 Hz, 1H), 7.47 (dd, *J*=7.7, 1.8 Hz, 2H), 7.43-7.36 (m, 3H), 7.22-7.17 (m, 2H), 7.17-7.12 (m, 1H), 6.88-6.83 (m, 2H), 6.39 (d, *J*=1.9 Hz, 1H), 3.76 (dd, *J*=8.4, 4.5 Hz, 1H), 1.84 (dd, *J*=6.2, 4.5 Hz, 1H), 1.67 (dd, *J*=8.4, 6.2 Hz, 1H), 1.00 (s, 3H). **¹³C NMR** (151 MHz, CDCl₃) δ 145.41, 144.22, 138.27, 131.11, 129.17, 128.79, 128.54, 128.42, 127.03, 126.38, 106.77, 44.39, 28.52, 19.50, 19.41. IR (ATR): 2956, 2922, 2853, 1458, 1378, 758, 721, 697 cm⁻¹. **HRMS** calculated for C₁₉H₁₈N₂ [M+Na]⁺ 297.1368, found 297.1365. **Chiral SFC**: 250 mm CHIRALCEL OD-H, 5% iPrOH, 2.5 mL/min, 230.4 nm, 44 °C, nozzle pressure = 200 bar CO₂, t_{R1} (major) = 6.1 min, t_{R2} (minor) = 7.9 min.

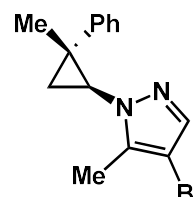
1-((1*S*,2*R*)-2-methyl-2-phenylcyclopropyl)-1*H*-pyrazol-3-amine (3l)


 Yellow oil, 70% yield, 94:6 *er*, >20:1 *rr*, >20:1 *dr*, $[\alpha]^{24}_D = +9^\circ$ (*c* 0.12, CHCl₃). **¹H NMR** (600 MHz, CDCl₃) δ 7.38-7.35 (m, 4H), 7.28 (d, *J* = 1.9 Hz, 1H), 7.26-7.24 (m, 1H), 5.54 (d, *J* = 2.0 Hz, 1H), 3.75 (s, 2H), 3.33 (dd, *J* = 8.4, 4.4 Hz, 1H), 1.87 (dd, *J* = 6.0, 4.5 Hz, 1H), 1.73 (dd, *J* = 8.4, 6.0 Hz, 1H), 1.24 (s, 3H). **¹³C NMR** (151 MHz, CDCl₃) δ 146.70, 144.34, 138.55, 128.86, 126.66, 126.64, 90.12, 41.16, 27.81, 19.59, 19.22. **IR** (ATR): 3305, 3197, 2925, 1556, 1496, 1445, 1416, 1068, 1029, 922, 763, 697 cm⁻¹. **HRMS** calculated for C₁₃H₁₅N₃ [M+Na]⁺ 236.1164, found 236.1166. **Chiral SFC**: 250 mm CHIRALCEL OD-H, 10% iPrOH, 2.5 mL/min, 230.4 nm, 44 °C, nozzle pressure = 200 bar CO₂, t_{R1} (major) = 7.5 min, t_{R2} (minor) = 11.0 min.

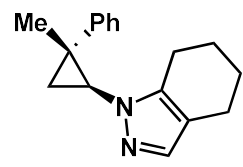
3-bromo-1-((1*S*,2*R*)-2-methyl-2-phenylcyclopropyl)-1*H*-pyrazole (3m)


 Colorless oil, 65% yield, 92:8 *er*, >20:1 *rr*, >20:1 *dr*, $[\alpha]^{24}_D = +18.3^\circ$ (*c* 0.16, CHCl₃). **¹H NMR** (600 MHz, CDCl₃) δ 7.53-7.48 (m, 3H), 7.36 (t, *J* = 7.7 Hz, 2H), 7.29-7.23 (m, 2H), 6.38 (d, *J* = 1.9 Hz, 1H), 3.67 (dd, *J* = 8.4, 4.3 Hz, 1H), 1.96 (dd, *J* = 6.2, 4.3 Hz, 1H), 1.71 (dd, *J* = 8.4, 6.2 Hz, 1H), 1.14 (s, 3H). **¹³C NMR** (151 MHz, CDCl₃) δ 144.39, 139.62, 128.70, 127.58, 126.75, 115.34, 109.37, 43.84, 28.82, 19.65, 18.90. **IR** (ATR): 2926, 1495, 1446, 1394, 990, 917, 761, 697 cm⁻¹. **HRMS** calculated for C₁₃H₁₃BrN₂ [M+H]⁺ 277.0340, found 277.0331. **Chiral SFC**: 250 mm CHIRALCEL OD-H, 2.5% iPrOH, 2 mL/min, 230.4 nm, 44 °C, nozzle pressure = 200 bar CO₂, t_{R1} (major) = 7.4 min, t_{R2} (minor) = 8.1 min.

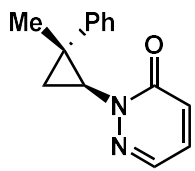
4-bromo-3-methyl-1-((1*S*,2*R*)-2-methyl-2-phenylcyclopropyl)-1*H*-pyrazole (3n)


 Yellow oil, 77% yield, 97:3 *er*, >20:1 *rr*, >20:1 *dr*, $[\alpha]^{24}_D = +44.3^\circ$ (*c* 0.31, CHCl₃). **¹H NMR** (400 MHz, CDCl₃) δ 7.44-7.31 (m, 5H), 7.30-7.21 (m, 1H), 3.54 (ddd, *J* = 8.6, 4.6, 1.5 Hz, 1H), 2.35 (s, 3H), 1.93 (ddd, *J* = 5.8, 4.4, 1.4 Hz, 1H), 1.71 (dd, *J* = 8.6, 6.3 Hz, 1H), 1.13 (s, 3H). **¹³C NMR** (101 MHz, CDCl₃) δ 144.18, 138.99, 138.31, 128.85, 126.74, 126.72, 122.97, 44.10, 27.98, 19.19, 18.98, 10.36. **IR** (ATR): 2926, 1496, 1445, 1400, 927, 839, 762, 697, 635 cm⁻¹. **HRMS** calculated for C₁₄H₁₅BrN₂ [M+H]⁺ 291.0497, found 291.0500. **Chiral SFC**: 250 mm CHIRALCEL OD-H, 2% iPrOH, 2.5 mL/min, 230.4 nm, 44 °C, nozzle pressure = 200 bar CO₂, t_{R1} (major) = 7.2 min, t_{R2} (minor) = 8.0 min.

2-((1*S*,2*R*)-2-methyl-2-phenylcyclopropyl)-4,5,6,7-tetrahydro-2*H*-indazole (3o)


 Colorless oil, 74% yield, 99:1 *er*, >20:1 *rr*, >20:1 *dr*, $[\alpha]^{24}_D = +49.4^\circ$ (*c* 0.12, CHCl₃). **¹H NMR** (600 MHz, CDCl₃) δ 7.38-7.33 (m, 4H), 7.26 (s, 1H), 7.24 (ddd, *J* = 8.5, 4.2, 2.2 Hz, 1H), 3.49 (dd, *J* = 8.4, 4.4 Hz, 1H), 2.68 (tt, *J* = 6.4, 1.3 Hz, 2H), 2.54-2.50 (m, 2H), 1.91 (dd, *J* = 6.0, 4.5 Hz, 1H), 1.88-1.83 (m, 2H), 1.77-1.73 (m, 2H), 1.64 (dd, *J* = 8.4, 6.0 Hz, 1H), 1.14 (s, 3H). **¹³C NMR** (151 MHz, CDCl₃) δ 144.99, 140.15, 136.30, 128.73, 127.17, 126.52, 116.73, 42.57, 27.90, 23.32, 23.02, 22.14, 20.88, 19.61, 18.79. **IR** (ATR): 3061, 3027, 2954, 2922, 1465, 1454, 1420, 769, 753, 742, 708, 698, 634 cm⁻¹. **HRMS** calculated for C₁₇H₂₀N₂ [M+Na]⁺ 275.1524, found 275.1523. **Chiral SFC**: 250 mm CHIRALCEL OJ-H, 3% iPrOH, 2.5 mL/min, 230.4 nm, 44 °C, nozzle pressure = 200 bar CO₂, t_{R1} (major) = 8.6 min, t_{R2} (minor) = 11.0 min.

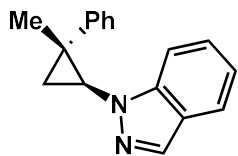
2-((1*S*,2*R*)-2-methyl-2-phenylcyclopropyl)pyridazin-3(2*H*)-one (3p)



Colorless oil, 55% yield, 87:13 *er*, >20:1 *rr*, >20:1 *dr*, $[\alpha]^{24}_D = -9.2^\circ$ (*c* 0.15, CHCl₃). **¹H NMR** (600 MHz, CDCl₃) δ 7.79 (dd, *J* = 3.8, 1.7 Hz, 1H), 7.67-7.62 (m, 2H), 7.34 (dd, *J* = 8.3, 7.1 Hz, 2H), 7.25-7.20 (m, 2H), 6.99 (dd, *J* = 9.4, 1.7 Hz, 1H), 3.86 (dd, *J* = 8.1, 4.8 Hz, 1H), 1.77 (dd, *J* = 6.2, 4.8 Hz, 1H), 1.56 (dd, *J* = 8.1, 6.2 Hz, 1H), 1.11 (s, 3H). **¹³C NMR** (151 MHz, CDCl₃) δ 162.42, 145.31, 135.67, 130.96, 129.46, 128.65, 128.62, 126.72, 46.28, 28.94, 20.28, 17.16. **IR** (ATR): 2926, 2360, 1660, 1590, 1445, 1154, 1024, 820, 763, 699, 599 cm⁻¹. **HRMS** calculated for C₁₄H₁₄N₂O [M+Na]⁺ 249.1004, found 249.1005.

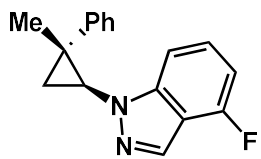
Chiral SFC: 100 mm CHIRALCEL OD-H, 5% ⁱPrOH, 2.5 mL/min, 220.2 nm, 44 °C, nozzle pressure = 200 bar CO₂, t_{R1} (major) = 5.3 min, t_{R2} (minor) = 6.5 min.

2-((1*S*,2*R*)-2-methyl-2-phenylcyclopropyl)-2*H*-indazole (3q)



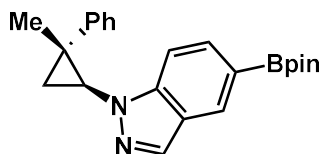
Colorless oil, 66% yield, 91:9 *er*, 3.8:1 *rr*, >20:1 *dr*, $[\alpha]^{24}_D = +33.8^\circ$ (*c* 0.21, CHCl₃). **¹H NMR** (600 MHz, CDCl₃) δ 8.03 (s, 1H), 7.76 (d, *J* = 8.1 Hz, 1H), 7.60 (d, *J* = 8.4 Hz, 1H), 7.51-7.47 (m, 2H), 7.44-7.39 (m, 3H), 7.29 (s, 1H), 7.19 (t, *J* = 7.4 Hz, 1H), 3.81 (dd, *J* = 8.3, 4.4 Hz, 1H), 1.97 (dd, *J* = 6.0, 4.4 Hz, 1H), 1.86 (dd, *J* = 8.3, 5.9 Hz, 1H), 1.16 (s, 3H). **¹³C NMR** (151 MHz, CDCl₃) δ 144.76, 141.32, 133.18, 128.85, 127.19, 126.65, 126.60, 124.59, 121.27, 121.08, 109.87, 42.36, 28.32, 19.97, 19.63. **IR** (ATR): 3059, 2960, 2924, 1633, 1579, 1506, 1421, 1240, 1199, 980, 763, 698 cm⁻¹. **HRMS** calculated for C₁₇H₁₆N₂ [M+H]⁺ 249.1392, found 249.1384. **Chiral SFC:** 250 mm CHIRALCEL OD-H, 5% ⁱPrOH, 2.5 mL/min, 230.4 nm, 44 °C, nozzle pressure = 200 bar CO₂, t_{R1} (major) = 9.6 min, t_{R2} (minor) = 11.3 min.

4-fluoro-2-((1*S*,2*R*)-2-methyl-2-phenylcyclopropyl)-2*H*-indazole (3r)



Colorless oil, 58% yield, 92:8 *er*, 3.1:1 *rr*, >20:1 *dr*, $[\alpha]^{24}_D = +38.3^\circ$ (*c* 0.094, CHCl₃). **¹H NMR** (600 MHz, CDCl₃) δ 8.08 (s, 1H), 7.49-7.44 (m, 2H), 7.41 (t, *J* = 7.7 Hz, 2H), 7.38-7.31 (m, 2H), 7.31-7.27 (m, 1H), 6.82 (ddd, *J* = 9.9, 7.0, 1.2 Hz, 1H), 3.80 (dd, *J* = 8.3, 4.4 Hz, 1H), 1.96 (dd, *J* = 6.0, 4.4 Hz, 1H), 1.86 (dd, *J* = 8.3, 6.0 Hz, 1H), 1.15 (s, 3H). **¹³C NMR** (151 MHz, CDCl₃) δ 156.82, 155.15, 144.50, 143.99, 129.61, 129.60, 128.89, 127.61, 127.56, 127.17, 126.77, 114.95, 114.80, 105.96, 105.94, 105.49, 105.36, 42.54, 28.43, 20.00, 19.66. **IR** (ATR): 3025, 2927, 1633, 1579, 1457, 1421, 1240, 1199, 980, 777, 730, 763, 698 cm⁻¹. **HRMS** calculated for C₁₇H₁₅FN₂ [M+H]⁺ 267.1298, found 267.1304. **Chiral SFC**: 250 mm CHIRALCEL OD-H, 5% iPrOH, 2.5 mL/min, 230.4 nm, 44 °C, nozzle pressure = 200 bar CO₂, t_{R1} (major) = 25.0 min, t_{R2} (minor) = 32.4 min.

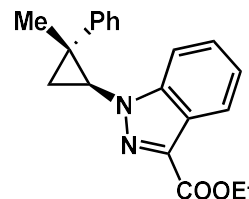
2-((1*S*,2*R*)-2-methyl-2-phenylcyclopropyl)-5-(4,4,5,5-tetramethyl-1,3,2-dioxaborolan-2-yl)-2*H*-indazole (3s)



White solid, 22% yield, 91:9 *er*, 3.8:1 *rr*, >20:1 *dr*, $[\alpha]^{24}_D = +31.8^\circ$ (*c* 0.064, CHCl₃). **¹H NMR** (600 MHz, CDCl₃) δ 8.28 (s, 1H), 8.02 (s, 1H), 7.82 (dd, *J* = 8.4, 1.0 Hz, 1H), 7.56 (dt, *J* = 8.5, 1.0 Hz, 1H), 7.49-7.45 (m, 2H), 7.40 (dd, *J* = 8.4, 7.0 Hz, 2H), 7.30-7.27 (m, 1H), 3.81 (dd, *J* = 8.2, 4.4 Hz, 1H), 1.95 (dd, *J* = 6.0, 4.4 Hz, 1H), 1.85 (dd, *J* = 8.3, 6.0 Hz, 1H), 1.37 (s, 12H), 1.13 (s, 3H). **¹³C NMR** (151 MHz, CDCl₃) δ 144.71, 142.84, 133.96, 132.22, 129.59, 128.86, 127.18, 126.66, 124.55, 109.17, 83.92, 42.36, 28.33, 25.06, 25.04, 19.94, 19.68. **IR** (ATR): 2977, 2927, 1615, 1398, 1302, 1145, 859, 699, 683 cm⁻¹. **HRMS** calculated for C₂₃H₂₇BN₂O₂ [M+H]⁺ 375.2248, found 375.2262.

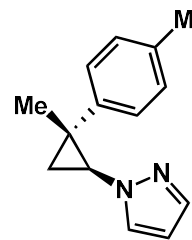
Chiral SFC: 100 mm CHIRALCEL OD-H, 7% ⁱPrOH, 2.5 mL/min, 230.4 nm, 44 °C, nozzle pressure = 200 bar CO₂, t_{R1} (major) = 2.9 min, t_{R2} (minor) = 3.3 min.

Methyl 2-((1*S*,2*R*)-2-methyl-2-phenylcyclopropyl)-2*H*-indazole-3-carboxylate (3t)



White solid, 9% yield, 89:11 *er*, >20:1 *rr*, >20:1 *dr*, [α]²⁴D = +20.1° (c 0.048, CHCl₃). **¹H NMR** (600 MHz, CDCl₃) δ 8.07 (dt, *J* = 8.4, 1.1 Hz, 1H), 7.81 (dt, *J* = 8.7, 1.0 Hz, 1H), 7.56-7.52 (m, 2H), 7.41-7.35 (m, 3H), 7.31 (ddd, *J* = 8.4, 6.7, 1.0 Hz, 1H), 7.28-7.26 (m, 1H), 4.71 (dd, *J* = 8.0, 4.7 Hz, 1H), 3.95 (s, 3H), 2.41 (dd, *J* = 6.3, 4.7 Hz, 1H), 1.81 (dd, *J* = 8.0, 6.3 Hz, 1H), 1.07 (s, 3H). **¹³C NMR** (151 MHz, CDCl₃) δ 160.57, 146.78, 144.54, 128.60, 127.23, 126.60, 126.57, 125.34, 124.43, 121.32, 118.57, 52.10, 47.95, 29.18, 19.68, 18.70. **IR** (ATR): 2930, 1716, 1458, 1364, 1244, 1210, 1094, 1051, 758, 699 cm⁻¹. **HRMS** calculated for C₁₉H₁₈N₂O₂ [M+H]⁺ 307.1447, found 307.1445. **Chiral SFC:** 100 mm CHIRALCEL OJ-H, 2.5% ⁱPrOH, 2.5 mL/min, 230.4 nm, 44 °C, nozzle pressure = 200 bar CO₂, t_{R1} (major) = 3.6 min, t_{R2} (minor) = 3.1 min.

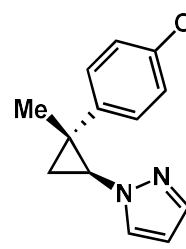
1-((1*S*,2*R*)-2-methyl-2-(p-tolyl)cyclopropyl)-1*H*-pyrazole (4b)



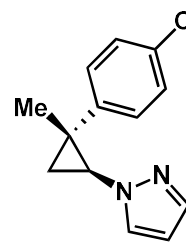
Colorless oil, 72% yield, 94:6 *er*, >20:1 *dr*, [α]²⁴D = +55.4° (c 0.11, CHCl₃). **¹H NMR** (600 MHz, CDCl₃) δ 7.57 (d, *J* = 1.8 Hz, 1H), 7.50 (d, *J* = 2.3 Hz, 1H), 7.32-7.27 (m, 2H), 7.18-7.14 (m, 2H), 6.29 (t, *J* = 2.1 Hz, 1H), 3.75 (dd, *J* = 8.0, 4.6 Hz, 1H), 2.35 (s, 3H), 1.66-1.58 (m, 2H), 1.15 (s, 3H). **¹³C NMR** (151 MHz, CDCl₃) δ 141.75, 139.58, 136.33, 130.42, 129.40, 127.50, 105.60, 44.37, 28.03, 21.14, 20.41, 19.27. **IR** (ATR): 2923, 1514, 1446, 1396, 1084, 1033, 952, 818, 747, 722, 651, 615 cm⁻¹. **HRMS**

calculated for C₁₄H₁₆N₂ [M+H]⁺ 213.1392, found 213.1393. **Chiral SFC:** 250 mm CHIRALCEL OD-H, 5% ⁱPrOH, 2.5 mL/min, 230.4 nm, 44 °C, nozzle pressure = 200 bar CO₂, t_{R1} (major) = 16.7 min, t_{R2} (minor) = 24.3 min.

1-((1*S*,2*R*)-2-(4-methoxyphenyl)-2-methylcyclopropyl)-1*H*-pyrazole (4c)

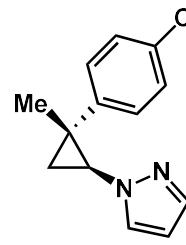
 White solid, 75% yield, 94:6 *er*, >20:1 *dr*, [α]²⁴_D = +47.0° (c 0.23, CHCl₃). **¹H NMR** (600 MHz, CDCl₃) δ 7.56 (d, *J* = 1.8 Hz, 1H), 7.49 (d, *J* = 2.3 Hz, 1H), 7.35-7.30 (m, 2H), 6.91-6.85 (m, 2H), 6.29 (t, *J* = 2.1 Hz, 1H), 3.80 (s, 3H), 3.73 (dd, *J* = 8.0, 4.5 Hz, 1H), 1.63-1.55 (m, 2H), 1.13 (s, 3H). **¹³C NMR** (151 MHz, CDCl₃) δ 158.40, 139.62, 136.89, 130.39, 128.78, 114.09, 105.57, 55.46, 44.31, 29.84, 20.67, 19.22. **IR (ATR):** 2926, 1612, 1513, 1443, 1396, 1299, 1244, 1179, 1030, 953, 831, 789, 749, 615 cm⁻¹. **HRMS** calculated for C₁₄H₁₆N₂O [M+H]⁺ 229.1341, found 229.1341. **Chiral SFC:** 250 mm CHIRALCEL OD-H, 5% ⁱPrOH, 2.5 mL/min, 230.4 nm, 44 °C, nozzle pressure = 200 bar CO₂, t_{R1} (major) = 6.0 min, t_{R2} (minor) = 6.7 min.

1-((1*S*,2*R*)-2-(4-chlorophenyl)-2-methylcyclopropyl)-1*H*-pyrazole (4d)

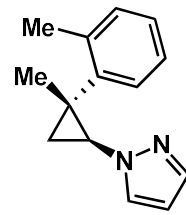
 White solid, 77% yield, 94:6 *er*, >20:1 *dr*, [α]²⁴_D = +4.2° (c 0.62, CHCl₃). **¹H NMR** (600 MHz, CDCl₃) δ 7.56 (d, *J* = 1.8 Hz, 1H), 7.48 (d, *J* = 2.3 Hz, 1H), 7.35-7.28 (m, 4H), 6.29 (t, *J* = 2.1 Hz, 1H), 3.74 (dd, *J* = 7.6, 5.2 Hz, 1H), 1.63 (h, *J* = 7.3 Hz, 3H), 1.14 (s, 3H). **¹³C NMR** (151 MHz, CDCl₃) δ 143.20, 139.85, 132.49, 130.30, 129.02, 128.86, 105.70, 44.35, 27.87, 20.18, 19.36. **IR (ATR):** 2956, 2922, 2853, 1497, 1466, 1092, 829, 746, 721 cm⁻¹. **HRMS** calculated for C₁₃H₁₃ClN₂ [M+H]⁺ 233.0845, found

233.0845. **Chiral SFC:** 100 mm CHIRALCEL OD-H, 5% ⁱPrOH, 2.5 mL/min, 220.2 nm, 44 °C, nozzle pressure = 200 bar CO₂, t_{R1} (major) = 2.3 min, t_{R2} (minor) = 2.7 min.

1-((1*S*,2*R*)-2-methyl-2-(4-(trifluoromethyl)phenyl)cyclopropyl)-1*H*-pyrazole (4e)

 White solid, 89% yield, 93:7 *er*, >20:1 *dr*, [α]²⁴_D = +10.3° (c 0.43, CHCl₃). ¹**H** NMR (600 MHz, CDCl₃) δ 7.62-7.56 (m, 3H), 7.52-7.47 (m, 3H), 6.30 (t, *J* = 2.1 Hz, 1H), 3.79 (dd, *J* = 8.0, 4.8 Hz, 1H), 1.73-1.66 (m, 2H), 1.18 (s, 3H). ¹³C NMR (151 MHz, CDCl₃) δ 148.63, 139.94, 130.32, 129.01 (q, 16.6 Hz), 127.84, 125.72 (q, *J* = 3.8 Hz), 123.41, 105.82, 44.48, 28.13, 19.81, 19.57. IR (ATR): 2923, 2854, 1619, 1402, 1327, 1159, 1110, 1042, 1014, 844, 764, 697, 620 cm⁻¹. HRMS calculated for C₁₄H₁₃F₃N₂ [M+H]⁺ 267.1109, found 267.1118. **Chiral SFC:** 250 mm CHIRALCEL OD-H, 5% ⁱPrOH, 2.5 mL/min, 230.4 nm, 44 °C, nozzle pressure = 200 bar CO₂, t_{R1} (major) = 15.4 min, t_{R2} (minor) = 13.1 min.

1-((1*S*,2*R*)-2-methyl-2-(*o*-tolyl)cyclopropyl)-1*H*-pyrazole (4f)

 Colorless oil, 60% yield, 92:8 *er*, >20:1 *dr*, [α]²⁴_D = +51.6° (c 0.17, CHCl₃). ¹**H** NMR (600 MHz, CDCl₃) δ 7.62-7.58 (m, 1H), 7.58-7.55 (m, 1H), 7.47-7.41 (m, 1H), 7.24-7.15 (m, 3H), 6.31 (s, 1H), 3.81 (dd, *J* = 8.3, 4.3 Hz, 1H), 2.58 (s, 3H), 1.63 (dd, *J* = 5.9, 4.3 Hz, 1H), 1.54 (dd, *J* = 8.2, 5.8 Hz, 1H), 1.10 (s, 3H). ¹³C NMR (151 MHz, CDCl₃) δ 142.57, 139.75, 137.54, 130.83, 130.27, 129.97, 127.17, 126.32, 105.50, 43.82, 28.56, 19.75, 19.57, 19.42. IR (ATR): 2924, 1513, 1490, 1444, 1396, 1087, 1031, 953, 746, 728, 616 cm⁻¹. HRMS calculated for C₁₄H₁₆N₂ [M+H]⁺ 213.1392, found 213.1392. **Chiral SFC:** 250 mm

CHIRALCEL OD-H, 5% i PrOH, 2.5 mL/min, 230.4 nm, 44 °C, nozzle pressure = 200 bar CO₂, t_{R1} (major) = 14.6 min, t_{R2} (minor) = 28.6 min.

1-((1*S*,2*R*)-2-methyl-2-(*m*-tolyl)cyclopropyl)-1*H*-pyrazole (4g)

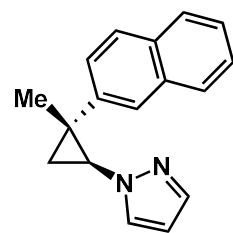
Yellow oil, 68% yield, 92:8 *er*, >20:1 *dr*, $[\alpha]^{24}_D = +46.1^\circ$ (*c* 0.17, CHCl₃). **¹H NMR** (500 MHz, CDCl₃) δ 7.57 (d, *J* = 1.9 Hz, 1H), 7.50 (d, *J* = 2.3 Hz, 1H), 7.26-7.21 (m, 2H), 7.21-7.17 (m, 1H), 7.06 (d, *J* = 7.0 Hz, 1H), 6.29 (t, *J* = 2.1 Hz, 1H), 3.77 (dd, *J* = 8.1, 4.5 Hz, 1H), 2.37 (s, 3H), 1.67-1.59 (m, 2H), 1.15 (s, 3H). **¹³C NMR** (125 MHz, CDCl₃) δ 144.66, 139.65, 138.39, 130.40, 128.64, 128.42, 127.47, 124.64, 105.59, 44.33, 28.35, 21.57, 20.40, 19.25. **IR** (ATR): 3017, 2927, 1513, 1446, 1396, 954, 784, 748, 704, 617 cm⁻¹. **HRMS** calculated for C₁₄H₁₆N₂ [M+H]⁺ 213.1392, found 213.1385. **Chiral SFC**: 100 mm CHIRALCEL OD-H, 5% i PrOH, 2.5 mL/min, 230.4 nm, 44 °C, nozzle pressure = 200 bar CO₂, t_{R1} (major) = 1.7 min, t_{R2} (minor) = 2.1 min.

1-((1*S*,2*S*)-2-methyl-2-(thiophen-2-yl)cyclopropyl)-1*H*-pyrazole (4h)

Colorless oil, 96% yield, 93:7 *er*, >20:1 *dr*, $[\alpha]^{24}_D = +49.5^\circ$ (*c* 0.28, CHCl₃). **¹H NMR** (600 MHz, CDCl₃) δ 7.54 (d, *J* = 1.9 Hz, 1H), 7.48 (d, *J* = 2.4 Hz, 1H), 7.14 (dd, *J* = 5.2, 1.3 Hz, 1H), 6.95 (dd, *J* = 5.1, 3.5 Hz, 1H), 6.88 (dd, *J* = 3.5, 1.3 Hz, 1H), 6.29 (t, *J* = 2.1 Hz, 1H), 3.82 (dd, *J* = 8.3, 4.7 Hz, 1H), 1.82 (dd, *J* = 6.3, 4.7 Hz, 1H), 1.73 (dd, *J* = 8.3, 6.3 Hz, 1H), 1.24 (s, 3H). **¹³C NMR** (151 MHz, CDCl₃) δ 149.85, 139.54, 130.49, 127.04, 123.18, 122.89, 105.94, 46.42, 29.84, 21.97, 19.44. **IR** (ATR): 2926, 1514, 1445, 1395, 1265, 1055, 951, 852, 749, 692, 616 cm⁻¹. **HRMS** calculated for C₁₁H₁₂N₂S [M+H]⁺ 205.0799,

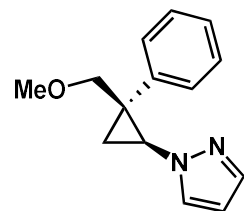
found 205.0793. **Chiral SFC:** 250 mm CHIRALCEL OD-H, 5% i PrOH, 2.5 mL/min, 230.4 nm, 44 °C, nozzle pressure = 200 bar CO₂, t_{R1} (major) = 5.0 min, t_{R2} (minor) = 6.4 min.

1-((1*S*,2*R*)-2-methyl-2-(naphthalen-2-yl)cyclopropyl)-1*H*-pyrazole (4i)



White solid, 74% yield, 93:7 *er*, >20:1 *dr*, $[\alpha]^{24}_D = +6.1^\circ$ (*c* 0.060, CHCl₃). **¹H NMR** (600 MHz, CDCl₃) δ 7.87-7.81 (m, 4H), 7.60 (d, *J* = 1.8 Hz, 1H), 7.55 (td, *J* = 4.0, 1.8 Hz, 2H), 7.47 (dddd, *J* = 17.1, 8.1, 6.8, 1.3 Hz, 2H), 6.32 (t, *J* = 2.1 Hz, 1H), 3.88 (dd, *J* = 8.2, 4.5 Hz, 1H), 1.77 (dd, *J* = 8.2, 6.1 Hz, 1H), 1.70 (dd, *J* = 6.1, 4.5 Hz, 1H), 1.26 (s, 3H). **¹³C NMR** (151 MHz, CDCl₃) δ 142.06, 139.79, 133.58, 132.39, 130.41, 128.52, 127.78, 127.74, 126.37, 126.14, 126.11, 125.87, 105.64, 44.29, 28.69, 20.39, 19.25. **IR** (ATR): 2925, 1496, 1445, 1396, 1027, 952, 749, 698, 615 cm⁻¹. **HRMS** calculated for C₁₇H₁₆N₂ [M+H]⁺ 249.1392, found 249.1390. **Chiral SFC:** 250 mm CHIRALCEL OD-H, 5% *i*PrOH, 2.5 mL/min, 230.4 nm, 44 °C, nozzle pressure = 200 bar CO₂, t_{R1} (major) = 15.2 min, t_{R2} (minor) = 13.2 min.

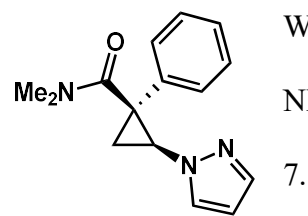
1-((1*S*,2*S*)-2-(methoxymethyl)-2-phenylcyclopropyl)-1*H*-pyrazole (4j)



Colorless oil, 94% yield, 96:4 *er*, >20:1 *dr*, $[\alpha]^{24}_D = +55.4^\circ$ (*c* 0.15, CHCl₃). **¹H NMR** (600 MHz, CDCl₃) δ 7.64 (d, *J* = 2.3 Hz, 1H), 7.55 (d, *J* = 1.9 Hz, 1H), 7.50-7.45 (m, 2H), 7.36 (dd, *J* = 8.5, 6.9 Hz, 2H), 7.30-7.25 (m, 1H), 6.30 (t, *J* = 2.1 Hz, 1H), 3.88 (dd, *J* = 8.0, 4.5 Hz, 1H), 3.28 (q, *J* = 18.3, 10.3 Hz, 2H), 3.08 (s, 3H), 1.87 (dd, *J* = 6.2, 4.5 Hz, 1H), 1.66 (dd, *J* = 8.0, 6.1 Hz, 1H). **¹³C NMR** (151 MHz, CDCl₃) δ 141.54, 139.60, 131.07, 129.09, 128.63, 127.22, 105.86, 75.21, 58.90, 43.50, 33.46, 17.13. **IR**

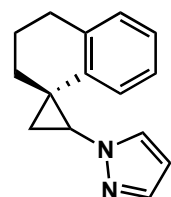
(ATR): 2924, 1514, 1496, 1447, 1395, 1195, 1106, 964, 751, 699, 616 cm⁻¹. **HRMS** calculated for C₁₄H₁₆N₂O [M+H]⁺ 229.1341, found 229.1344. **Chiral SFC:** 250 mm CHIRALCEL OJ-H, 5% iPrOH, 2.5 mL/min, 230.4 nm, 44 °C, nozzle pressure = 200 bar CO₂, t_{R1} (major) = 3.4 min, t_{R2} (minor) = 2.9 min.

(1*S*,2*S*)-*N,N*-dimethyl-1-phenyl-2-(1*H*-pyrazol-1-yl)cyclopropane-1-carboxamide (4k)



White solid, 51% yield, 99:1 *er*, >20:1 *dr*, [α]²⁴_D = +14.7° (c 0.4, CHCl₃). ¹H NMR (600 MHz, CDCl₃) δ 7.54-7.50 (m, 1H), 7.41 (s, 1H), 7.34 (dd, *J* = 8.2, 7.1 Hz, 2H), 7.30-7.24 (m, 3H), 6.24 (s, 1H), 4.68 (dd, *J* = 8.7, 5.5 Hz, 1H), 2.69 (d, *J* = 15.0 Hz, 7H), 2.68-2.66 (m, 1H), 1.52 (dd, *J* = 8.7, 6.7 Hz, 1H). ¹³C NMR (151 MHz, CDCl₃) δ 167.78, 139.95, 138.89, 129.14, 128.14, 127.20, 125.92, 105.67, 44.08, 38.18, 38.15, 35.82, 20.76. **IR** (ATR): 2956, 2922, 2853, 1633, 1466, 1379, 780, 699 cm⁻¹. **HRMS** calculated for C₁₅H₁₇N₃O [M+Na]⁺ 278.1269, found 278.1261. **Chiral SFC:** 250 mm CHIRALCEL OJ-H, 2% iPrOH, 2.5 mL/min, 230.4 nm, 44 °C, nozzle pressure = 200 bar CO₂, t_{R1} (major) = 4.7 min, t_{R2} (minor) = 5.6 min.

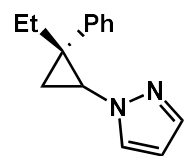
1-((1*R*,2*S*)-3',4'-dihydro-2'H-spiro[cyclopropane-1,1'-naphthalen]-2-yl)-1*H*-pyrazole (4l)



Colorless oil, 80% yield, 95:5 *er*, >20:1 *dr*, [α]²⁴_D = +33.9° (c 0.11, CHCl₃). ¹H NMR (600 MHz, CDCl₃) δ 7.52 (d, *J* = 1.8 Hz, 1H), 7.47 (d, *J* = 2.3 Hz, 1H), 7.19-7.12 (m, 2H), 7.12-7.08 (m, 1H), 6.73 (dd, *J* = 7.4, 1.3 Hz, 1H), 6.28 (t, *J* = 2.1 Hz, 1H), 3.83 (dd, *J* = 8.2, 5.0 Hz, 1H), 2.86 (dd, *J* = 7.0, 5.7 Hz, 2H), 1.85-1.79 (m, 2H), 1.79-1.72 (m, 2H), 1.60 (ddd, *J* = 13.5, 9.7, 3.7 Hz, 1H), 1.24 (ddd, *J* = 13.7, 6.7, 3.4 Hz, 1H). ¹³C NMR

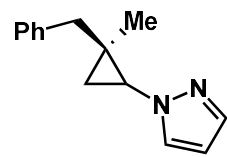
(151 MHz, CDCl₃) δ 139.27, 139.05, 137.88, 130.42, 129.14, 126.42, 125.70, 121.86, 105.82, 47.74, 30.65, 28.01, 26.27, 22.07, 21.45. **IR** (ATR): 2927, 1683, 1599, 1493, 1453, 1395, 1284, 1197, 1043, 973, 807, 752, 726, 618 cm⁻¹. **HRMS** calculated for C₁₅H₁₆N₂ [M+Na]⁺ 247.1211, found 247.1213. **Chiral SFC:** 100 mm CHIRALCEL OD-H, 5% iPrOH, 2.5 mL/min, 230.4 nm, 44 °C, nozzle pressure = 200 bar CO₂, t_{R1} (major) = 3.5 min, t_{R2} (minor) = 4.9 min.

1-((1*S*,2*R*)-2-ethyl-2-phenylcyclopropyl)-1*H*-pyrazole (4m)



Colorless oil, 63% yield, 94:6 *er*, >20:1 *dr*, [α]²⁴_D = +39.2° (c 0.08, CHCl₃). **1H NMR** (600 MHz, CDCl₃) δ 7.57 (d, *J* = 1.8 Hz, 1H), 7.52 (d, *J* = 2.2 Hz, 1H), 7.45-7.40 (m, 2H), 7.35 (dd, *J* = 8.5, 6.9 Hz, 2H), 7.28-7.22 (m, 1H), 6.29 (t, *J* = 2.1 Hz, 1H), 3.78 (dd, *J* = 8.1, 4.5 Hz, 1H), 1.70-1.59 (m, 2H), 1.56 (dd, *J* = 6.0, 4.4 Hz, 1H), 1.03-0.93 (m, 1H), 0.77 (t, *J* = 7.4 Hz, 3H). **13C NMR** (151 MHz, CDCl₃) δ 142.82, 139.60, 130.41, 129.42, 128.56, 126.88, 105.55, 44.65, 34.87, 27.05, 17.01, 11.05. **IR** (ATR): 2964, 1602, 1513, 1495, 1446, 1396, 1322, 1041, 963, 748, 700, 616 cm⁻¹. **HRMS** calculated for C₁₄H₁₆N₂ [M+H]⁺ 213.1392, found 213.1396. **Chiral SFC:** 250 mm CHIRALCEL OJ-H, 5% iPrOH, 2.5 mL/min, 230.4 nm, 44 °C, nozzle pressure = 200 bar CO₂, t_{R1} (major) = 3.5 min, t_{R2} (minor) = 2.8 min.

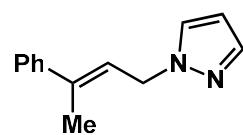
1-((1*S*,2*R*)-2-benzyl-2-methylcyclopropyl)-1*H*-pyrazole (4n)



Colorless oil, 80% yield, 89:11 *er*, 1:1 *dr*. **1H NMR** (600 MHz, CDCl₃) δ 7.56 (s, 1H), 7.28-7.23 (m, 3H), 7.19 (t, *J* = 7.3 Hz, 1H), 7.11 (d, *J* = 7.5 Hz, 2H), 6.29 (s, 1H), 3.50-3.48 (m, 1H), 2.71 (d, *J* = 14.2 Hz, 1H), 1.97 (d, *J* = 14.2 Hz, 1H), 1.70-1.60 (m, 2H), 1.12 (s, 3H). **13C NMR** (151 MHz, CDCl₃) δ 139.66, 129.34, 128.52,

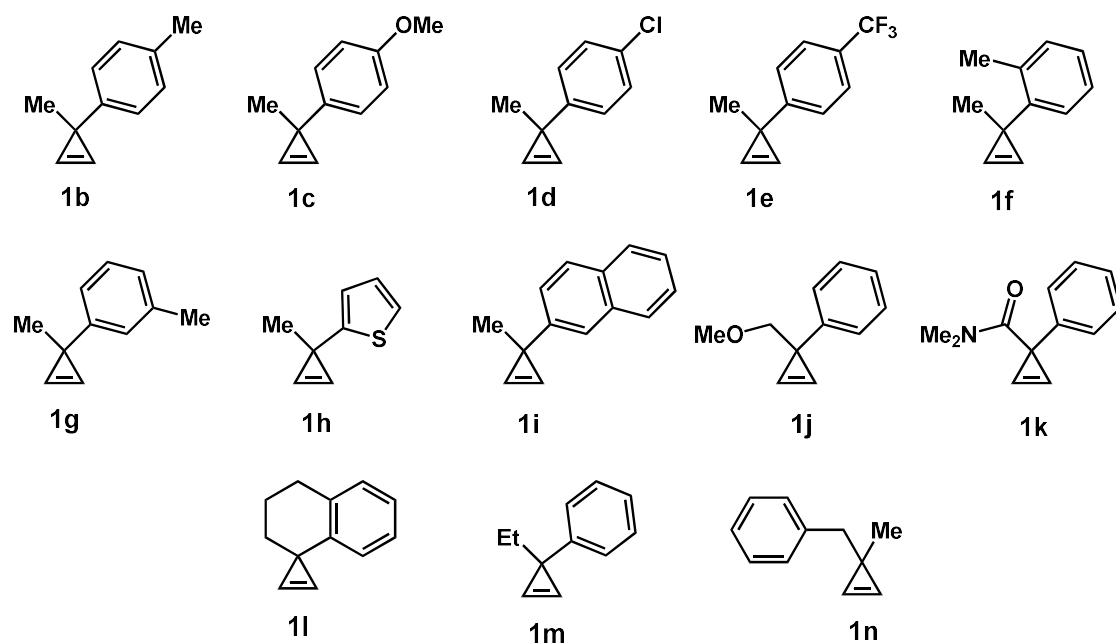
128.32, 126.58, 126.21, 43.83, 38.77, 24.40, 22.51, 18.51. **IR** (ATR): 2922, 2851, 1669, 1514, 1454, 1397, 966, 750, 700, 616 cm⁻¹. **HRMS** calculated for C₁₄H₁₆N₂ [M+H]⁺ 213.1392, found 213.1392. **Chiral SFC:** 100 mm CHIRALCEL AD-H, 1% ⁱPrOH, 2.5 mL/min, 220.2 nm, 44 °C, nozzle pressure = 200 bar CO₂, t_{R1} (major) = 7.6 min, t_{R2} (minor) = 11.3 min.

(E)-1-(3-phenylbut-2-en-1-yl)-1*H*-pyrazole (5a)

 Colorless oil, 66% yield, >20:1 E/Z. **¹H NMR** (600 MHz, CDCl₃) δ 7.53 (d, J = 1.9 Hz, 1H), 7.44-7.38 (m, 3H), 7.32 (dd, J = 8.6, 6.6 Hz, 2H), 7.26 (t, J = 7.1 Hz, 1H), 6.26 (t, J = 2.1 Hz, 1H), 5.99 (t, J = 6.9 Hz, 1H), 4.96 (d, J = 6.9 Hz, 2H), 2.17 (s, 3H). **¹³C NMR** (151 MHz, CDCl₃) δ 142.55, 139.62, 139.46, 128.58, 128.45, 127.69, 126.00, 121.91, 105.79, 50.41, 16.34. **IR** (ATR) 2923, 1510, 1494, 1445, 1395, 1046, 754, 654, 618 cm⁻¹. **HRMS** calculated for C₁₃H₁₄N₂ [M]⁺ 198.1157, found 198.1154.

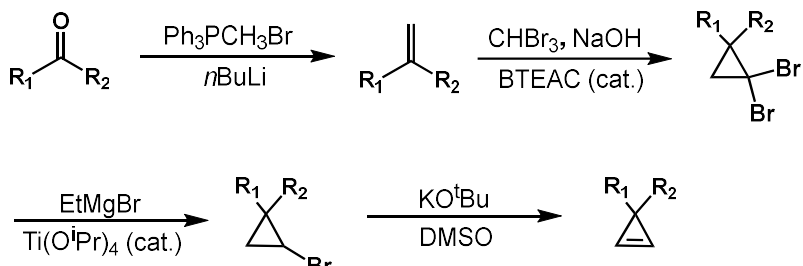
3.4 Synthesis of Cyclopropenes

Figure 16 : Synthesized Cyclopropenes



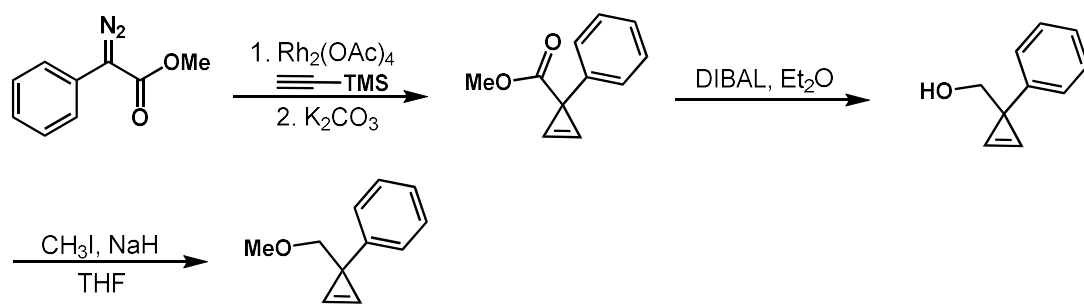
3.4.1 Synthesis of Cyclopropenes (1a-1i, 1l-1n)

Cyclopropenes **1a-1i, 1l-1n** (Figure 16) were synthesized following reported procedures.¹⁻²



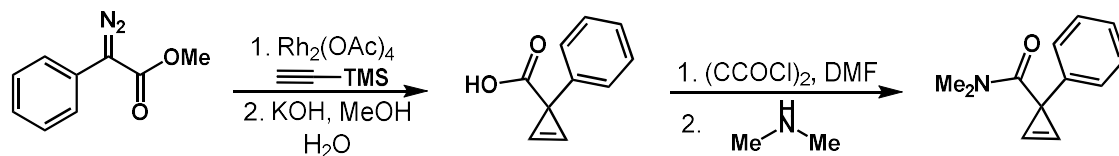
3.4.2 Synthesis of Cyclopropene (1j)

Cyclopropene **1j** was synthesized from 2-phenylacetophenone following reported procedures.²



3.4.3 Synthesis of Cyclopropene (1k)

Cyclopropene **1k** was synthesized from 2-phenylacetophenone following reported procedures.³



3.5 Rate Studies

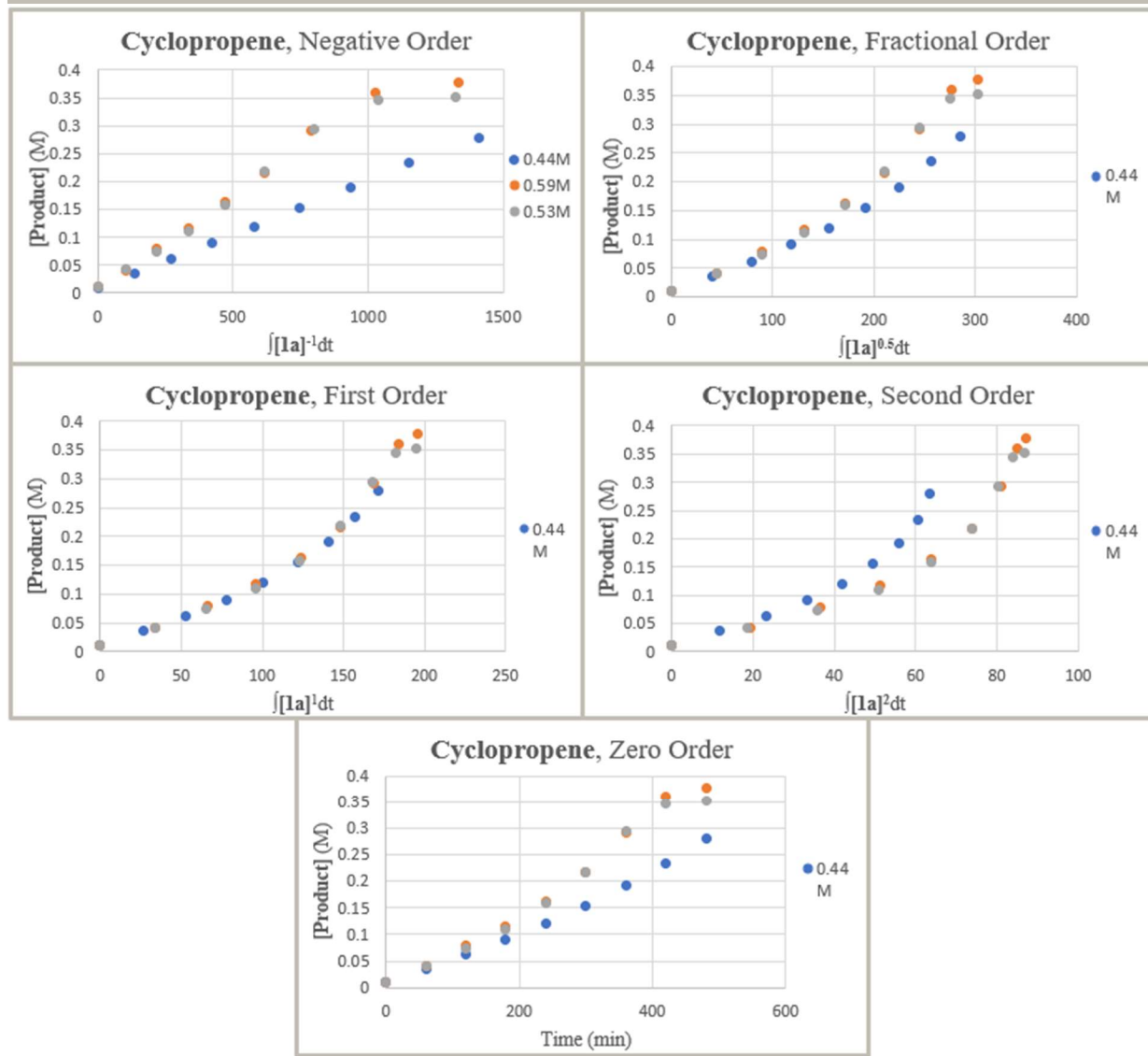
3.5.1 General Information

The kinetic profile of the reaction was determined using the variable time normalization analysis (VTNA) method described by Burés.⁴ Rates were monitored using GC-FID analysis with 1,3,5-trimethoxybenzene as a standard. ⁱPr-Duphos was utilized to ensure full dissolution. 1,3,5-trimethoxybenzene was determined to have no effect on the reaction. Catalyst concentration was assumed to remain constant over the duration of the reaction. Integrals were calculated using the trapezoid rule approximation.

3.5.2 Representative Procedure for Determination of the Reaction Order of Cyclopropene (**1**)

In a N₂-filled glove box, solutions of Cu(CH₃CN)₄PF₆ (13.3 mg, 0.0357 mmol) and **L3** (17.5 mg, 0.0418 mmol) in MeCN (700 μL), DBU (80.0 μL, 0.540 mmol) in MeCN (320 μL), cyclopropene **1a** (130.2 mg, 1.000 mmol) in MeCN (1000 μL), pyrazole **2a** (76.5 mg, 1.12 mmol) in MeCN (340 μL), and 1,3,5-trimethoxybenzene (156.0 mg, 0.928 mmol) in MeCN (310 μL) were prepared. The catalyst solution was stirred for 30 minutes to establish complexation. An oven-dried 1-dram vial was charged with a stir bar, the catalyst solution (100.0 μL), DBU solution (30.0 μL), **2a** solution (30.0 μL), 1,3,5-trimethoxybenzene solution (40.0 μL), **1a** solution (120.0 μL), and additional MeCN (80.0 μL). The mixture was held at 30 °C in the glove box, aliquots (approximately 25 μL) were taken every 60 minutes, quenched with methanol (approximately 0.5 mL), and diluted with ethyl acetate. The amount of **3a** was monitored using GC-FID analysis. By visual analysis, it is concluded that the reaction rate is first order with respect to cyclopropene (**Figure 17**).

Figure 17 : VTNA Graphs for Cyclopropene **1a**

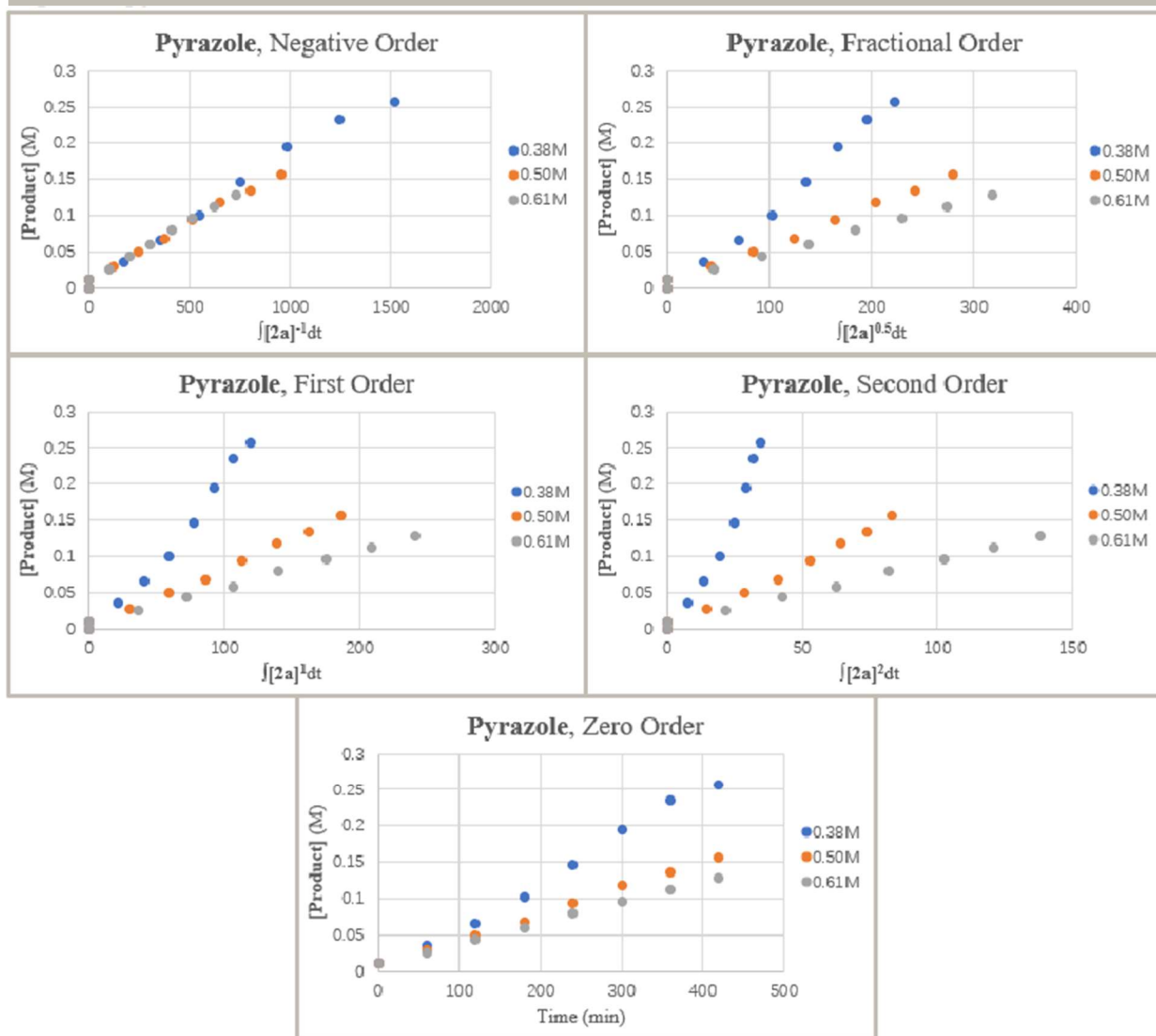


3.5.3 Representative Procedure for Determination of the Reaction Order of Pyrazole (2)

In a N₂-filled glove box, solutions of Cu(CH₃CN)₄PF₆ (23.4 mg, 0.0628 mmol) and **L3** (30.8 mg, 0.0736 mmol) in MeCN (740 μL), DBU (80.0 μL, 0.540 mmol) in MeCN (320 μL), cyclopropene **1a** (130.2 mg, 1.000 mmol) in MeCN (1000 μL), pyrazole **2a** (86.6 mg, 1.27 mmol) in MeCN (382 μL), and 1,3,5-trimethoxybenzene (204.5 mg, 1.22 mmol) in MeCN (405 μL) were prepared. The catalyst solution was stirred for 30 minutes to establish complexation. An oven-dried 1-dram vial

was charged with a stir bar, the catalyst solution (60.0 μ L), DBU solution (30.0 μ L), **2a** solution (30.0 μ L), 1,3,5-trimethoxybenzene solution (40.0 μ L), **1a** solution (120.0 μ L), and additional MeCN (120.0 μ L). The mixture was held at 30 °C in the glove box, aliquots (approximately 25 μ L) were taken every 60 minutes, quenched with methanol (approximately 0.5 mL), and diluted with ethyl acetate. The amount of **3a** was monitored using GC-FID analysis. By visual analysis, it is concluded that the reaction rate is **negative order** with respect to pyrazole (**Figure 18**).

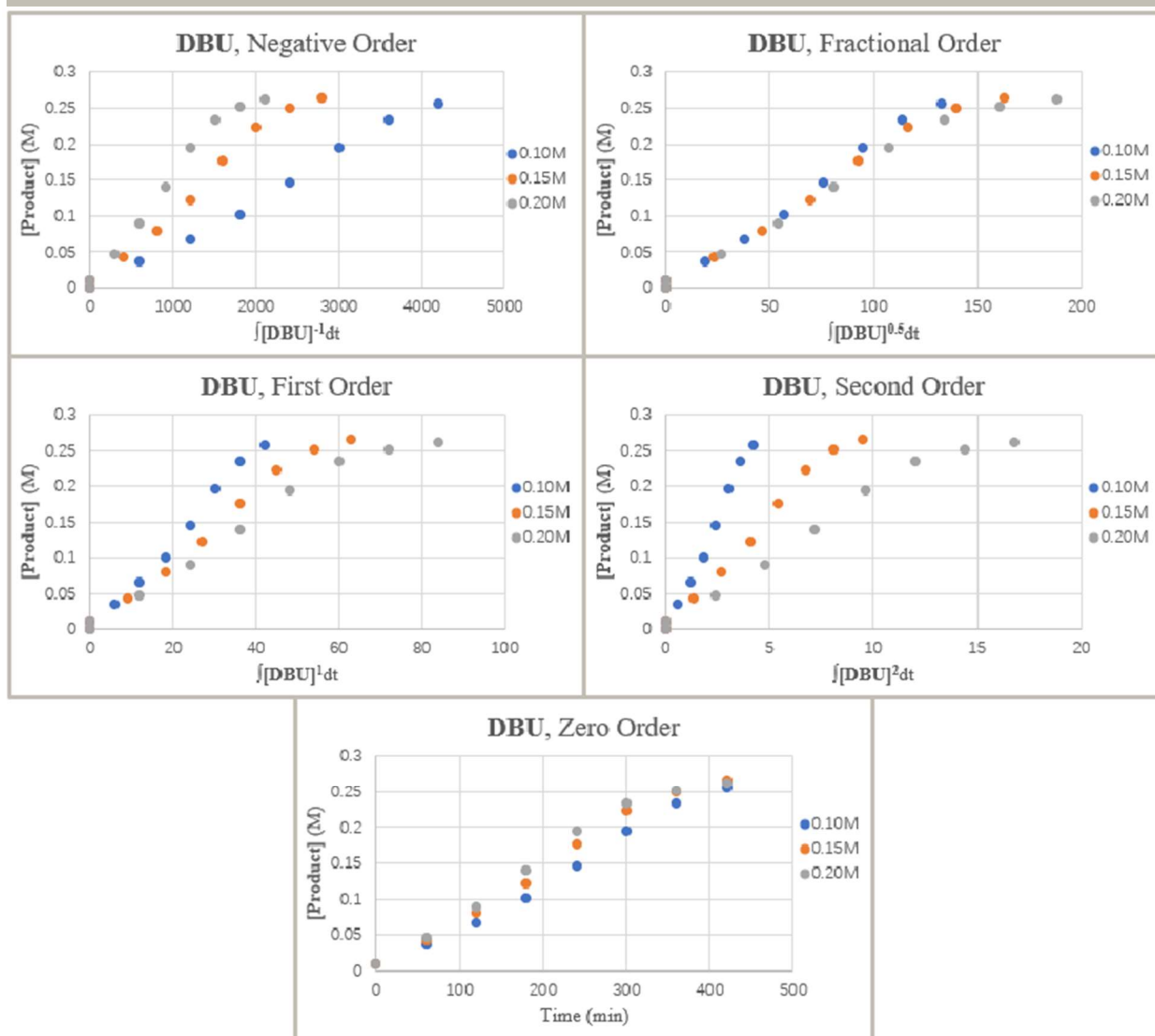
Figure 18 : VTNA Graphs for Pyrazole **2a**



3.5.4 Representative Procedure for Determination of the Reaction Order of DBU

In a N₂-filled glove box, solutions of Cu(CH₃CN)₄PF₆ (23.4 mg, 0.0628 mmol) and **L3** (30.8 mg, 0.0736 mmol) in MeCN (740 μ L), DBU (80.0 μ L, 0.540 mmol) in MeCN (320 μ L), cyclopropene **1a** (130.2 mg, 1.000 mmol) in MeCN (1000 μ L), pyrazole **2a** (86.6 mg, 1.27 mmol) in MeCN (382 μ L), and 1,3,5-trimethoxybenzene (204.5 mg, 1.22 mmol) in MeCN (405 μ L) were prepared. The catalyst solution was stirred for 30 minutes to establish complexation. An oven-dried 1-dram vial was charged with a stir bar, the catalyst solution (60.0 μ L), DBU solution (45.0 μ L),

Figure 19 : VTNA Graphs for DBU

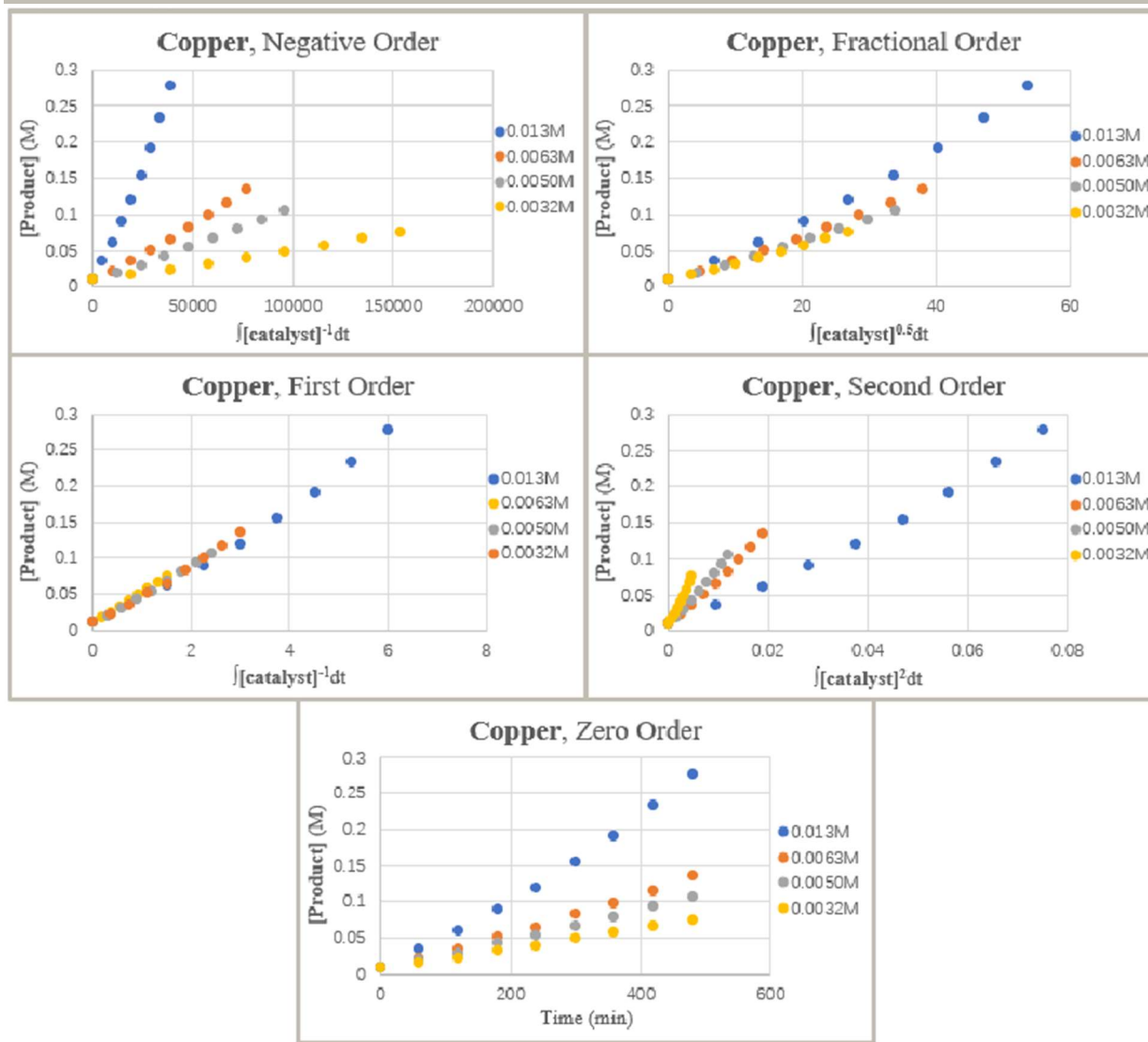


2a solution (30.0 μL), 1,3,5-trimethoxybenzene solution (40.0 μL), **1a** solution (120.0 μL), and additional MeCN (105.0 μL). The mixture was held at 30 °C in the glove box, aliquots (approximately 25 μL) were taken every 60 minutes, quenched with methanol (approximately 0.5 mL), and diluted with ethyl acetate. The amount of **3a** was monitored using GC-FID analysis. By visual analysis, it is concluded that the reaction rate is fractional order with respect to DBU (**Figure 19**).

3.5.5 Representative Procedure for Determination of the Reaction Order of Copper Catalyst at Low Loading

In a N₂-filled glove box, solutions of Cu(CH₃CN)₄PF₆ (13.3 mg, 0.0357 mmol) and **L3** (17.5 mg, 0.0418 mmol) in MeCN (700 μL), DBU (80.0 μL , 0.540 mmol) in MeCN (320 μL), cyclopropene **1a** (130.2 mg, 1.000 mmol) in MeCN (1000 μL), pyrazole **2a** (76.5 mg, 1.12 mmol) in MeCN (340 μL), and 1,3,5-trimethoxybenzene (156.0 mg, 0.928 mmol) in MeCN (310 μL) were prepared. The catalyst solution was stirred for 30 minutes to establish complexation. An oven-dried 1-dram vial was charged with a stir bar, the catalyst solution (50.0 μL), DBU solution (30.0 μL), **2a** solution (30.0 μL), 1,3,5-trimethoxybenzene solution (40.0 μL), **1a** solution (120.0 μL), and additional MeCN (130.0 μL). The mixture was held at 30 °C in the glove box, aliquots (approximately 25 μL) were taken every 60 minutes, quenched with methanol (approximately 0.5 mL), and diluted with ethyl acetate. The amount of **3a** was monitored using GC-FID analysis. By visual analysis, it is concluded that the reaction rate is first order with respect to copper catalyst (**Figure 20**).

Figure 20 : VTNA Graphs for Copper at Low Loading



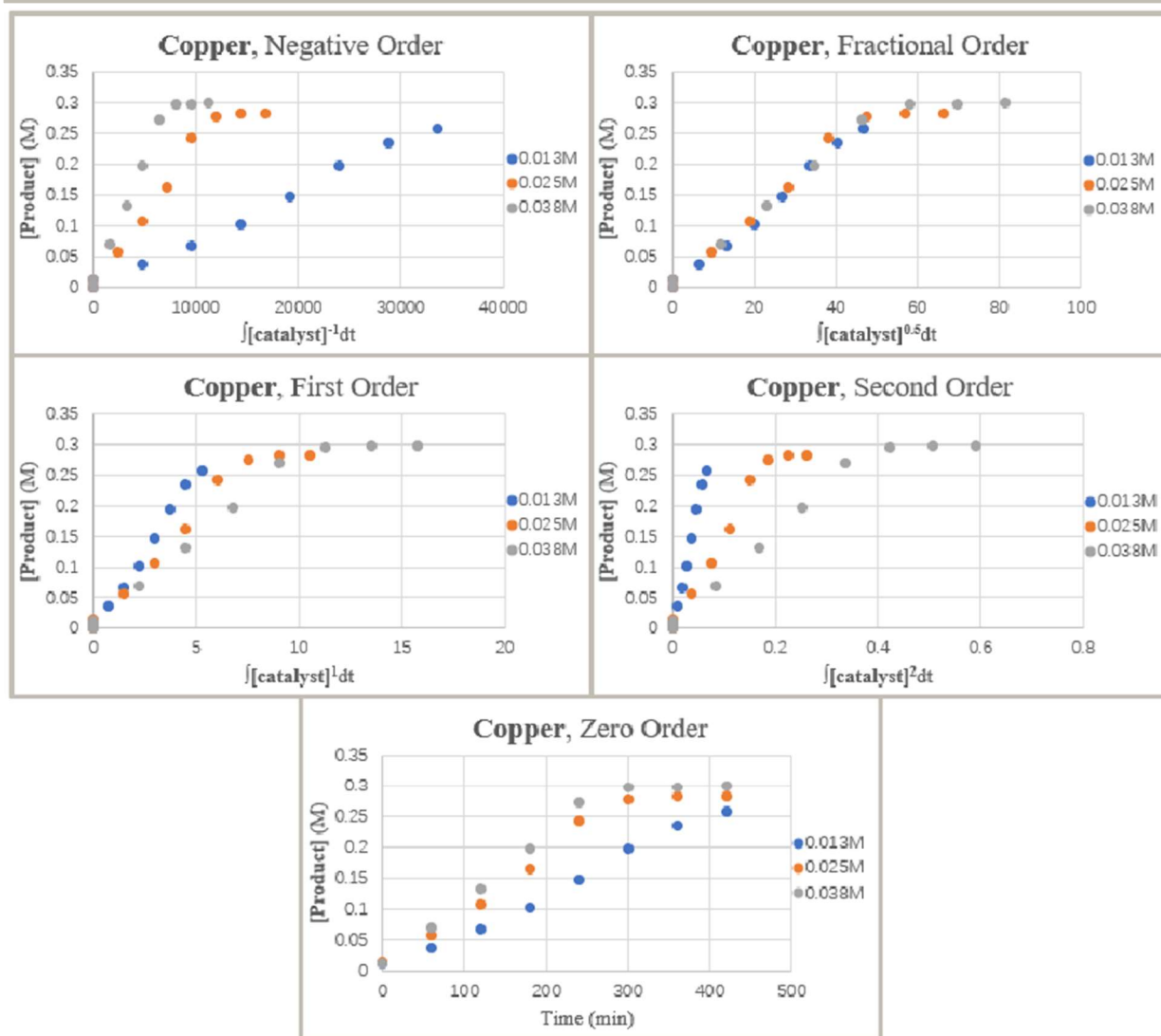
3.5.6 Representative Procedure for Determination of the Reaction Order of Copper

Catalyst at High Loading

In a N₂-filled glove box, solutions of Cu(CH₃CN)₄PF₆ (23.4 mg, 0.0628 mmol) and **L3** (30.8 mg, 0.0736 mmol) in MeCN (740 μL), DBU (80.0 μL, 0.540 mmol) in MeCN (320 μL), cyclopropene **1a** (130.2 mg, 1.000 mmol) in MeCN (1000 μL), pyrazole **2a** (86.6 mg, 1.27 mmol) in MeCN (382 μL), and 1,3,5-trimethoxybenzene (204.5 mg, 1.22 mmol) in MeCN (405 μL) were prepared. The

catalyst solution was stirred for 30 minutes to establish complexation. An oven-dried 1-dram vial was charged with a stir bar, the catalyst solution (120.0 μ L), DBU solution (30.0 μ L), **2a** solution (30.0 μ L), 1,3,5-trimethoxybenzene solution (40.0 μ L), **1a** solution (120.0 μ L), and additional MeCN (60.0 μ L). The mixture was held at 30 °C in the glove box, aliquots (approximately 25 μ L) were taken every 60 minutes, quenched with methanol (approximately 0.5 mL), and diluted with ethyl acetate. The amount of **3a** was monitored using GC-FID analysis. By visual analysis, it is concluded that the reaction rate is **fractional order** with respect to copper catalyst (**Figure 21**).

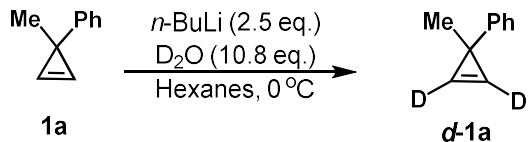
Figure 21 : VTNA Graphs for Copper at High Loading



3.6 Deuterium Labeling Studies

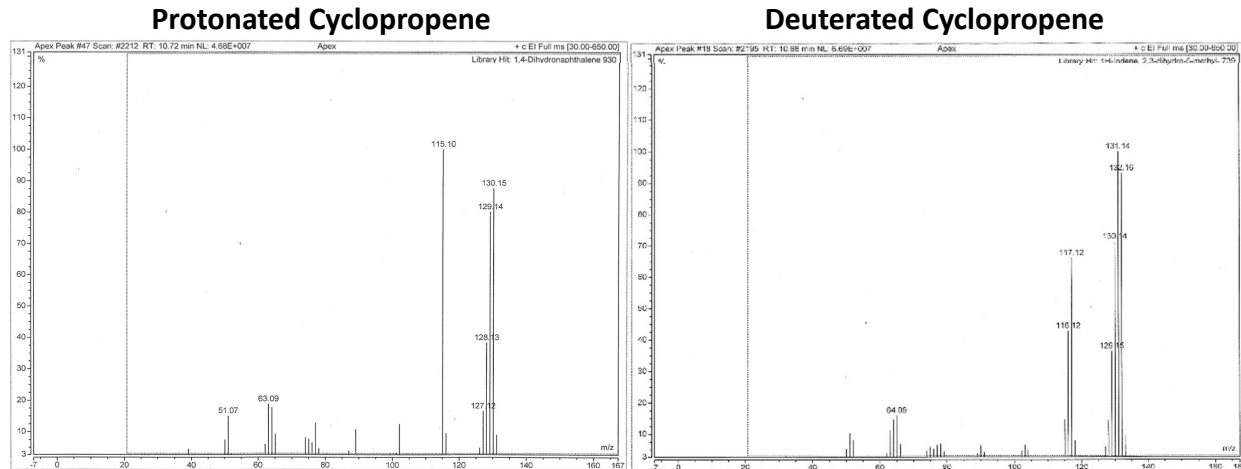
3.6.1 Synthesis of (1-methylcyclopropyl-2,3-²H₂)benzene (**d-1a**)

Deuterated cyclopropene **d-1a** was synthesized from **1a** following reported procedures.⁵

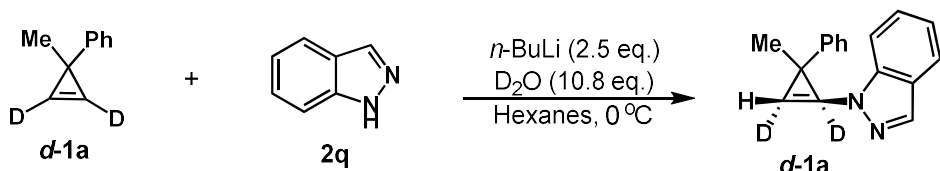


To a stirred solution of **1a** (200 mg, 1.54 mmol, 1.0 equiv.) in anhydrous hexane (2 mL) under N₂ at -78 °C a solution of 2.5 M *n*-BuLi (1.54 mL, 3.84 mmol, 2.5 equiv.) was added dropwise via syringe. The mixture was stirred for 30 minutes at 0 °C and quenched with deuterium oxide (300 μL, 16.6 mmol, 10.8 equiv.). The solution was stirred for 15 minutes, then the organic phase was separated, dried over MgSO₄, filtered, and concentrated under reduced pressure. The crude mixture was purified by column chromatography on silica gel (hexanes) to yield the desired product **d-1a**. Percent deuterium incorporation (%D) of **75% D** was determined by ¹H NMR. Double deuteration was confirmed by GCMS (Figure 22).

Figure 22 : GCMS of Cyclopropene **1a** and **d-1a**



3.6.2 Synthesis of 1-((1*S*,2*R*,3*R*)-2-methyl-2-phenylcyclopropyl-1,3-²H₂)-1*H*-indazole (*d*-3q)



Following the “General Procedure for Asymmetric Hydroamination” (Section 3.3.1), **d-1a** was used as the cyclopropene coupling partner. The target compound **d-3q** was obtained. Deuterium incorporation was determined by ¹H NMR. Percent deuterium (% D) incorporation is depicted as the amount of deuterium in place of a single hydrogen atom at that site.

3.7 NMR Studies

3.7.1 Reaction Observation

In a N₂-filled glove box, Cu(CH₃CN)₄PF₆ (1.9 mg, 0.0050 mmol, 5 mol%), **L3** (2.5 mg, 0.0060 mmol, 6 mol%), and MeCN-*d*₃ (0.30 mL) were added to a 1-dram vial containing a stir bar. The resulting mixture was stirred for 10 min. DBU (6.0 μ L, 0.040 mmol, 0.4 equiv.) and pyrazole **2a** (0.10 mmol, 1.0 equiv.) were added sequentially, followed by cyclopropene **1a** (0.10 mL, 1.2 M solution in MeCN-*d*₃, 0.12 mmol) to initiate the reaction. The reaction mixture was transferred to an NMR tube and removed from the glovebox to perform ³¹P NMR spectroscopy. A resonance at **-2.4 ppm** was observed at rt in the ³¹P NMR spectroscopy. Near the end of reaction, a resonance at **-4.7 ppm** was identified. PF₆⁻ was used as reference.

3.7.2 NMR Titration

3.7.2.1 Cu + L3

In a N₂-filled glove box, Cu(CH₃CN)₄PF₆ (3.8 mg, 0.0102 mmol, 1 equiv.), **L3** (5.1 mg, 0.0122 mmol, 1.2 equiv.), and MeCN-*d*₃ (0.30 mL) were added to a 1-dram vial containing a stir bar. The resulting mixture was stirred for 10 min, transferred to an NMR tube and removed from the glovebox for ³¹P NMR spectroscopy. While excess **L3** appeared at -11.4 ppm, a broad peak at 2.4 ppm was observed, representing the formation of Cu–**L3** complex (**Solution 1**).

3.7.2.2 Cu + L3 + DBU

DBU (9.1 μ l, 0.0612 mmol, 6 equiv.) was diluted with MeCN-*d*₃ (0.30 mL). The resulting DBU stock solution was used to titrate **Solution 1** via microsyringe (10 μ l, 0.2 equiv. per time). After 1 equiv. of DBU was added, a resonance at -4.7 ppm was monitored on ³¹P NMR spectroscopy, which we labeled as Cu–**L3**–DBU complex.

3.7.2.3 Cu + L3 + 3Py

Pyrazole **2a** (8.3 mg, 0.122 mmol, 12 equiv.) was dissolved in MeCN-*d*₃ (0.60 mL). The resulting **2a** stock solution was used to titrate **Solution 1** via microsyringe (10 μ L, 0.2 equiv. per time). Even after 3 equiv. of pyrazole was added, no significant difference from **Solution 1** was observed by ³¹P NMR spectroscopy, indicating the lack of copper-pyrazolate formation (**Solution 2**).

3.7.2.4 Cu + L3 + 3Py + DBU

DBU stock solution was used to titrate **Solution 2** via microsyringe (10 μ L, 0.2 equiv. per time). After 1 equiv. of DBU was added, a resonance at -2.5 ppm was observed by ³¹P NMR spectroscopy, which we labeled as Cu–**L3**–pyrazolate complex.

3.7.2.5 Cu + L3 + 3Py + 3KO^tBu

KO^tBu (6.9 mg, 0.0612 mmol, 6 equiv.) was dissolved in MeCN-*d*₃ (0.60 mL). The resulting stock solution was used to titrate **Solution 2** via microsyringe (20 μ L, 0.2 equiv. per time). After 3 equiv. of KO^tBu was added, a resonance at **-2.2 ppm** was observed by ³¹P NMR spectroscopy, which we labeled as copper-pyrazolate formation. We attributed the lower solubility of KO^tBu to the increased equivalents of base needed to deprotonate pyrazole.

3.7.3 Varying Copper Loading

3.7.3.1 Low Loading (0.005M)

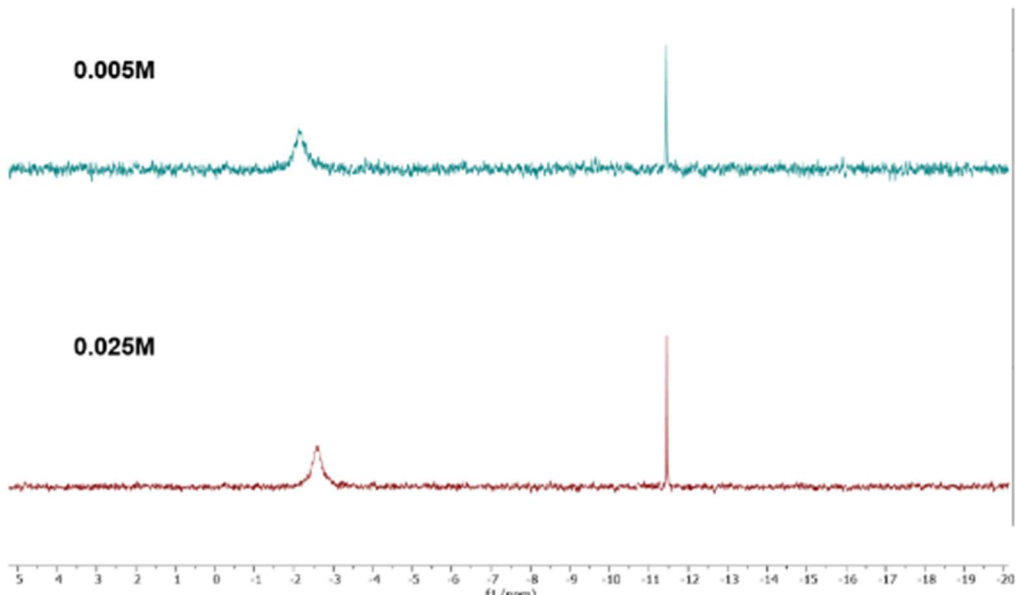
In a N₂-filled glove box, Cu(CH₃CN)₄PF₆ (1.9 mg, 0.0050 mmol), **L3** (2.5 mg, 0.0060 mmol), and MeCN-*d*₃ (1.00 mL) were added to a 1-dram vial containing a stir bar. The resulting mixture was stirred for 10 min. DBU (6.0 μ L, 0.040 mmol, 0.4 equiv.) and pyrazole **2a** (6.8 mg, 0.10 mmol, 1.0 equiv.) were added sequentially. The reaction mixture was transferred to an NMR tube and removed from the glovebox for ³¹P NMR spectroscopy. A resonance at **-2.2 ppm** was observed (**Figure 23**).

3.7.3.2 High Loading (0.025M)

In a N₂-filled glove box, Cu(CH₃CN)₄PF₆ (3.8 mg, 0.010 mmol, 5 mol%), **L3** (5.1 mg, 0.0060 mmol, 6 mol%), and MeCN-*d*₃ (0.40 mL) were added to a 1-dram vial containing a stir bar. The resulting mixture was stirred for 10 min. DBU (6.0 μ L, 0.040 mmol, 0.4 equiv.) and pyrazole **2a** (6.8 mg, 0.10 mmol, 1.0 equiv.) were added sequentially. The reaction mixture was transferred to an NMR tube and removed from the glovebox for ³¹P NMR spectroscopy. Based on these results, we envision copper-pyrazolate as a plausible resting state. NMR titration studies revealed the dual

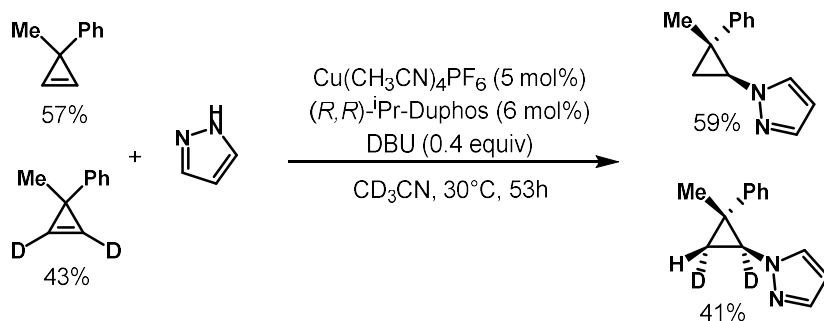
role of DBU in both as a base to deprotonate pyrazole and a ligand to copper. A resonance at **-2.5 ppm** was observed.

Figure 23 : ^{31}P NMR with Varied Copper Loadings



3.8 Kinetic Isotope Effect Study

3.8.1 Procedure for Competition Kinetic Isotope Effect Study



In a N_2 -filled glove box, $\text{Cu}(\text{CH}_3\text{CN})_4\text{PF}_6$ (3.0 mg, 0.0080 mmol, 5 mol%), **L3** (4.0 mg, 0.0096 mmol, 6 mol%), and CD_3CN (0.44 mL) were added to a 1-dram vial containing a stir bar. The resulting mixture was stirred for 10 min. DBU (12.1 μl , 0.080 mmol, 0.5 equiv.) and pyrazole **2**

(10.9 mg, 0.16 mmol, 1.0 equiv.) were added sequentially, followed by 67% deuterated cyclopropene **d-1a** (0.149 mL, 1.0 M solution in MeCN, 0.149 mmol) and cyclopropene **1a** (0.051 mL, 1.0 M solution in MeCN, 0.051 mmol)^{*} to initiate the reaction. The mixture was transferred to an NMR tube and sealed. The tube was removed from the glovebox and placed in a sonicator bath at 30 °C, removed only to take timepoint measurements. Conversion and deuteration ratio of the product was determined by ¹H NMR analysis of the reaction in progress. These data were used to calculate the KIE of the reaction reported (**Figure 24**).⁶

^{*}This ratio was used to target a 50% deuterated starting material ratio. The measured cyclopropene starting material ratio was 43% deuterated by ¹H NMR taken 0.3 h after the reaction started.

Table 1 : Data from Competition KIE Study

Time Point (h)	Deuterated (%)	Conversion (%)	Calculated KIE
0.3 ^a	undetermined	negligible	N/A
2	24	12	-7.5 ^b
4	38	13	1.5 ^b
6	38	30	1.2 ^b
8	41	43	1.0
10	40	52	1.0
12	41	64	1.0
25	43	83	0.99
53 ^c	41	95 ^d	N/A

$$\text{KIE : } \mathbf{1.0 \pm 1.5 \text{ E-}2}$$

a. Time point was taken as quickly as possible after start of reaction and was used to establish starting material deuteration ratio. Included in this table for completeness. b. Data removed from calculation of reaction KIE due to lack of consistency resulting from low conversion. Employed technique's accuracy increases with % conversion.⁶ Included in this table for completeness. c. The atypically long reaction time is hypothesized to have resulted from the combination of variance in vessel shape and agitation technique from the standard conditions, and possibly minute air contamination resulting from running the reaction outside of a glove box. d. The reaction stalled at 95% conversion and did not proceed further. This measurement was used as the end of the reaction for the purposes of calculation.

3.8.2 Equation to Calculate Kinetic Isotope Effect

$$(k_L/k_H) = (\ln\{1 - F_T[(1 + R_{P,\infty}) / (1 + R_P)]\}) / [\ln(1 - F_T\{[R_P / R_{P,\infty}][(1 + R_{P,\infty}) / (1 + R_P)]\})]$$

k_L = concentration of light isotope

k_H = concentration of heavy isotope

F_T = total fractional conversion

R_P = isotopic ratio of the product

$R_{P,\infty}$ = isotopic ratio of the product at the end of the reaction

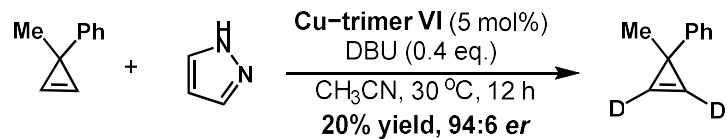
3.9 Synthesis and Reactivity of Copper–Trimer VI

3.9.1 Synthesis of Copper–Trimer VI



In a N₂-filled glove box, Cu(CH₃CN)₄PF₆ (3.8 mg, 0.010 mmol, 1 equiv.), **L3** (5.1 mg, 0.012 mmol, 1.2 equiv.), and MeCN-*d*₃ (0.20 mL) were added to a 1-dram vial containing a stir bar. The resulting mixture was stirred for 10 min. DBU (9 μL, 0.061 mmol, 6 equiv.) was diluted with MeCN-*d*₃ (0.30 mL). Pyrazole **2a** (8.3 mg, 0.122 mmol, 12 equiv.) was dissolved in MeCN-*d*₃ (0.60 mL). DBU (50 μL, 1 equiv.) and pyrazole **2a** (150 μL, 3 equiv.) were added sequentially to the complex solution. The mixture was transferred to an NMR tube and removed from the glovebox for ³¹P NMR spectroscopy. A resonance at -2.5 ppm was observed at rt in the ³¹P NMR spectroscopy. The NMR tube was then left for slow crystallization. A red crystal was observed at the bottom of NMR tube.

3.9.2 Reaction with Copper–Trimer VI

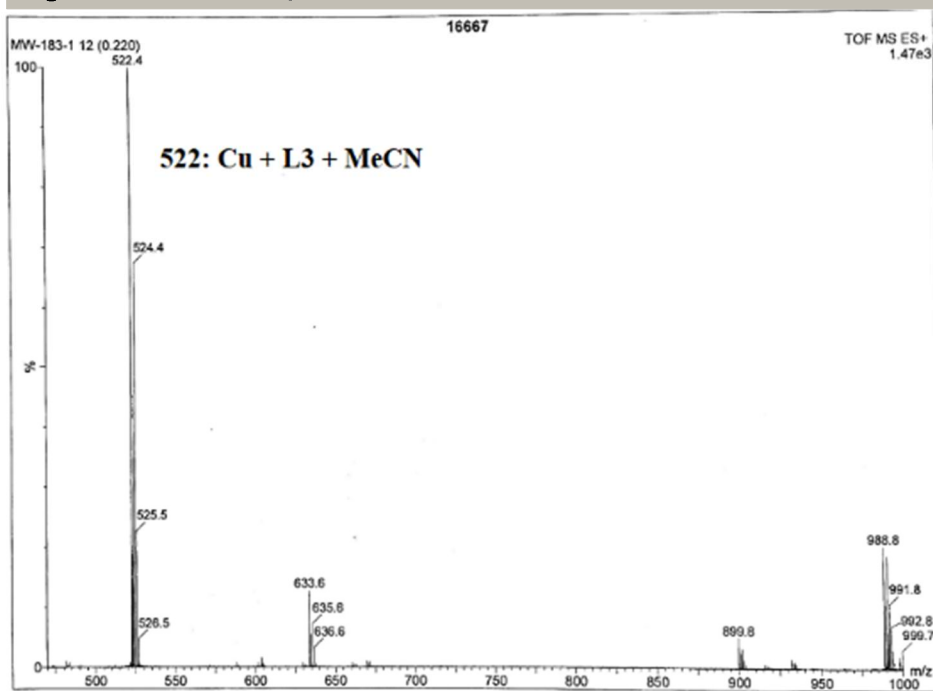


In a N₂-filled glove box, Copper-trimer **VI** (8.0 mg, 6.2 µmol, 5 mol%) and MeCN (0.30 mL) were added to a 1-dram vial containing a stir bar. The resulting mixture was stirred for 10 min. DBU (7.4 µL, 0.049 mmol, 0.4 equiv.) and pyrazole **2a** (8.4 mg, 0.12 mmol, 1.0 equiv.) were added sequentially, followed by cyclopropene **1a** (0.12 mL, 1.2 M solution in MeCN, 0.12 mmol) to initiate the reaction. The mixture was held at 30 °C until no starting material was observed by GC-MS. Diastereomeric ratio was determined by ¹H NMR analysis of the unpurified reaction mixture. Isolated yield of 20% for **3a** was obtained using preparative thin-layer chromatography. An enantiomeric ratio of 94:6 was collected using SFC.

3.10 Electrospray Ionization Mass Spectrometer Analysis

In a N₂-filled glove box, Cu(CH₃CN)₄PF₆ (3.8 mg, 0.010 mmol, 5 mol%), **L3** (5.1 mg, 0.0060 mmol, 6 mol%), and MeCN (0.40 mL) were added to a 1-dram vial containing a stir bar. The resulting mixture was stirred for 10 min. DBU (6.0 µL, 0.040 mmol, 0.4 equiv.) and pyrazole **2a** (6.8 mg, 0.10 mmol, 1.0 equiv.) were added sequentially. The catalytic solution was immediately subjected to ESI-MS analysis. We observed mostly the decomposition of the metal complex, with Cu + L3 + MeCN as the most dominant peak at approximately **522 m/z**. No desired mass of copper-pyrazolate monomer (549.2) or dimer (1098.4) was observed (**Figure 24**).

Figure 24 : ESI-MS Spectrum for Cu + L3 + MeCN



3.11

Density Functional Theory Calculations

DFT calculations were conducted to study the key selectivity determining aminocupration step in the hydroamination of cyclopropenes via the copper-phosphido catalyst. The coupling of 3-methyl-3-phenylcyclopropene **1a** and 3-methylpyrazole **2j** was chosen as the model substrate system for our theoretical study using Cu-(*R,R*)-ⁱPr-DuPhos **L3** as the catalytic species. All ground state and transition state optimizations as well as the calculation of vibrational frequencies were performed at the M062X/6-31G* level of theory in gas phase, as implemented in Gaussian 16.⁷⁻⁹ Single point energies were computed at three levels of theory: (1) M062X/6-311+G** // M062X/6-311+G**^{10,11}, (2) B3LYP-D3BJ/6-311+G** // B3LYP-D3BJ/6-31G*^{12,13}, and (3) ω B97XD/def2-TZVP // B97D/def2-SVP.¹⁴⁻¹⁷ All levels of theory were performed utilizing a polarized continuum solvation model (PCM) for acetonitrile. Thermal corrections to free energies were implemented using Grimme's quasi-rigid rotor harmonic oscillator (QRRHO) approximation.¹⁸ Transition

structures (TSs) were verified as exhibiting one sole imaginary frequency, and intrinsic reaction coordinate calculations were performed to confirm the TSs connect the minima along the potential energy surface. Conformational analysis was carried out for all TSs. Molecular graphics were generated using CYLview.¹⁹

3.12 X-Ray Crystallography

3.12.1 General Information

Crystal analysis was conducted using a Bruker X8 Prospector APEX II diffractometer system. The APEX3²⁰ program package was used to determine the unit-cell parameters and for data collection (10 sec/frame scan time). The raw frame data was processed using SAINT²¹ and SADABS²² to yield the reflection data file. Subsequent calculations were carried out using the SHELXTL²³ program package. The structures were solved by direct methods and refined on F^2 by full-matrix least-squares techniques. The analytical scattering factors²⁴ for neutral atoms were used throughout the analyses. The thermal ellipsoid plots are shown at the 50% probability level (see Appendix C).

3.12.2 Definitions

$$wR2 = [\sum[w(F_o^2 - F_c^2)^2] / \sum[w(F_o^2)^2]]^{1/2}$$

$$R1 = \sum||F_o| - |F_c|| / \sum|F_o|$$

Goof = S = $[\sum[w(F_o^2 - F_c^2)^2] / (n-p)]^{1/2}$ where n is the number of reflections and p is the total number of parameters refined.

3.12.3 Analysis of 3-methyl-1-((1*S*,2*R*)-2-methyl-2-phenylcyclopropyl)-1*H*-pyrazole (3j)

A colorless crystal of approximate dimensions 0.128 x 0.175 x 0.211 mm was mounted on a glass fiber and transferred to an X-ray diffractometer. The systematic absences were consistent with the monoclinic space groups $P2_1$ and $P2_1/m$. It was later determined that space group $P2_1$ was correct. Hydrogen atoms were located from a difference-map and refined (xyz and U_{iso}). Least-squares analysis yielded $wR2 = 0.1122$ and $Goof = 1.047$ for 209 variables refined against 2170 data (0.83 Å), $R1 = 0.0414$ for those 2072 data with $I > 2.0\sigma(I)$. The absolute structure could not be assigned by refinement of the Flack parameter.²⁵ The assignment was based on the synthetic method employed.

3.12.4 Analysis of 1-((1*S*,2*R*)-2-methyl-2-(naphthalen-2-yl)cyclopropyl)-1*H*-pyrazole (4i)

A colorless crystal of approximate dimensions 0.087 x 0.133 x 0.145 mm was mounted in a cryoloop and transferred to an X-ray diffractometer. The diffraction symmetry was mmm and the systematic absences were consistent with the orthorhombic space group $P2_12_12_1$ that was later determined to be correct. Hydrogen atoms were located from a difference-map and refined (xyz and U_{iso}). Least squares analysis yielded $wR2 = 0.0715$ and $Goof = 1.055$ for 237 variables refined against 2472 data (0.83 Å), $R1 = 0.0281$ for those 2368 data with $I > 2.0\sigma(I)$. The absolute structure was assigned by refinement of the Flack parameter.²⁵

3.12.5 Analysis of (1*S*,2*S*)-*N,N*-dimethyl-1-phenyl-2-(1*H*-pyrazol-1-yl)cyclopropane-1 carboxamide (4k)

A colorless crystal of approximate dimensions 0.035 x 0.095 x 0.253 mm was mounted in a cryoloop and transferred to an X-ray diffractometer. The systematic absences were consistent with the monoclinic space groups $P2_1$ and $P2_1/m$. It was later determined that space group $P2_1$ was correct. Hydrogen atoms were located from a difference-map and refined (xyz and U_{iso}).

Least-squares analysis yielded $wR_2 = 0.0839$ and $Goof = 1.091$ for 241 variables refined against 2434 data (0.83 \AA), $R_1 = 0.0338$ for those 2229 data with $I > 2.0\sigma(I)$. The absolute structure was assigned by refinement of the Flack parameter.²⁵

3.12.6 Analysis of Copper-trimer VI

An orange crystal of approximate dimensions $0.202 \times 0.241 \times 0.360 \text{ mm}$ was mounted on a glass fiber and transferred to an X-ray diffractometer. The diffraction symmetry was *mmm* and the systematic absences were consistent with the orthorhombic space group *P2₁2₁2₁* that was later determined to be correct. Hydrogen atoms were included using a riding model. There were two molecules of acetonitrile solvent present. Least squares analysis yielded $wR_2 = 0.1116$ and $Goof = 1.151$ for 770 variables refined against 17065 data (0.76 \AA), $R_1 = 0.0398$ for those 16689 data with $I > 2.0\sigma(I)$. The structure was refined as an inversion twin.

3.13 References

1. Li, Z.; Zhao, J.; Sun, B.; Zhou, T.; Liu, M.; Liu, S.; Zhang, M.; Zhang, Q. Asymmetric Nitrone Synthesis via Ligand-Enabled Copper-Catalyzed Cope-Type Hydroamination of Cyclopropene with Oxime. *J. Am. Chem. Soc.* **2017**, *139*, 11702–11705.
2. Phan, D. H. T.; Kou, K. G. M.; Dong, V. M. Enantioselective Desymmetrization of Cyclopropenes by Hydroacylation. *J. Am. Chem. Soc.* **2010**, *132*, 16354–16355.
3. Yamanushkin, P.; Lu-Diaz, M.; Edwards, A.; Aksenov, N. A.; Rubina, M.; Rubin, M. Directed Nucleophilic Addition of Phenoxides to Cyclopropenes. *Org. Biomol. Chem.* **2017**, *15*, 8153–8165.

4. Burés, J. Variable Time Normalization Analysis: General Graphical Elucidation of Reaction Orders from Concentration Profiles. *Angew. Chem. Int. Ed.* **2016**, *55*, 16084–16087.
5. Alnasleh, B. K.; Sherrill, W. M.; Rubin, M. Palladium-Catalyzed Hydrophosphorylation and Hydrophosphinylation of Cyclopropenes. *Org. Lett.* **2008**, *10*, 3231–3234.
6. Dale, H. J. A.; Leach, A. G.; Lloyd-Jones, G. C. Heavy-Atom Kinetic Isotope Effects: Primary Interest or Zero Point? *J. Am. Chem. Soc.* **2021**, *143*, 21079–21099.
7. Zhao, Y.; Truhlar, D. G. The M06 suite of density functionals for main group thermochemistry, thermochemical kinetics, noncovalent interactions, excited states, and transition elements: two new functionals and systematic testing of four M06-class functionals and 12 other functionals. *Theor. Chem. Acc.* **2008**, *120*, 215–241.
8. Hehre, W. J.; Stewart, R. F.; Pople, J. A. Self-Consistent Molecular-Orbital Methods. I. Use of Gaussian Expansions of Slater-Type Atomic Orbitals. *J. Chem. Phys.* **1969**, *51*, 2657–2664.
9. Frisch, M. J.; Trucks, G. W.; Schlegel, H. B.; Scuseria, G. E.; Robb, M. A.; Cheeseman, J. R.; Scalmani, G.; Barone, V.; Petersson, G. A.; Nakatsuji, H.; Li, X.; Caricato, M.; Marenich, A. V.; Bloino, J.; Janesko, B. G.; Gomperts, R.; Mennucci, B.; Hratchian, H. P.; Ortiz, J. V.; Izmaylov, A. F.; Sonnenberg, J. L.; Williams; Ding, F.; Lipparini, F.; Egidi, F.; Goings, J.; Peng, B.; Petrone, A.; Henderson, T.; Ranasinghe, D.; Zakrzewski, V. G.; Gao, J.; Rega, N.; Zheng, G.; Liang, W.; Hada, M.; Ehara, M.; Toyota, K.; Fukuda, R.; Hasegawa, J.; Ishida, M.; Nakajima, T.; Honda, Y.; Kitao, O.; Nakai, H.; Vreven, T.; Throssell, K.; Montgomery, J. A., Jr.; Peralta, J. E.; Ogliaro, F.; Bearpark, M. J.; Heyd, J. J.; Brothers, E. N.; Kudin, K. N.; Staroverov, V. N.; Keith, T. A.; Kobayashi, R.; Normand, J.

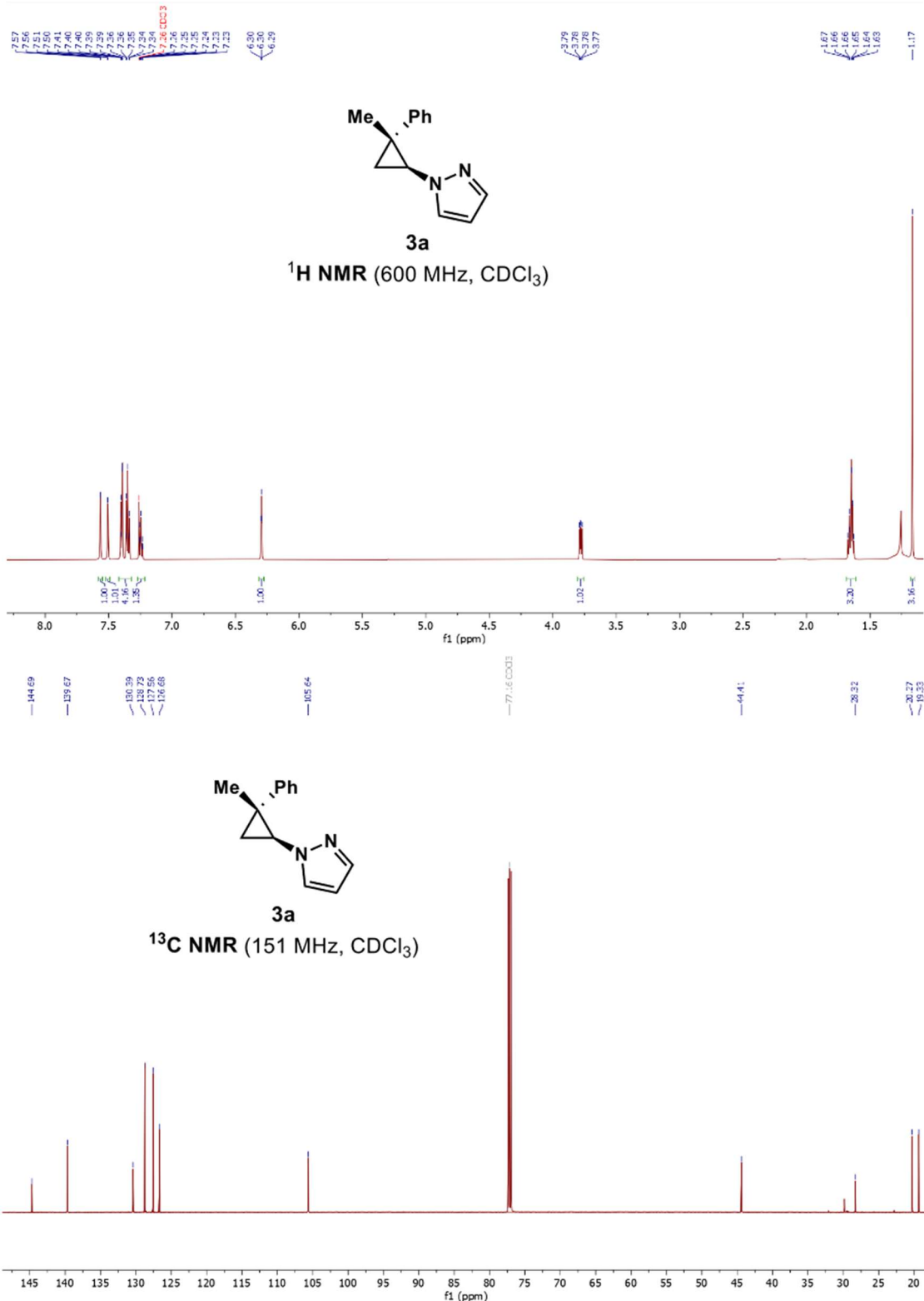
J.; Raghavachari, K.; Rendell, A. P.; Burant, J. C.; Iyengar, S. S.; Tomasi, J.; Cossi, M.; Millam, J. M.; Klene, M.; Adamo, C.; Cammi, R.; Ochterski, J. W.; Martin, R. L.; Morokuma, K.; Farkas, O.; Foresman, J. B.; Fox, D. J. *Gaussian 16*; rev. C.01; Gaussian, Inc.: Wallingford, CT, 2016.

10. Miertus, S.; Scrocco, E.; Tomasi, J. Electrostatic Interaction of a Solute with a Continuum – a Direct Utilization of Abinitio Molecular Potentials for the Prevision of Solvent Effects. *Chem. Phys.* **1981**, *55*, 117–129.
11. Tomasi, J.; Mennucci, B.; Cammi, R. Quantum mechanical continuum solvation models. *Chem. Rev.* **2005**, *105*, 2999–3093.
12. Becke, A. D. Density-functional thermochemistry. III. The role of exact exchange. *J. Chem. Phys.* **1993**, *98*, 5648–5652.
13. Grimme, S.; Ehrlich, S.; Goerigk, L. Effect of the damping function in dispersion corrected density functional theory. *J. Comput. Chem.* **2011**, *32*, 1456–1465.
14. Grimme, S. Semiempirical GGA-type density functional constructed with a long-range dispersion correction. *J. Comput. Chem.* **2006**, *27*, 1787–1799.
15. Becke, A. Density-Functional Thermochemistry. V. Systematic Optimization of Exchange-Correlation Functionals. *J. Chem. Phys.* **1997**, *107*, 8554–8560.
16. Chai, J. D.; Head-Gordon, M. Long-range corrected hybrid density functionals with damped atom-atom dispersion corrections. *Phys. Chem. Chem. Phys.* **2008**, *10*, 6615–6620.
17. Weigend, F.; Ahlrichs, R. Balanced basis sets of split valence, triple zeta valence and quadruple zeta valence quality for H to Rn: Design and assessment of accuracy. *Phys. Chem. Chem. Phys.* **2005**, *7*, 3297–3305.

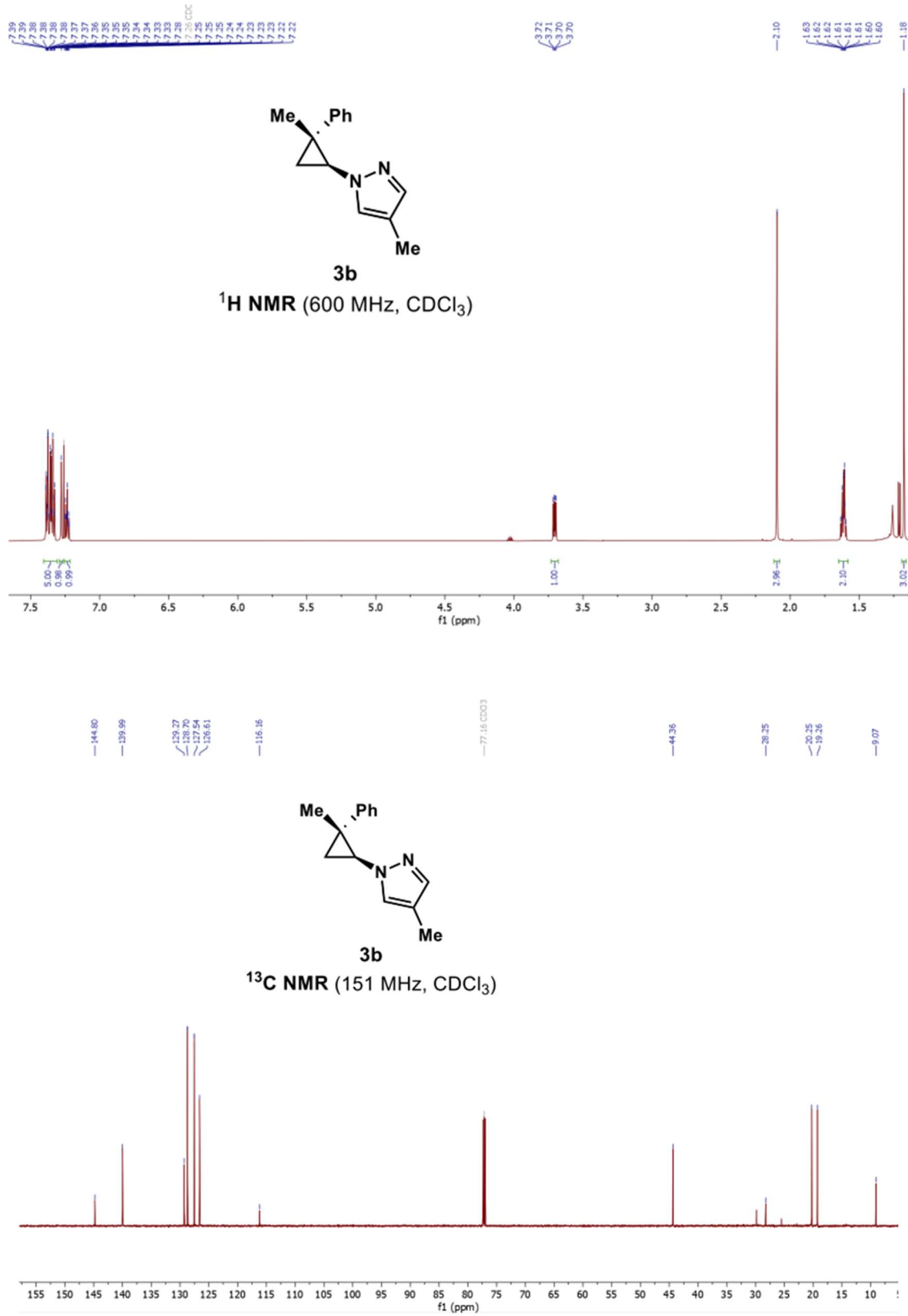
18. Grimme, S. Supramolecular binding thermodynamics by dispersion-corrected density functional theory. *Chem. Eur. J.* **2012**, *18*, 9955–9964.
19. Legault, C. Y.; CYLview, 1.0b; Université de Sherbrooke, **2009** (<http://www.cylview.org>).
20. APEX3 Version 2018.1-0, Bruker AXS, Inc.; Madison, WI 2018.
21. SAINT Version 8.38a, Bruker AXS, Inc.; Madison, WI 2013.
22. Sheldrick, G. M. SADABS, Version 2014/5, Bruker AXS, Inc.; Madison, WI 2014.
23. Sheldrick, G. M. SHELXTL, Version 2014/7, Bruker AXS, Inc.; Madison, WI 2014.
24. International Tables for Crystallography 1992, Vol. C., Dordrecht: Kluwer Academic Publishers.
25. Parsons, S.; Flack, H. D.; Wagner, T. Use of Intensity Quotients and Differences in Absolute Structure Refinement. *Acta Crystallogr., Sect. B: Struct. Sci., Cryst. Eng. Mater.* **2013**, *B69*, 249–259.

APPENDIX A: ^1H and ^{13}C NMR Spectral Data

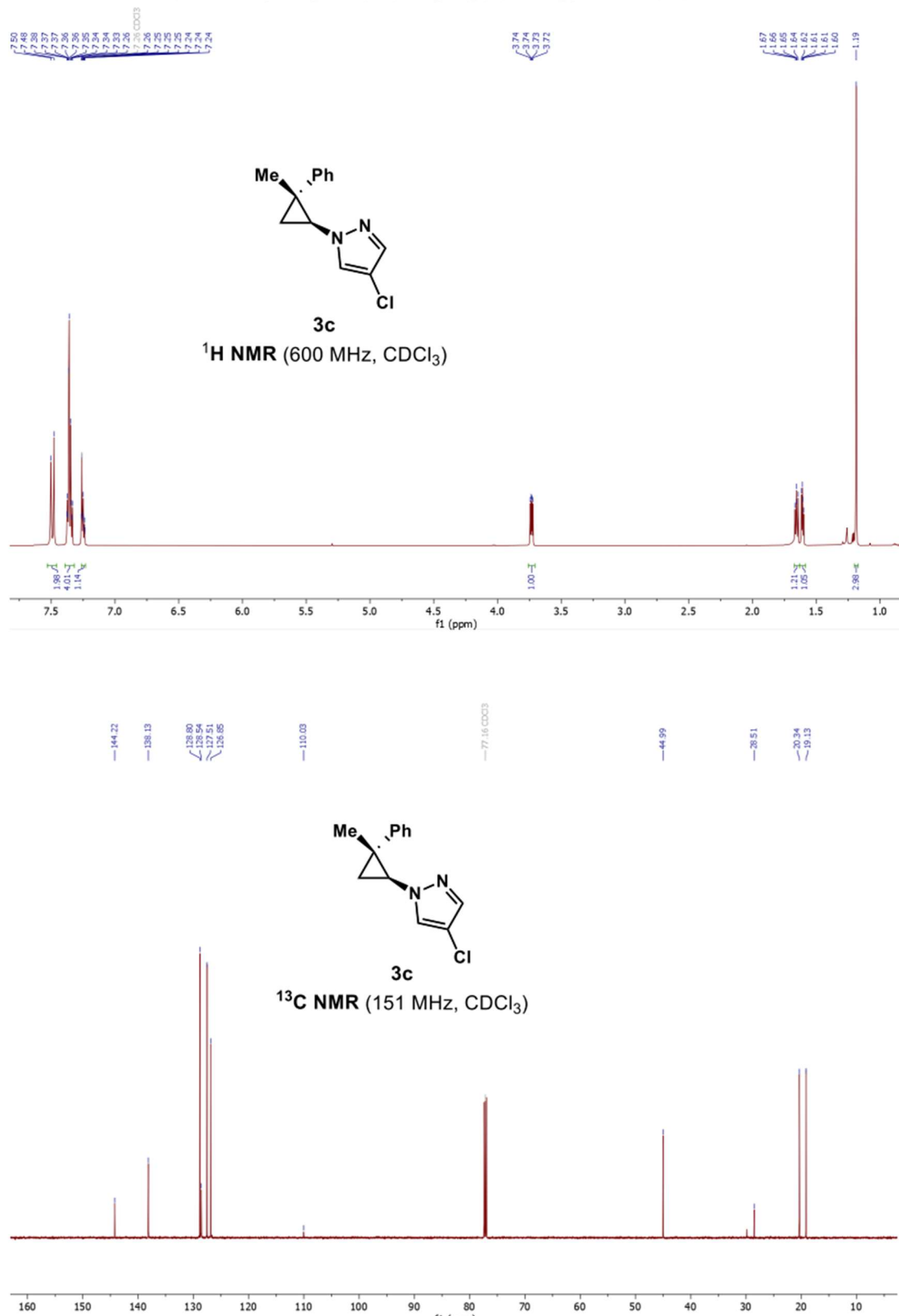
1-((1*S*,2*R*)-2-methyl-2-phenylcyclopropyl)-1*H*-pyrazole (3a)



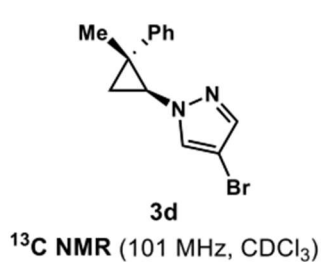
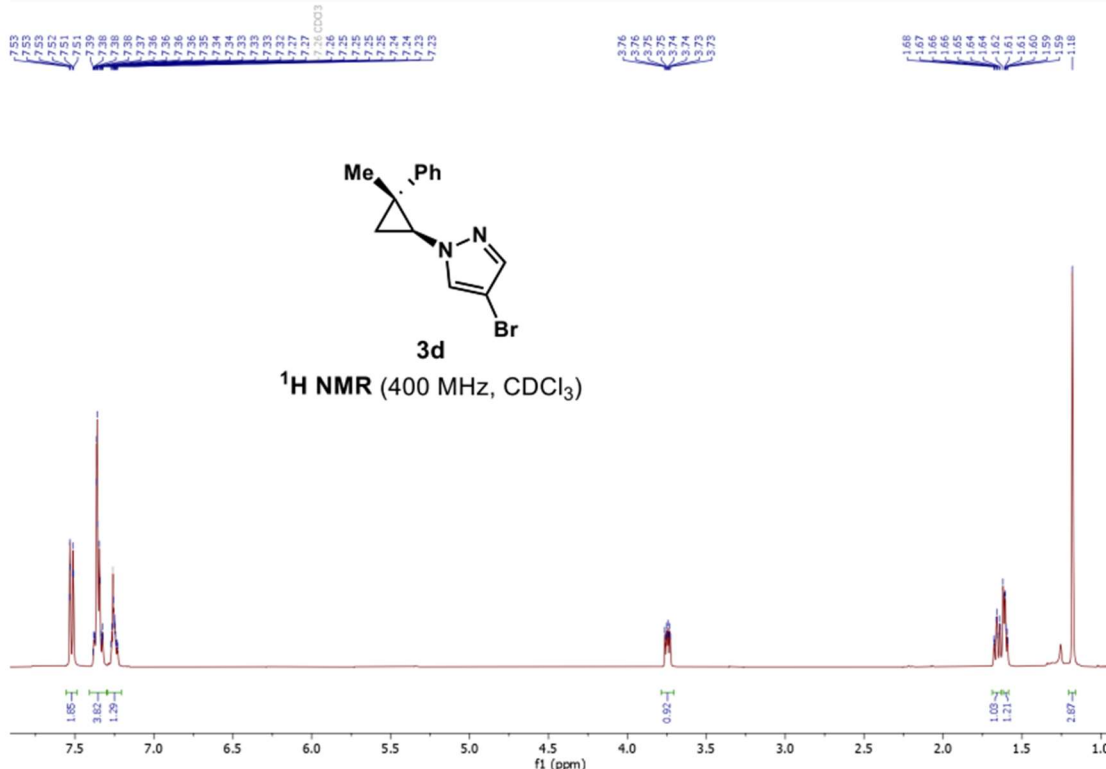
4-methyl-1-((1*S*,2*R*)-2-methyl-2-phenylcyclopropyl)-1*H*-pyrazole (3b)



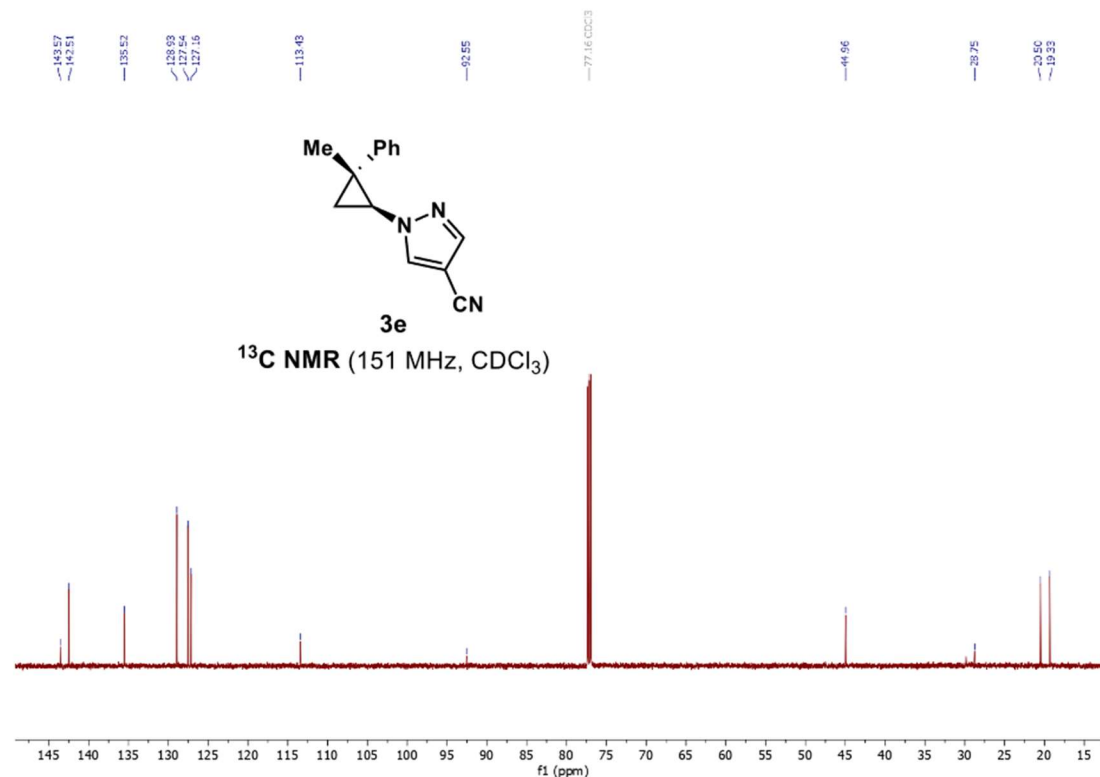
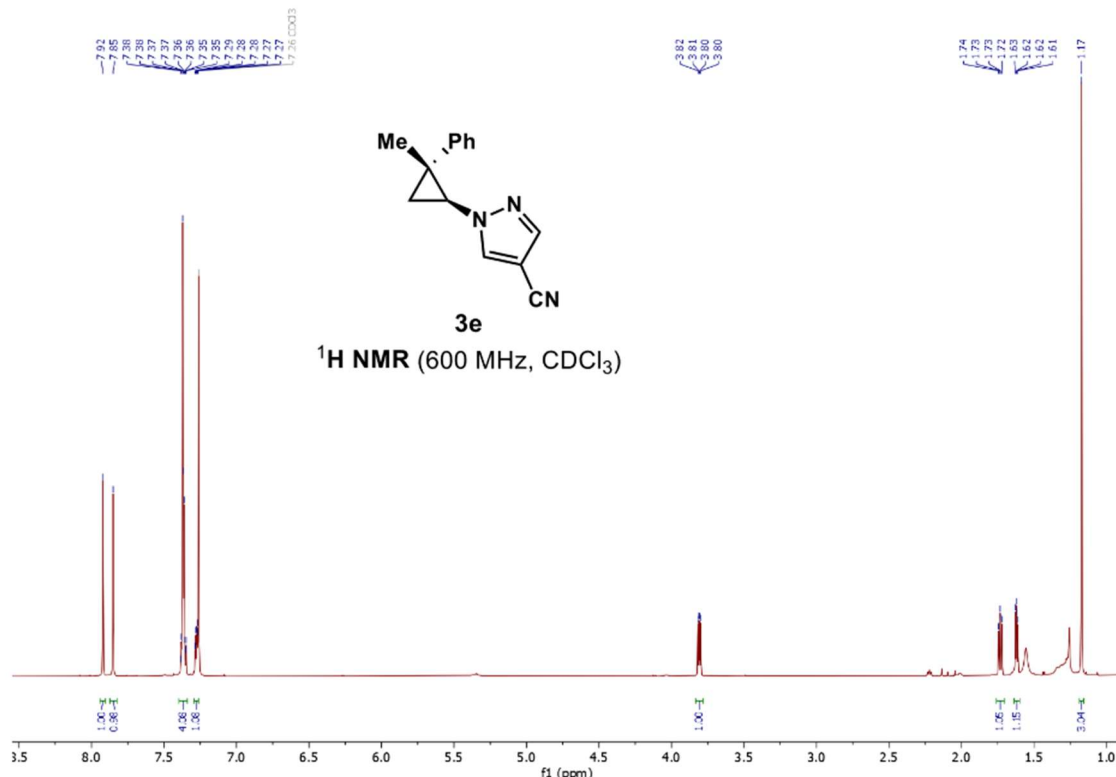
4-chloro-1-((1*S*,2*R*)-2-methyl-2-phenylcyclopropyl)-1*H*-pyrazole (3c)



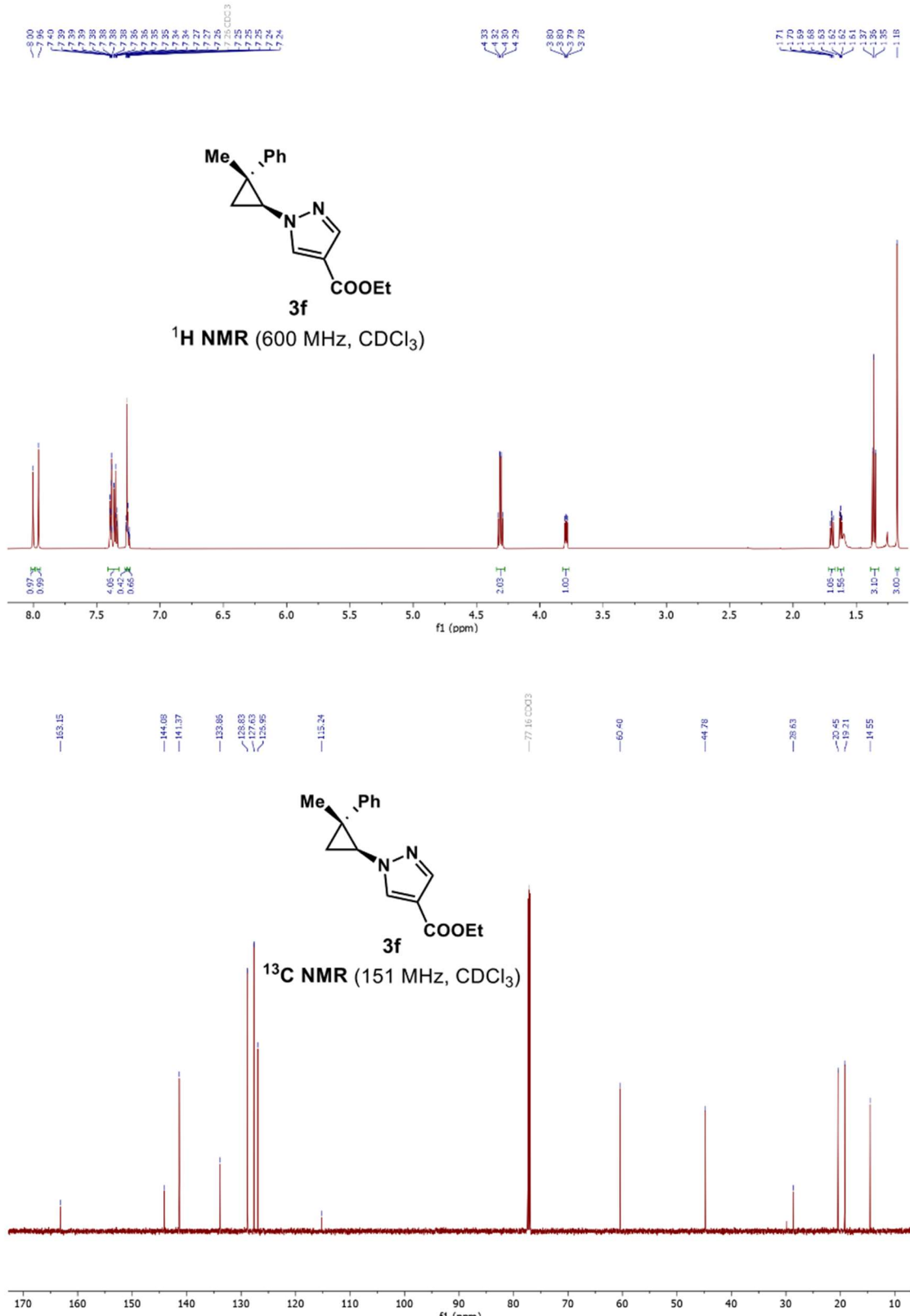
4-bromo-1-((1*S*,2*R*)-2-methyl-2-phenylcyclopropyl)-1*H*-pyrazole (3d)



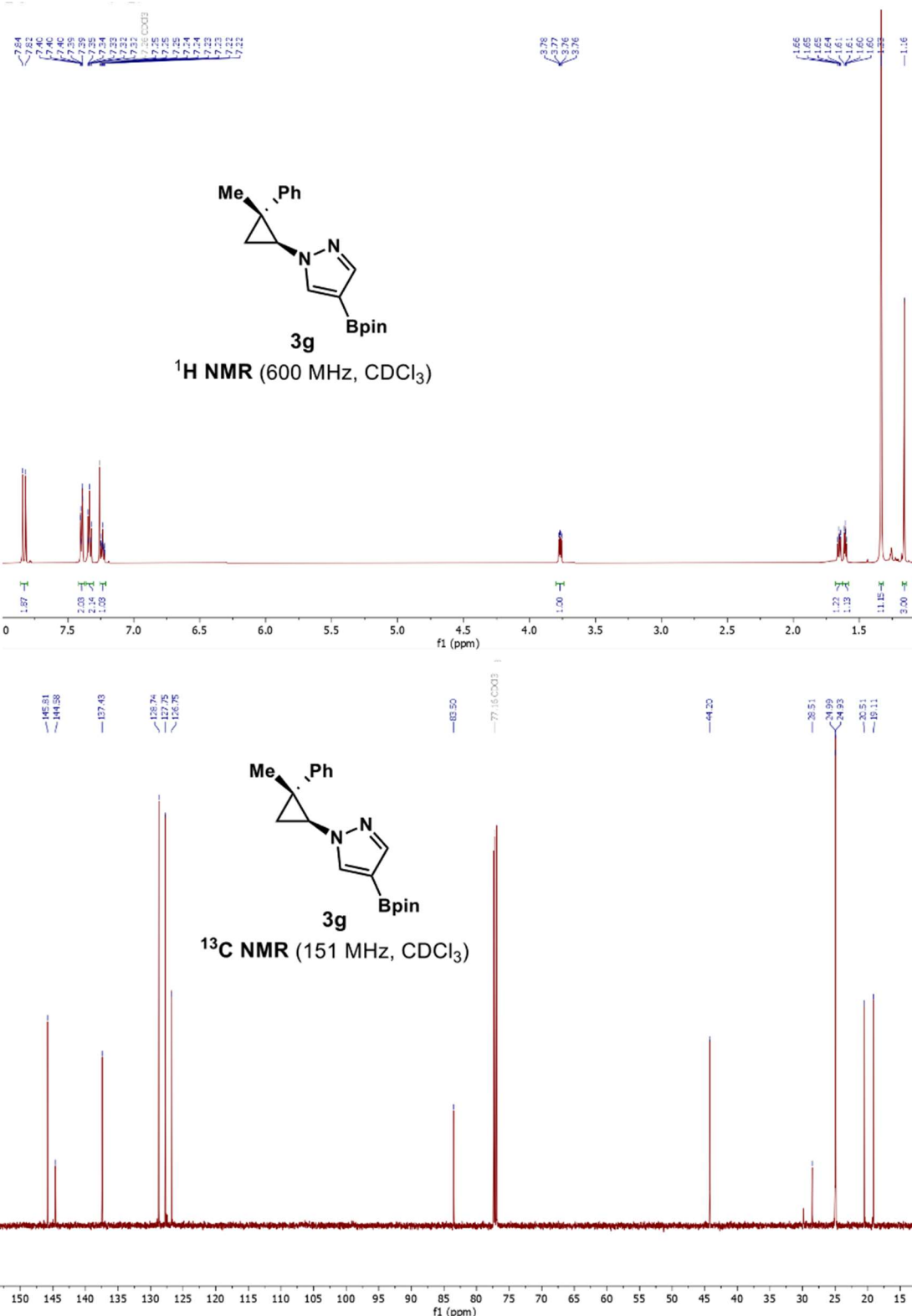
1-((1*S*,2*R*)-2-methyl-2-phenylcyclopropyl)-1*H*-pyrazole-4-carbonitrile (3e)



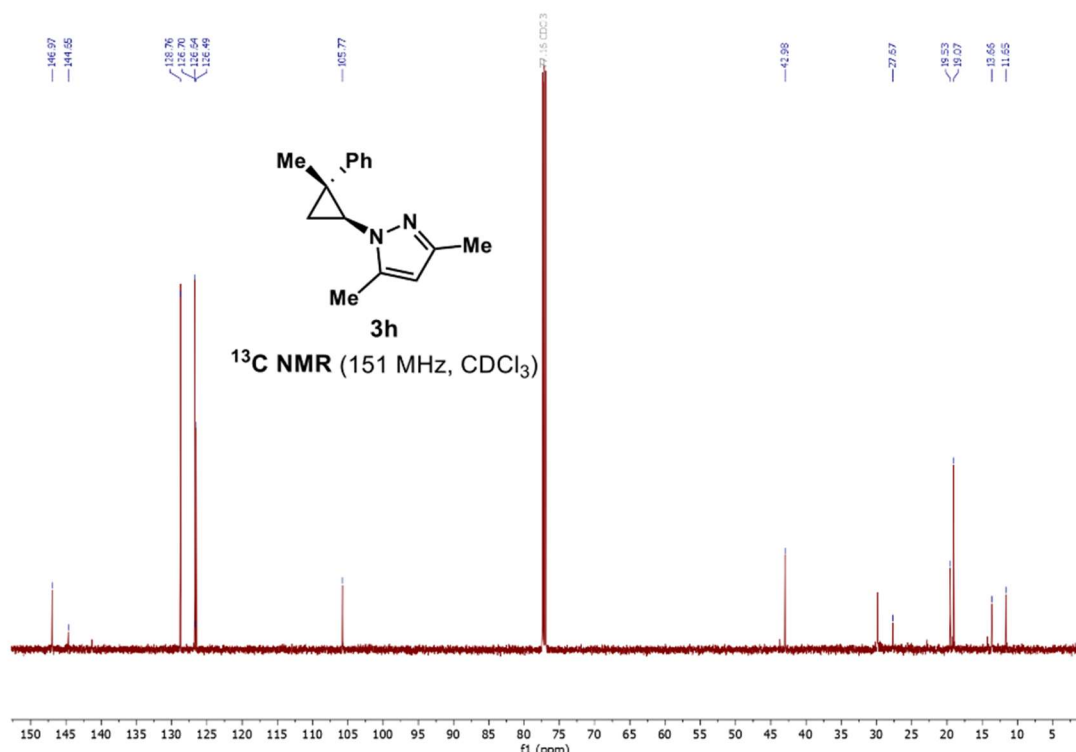
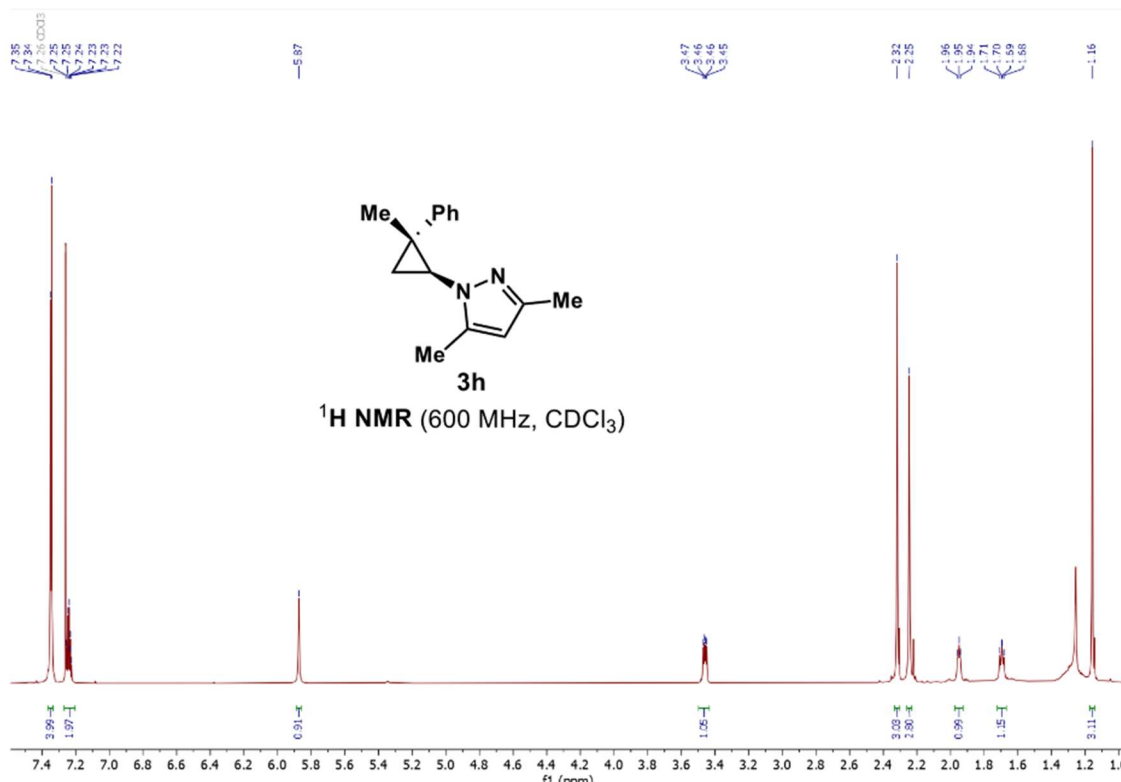
Ethyl 1-((1*S*,2*R*)-2-methyl-2-phenylcyclopropyl)-1*H*-pyrazole-4-carboxylate (3f**)**



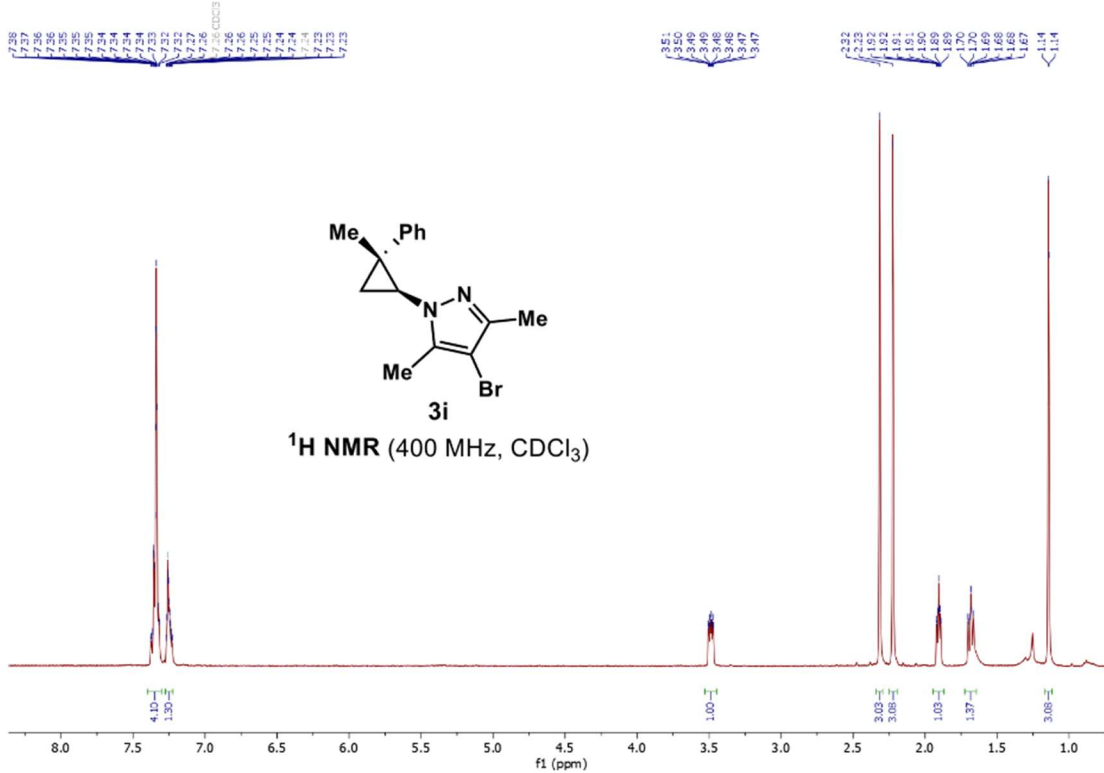
**1-((1*S*,2*R*)-2-methyl-2-phenylcyclopropyl)-4-(4,4,5,5-tetramethyl-1,3,2-dioxaborolan-2-yl)-
1*H*-pyrazole (3g)**



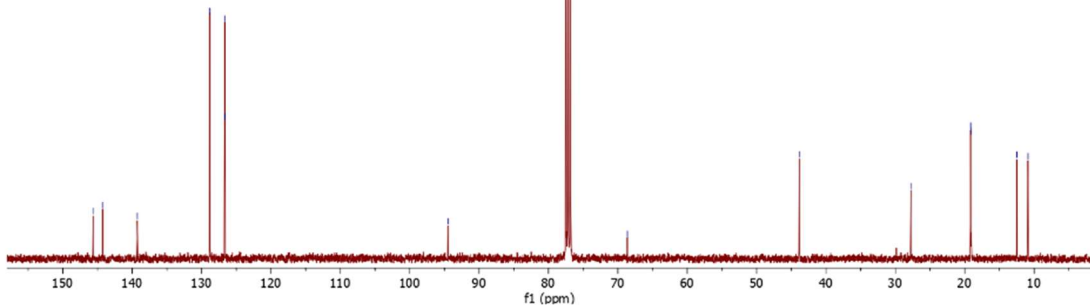
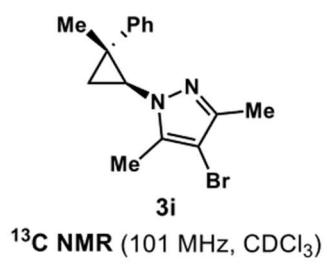
3,5-dimethyl-1-((1*S*,2*R*)-2-methyl-2-phenylcyclopropyl)-1*H*-pyrazole (3h)



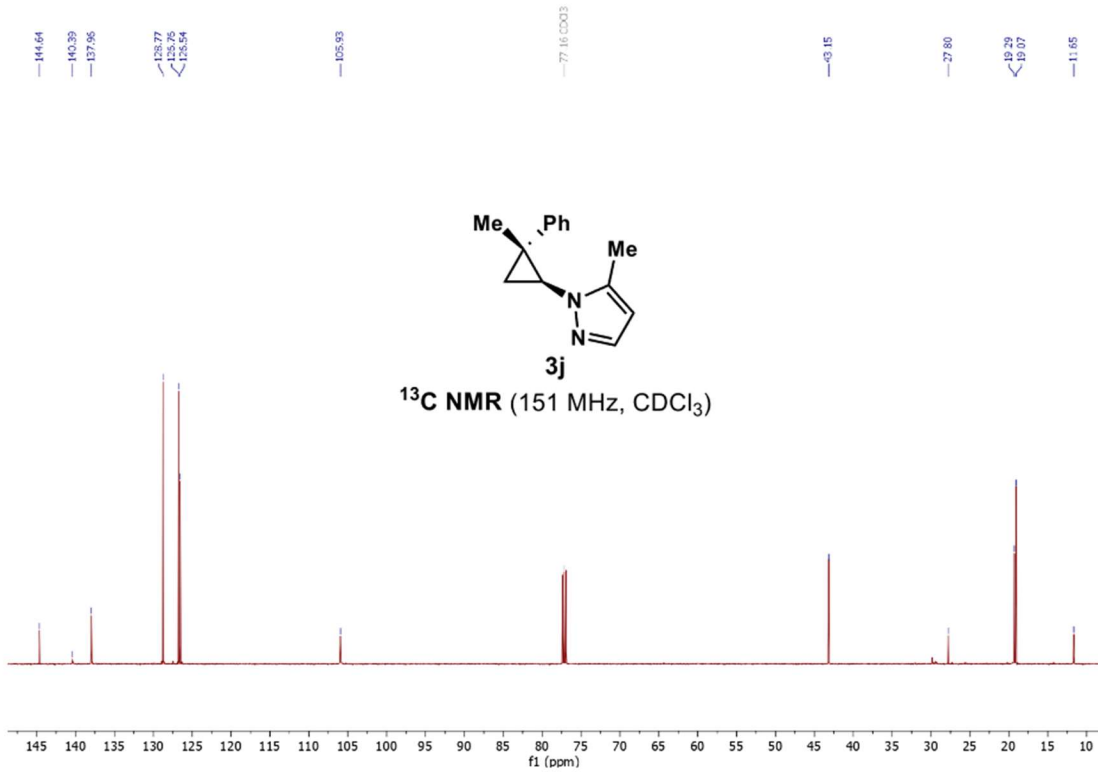
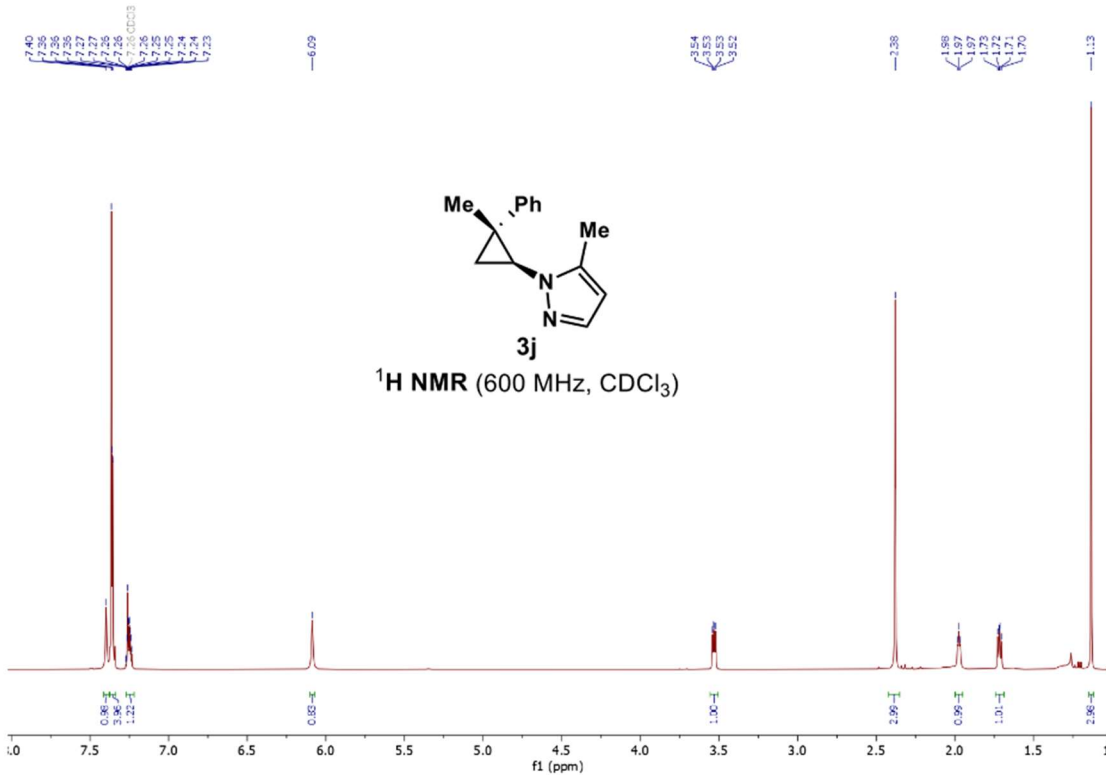
4-bromo-3,5-dimethyl-1-((1*S*,2*R*)-2-methyl-2-phenylcyclopropyl)-1*H*-pyrazole (3i)



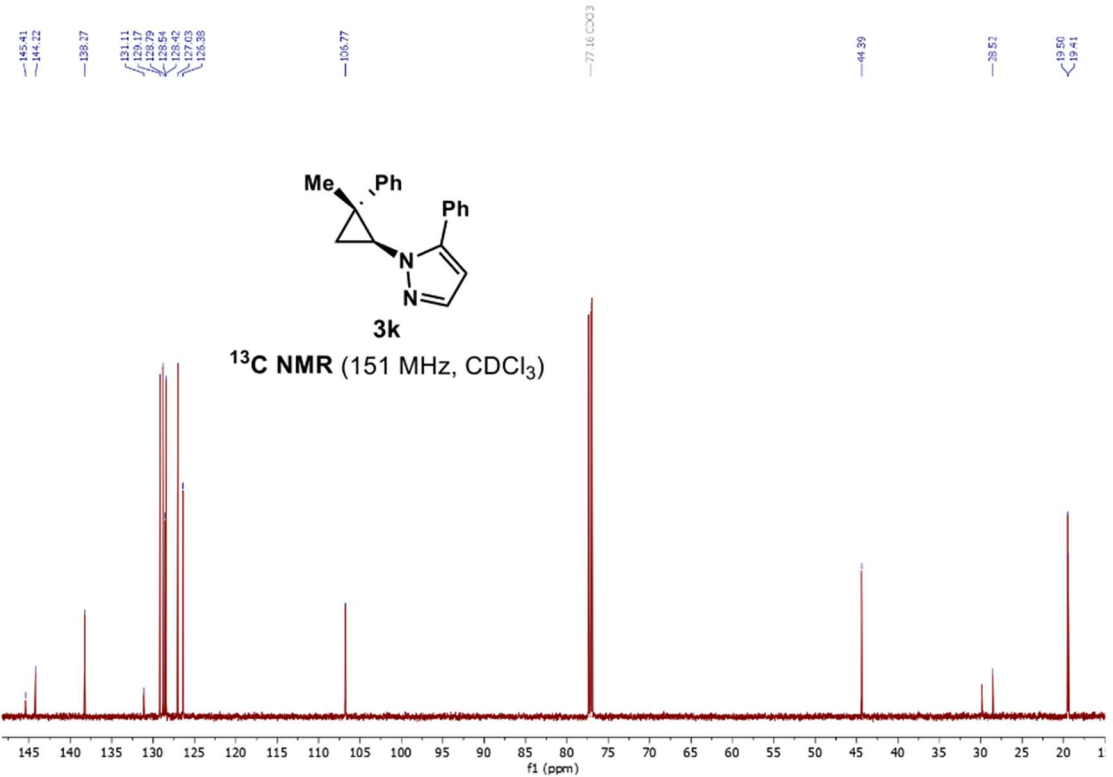
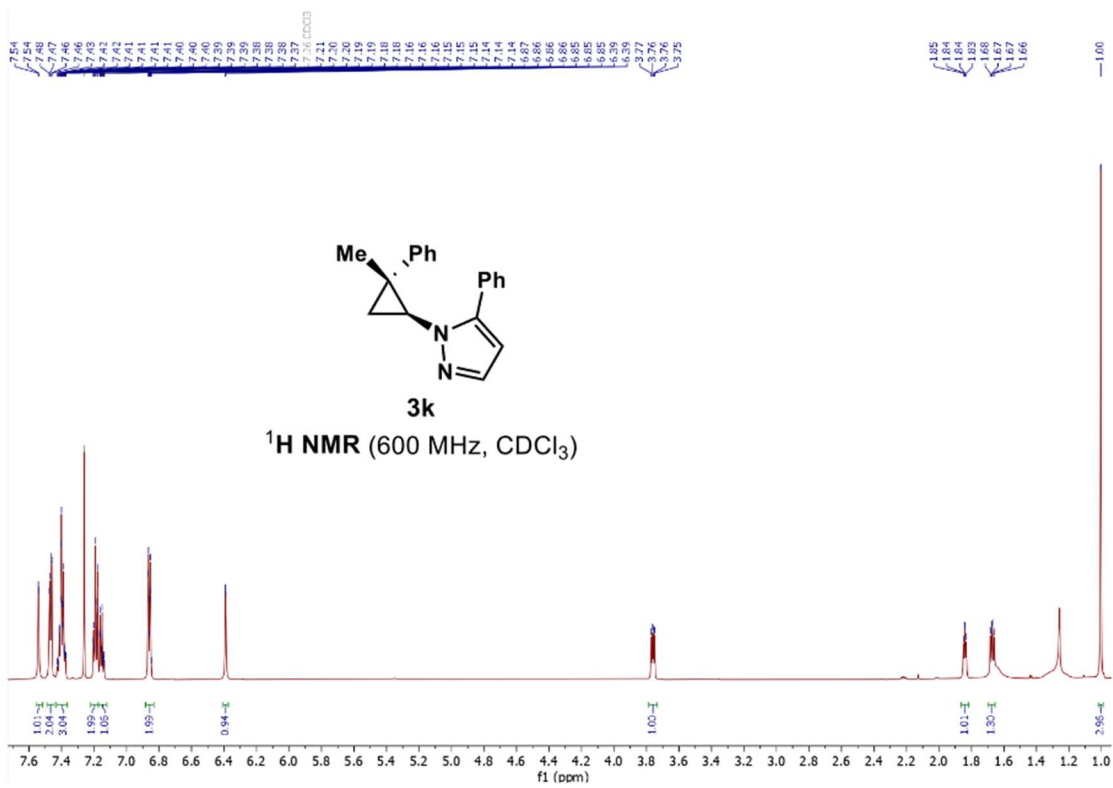
~ 145.65
 ~ 144.29
 ~ 139.26
 ~ 128.81
 ~ 128.67
 ~ 125.63
 ~ 94.49
 $\sim 77.16 \text{ CDCl}_3$
 ~ 68.63
 ~ 53.94
 ~ 27.77
 ~ 19.15
 ~ 19.08
 ~ 12.50
 ~ 10.88



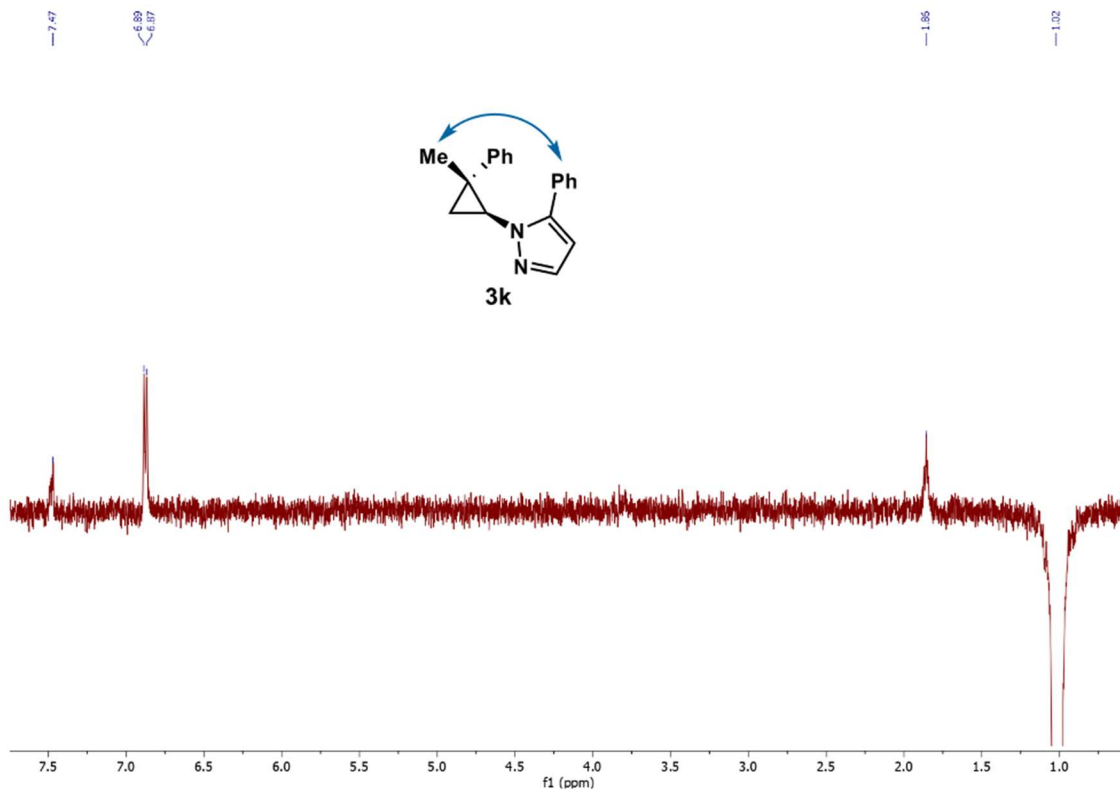
3-methyl-1-((1*S*,2*R*)-2-methyl-2-phenylcyclopropyl)-1*H*-pyrazole (3j)



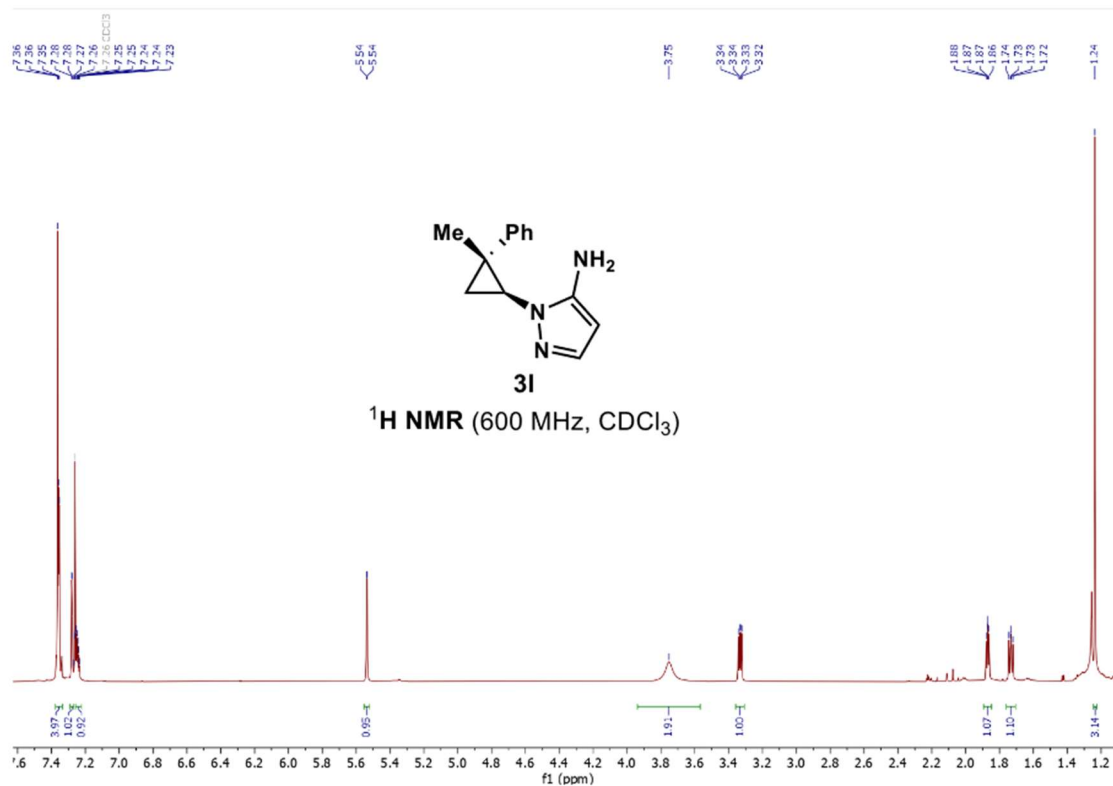
1-((1*S*,2*R*)-2-methyl-2-phenylcyclopropyl)-3-phenyl-1*H*-pyrazole (3k)



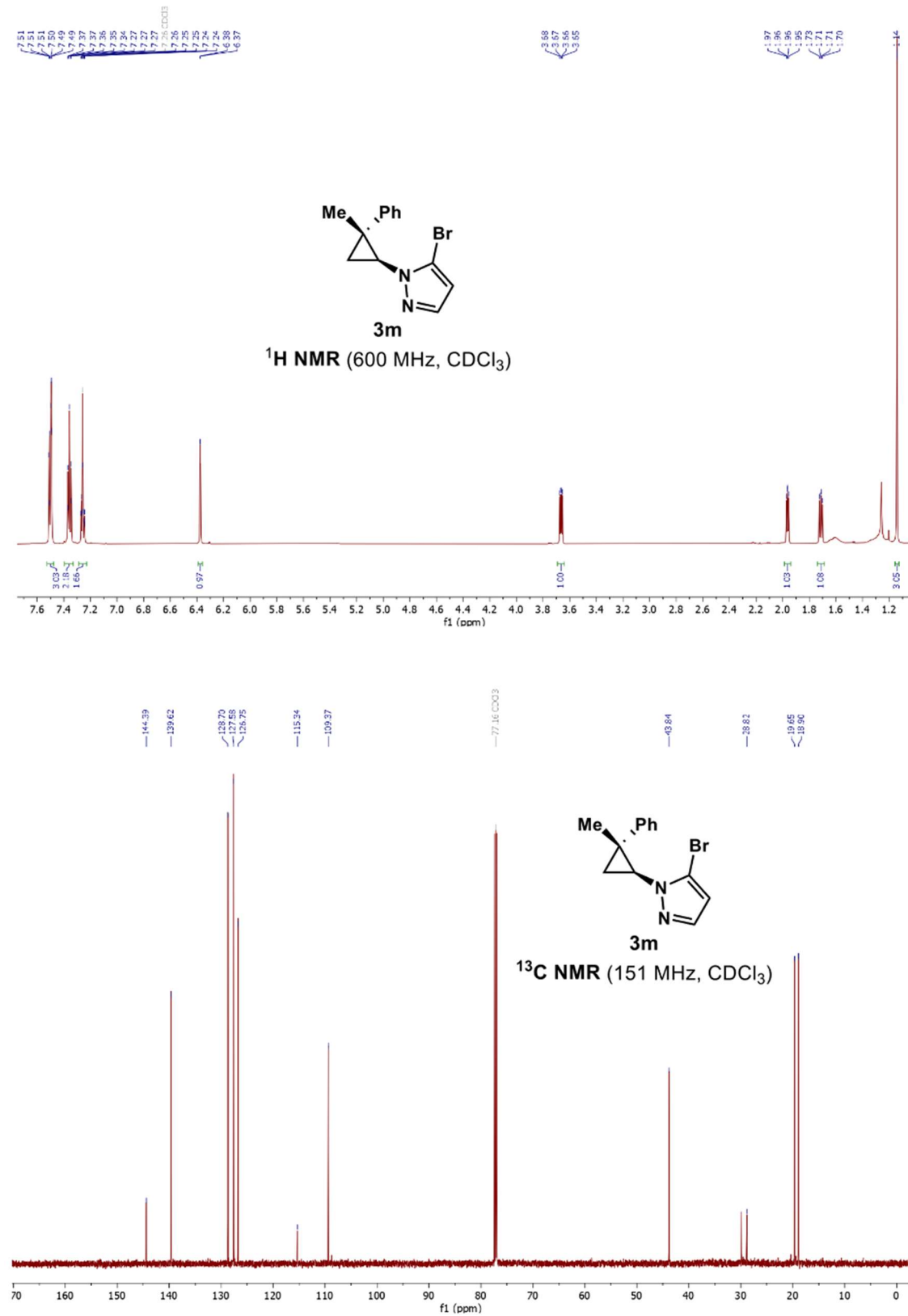
NOE-Experiment



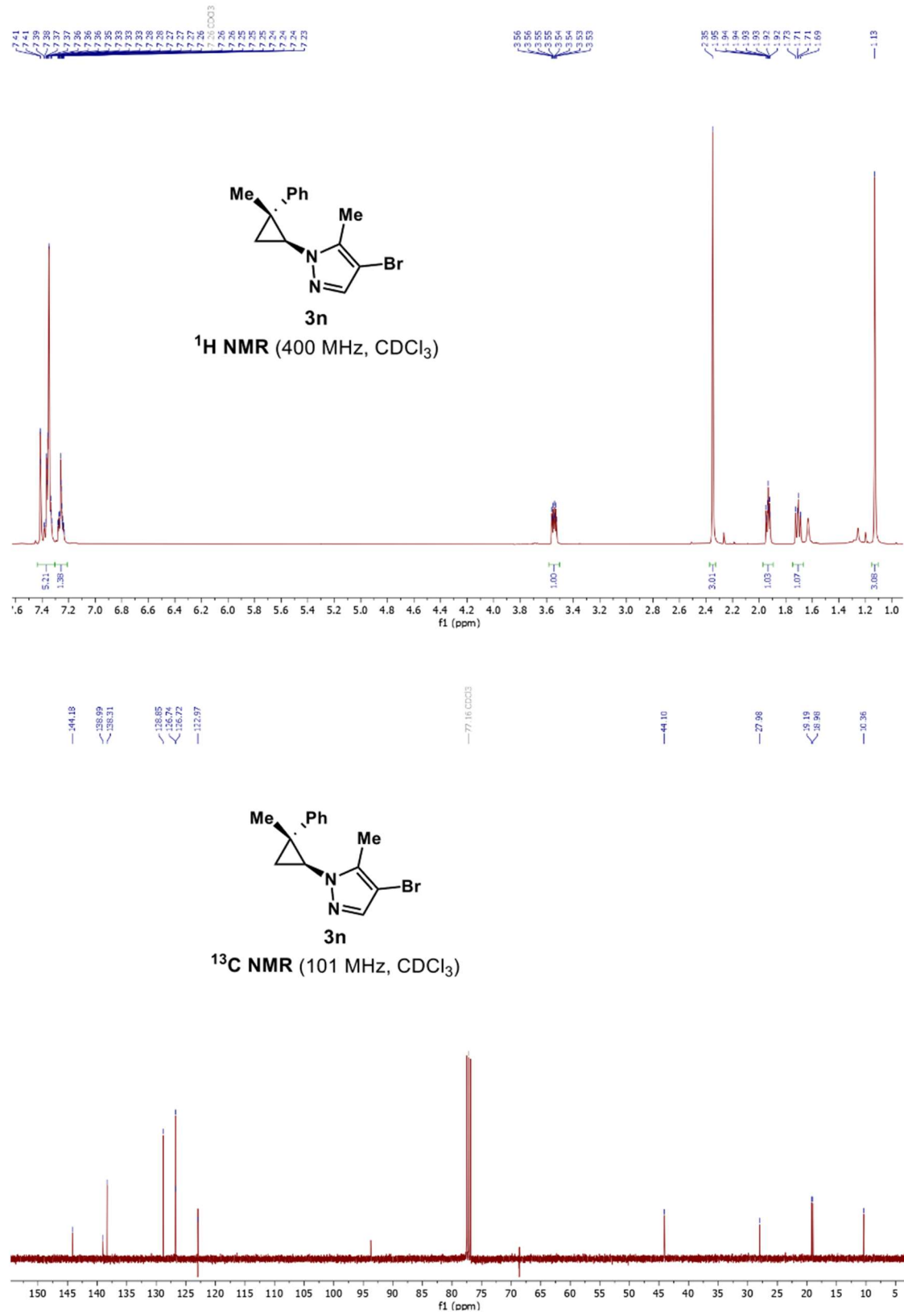
1-((1*S*,2*R*)-2-methyl-2-phenylcyclopropyl)-1*H*-pyrazol-3-amine (3l)



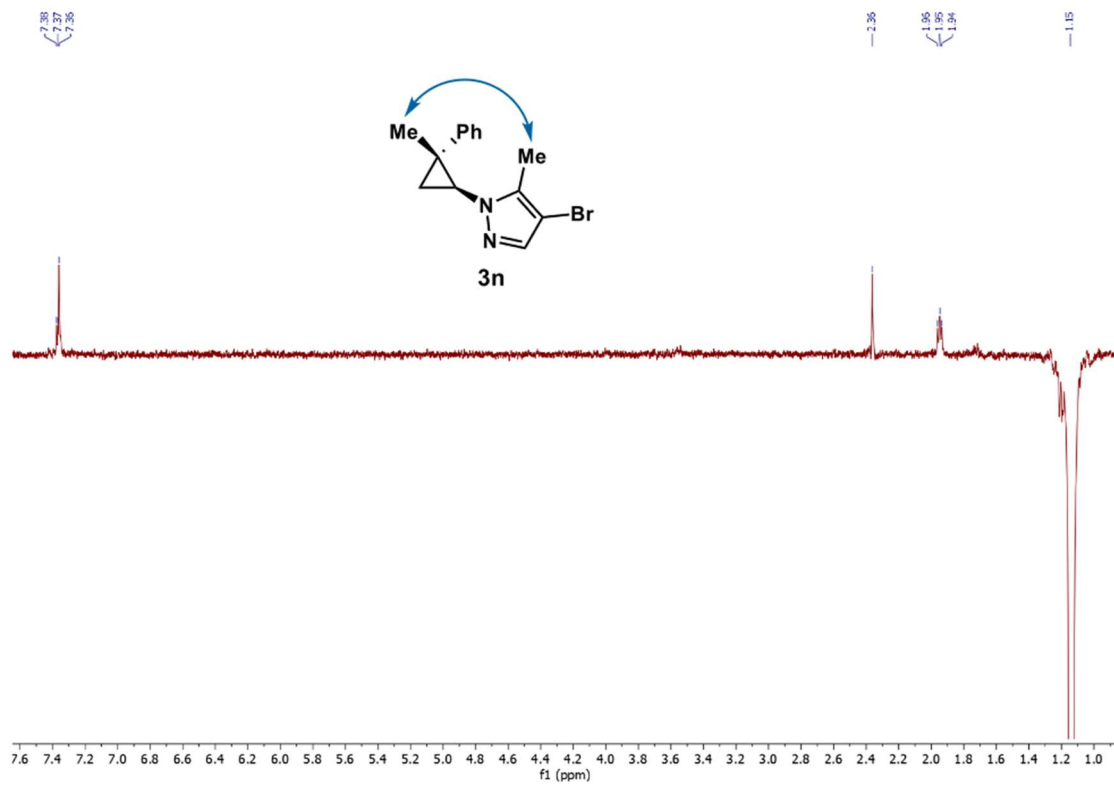
3-bromo-1-((1*S*,2*R*)-2-methyl-2-phenylcyclopropyl)-1*H*-pyrazole (3m)



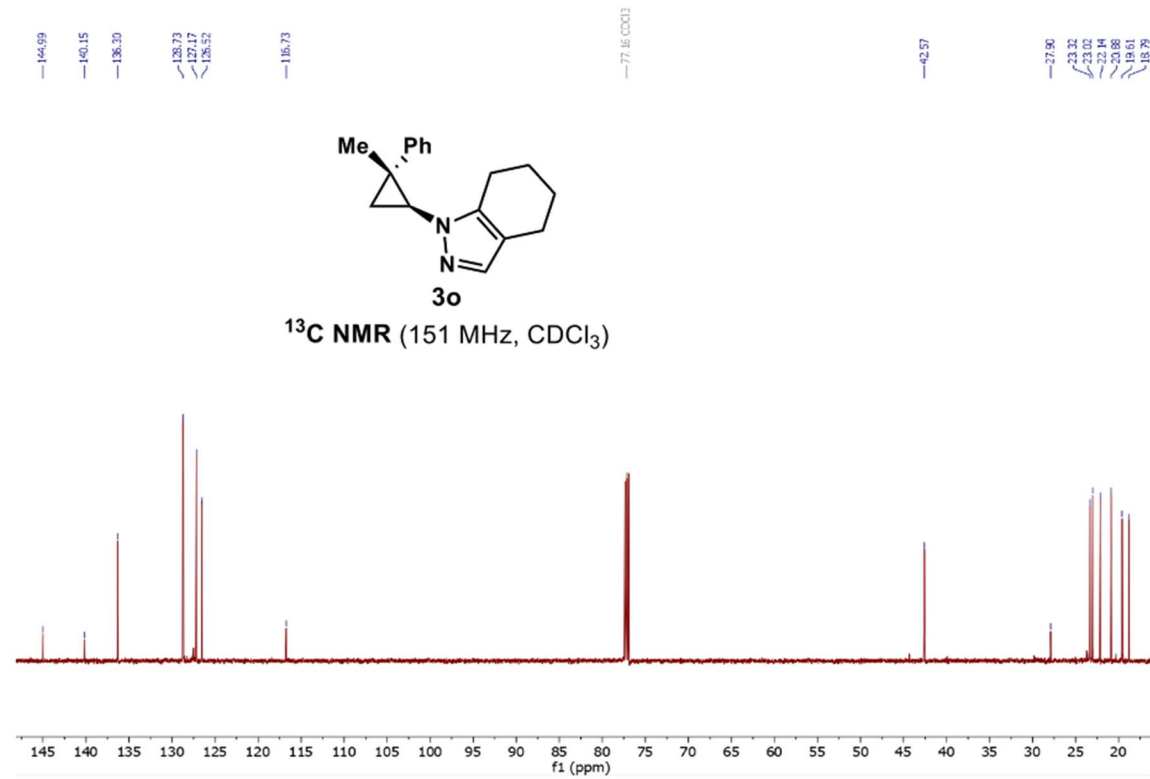
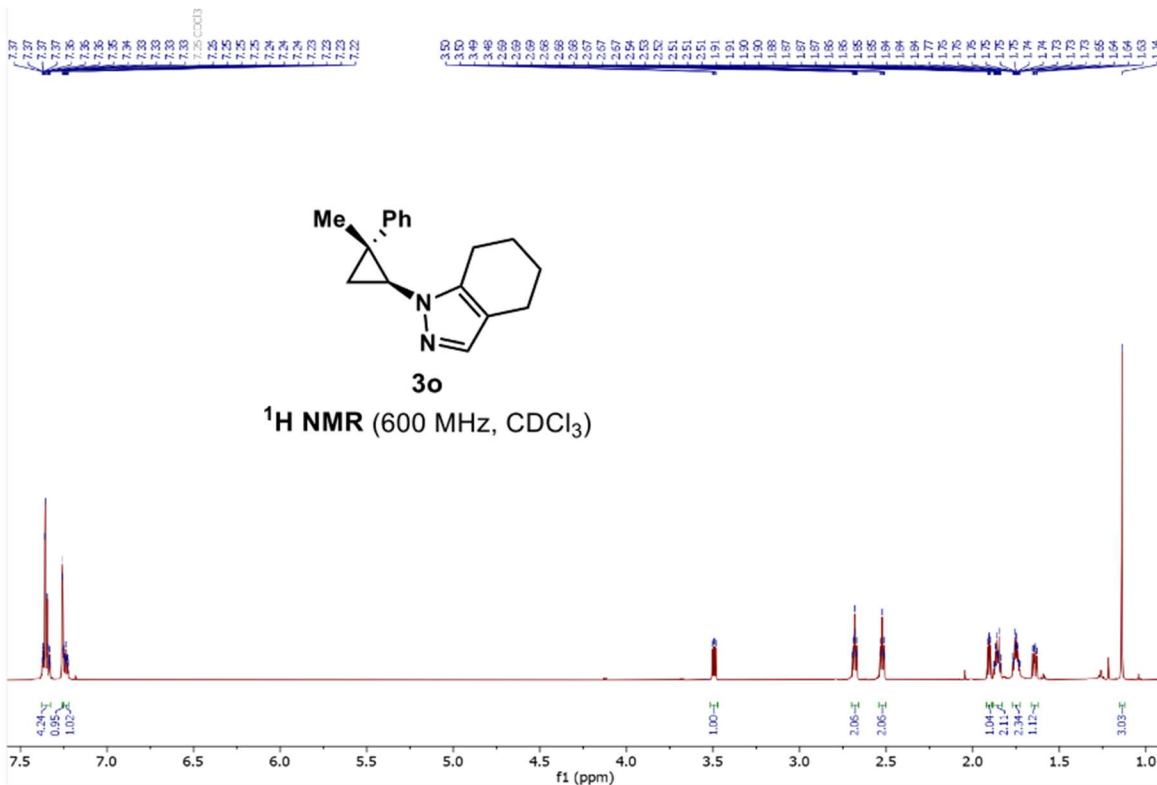
4-bromo-3-methyl-1-((1*S*,2*R*)-2-methyl-2-phenylcyclopropyl)-1*H*-pyrazole (3n)



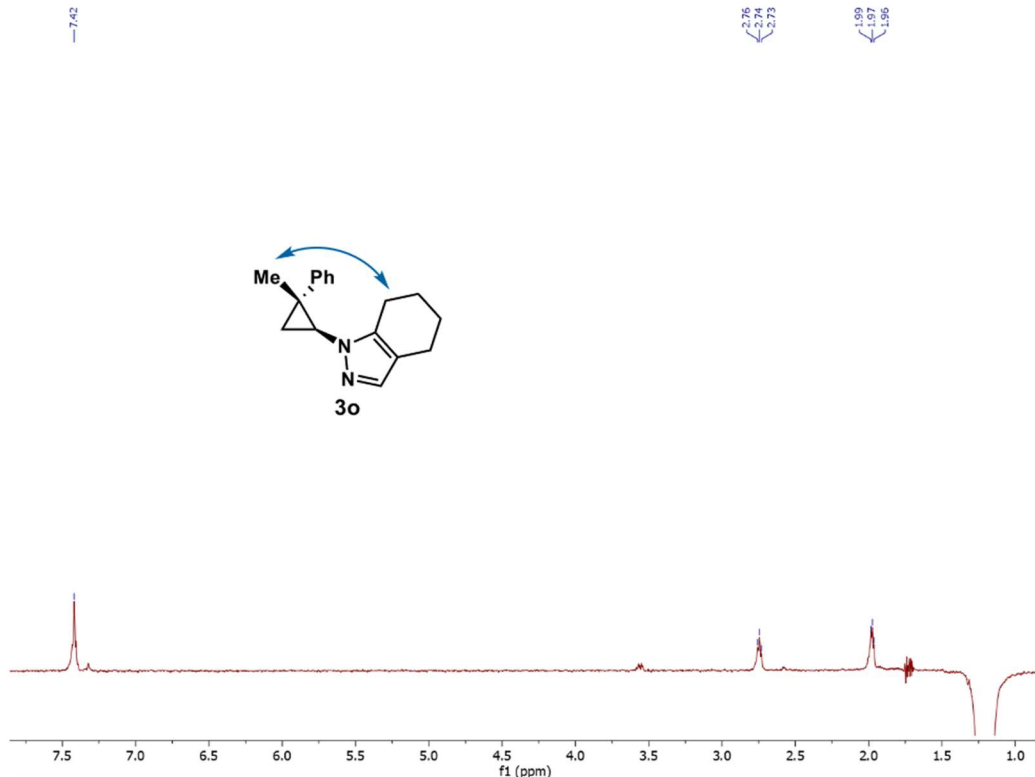
NOE-Experiment



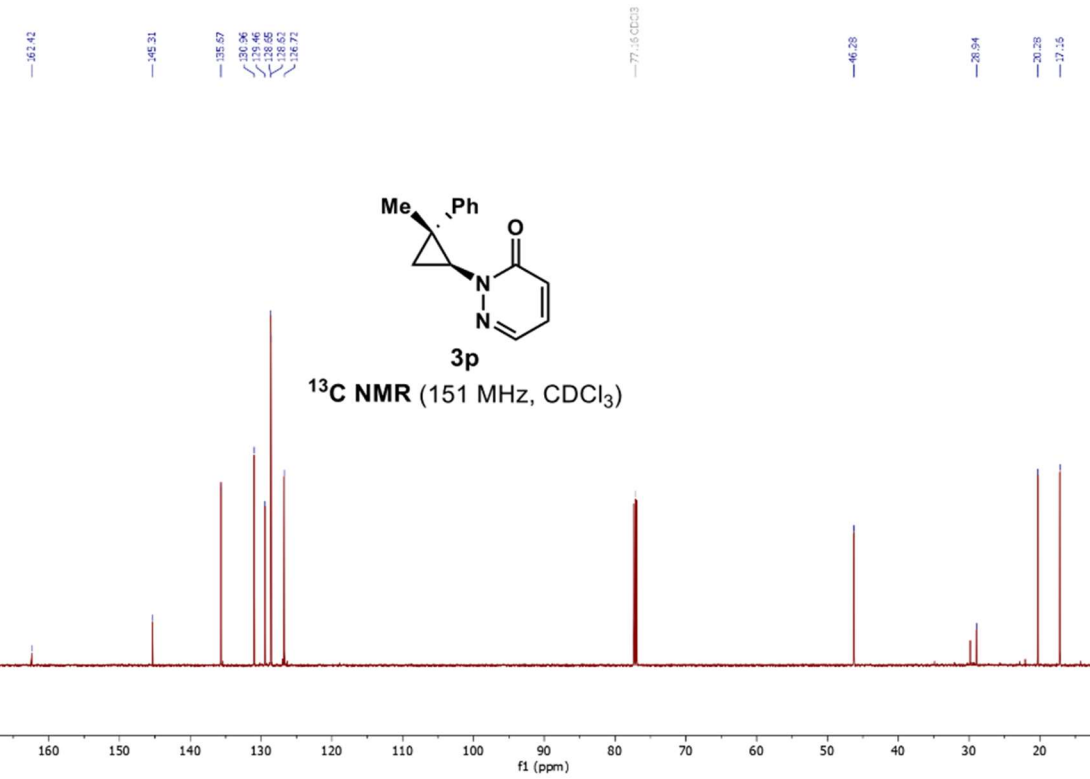
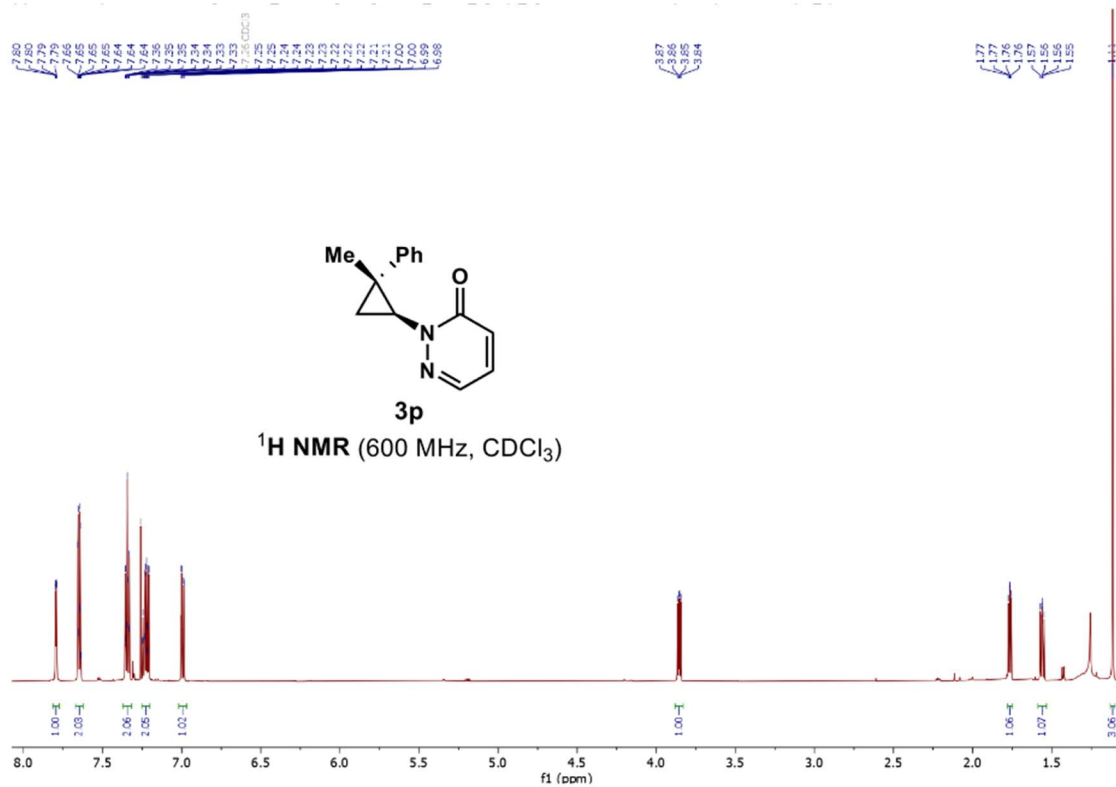
2-((1*S*,2*R*)-2-methyl-2-phenylcyclopropyl)-4,5,6,7-tetrahydro-2*H*-indazole (3o)



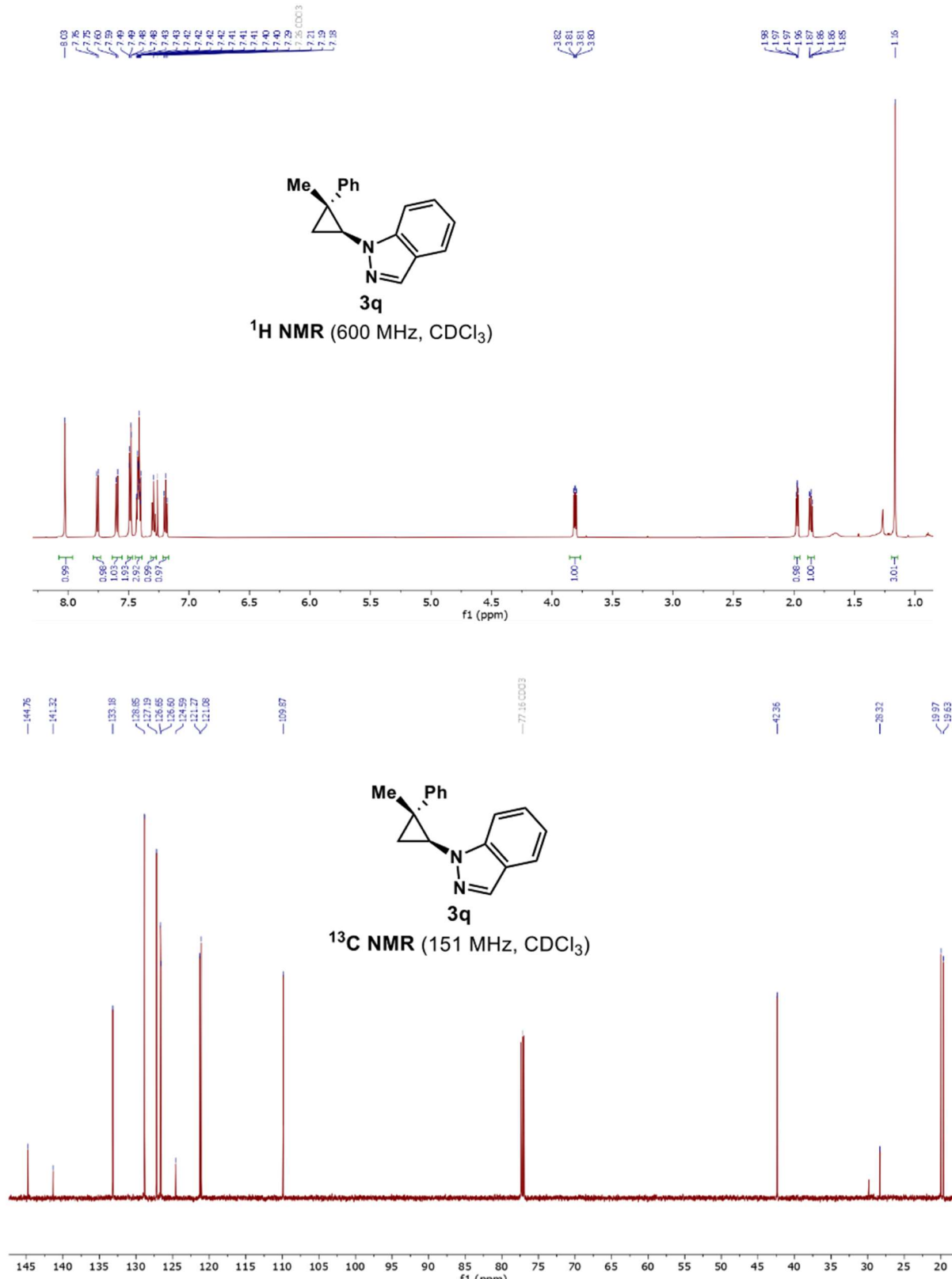
NOE-Experiment



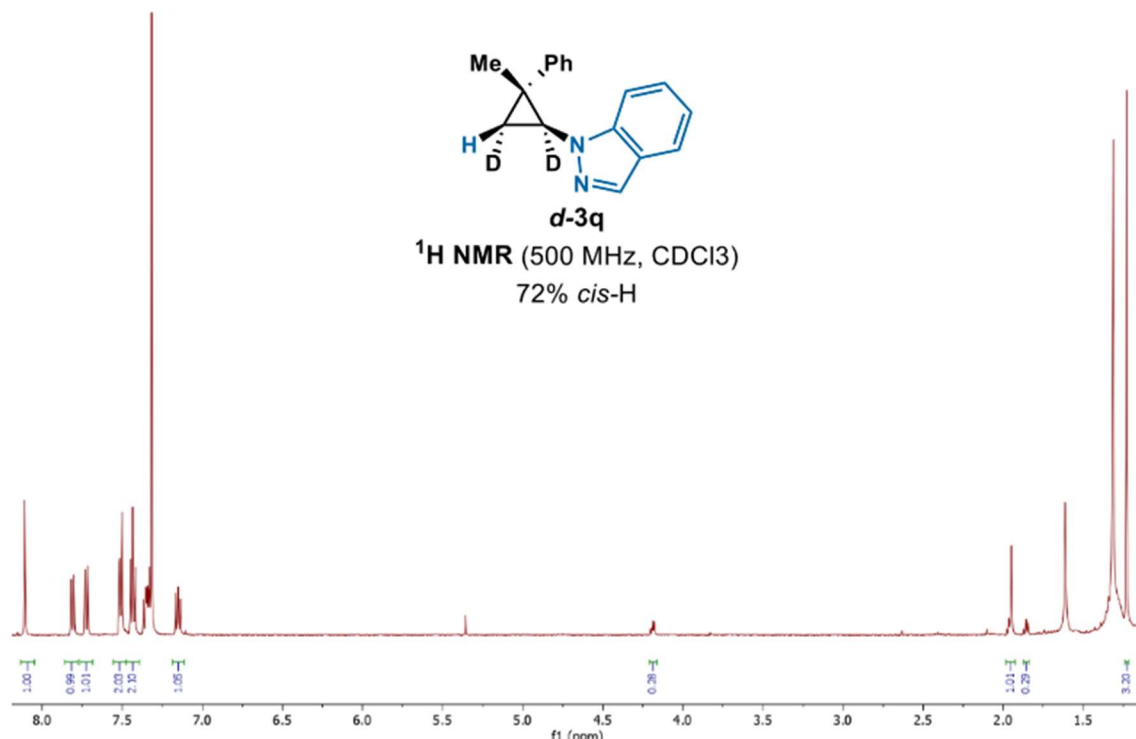
2-((1*S*,2*R*)-2-methyl-2-phenylcyclopropyl)pyridazin-3(2*H*)-one (3p)



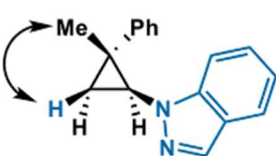
2-((1*S*,2*R*)-2-methyl-2-phenylcyclopropyl)-2*H*-indazole (3q)



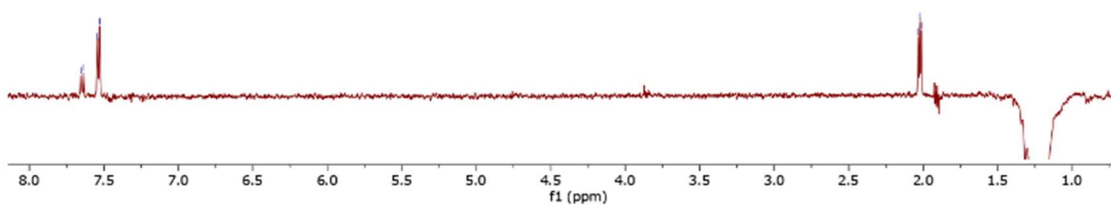
2-((1*S*,2*R*)-2-methyl-2-phenylcyclopropyl-1,3-²H₂)-1*H*-indazole (*d*-3q)



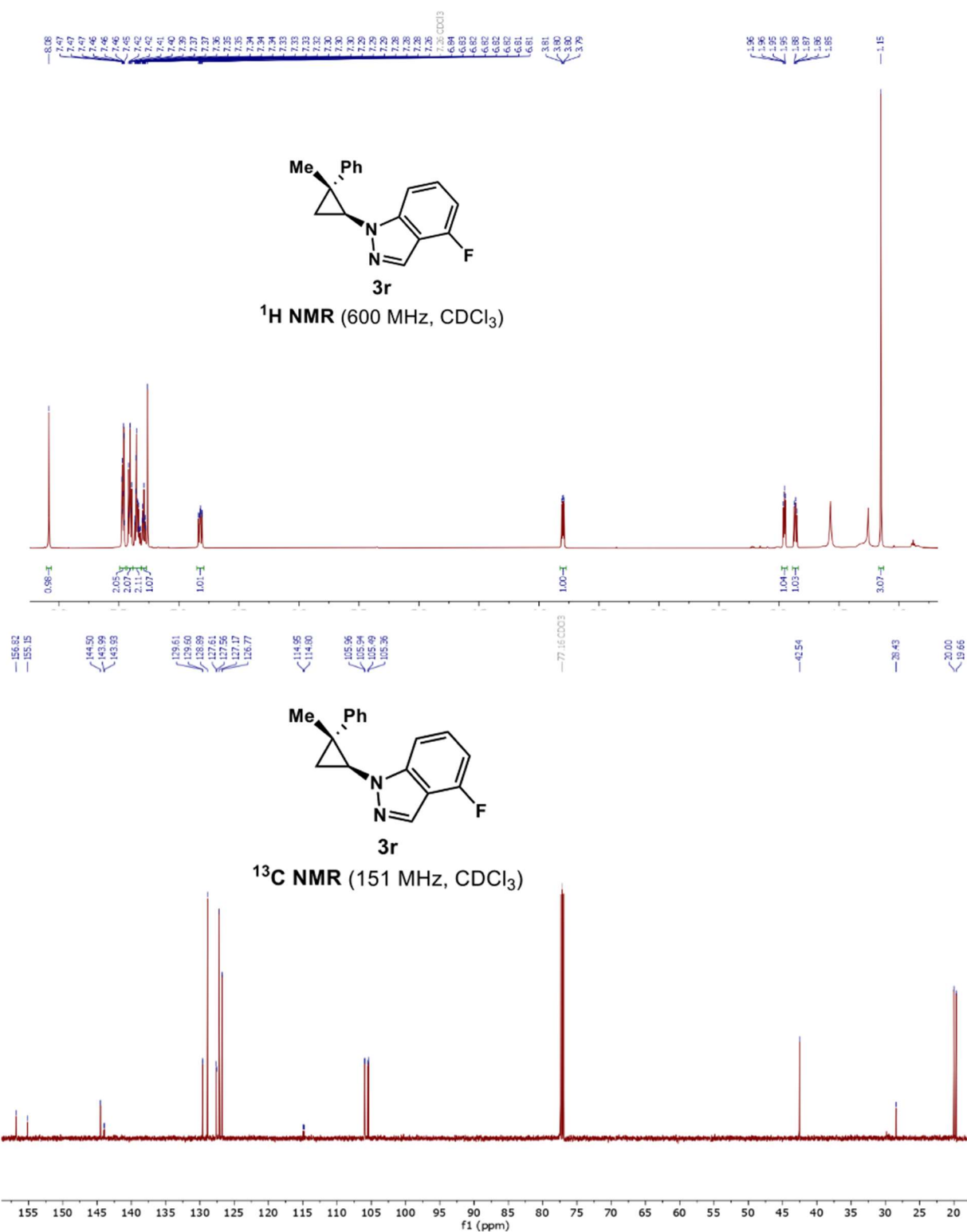
NOE Experiment



Proof of *syn*-addition
NOE Experiment on
3q

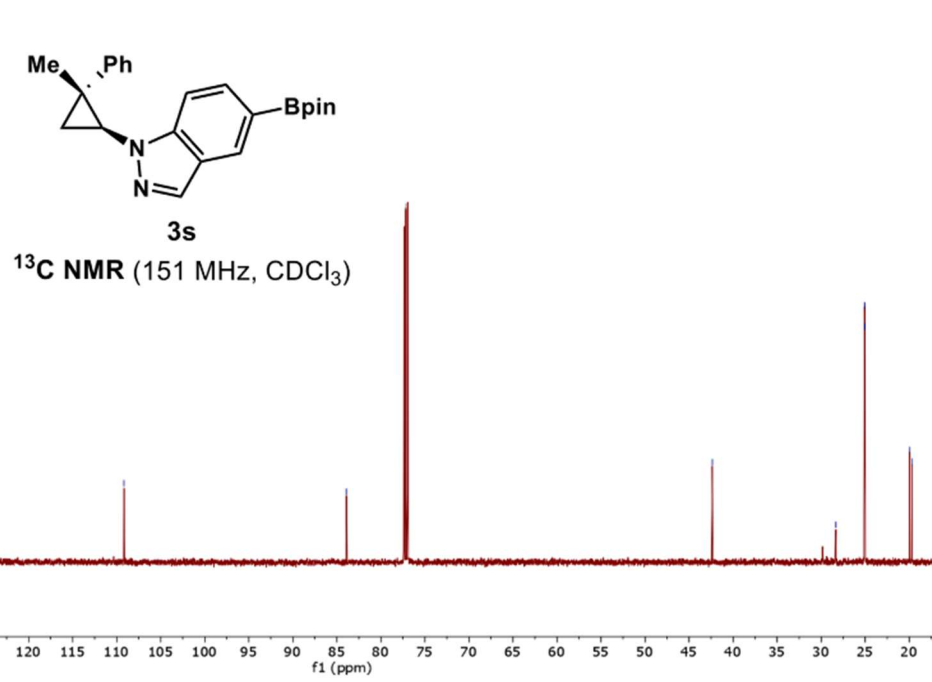
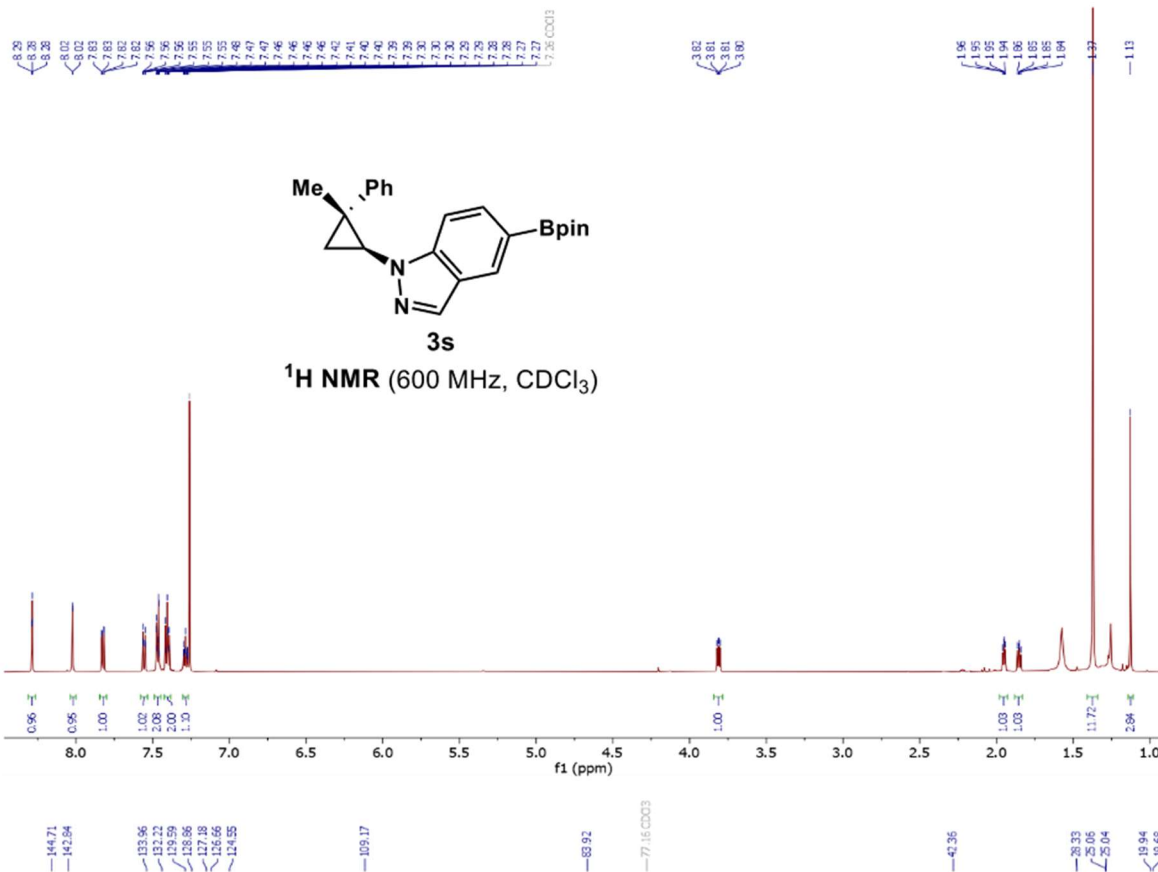


4-fluoro-2-((1*S*,2*R*)-2-methyl-2-phenylcyclopropyl)-2*H*-indazole (3r)

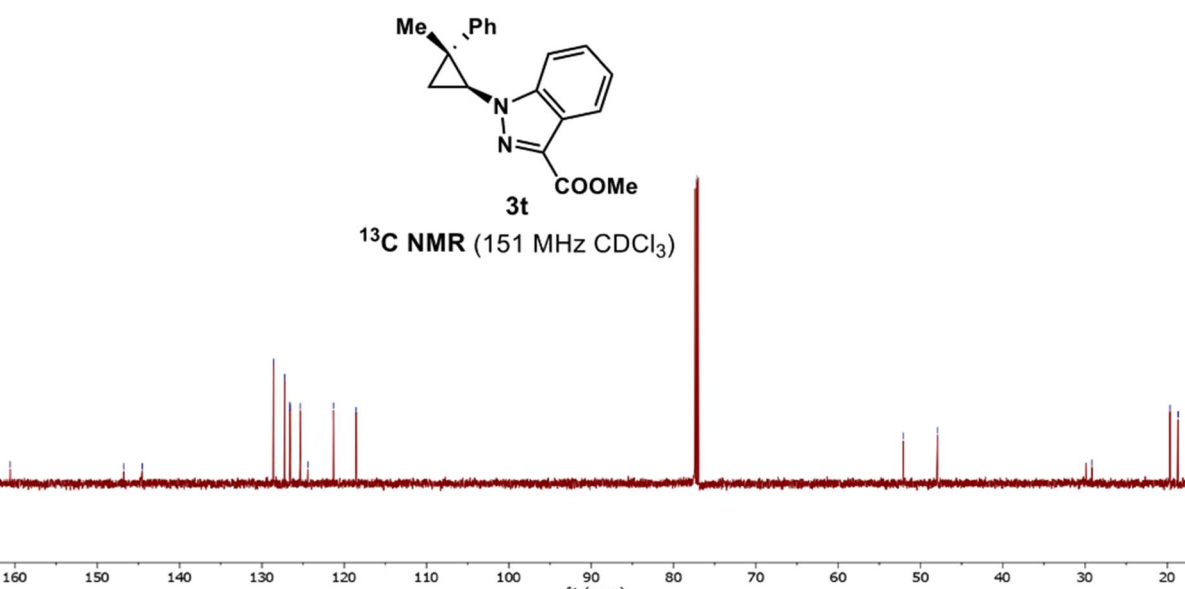
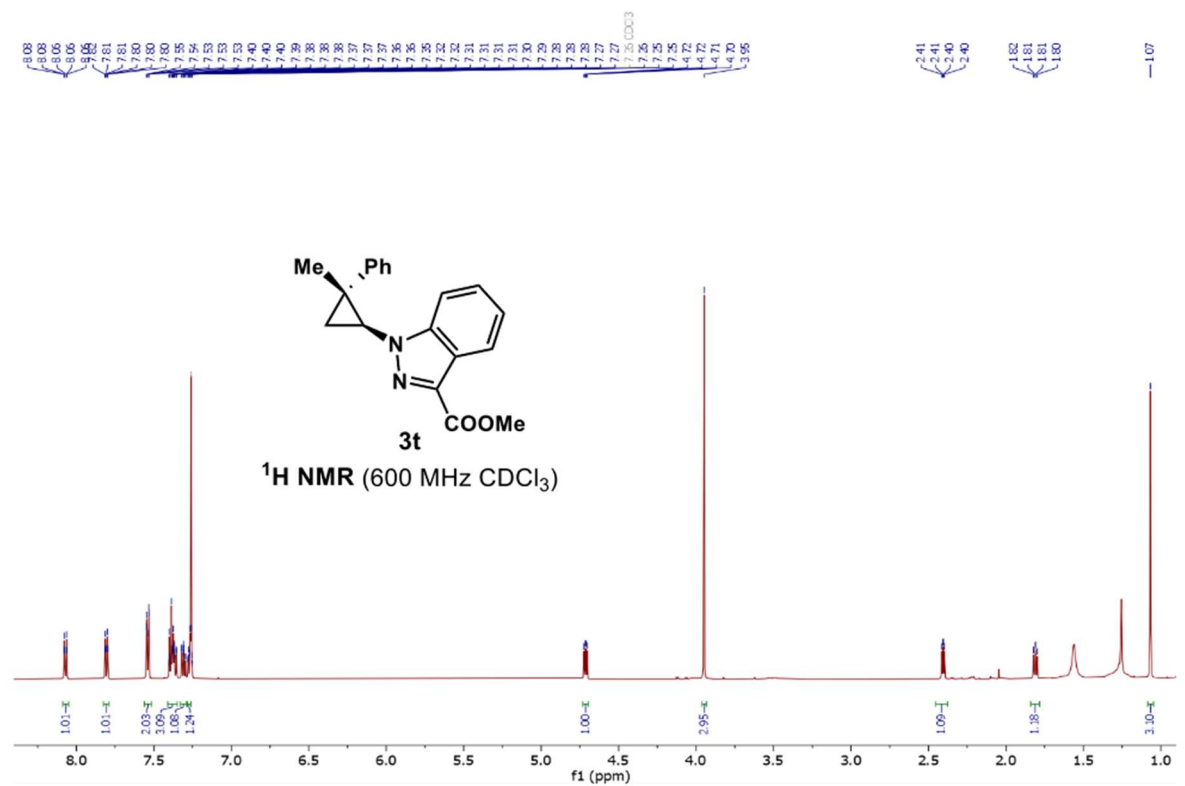


**2-((1*S*,2*R*)-2-methyl-2-phenylcyclopropyl)-5-(4,4,5,5-tetramethyl-1,3,2-dioxaborolan-2-yl)-
2*H*-indazole (3s)**

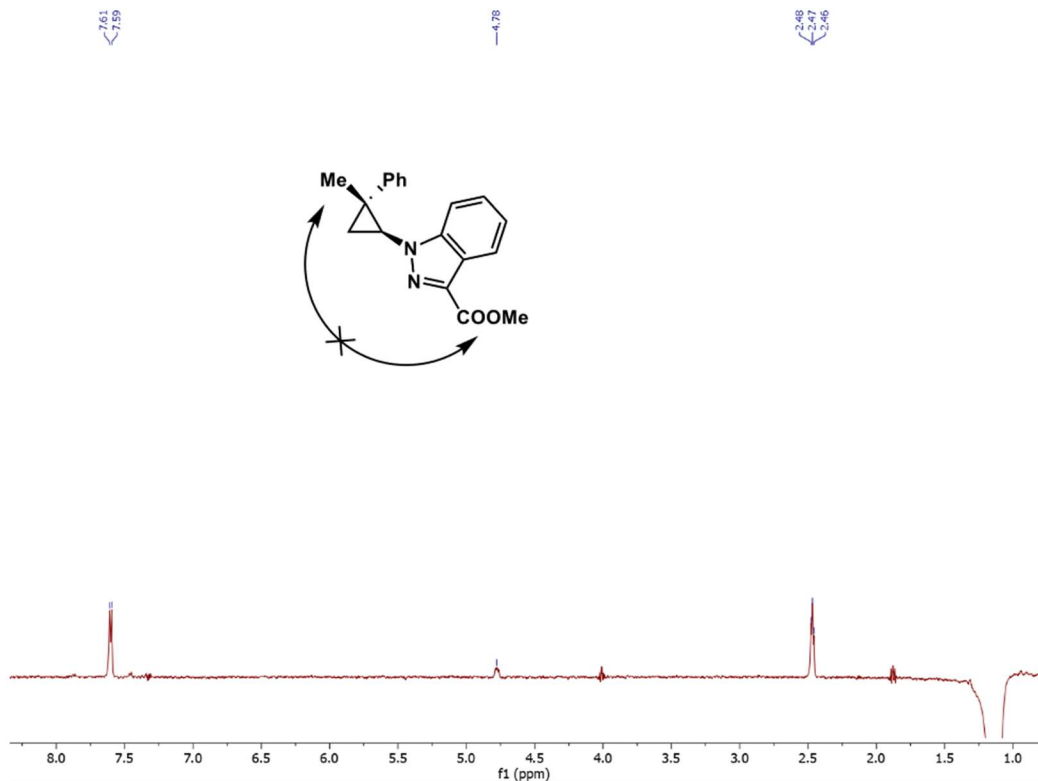
2*H*-indazole (3s)



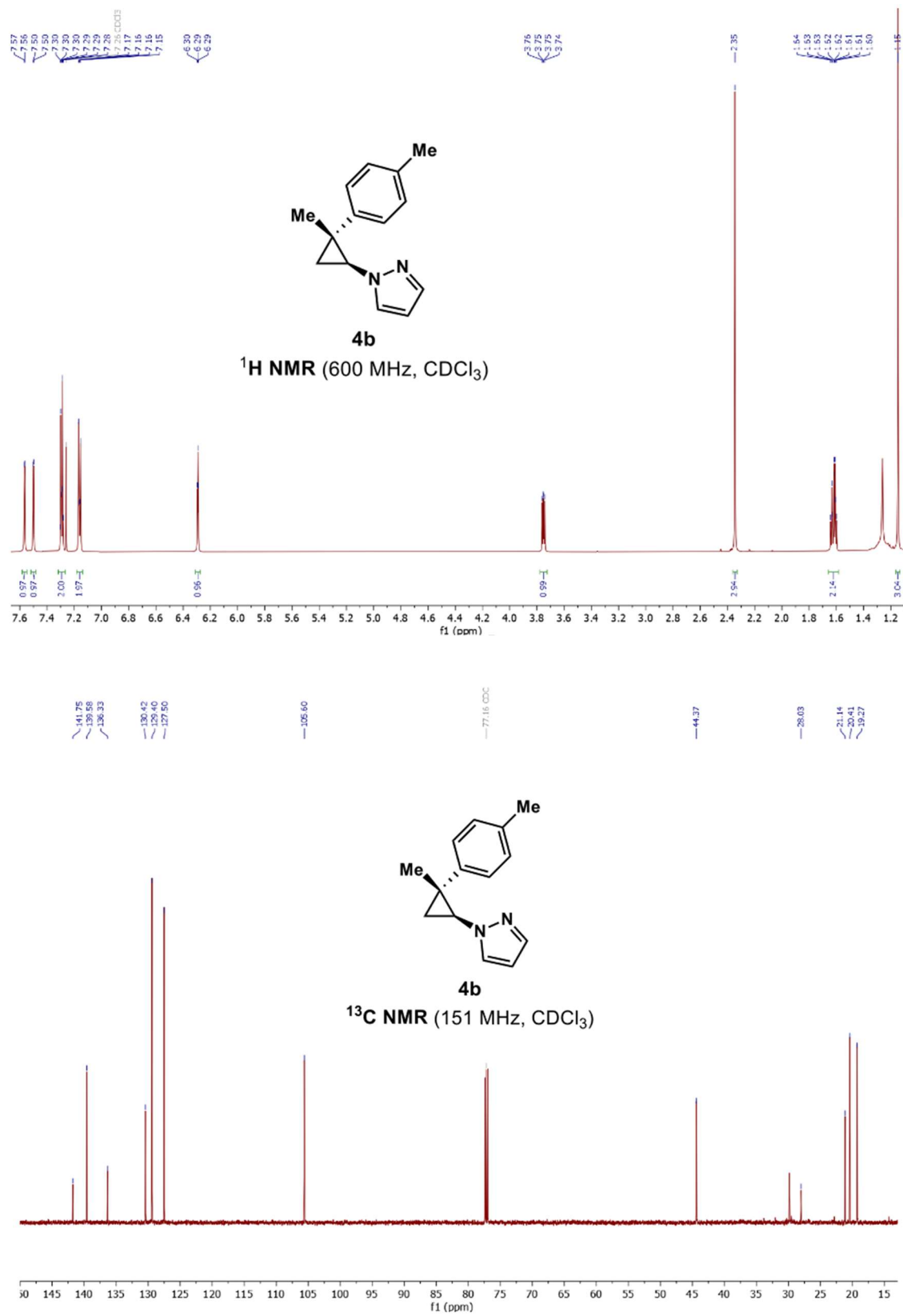
Methyl 2-((1*S*,2*R*)-2-methyl-2-phenylcyclopropyl)-2*H*-indazole-3-carboxylate (3t**)**



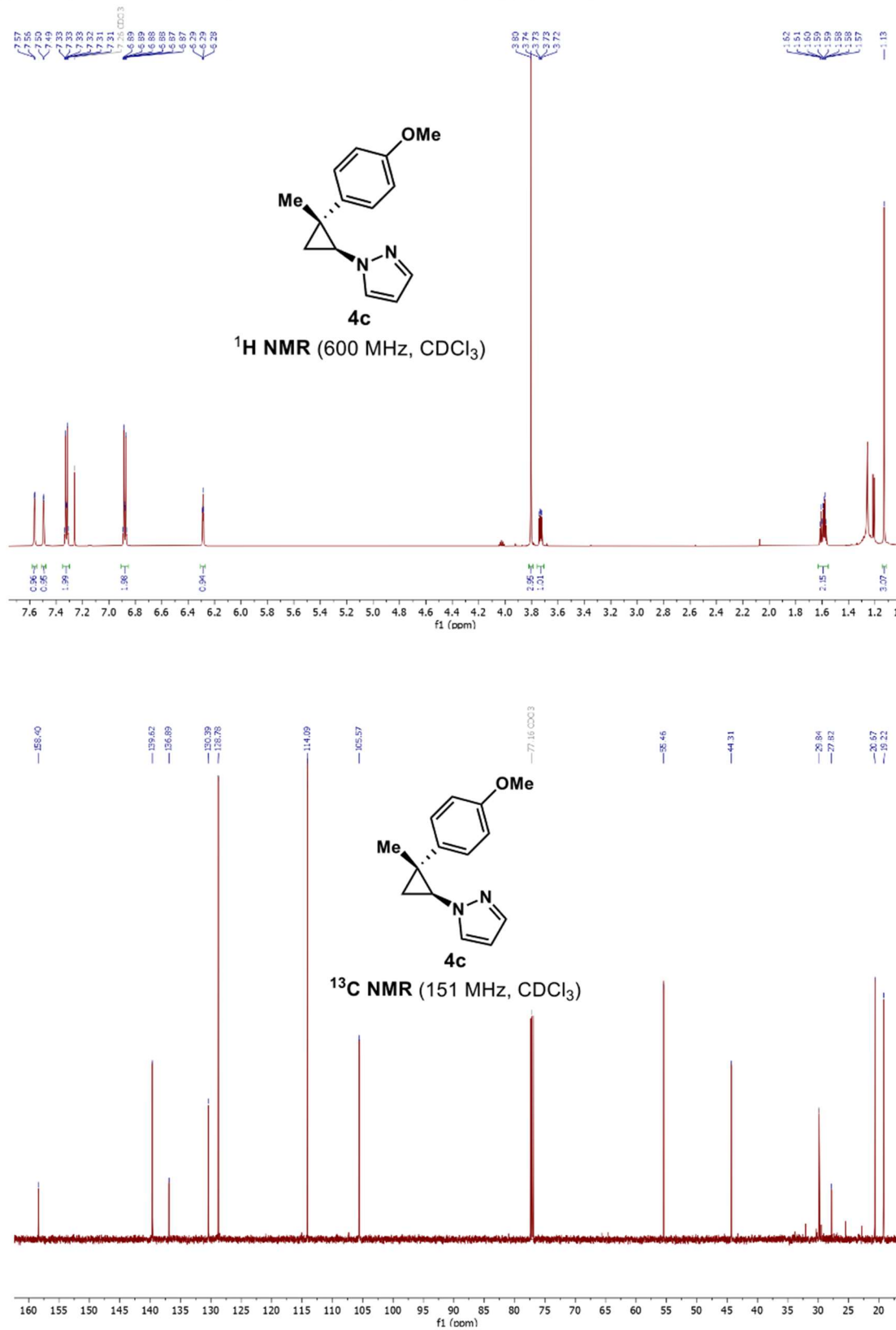
NOE-Experiment



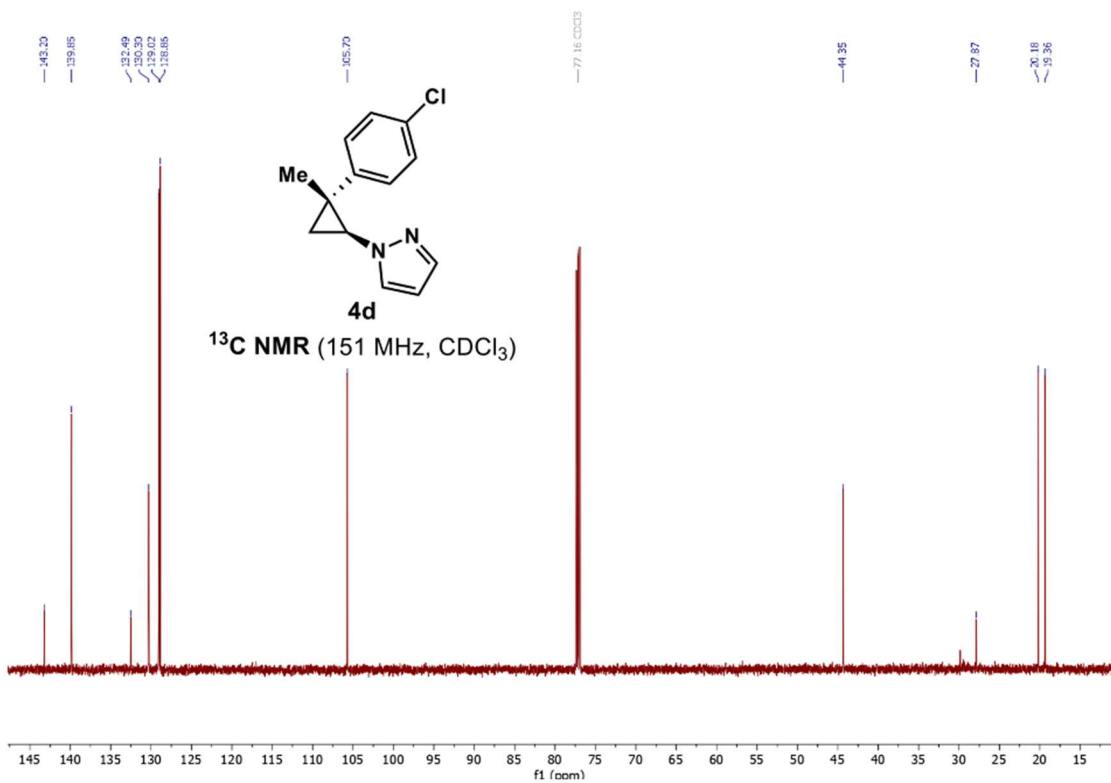
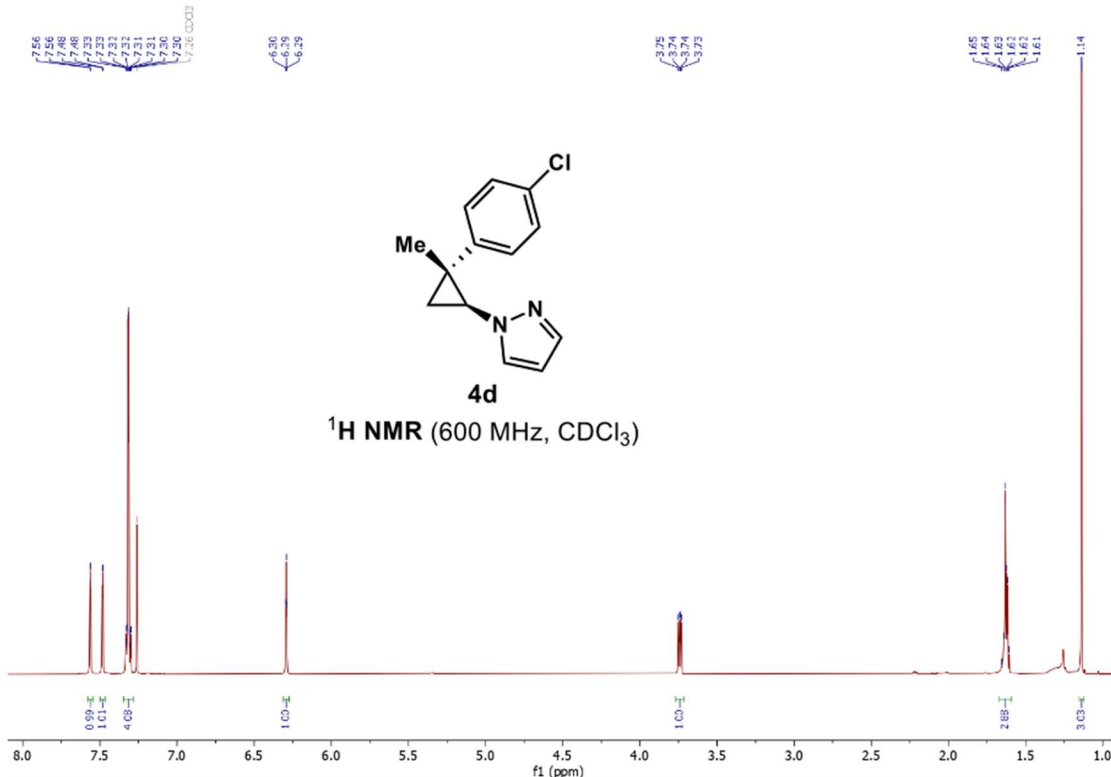
1-((1*S*,2*R*)-2-methyl-2-(*p*-tolyl)cyclopropyl)-1*H*-pyrazole (4b)



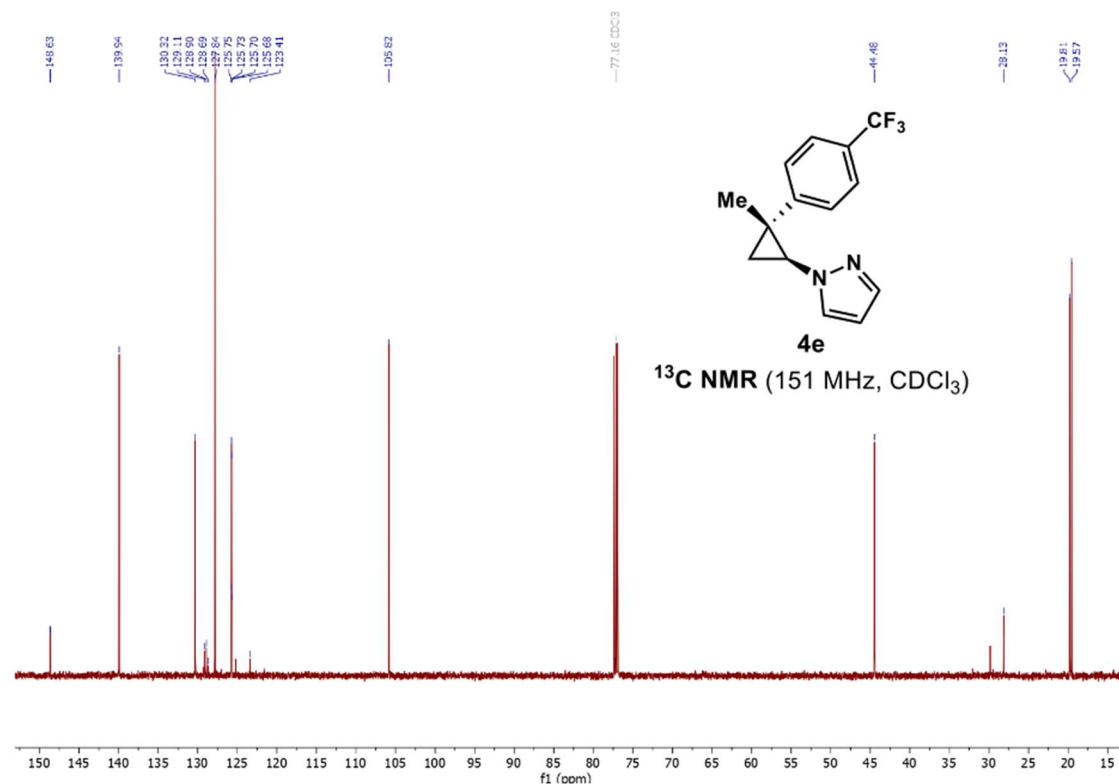
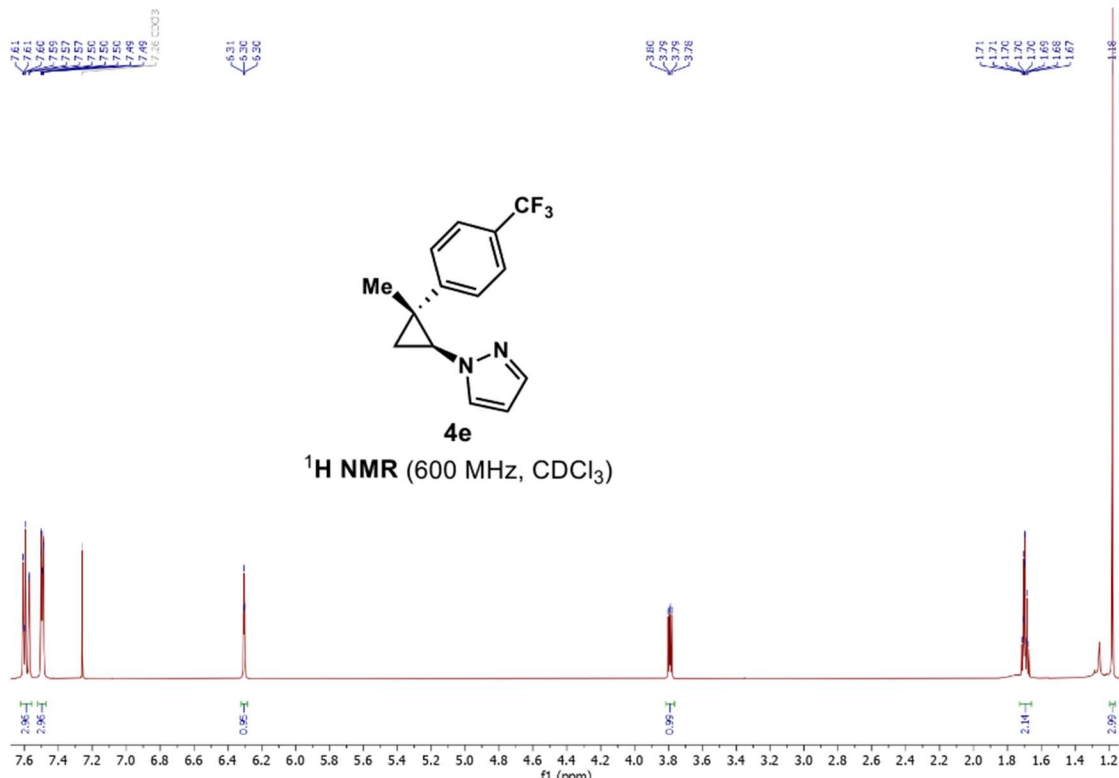
1-((1*S*,2*R*)-2-(4-methoxyphenyl)-2-methylcyclopropyl)-1*H*-pyrazole (4c)



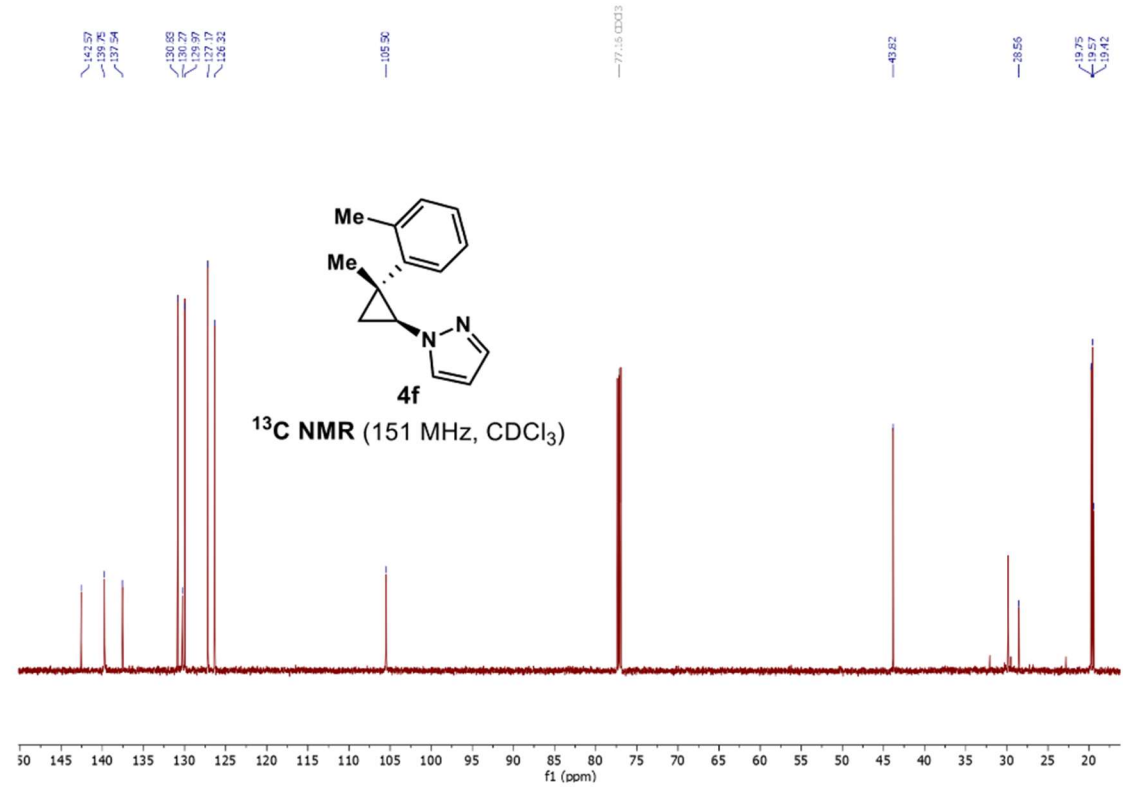
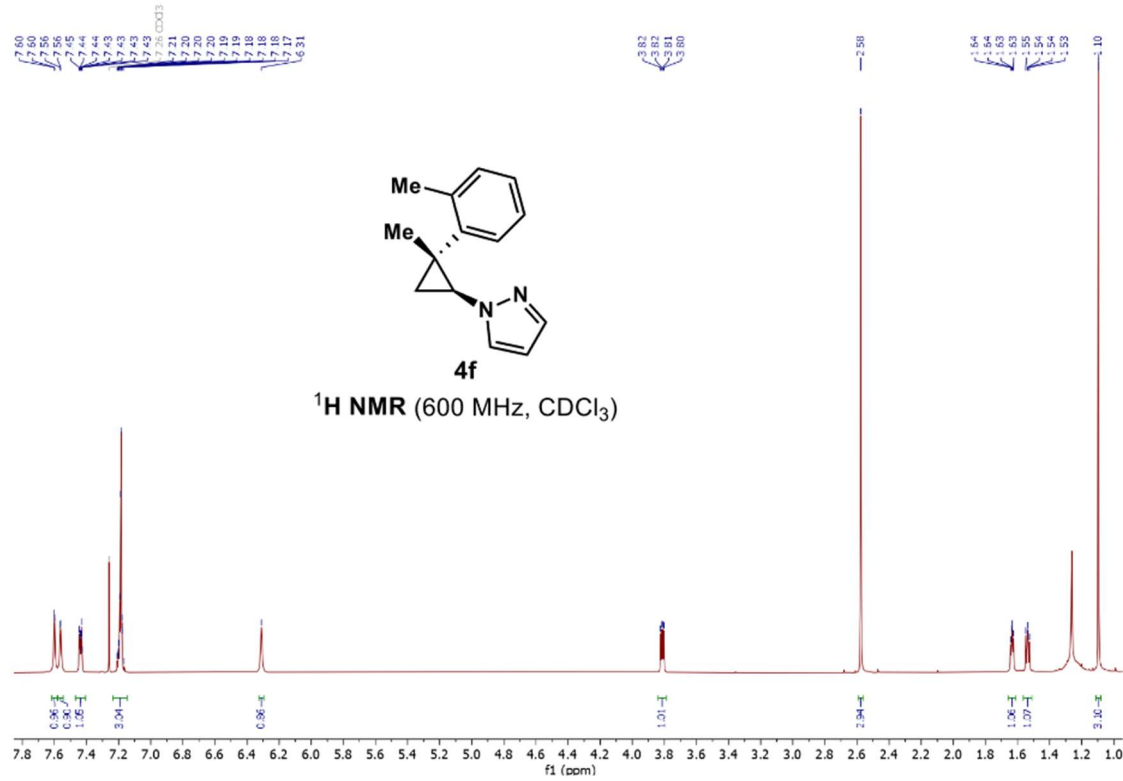
1-((1*S*,2*R*)-2-(4-chlorophenyl)-2-methylcyclopropyl)-1*H*-pyrazole (4d)



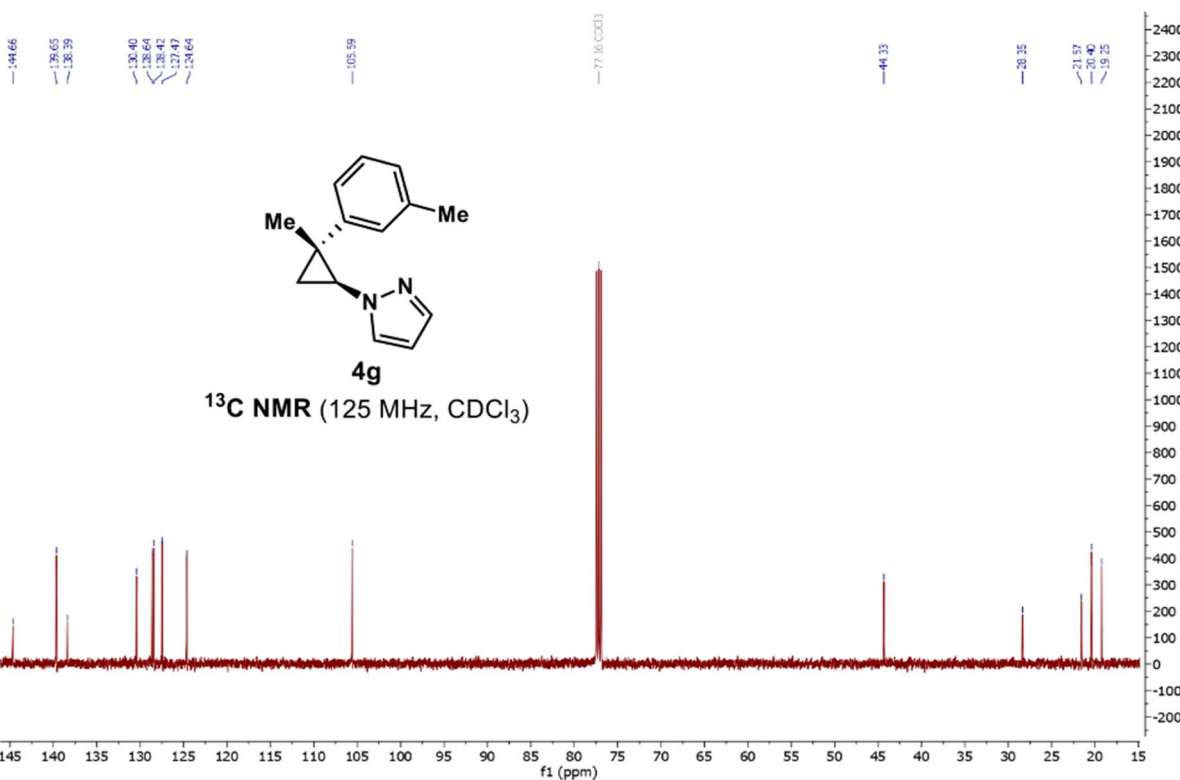
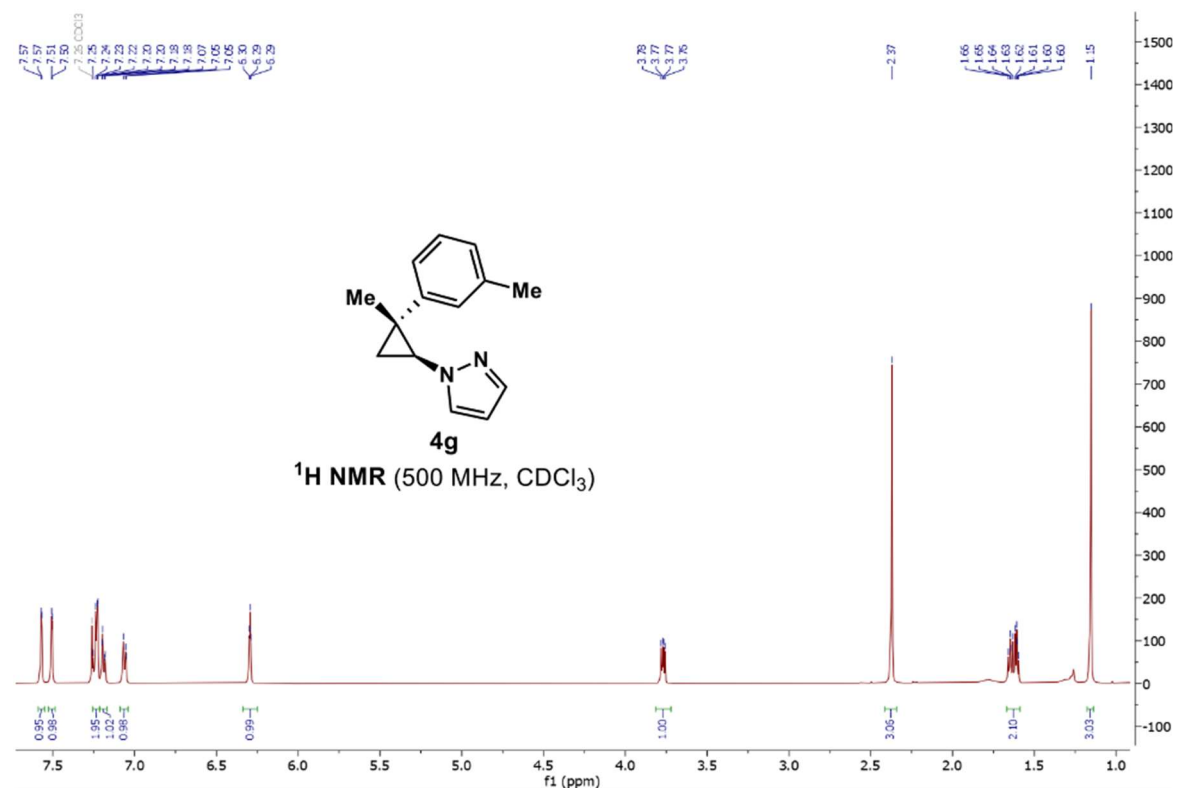
1-((1*S*,2*R*)-2-methyl-2-(4-(trifluoromethyl)phenyl)cyclopropyl)-1*H*-pyrazole (4e)



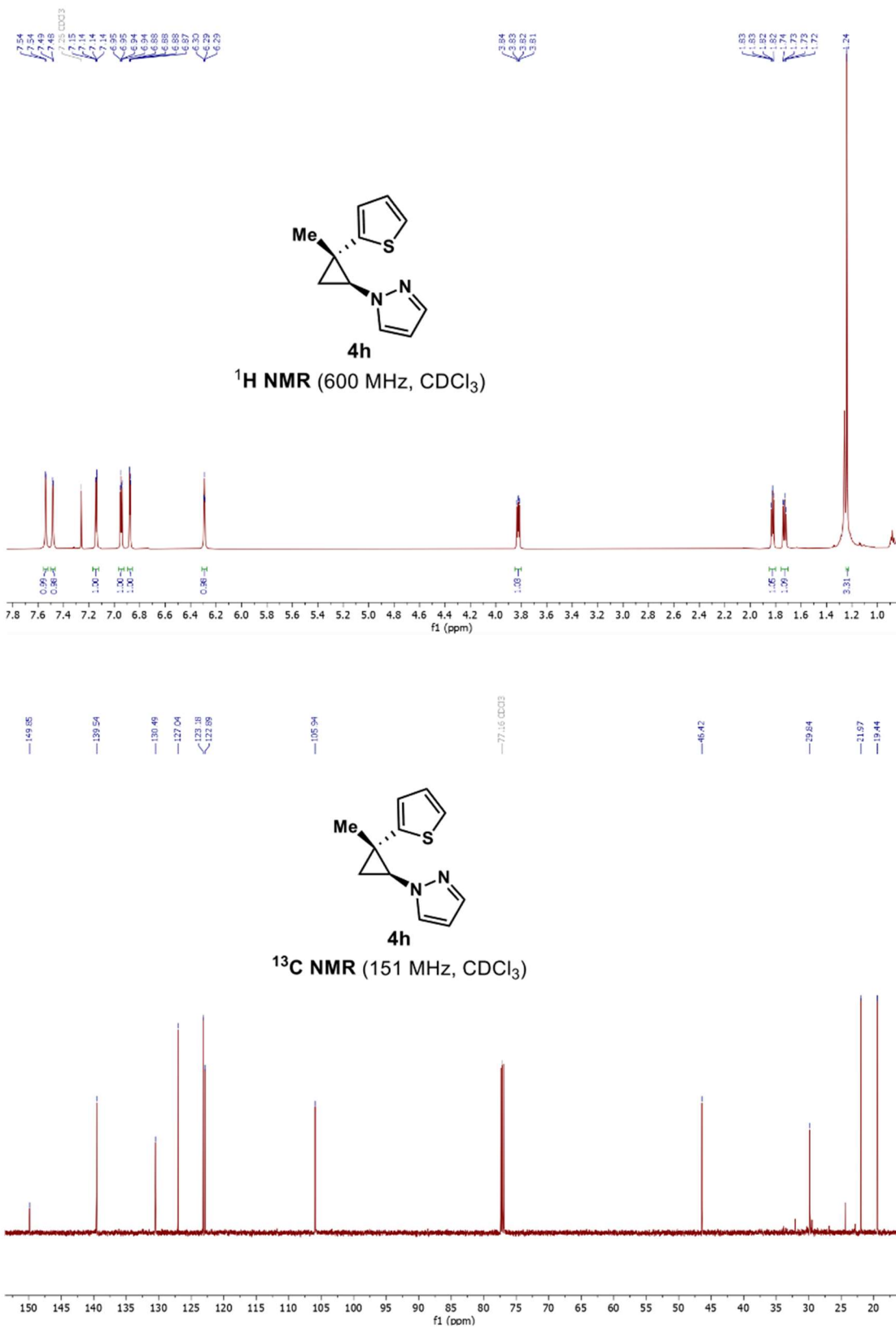
1-((1*S*,2*R*)-2-methyl-2-(*o*-tolyl)cyclopropyl)-1*H*-pyrazole (4f)



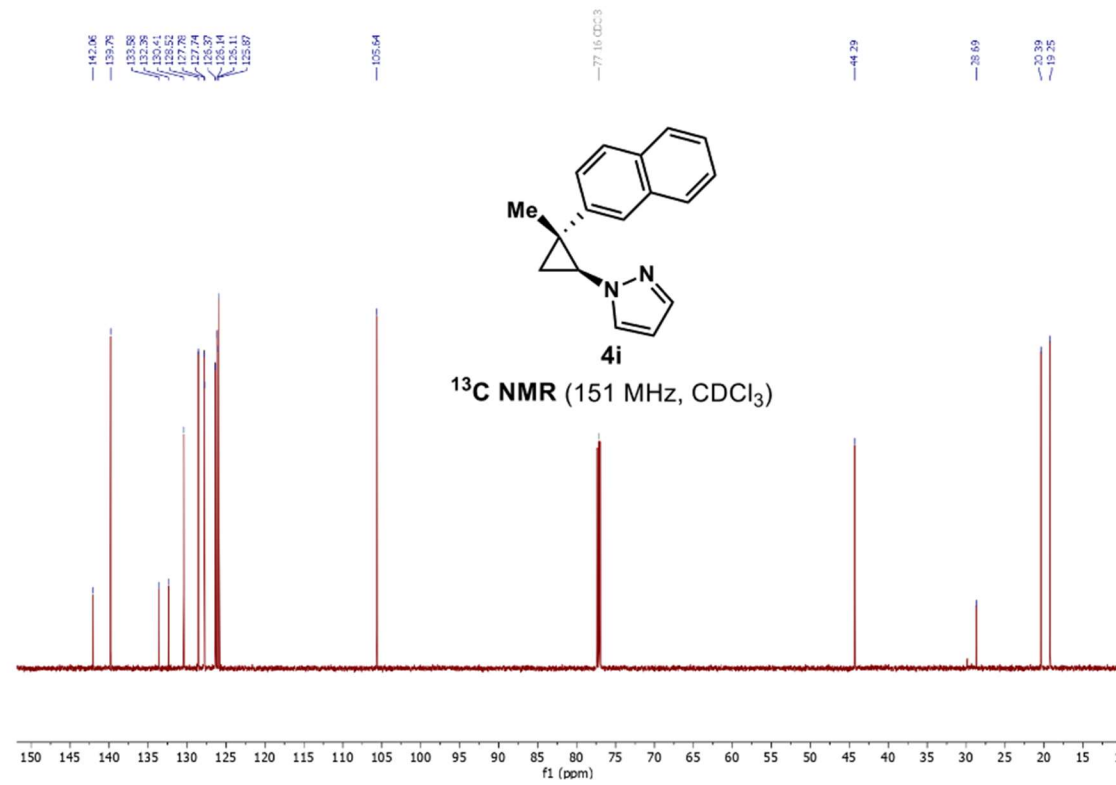
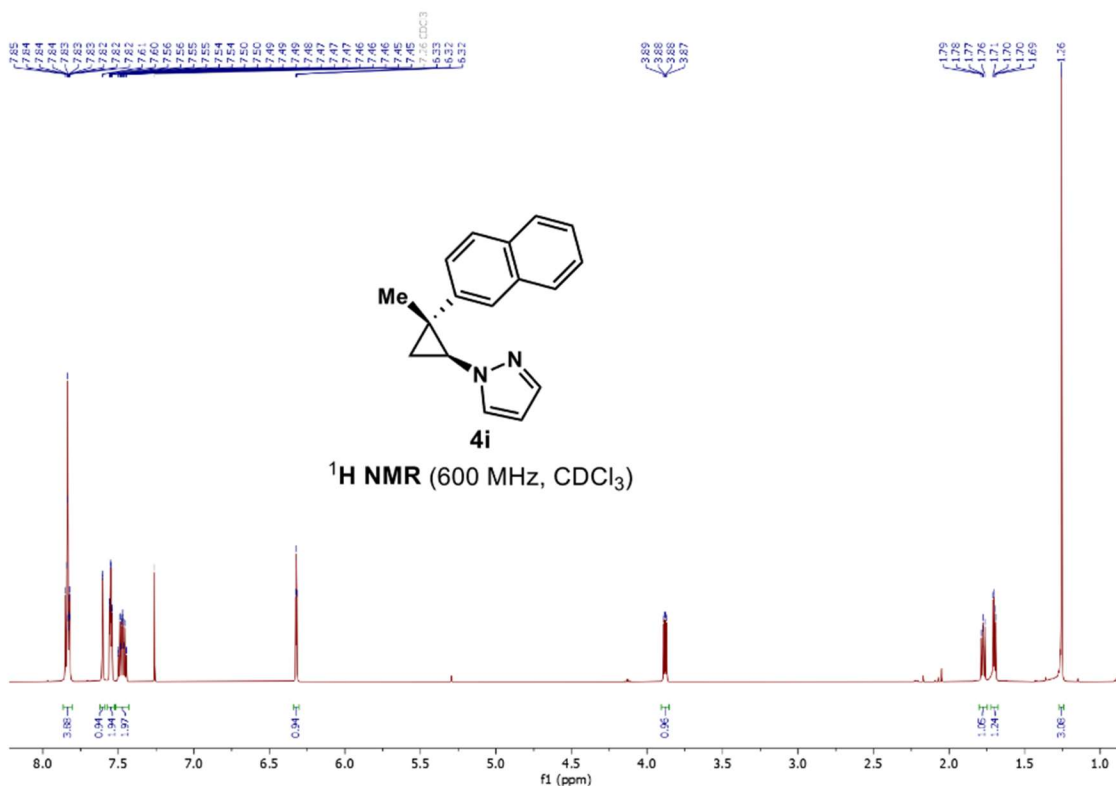
1-((1*S*,2*R*)-2-methyl-2-(*m*-tolyl)cyclopropyl)-1*H*-pyrazole (4g)



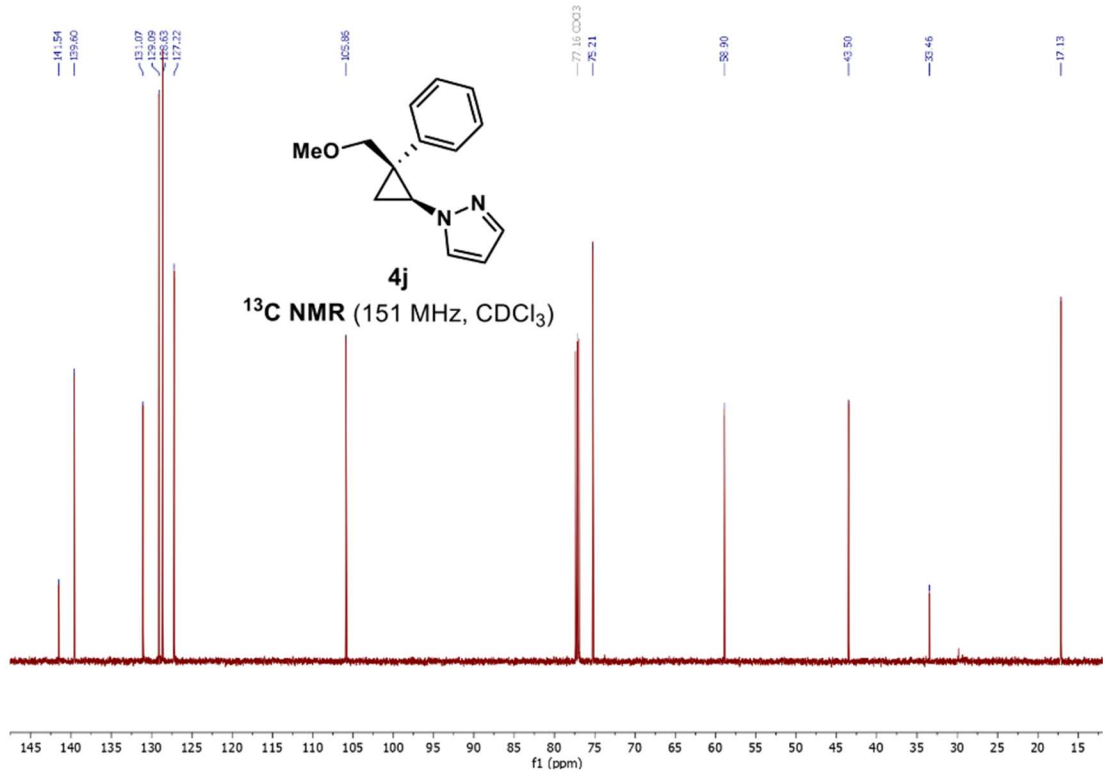
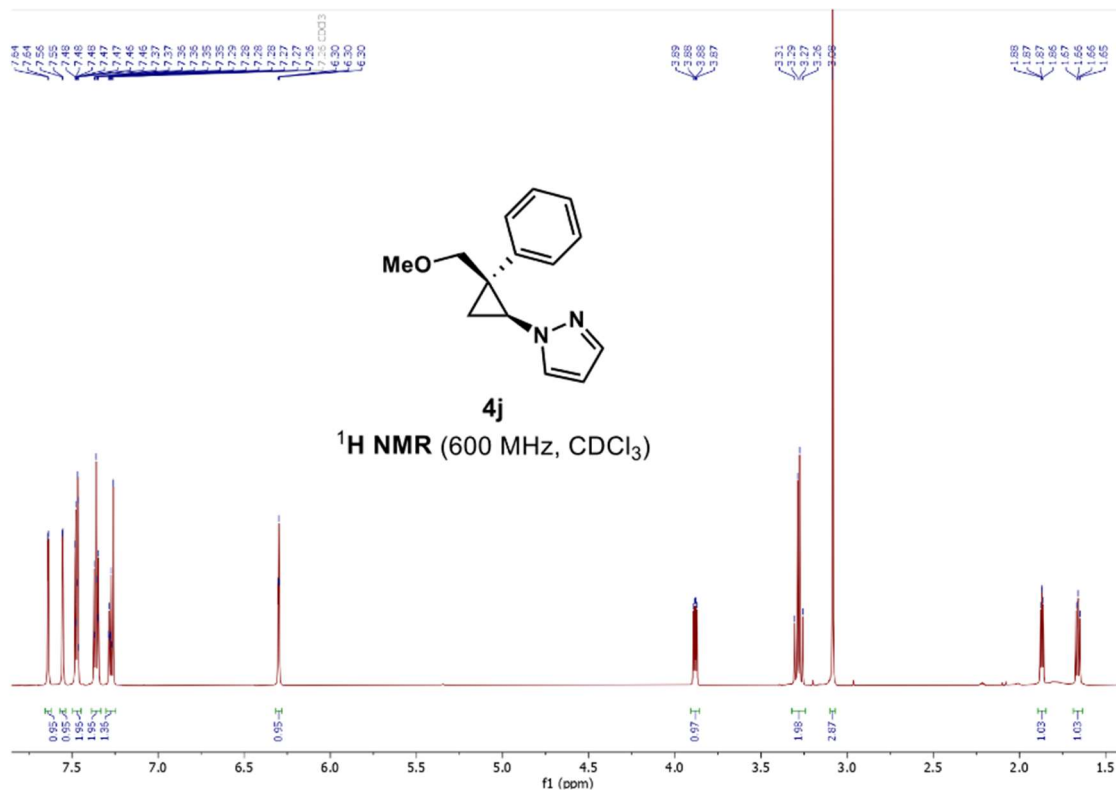
1-((1*S*,2*S*)-2-methyl-2-(thiophen-2-yl)cyclopropyl)-1*H*-pyrazole (4h)



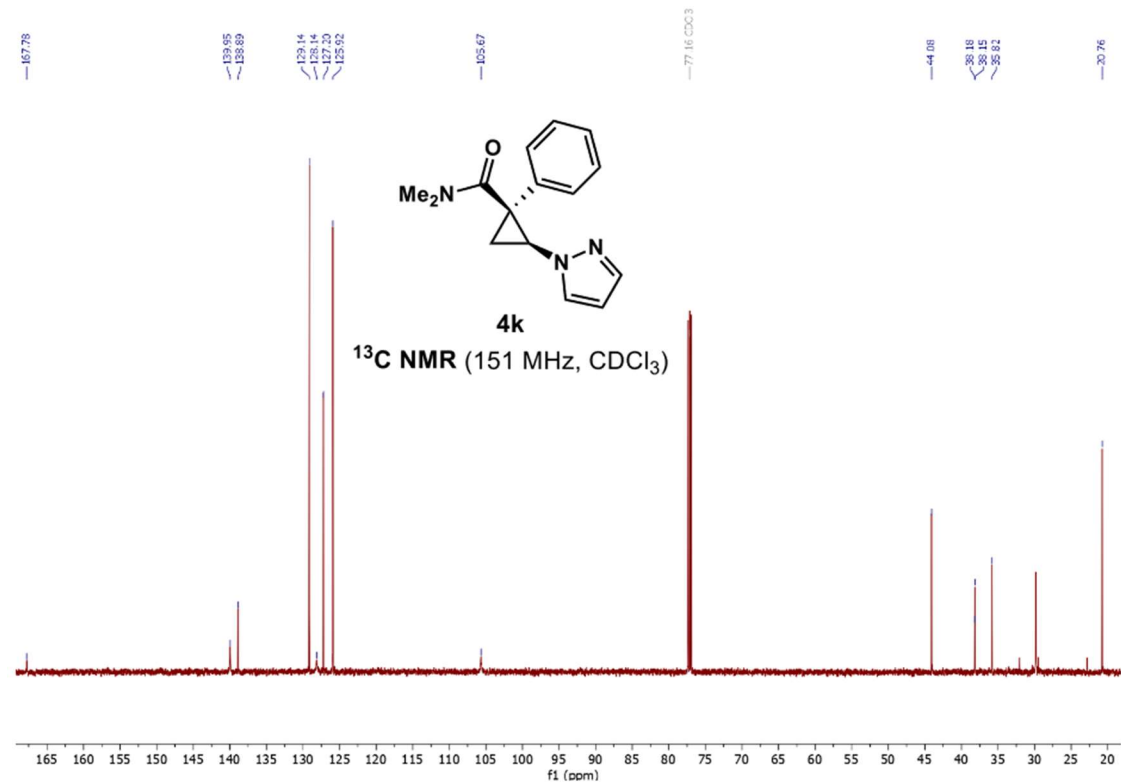
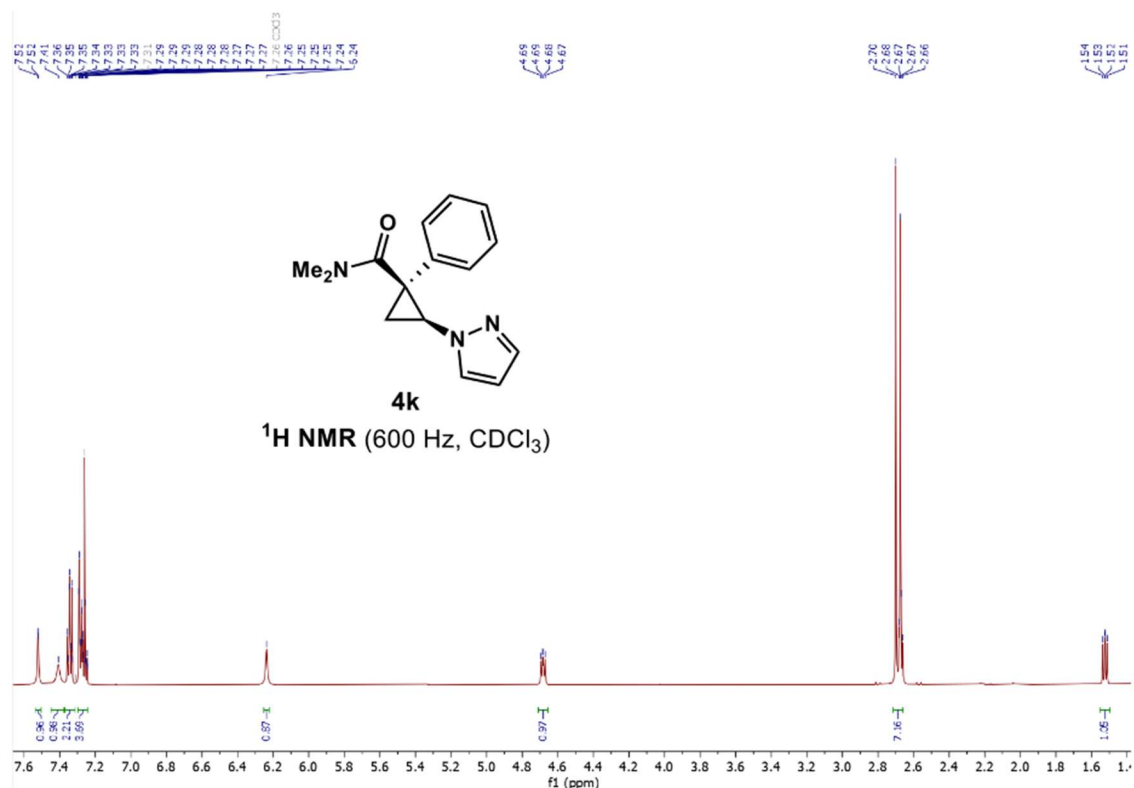
1-((1*S*,2*R*)-2-methyl-2-(naphthalen-2-yl)cyclopropyl)-1*H*-pyrazole (4i)



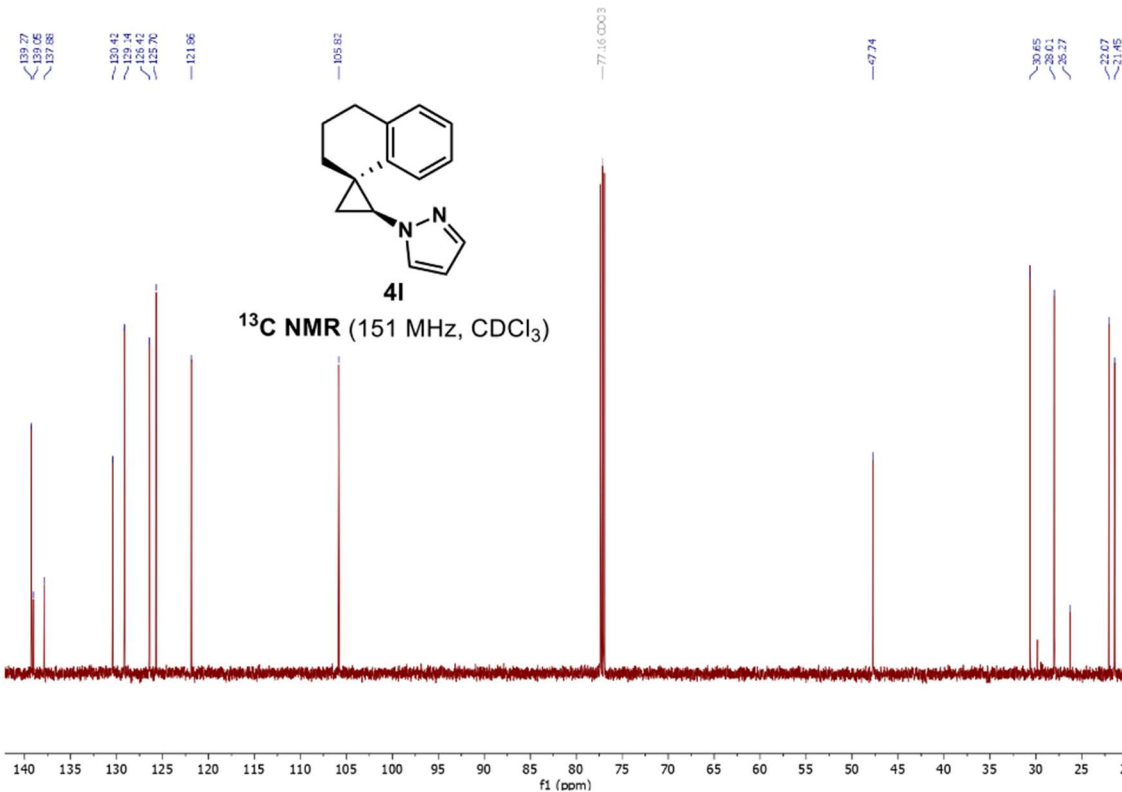
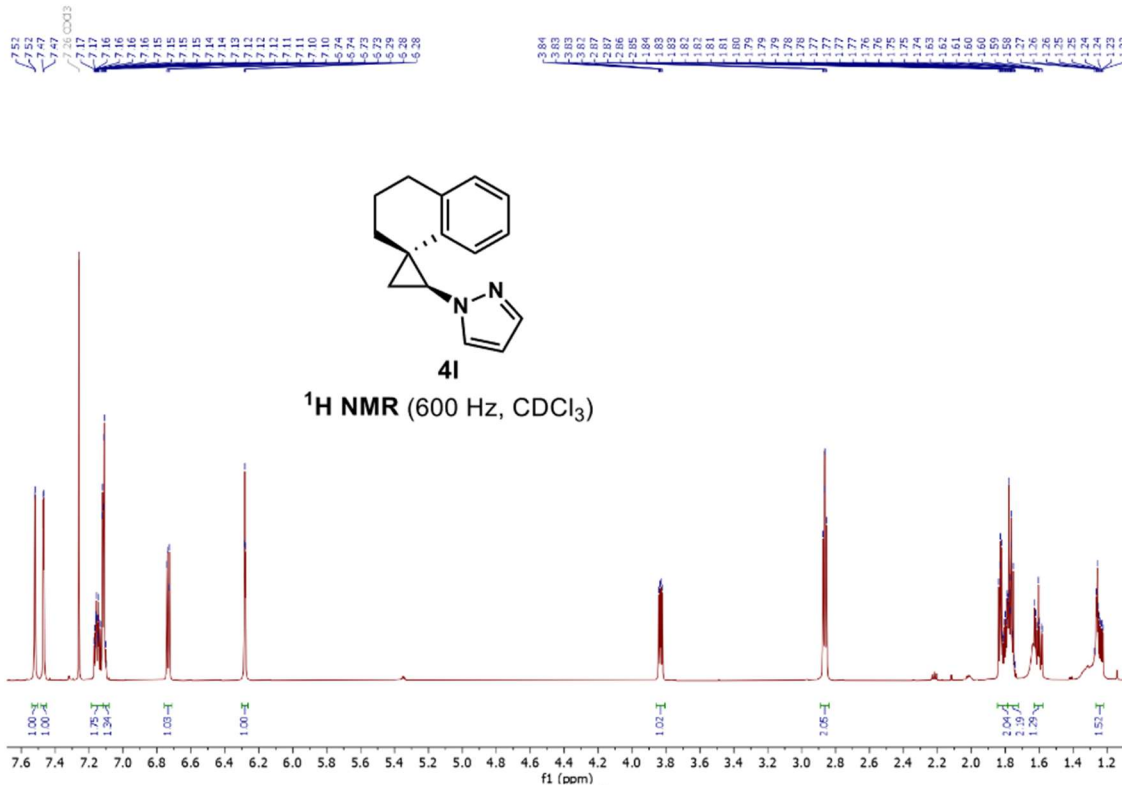
1-((1*S*,2*S*)-2-(methoxymethyl)-2-phenylcyclopropyl)-1*H*-pyrazole (4j)



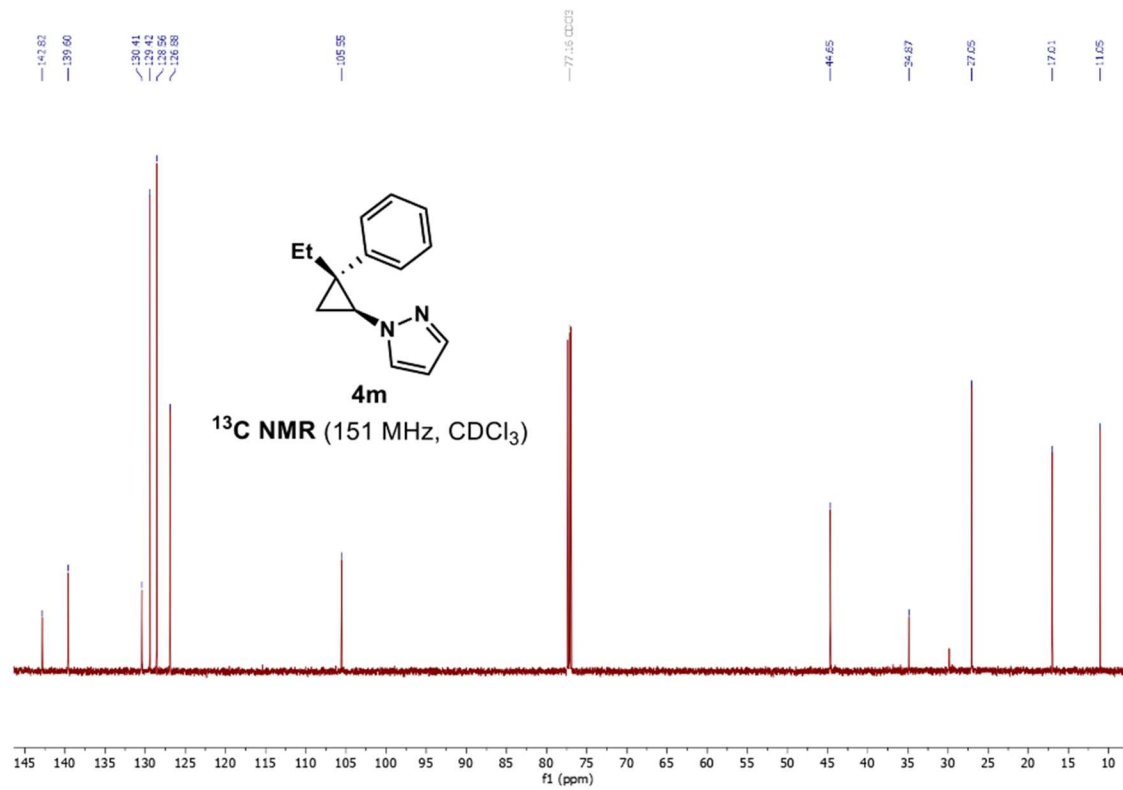
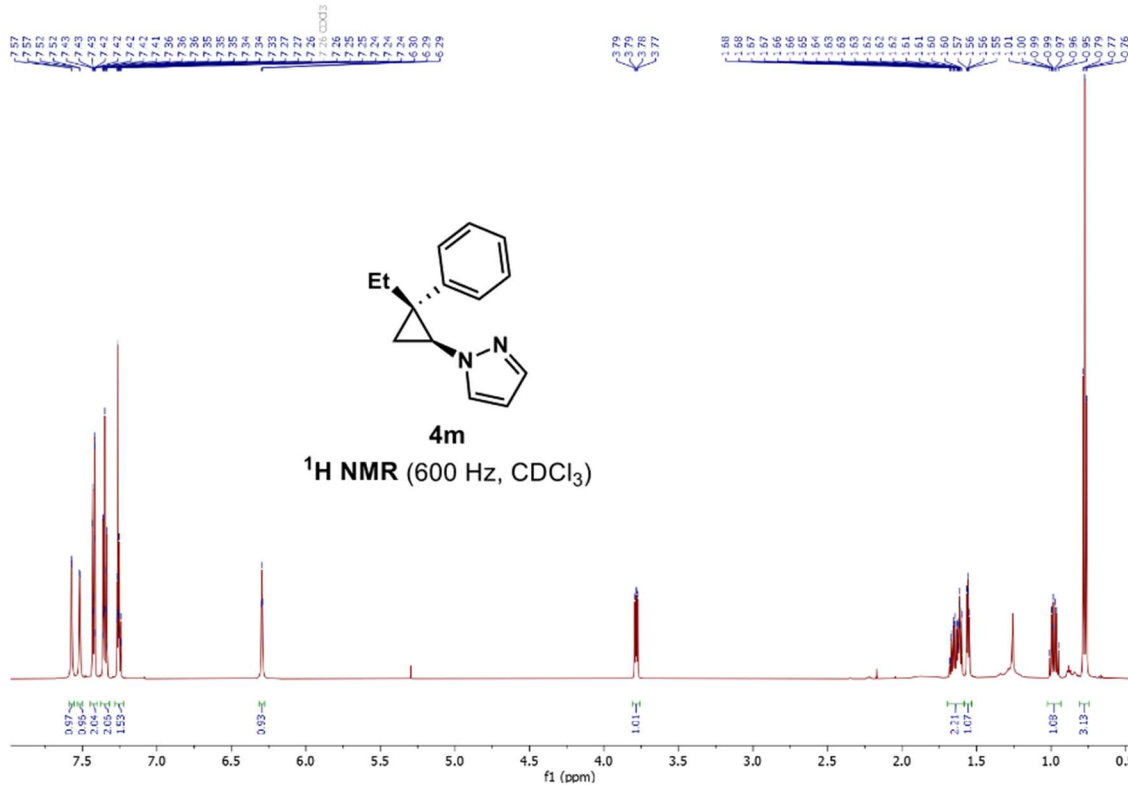
(1*S*,2*S*)-*N,N*-dimethyl-1-phenyl-2-(1*H*-pyrazol-1-yl)cyclopropane-1-carboxamide (4k)



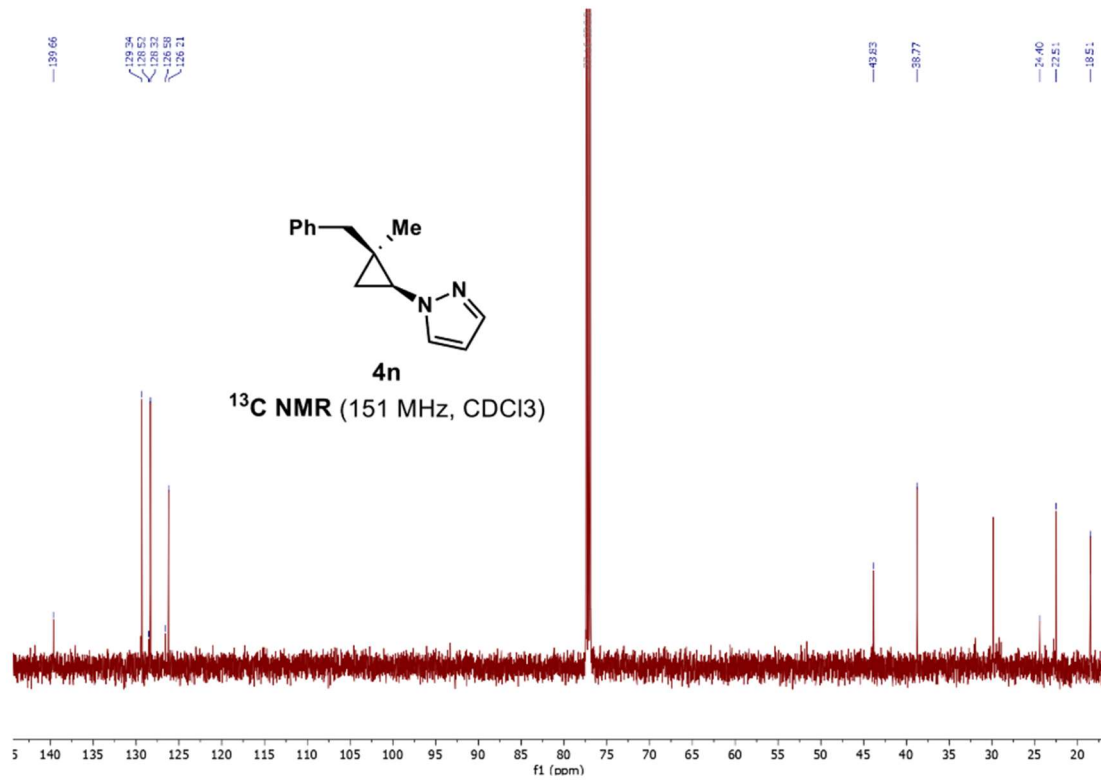
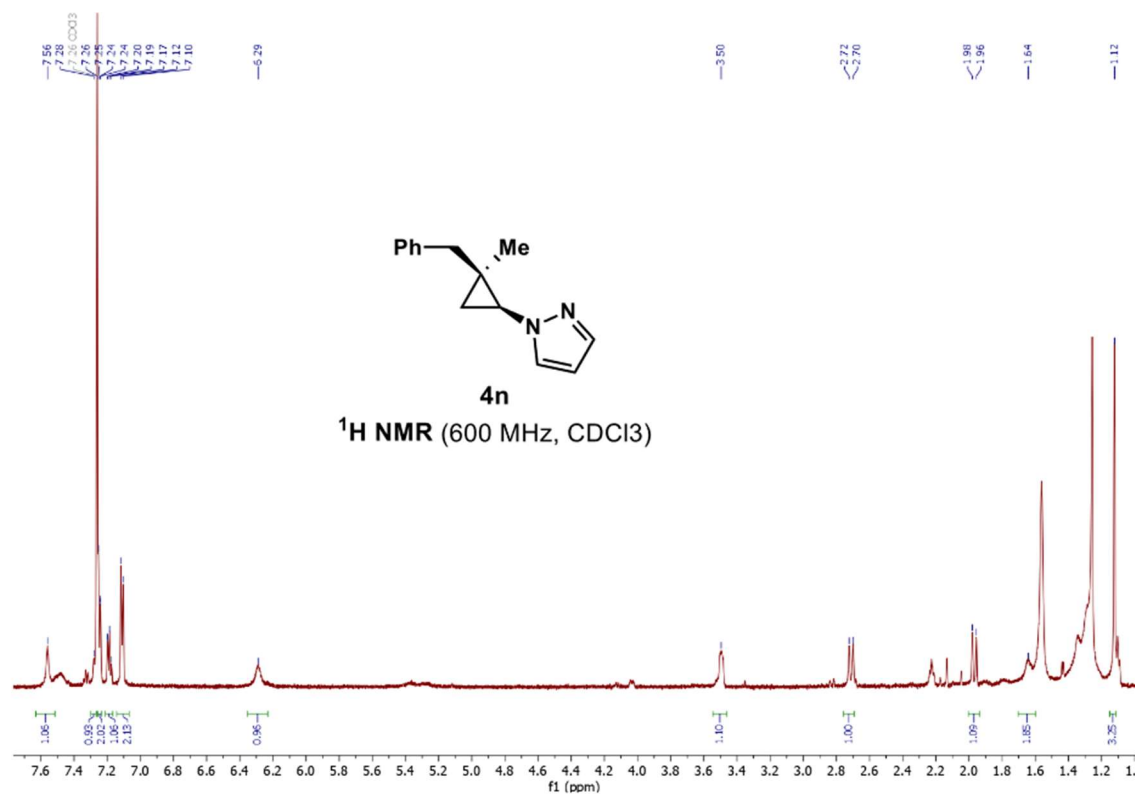
1-((1*R*,2*S*)-3',4'-dihydro-2'*H*-spiro[cyclopropane-1,1'-naphthalen]-2-yl)-1*H*-pyrazole (4l)

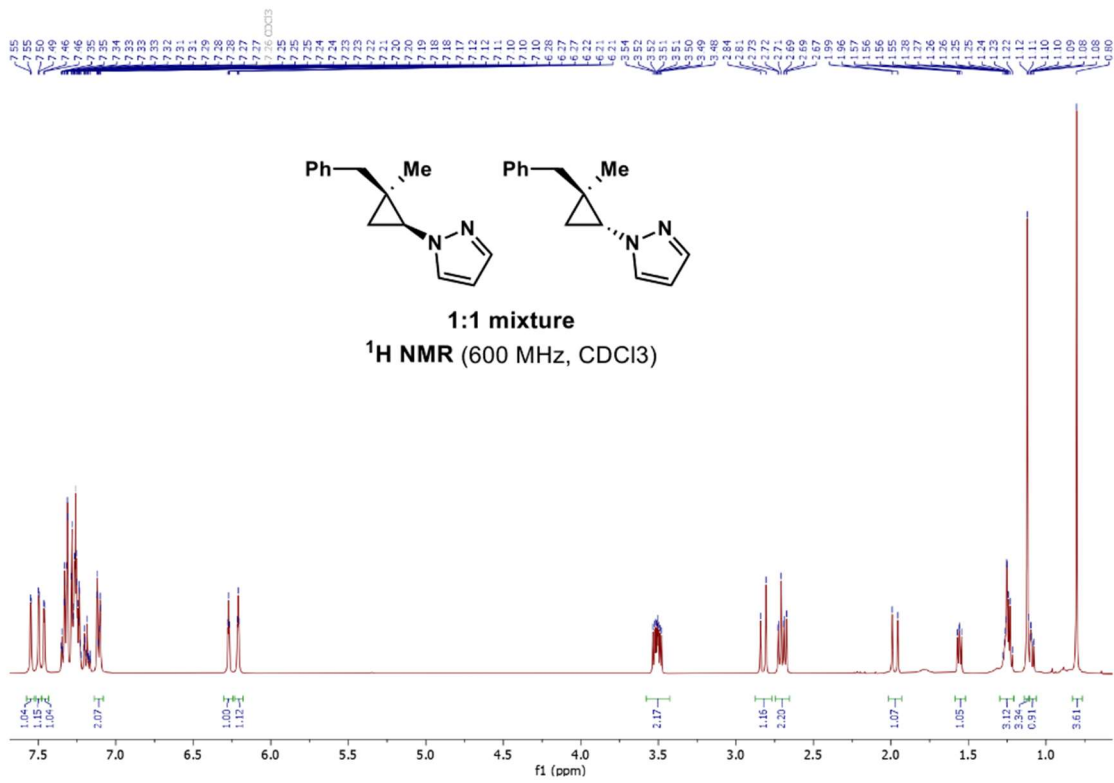


1-((1*S*,2*R*)-2-ethyl-2-phenylcyclopropyl)-1*H*-pyrazole (4m)

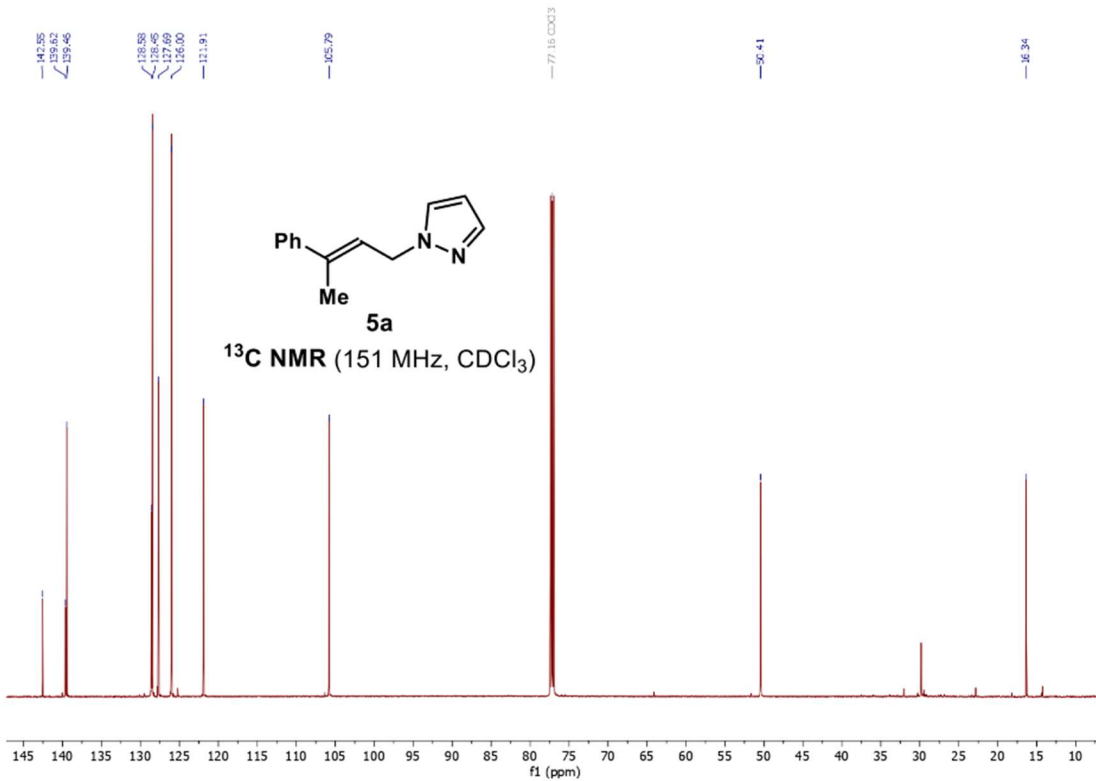
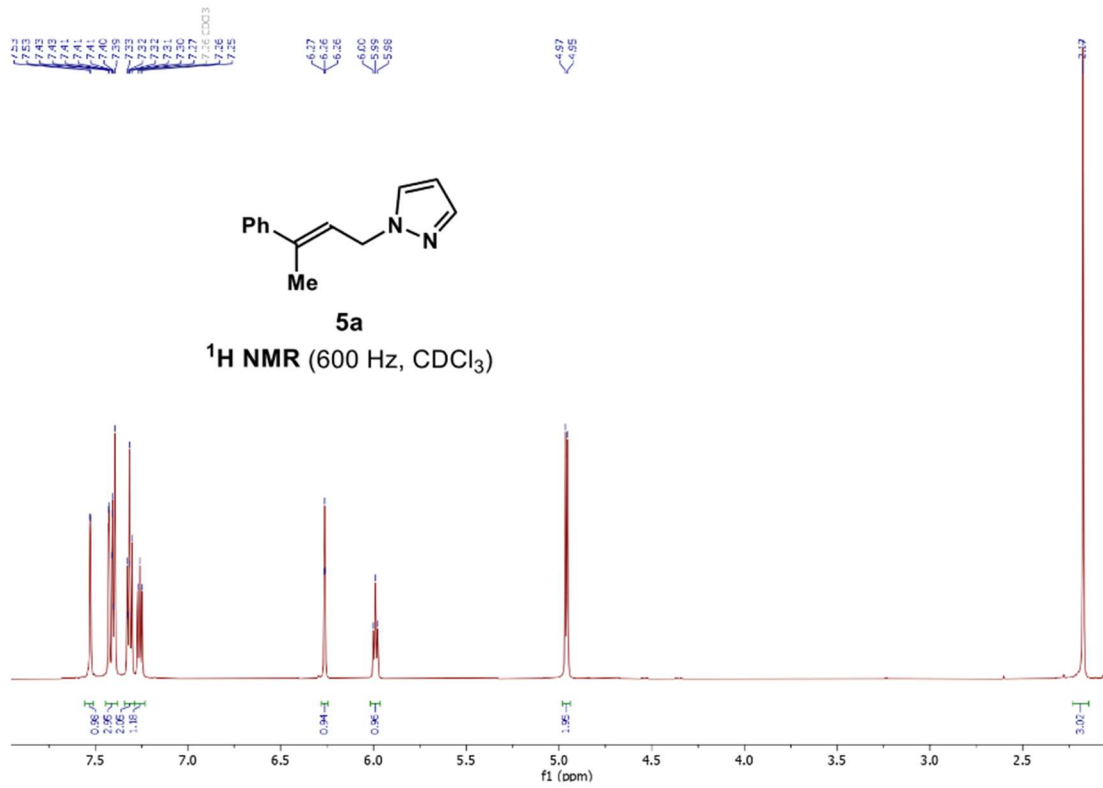


1-((1*S*,2*R*)-2-benzyl-2-methylcyclopropyl)-1*H*-pyrazole (4n)

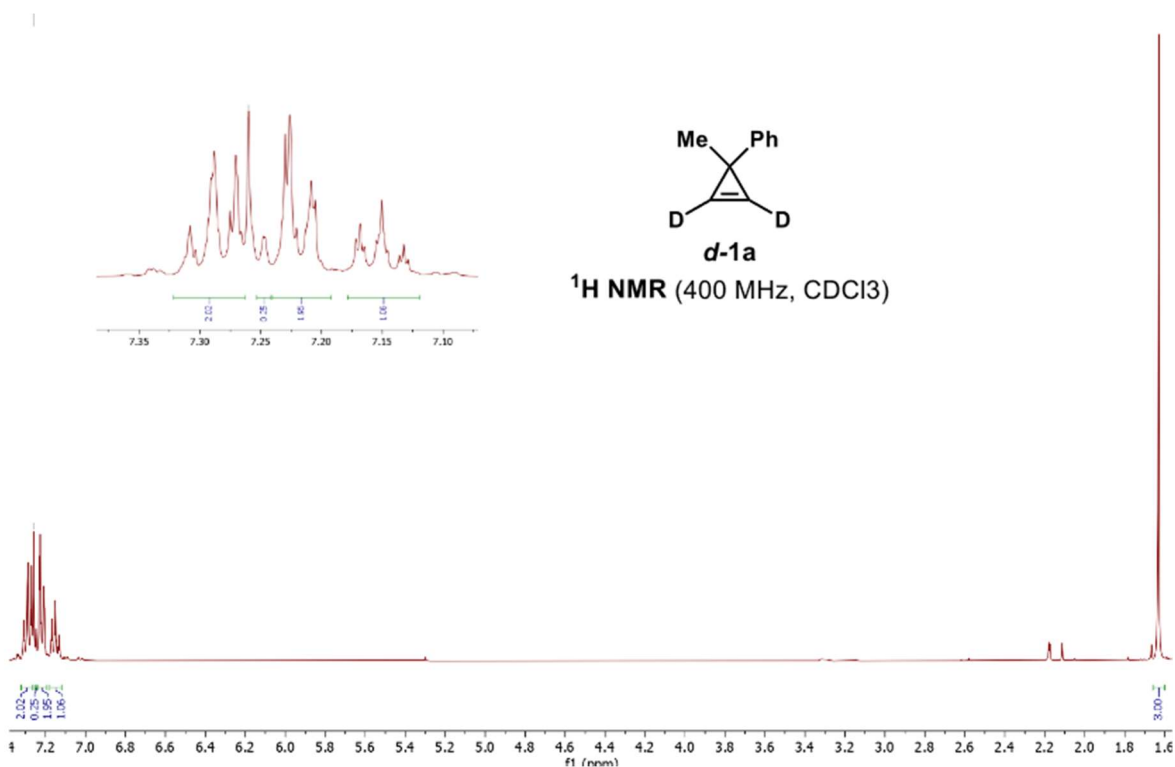




(E)-1-(3-phenylbut-2-en-1-yl)-1*H*-pyrazole (5a)

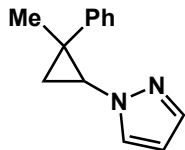


(1-methylcycloprop-2-en-1-yl-2,3-²H)benzene (*d*-1a)



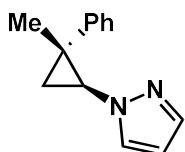
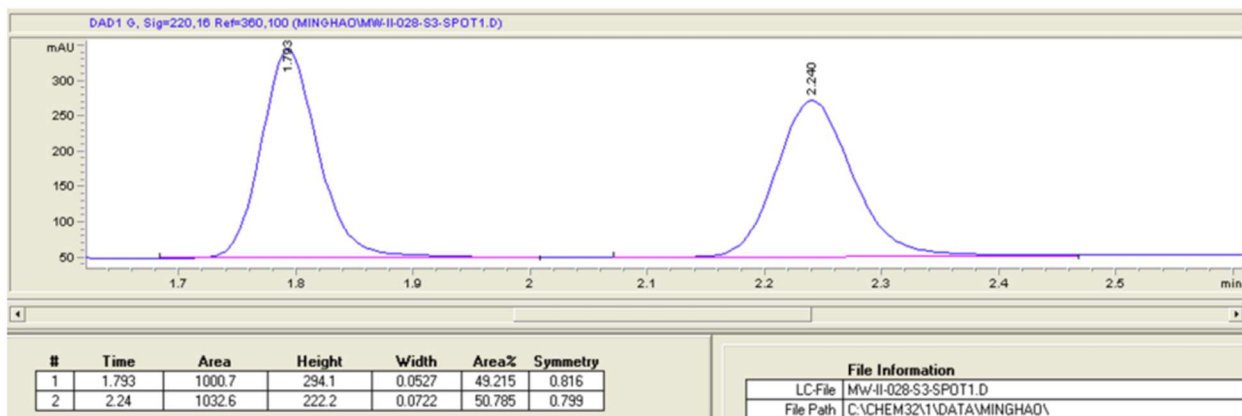
APPENDIX B: SFC Traces

1-((1*S*,2*R*)-2-methyl-2-phenylcyclopropyl)-1*H*-pyrazole (3a)



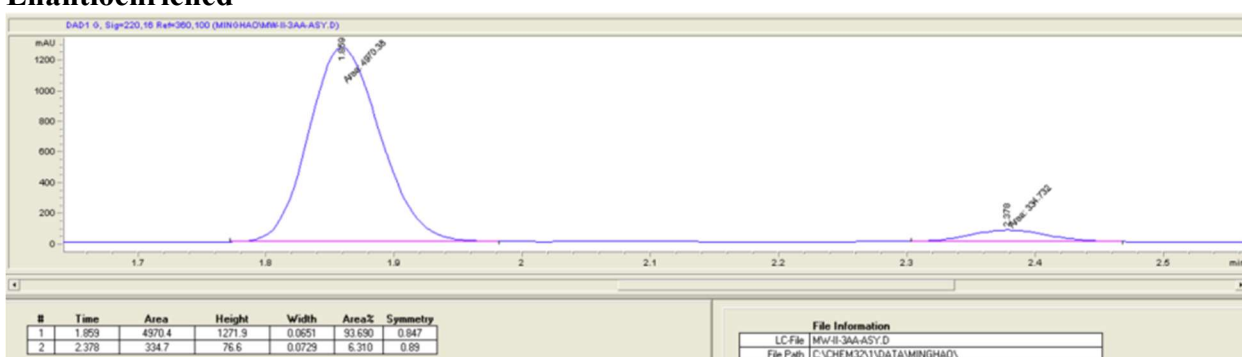
rac-3a

Racemic

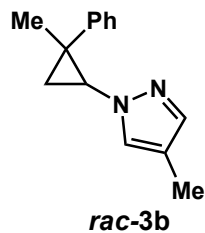


3a

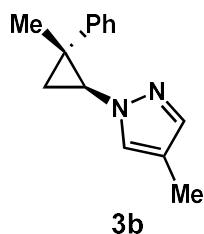
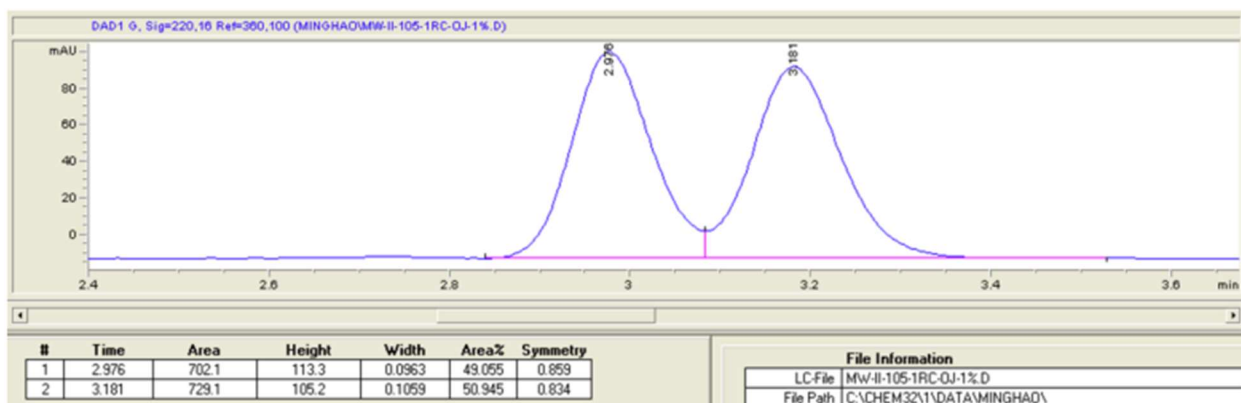
Enantioenriched



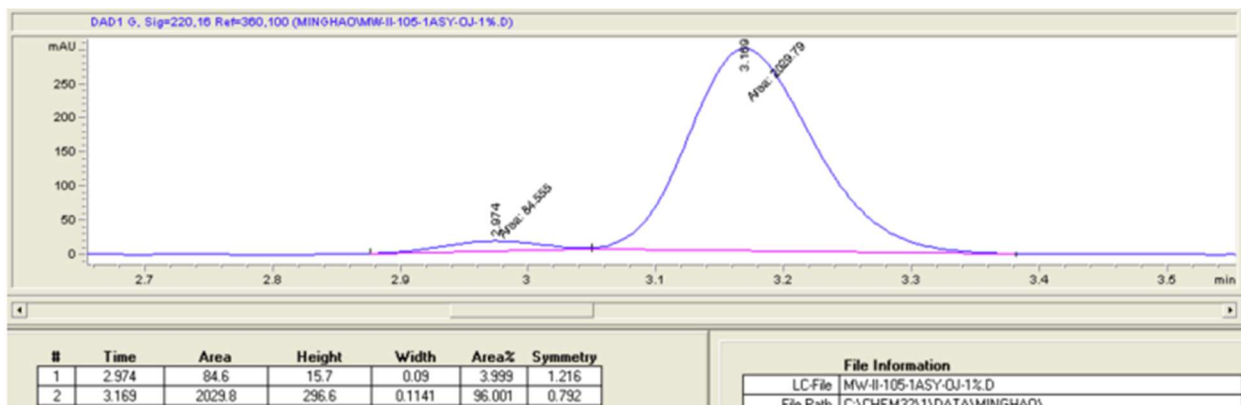
4-methyl-1-((1*S*,2*R*)-2-methyl-2-phenylcyclopropyl)-1*H*-pyrazole (3b)



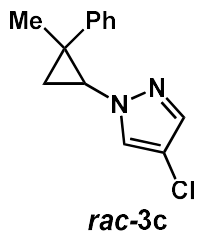
Racemic



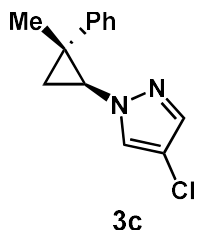
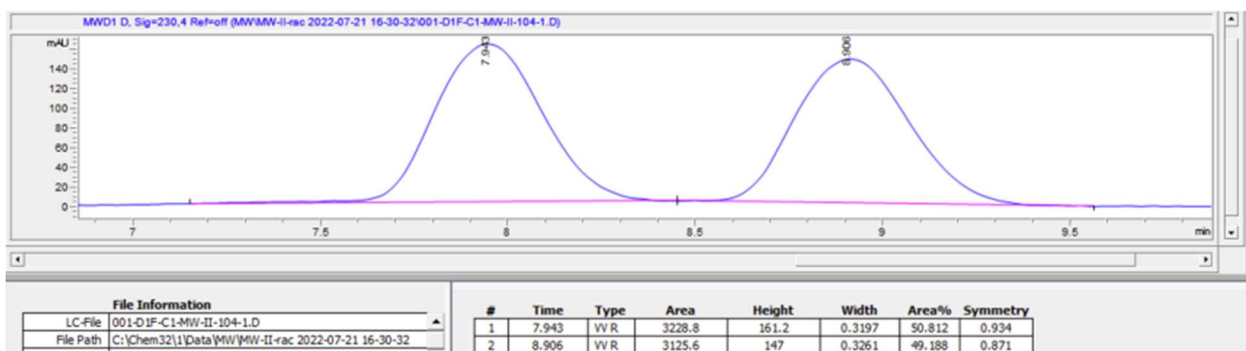
Enantioenriched



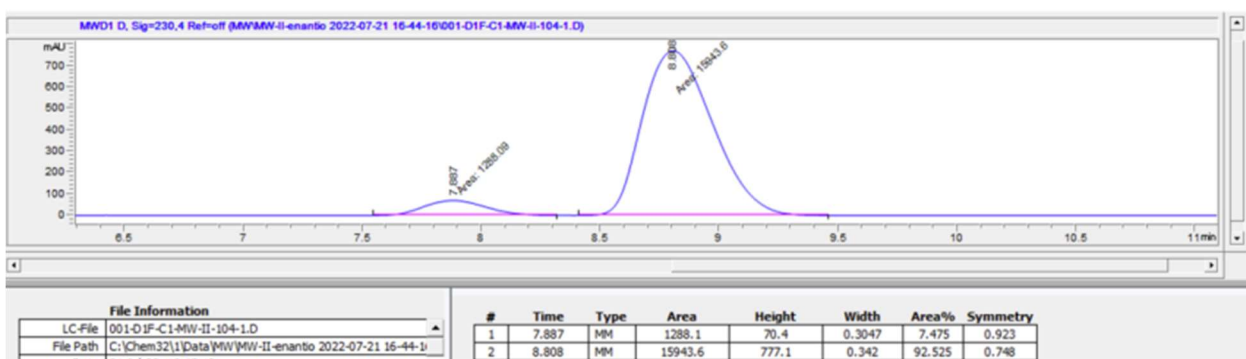
4-chloro-1-((1*S*,2*R*)-2-methyl-2-phenylcyclopropyl)-1*H*-pyrazole (3c)



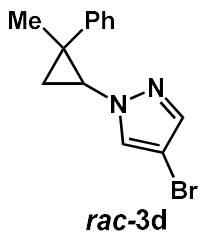
Racemic



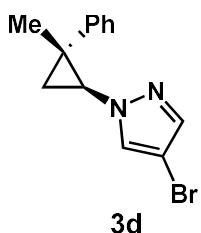
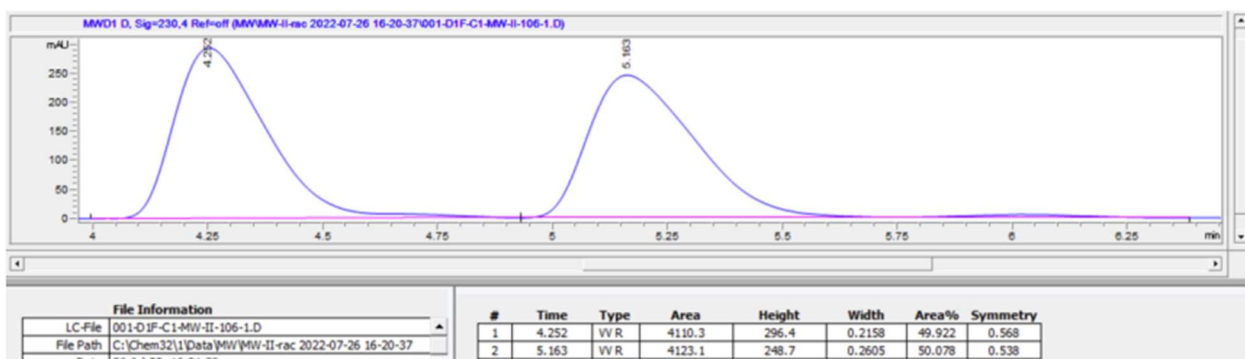
Enantioenriched



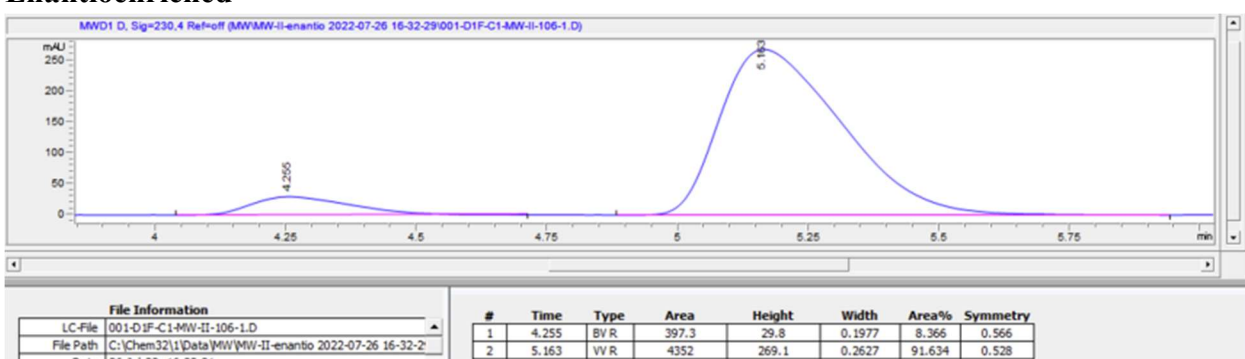
4-bromo-1-((1*S*,2*R*)-2-methyl-2-phenylcyclopropyl)-1*H*-pyrazole (3d)



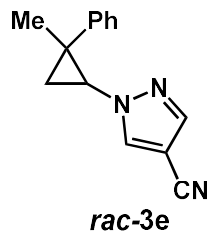
Racemic



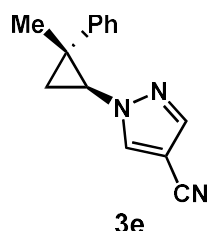
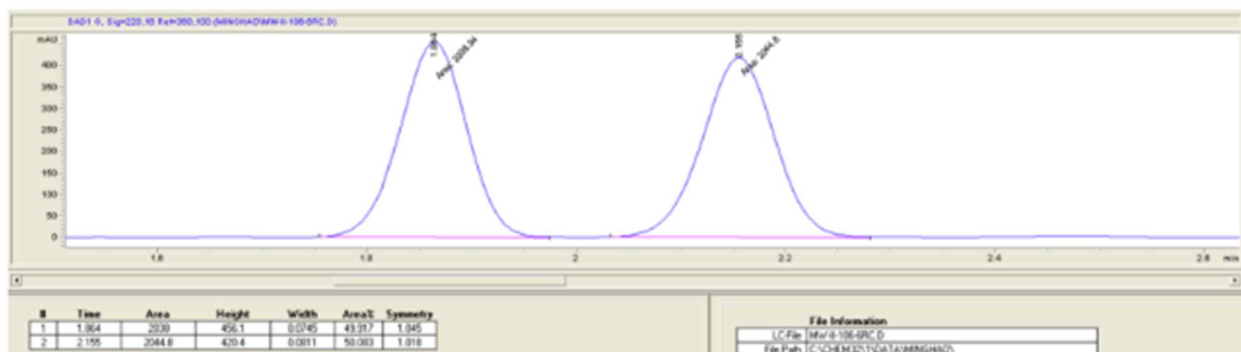
Enantioenriched



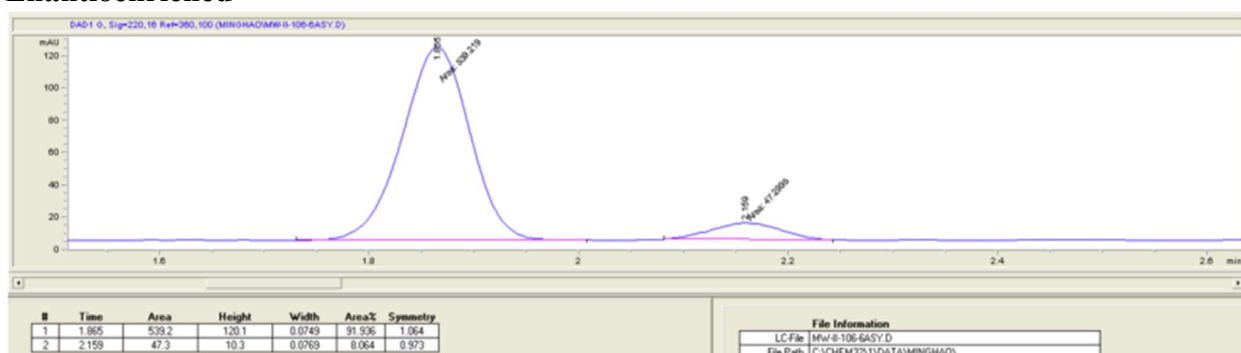
1-((1*S*,2*R*)-2-methyl-2-phenylcyclopropyl)-1*H*-pyrazole-4-carbonitrile (3e)



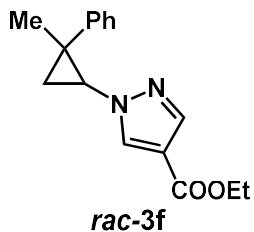
Racemic



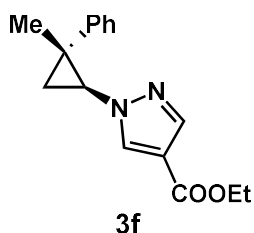
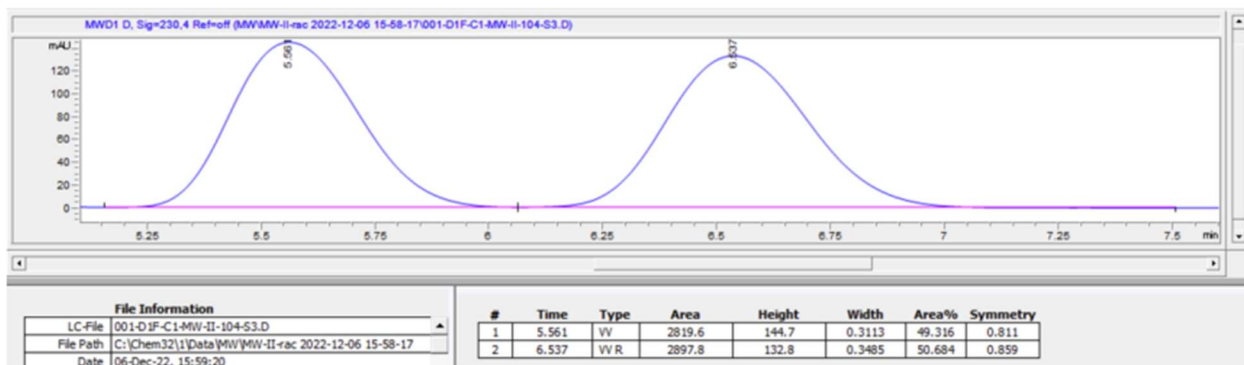
Enantioenriched



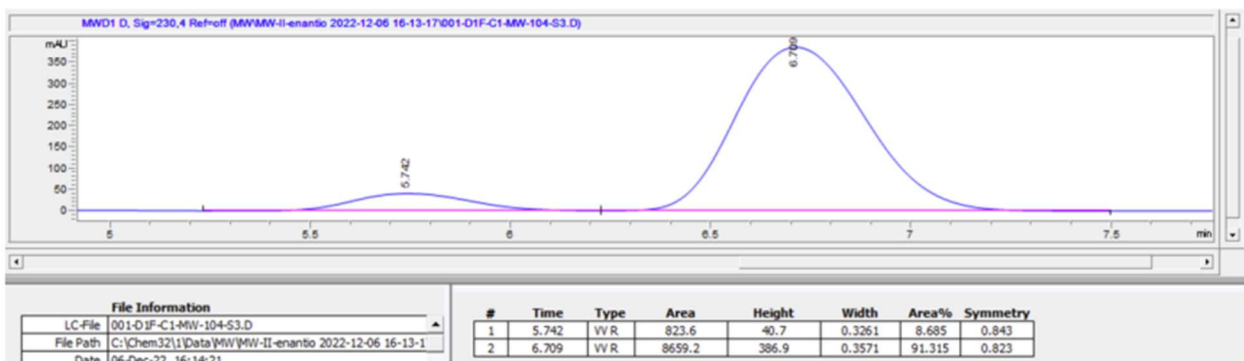
Ethyl 1-((1*S*,2*R*)-2-methyl-2-phenylcyclopropyl)-1*H*-pyrazole-4-carboxylate (3f**)**



Racemic

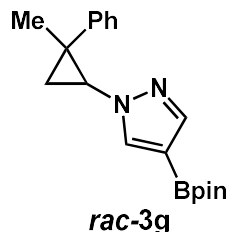


Enantioenriched

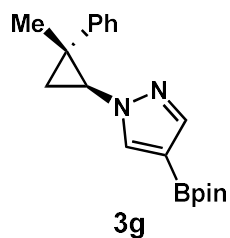
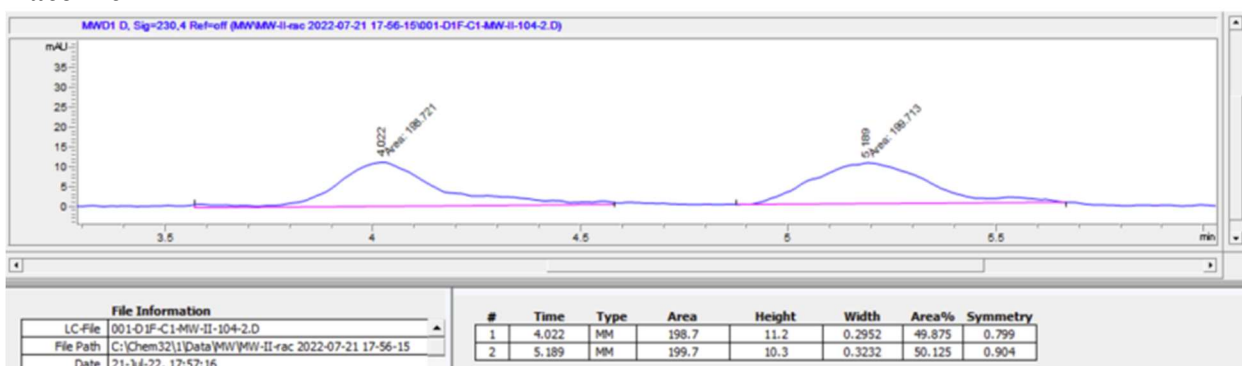


1-((1*S*,2*R*)-2-methyl-2-phenylcyclopropyl)-4-(4,4,5,5-tetramethyl-1,3,2-dioxaborolan-2-yl)-

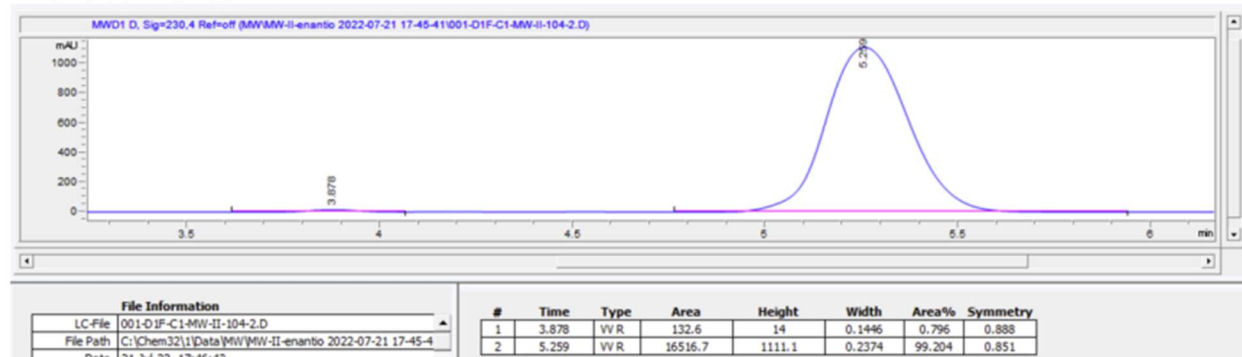
1*H*-pyrazole (3g)



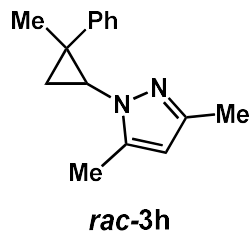
Racemic



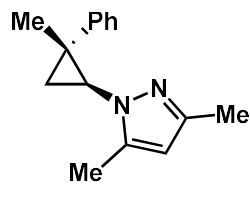
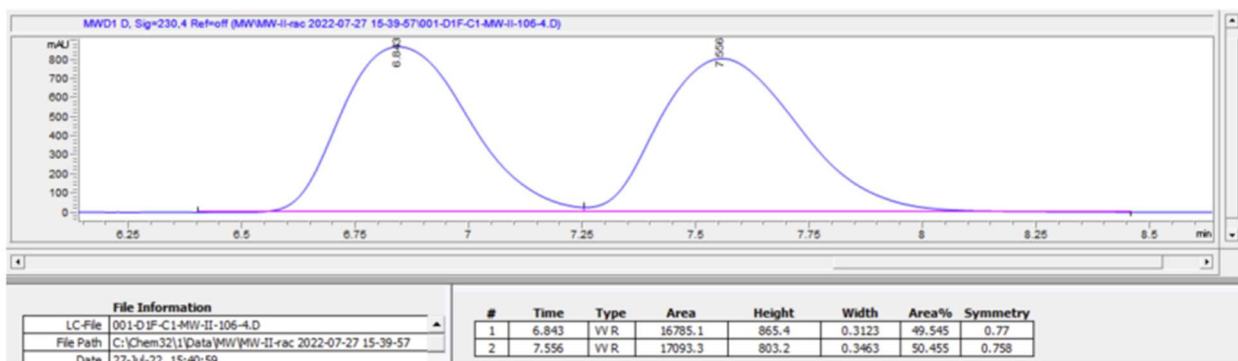
Enantioenriched



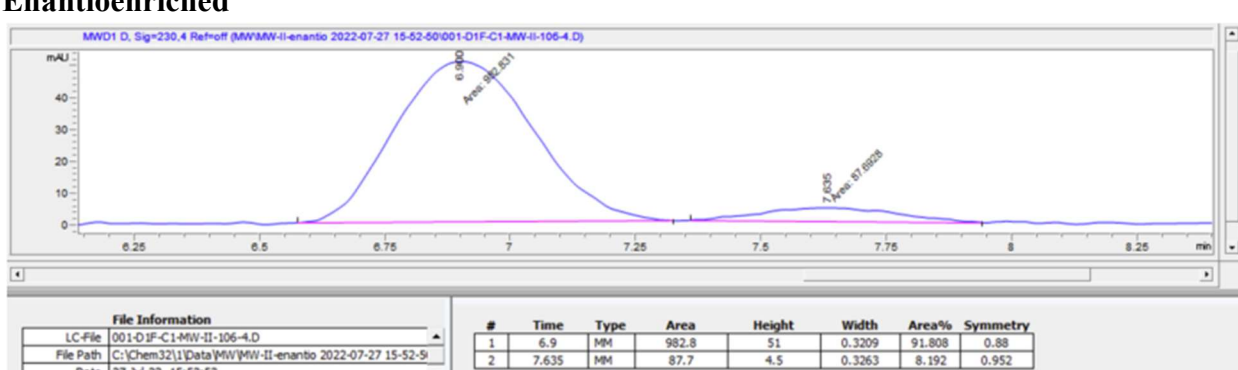
3,5-dimethyl-1-((1*S*,2*R*)-2-methyl-2-phenylcyclopropyl)-1*H*-pyrazole (3h)



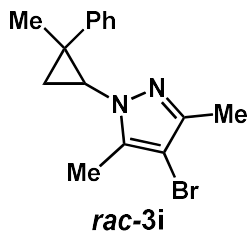
Racemic



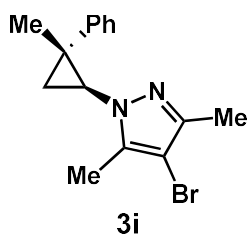
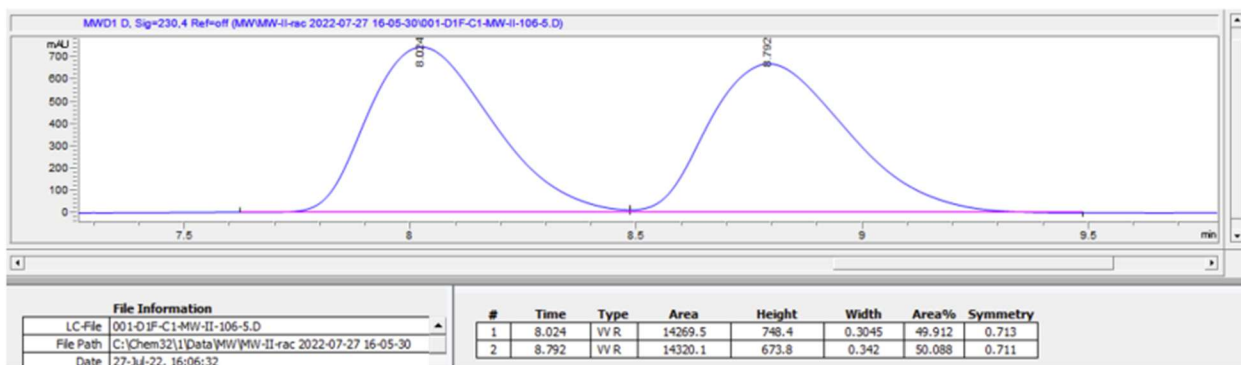
Enantioenriched



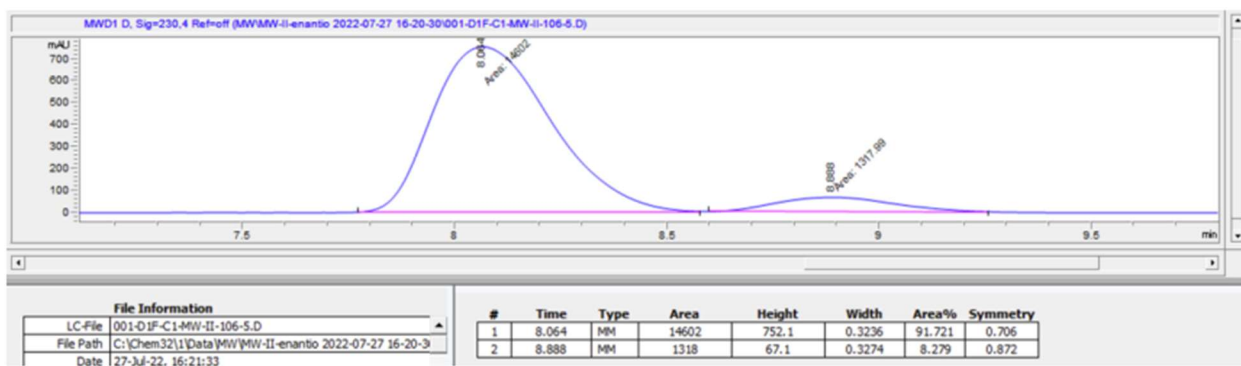
4-bromo-3,5-dimethyl-1-((1*S*,2*R*)-2-methyl-2-phenylcyclopropyl)-1*H*-pyrazole (3i)



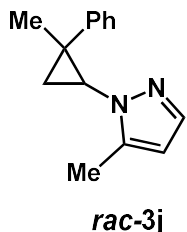
Racemic



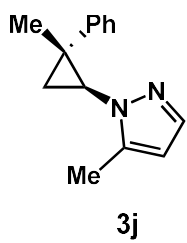
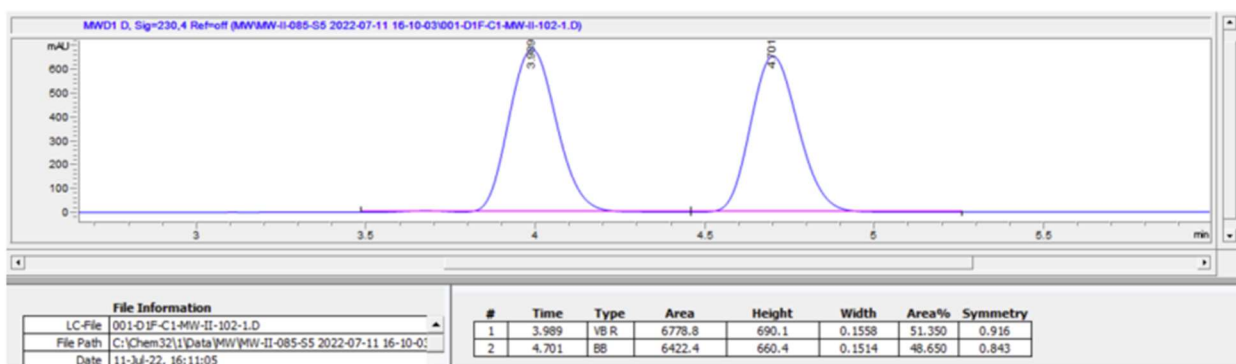
Enantioenriched



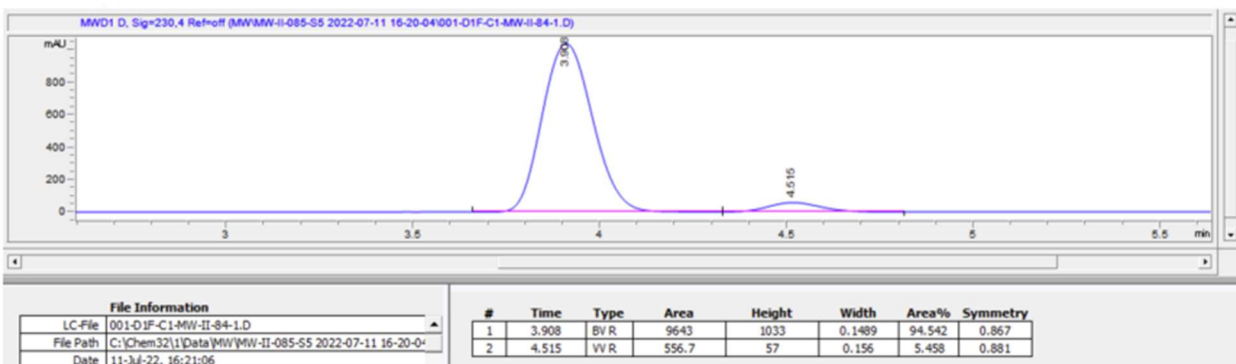
3-methyl-1-((1*S*,2*R*)-2-methyl-2-phenylcyclopropyl)-1*H*-pyrazole (3j)



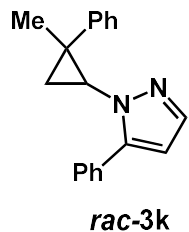
Racemic



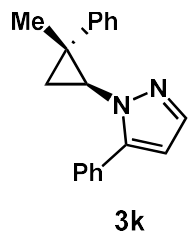
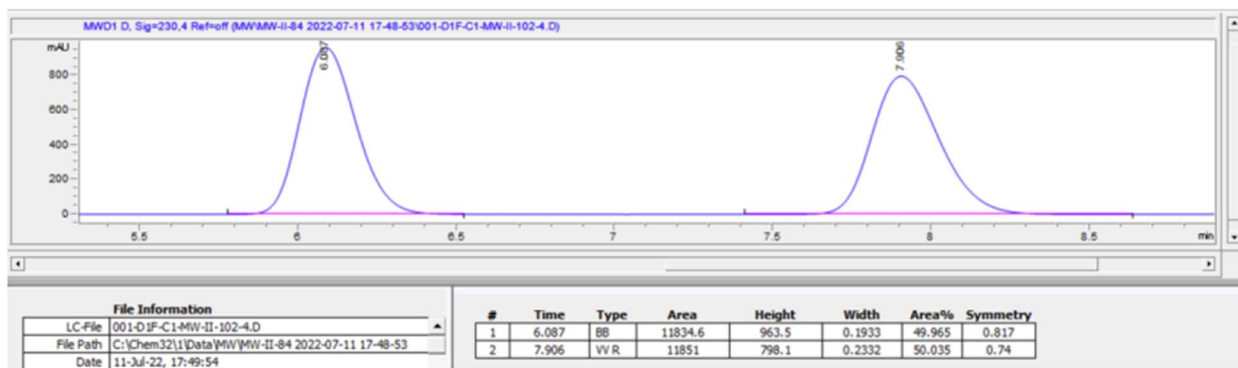
Enantioenriched



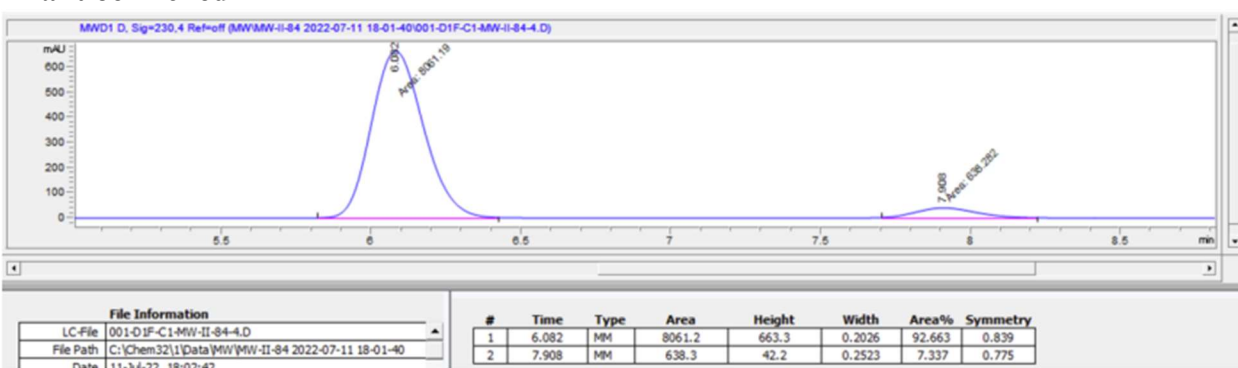
1-((1*S*,2*R*)-2-methyl-2-phenylcyclopropyl)-3-phenyl-1*H*-pyrazole (3k)



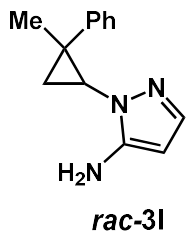
Racemic



Enantioenriched

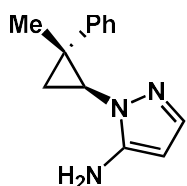
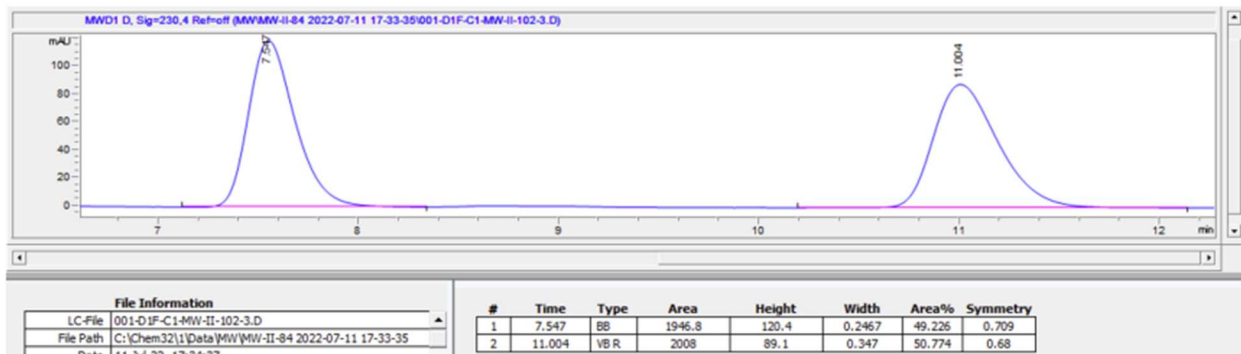


1-((1*S*,2*R*)-2-methyl-2-phenylcyclopropyl)-1*H*-pyrazol-3-amine (3l)



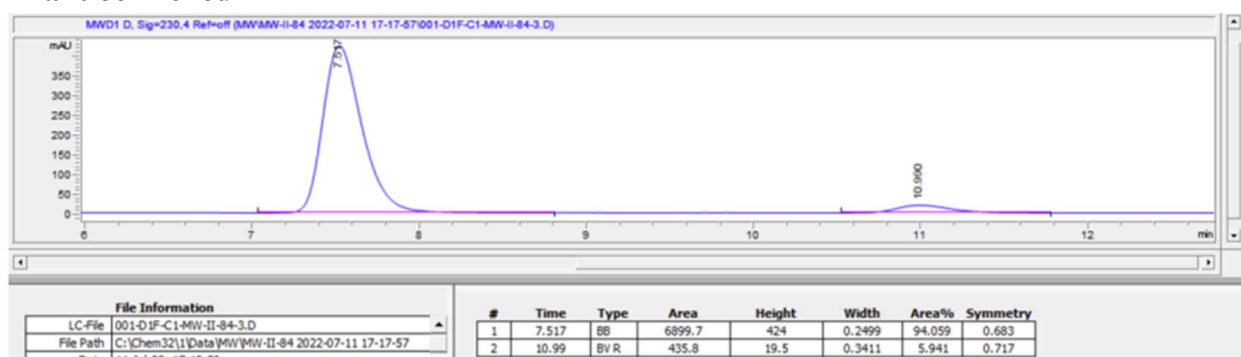
rac-3l

Racemic

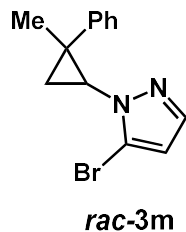


3l

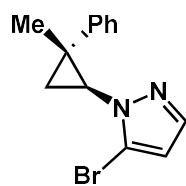
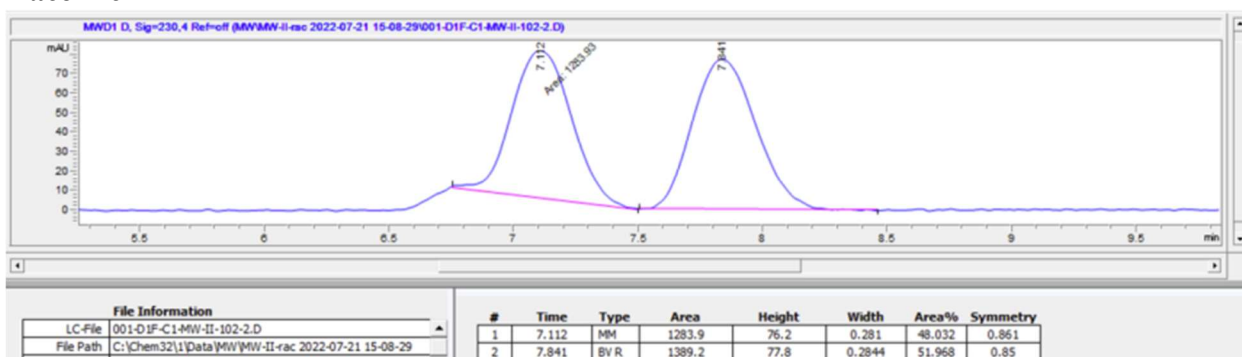
Enantioenriched



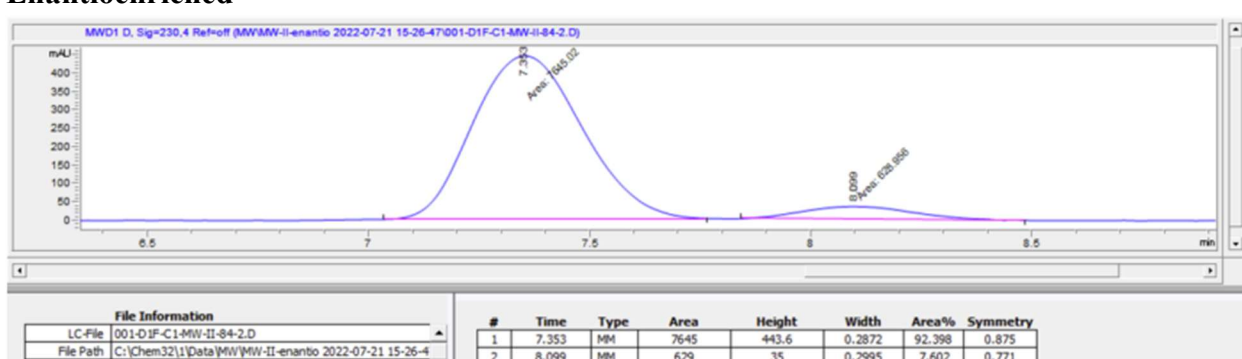
3-bromo-1-((1*S*,2*R*)-2-methyl-2-phenylcyclopropyl)-1*H*-pyrazole (3m)



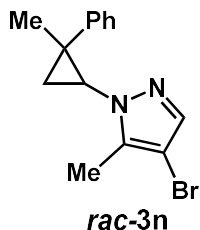
Racemic



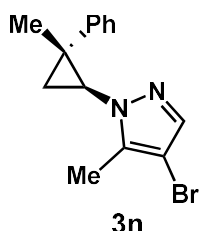
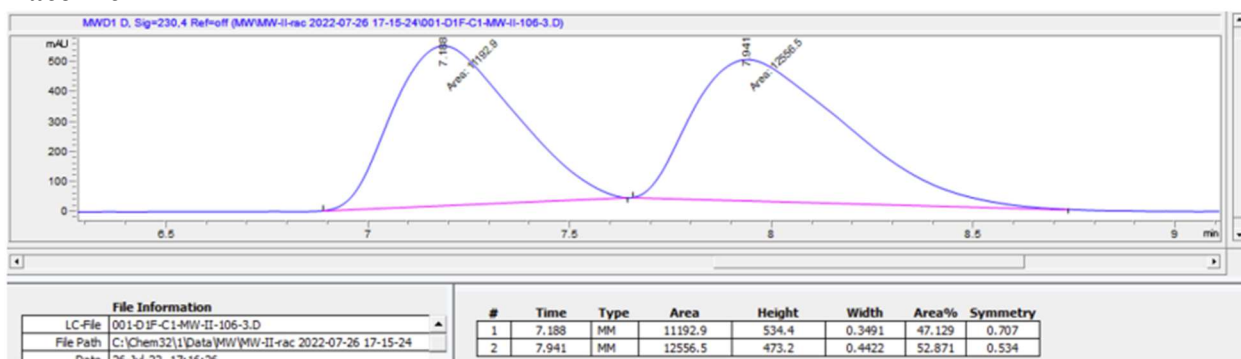
Enantioenriched



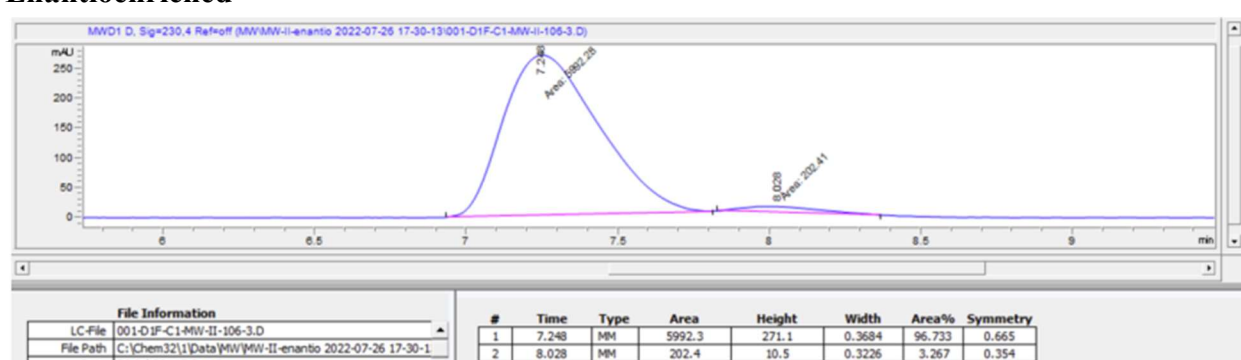
4-bromo-3-methyl-1-((1*S*,2*R*)-2-methyl-2-phenylcyclopropyl)-1*H*-pyrazole (3n)



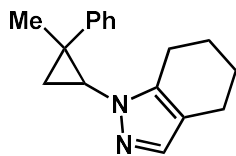
Racemic



Enantioenriched

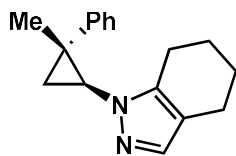
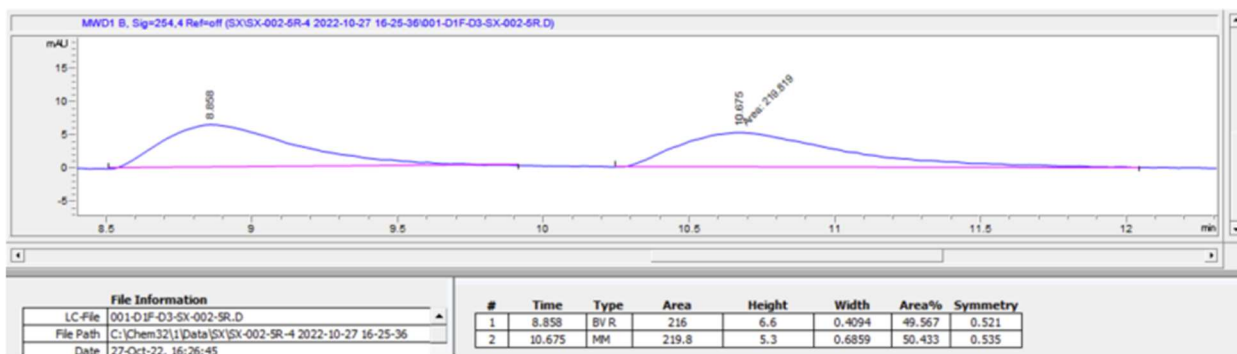


2-((1*S*,2*R*)-2-methyl-2-phenylcyclopropyl)-4,5,6,7-tetrahydro-2*H*-indazole (3o)



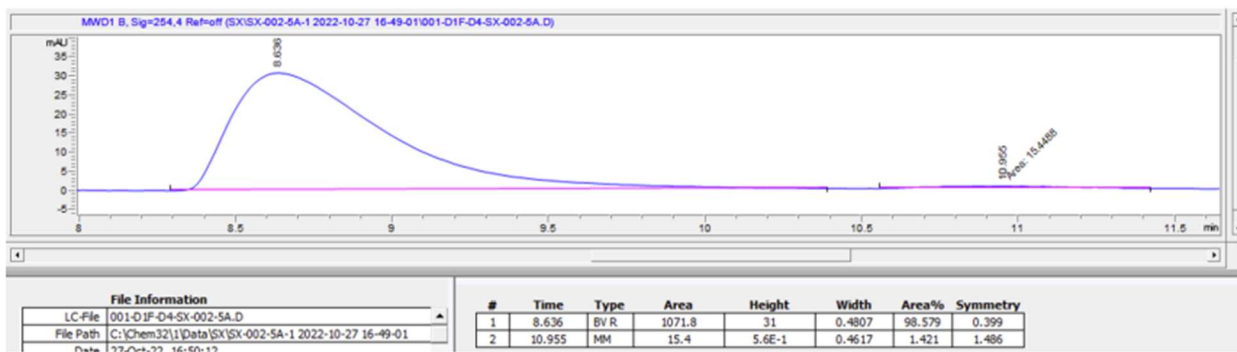
rac-3o

Racemic

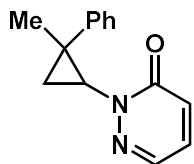


3o

Enantioenriched

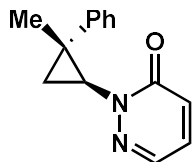
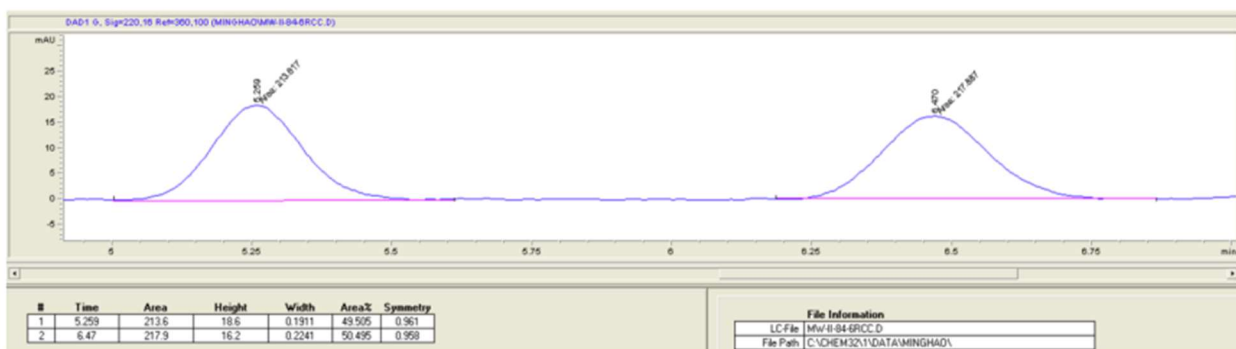


2-((1*S*,2*R*)-2-methyl-2-phenylcyclopropyl)pyridazin-3(2*H*)-one (3p)



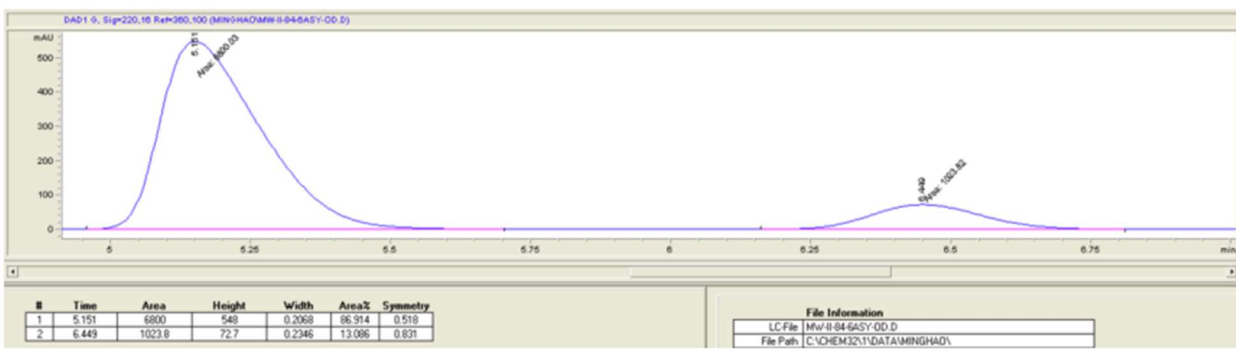
rac-3p

Racemic

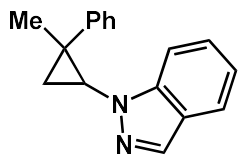


3p

Enantioenriched

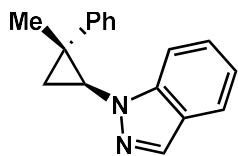
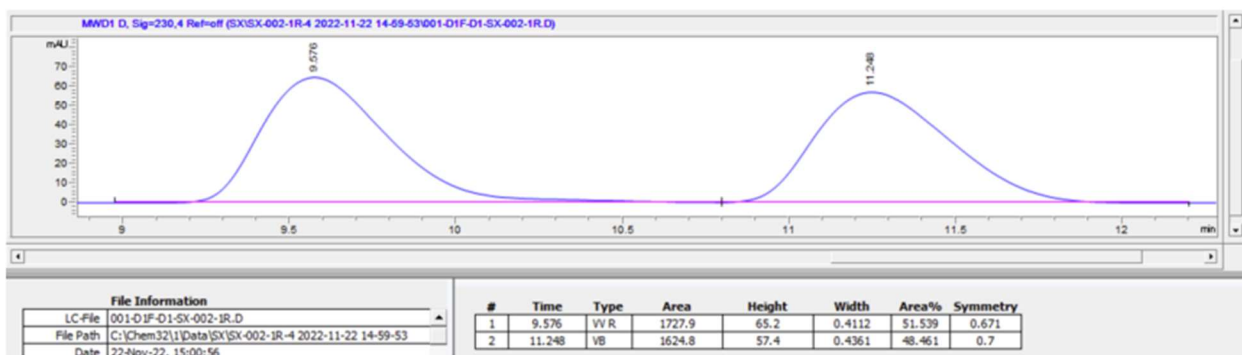


2-((1*S*,2*R*)-2-methyl-2-phenylcyclopropyl)-2*H*-indazole (3q)



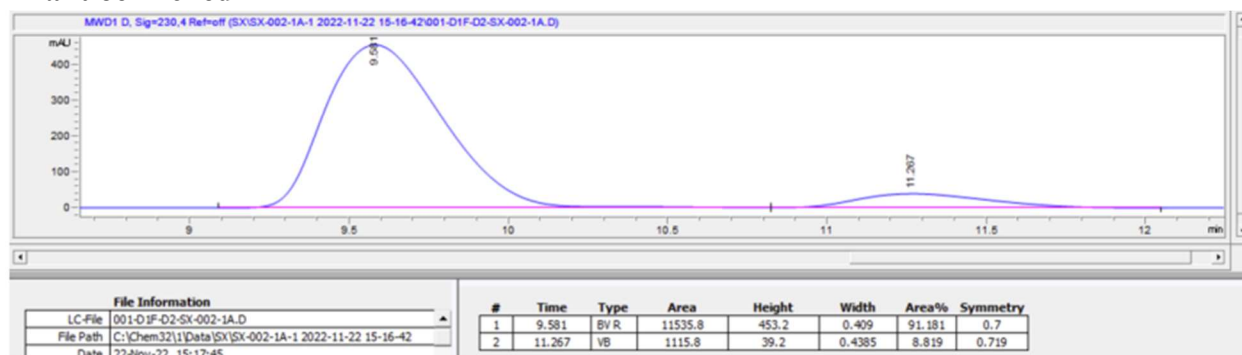
rac-3q

Racemic

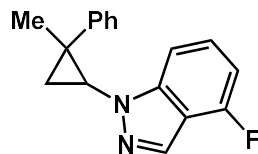


3q

Enantioenriched

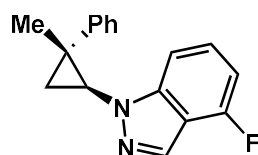
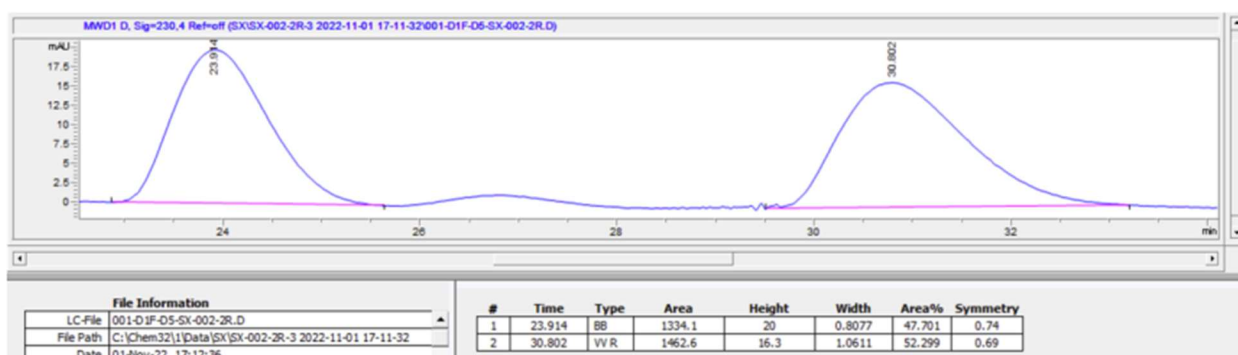


4-fluoro-2-((1*S*,2*R*)-2-methyl-2-phenylcyclopropyl)-2*H*-indazole (3r)



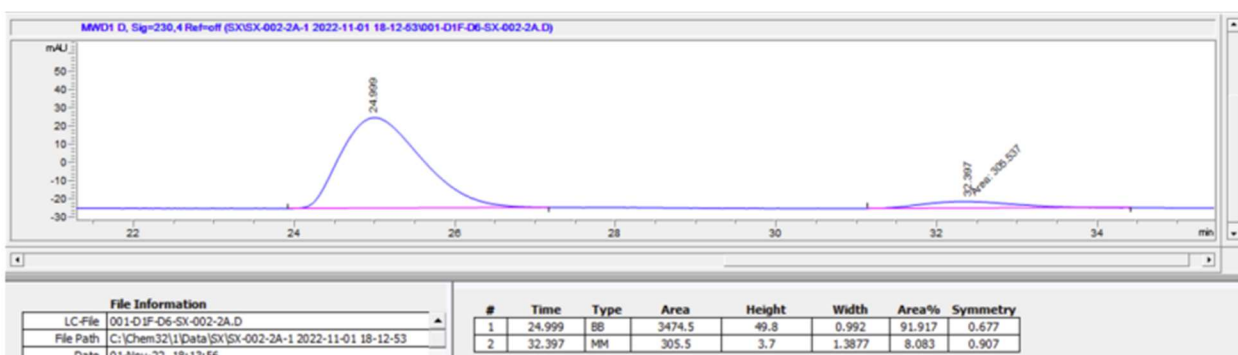
rac-3r

Racemic



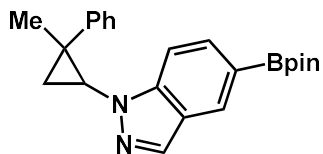
3r

Enantioenriched



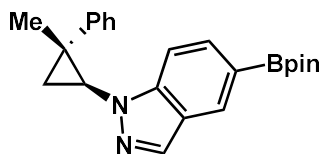
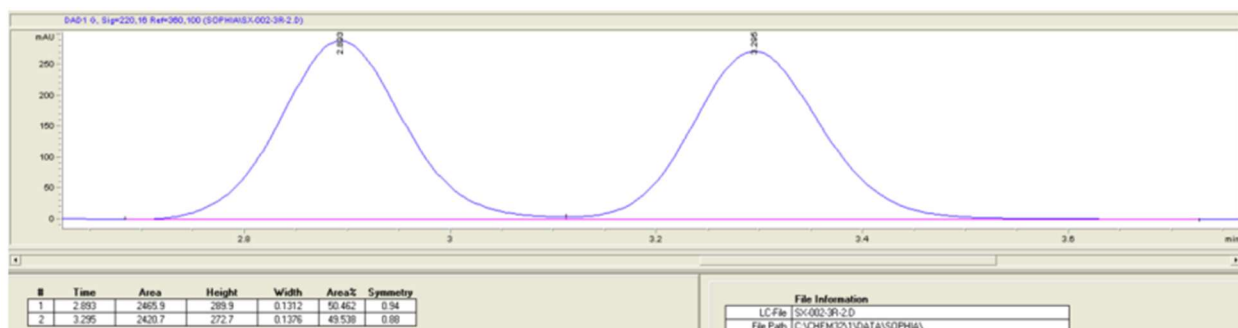
**2-((1*S*,2*R*)-2-methyl-2-phenylcyclopropyl)-5-(4,4,5,5-tetramethyl-1,3,2-dioxaborolan-2-yl)-
2*H*-indazole (3s)**

2*H*-indazole (3s)

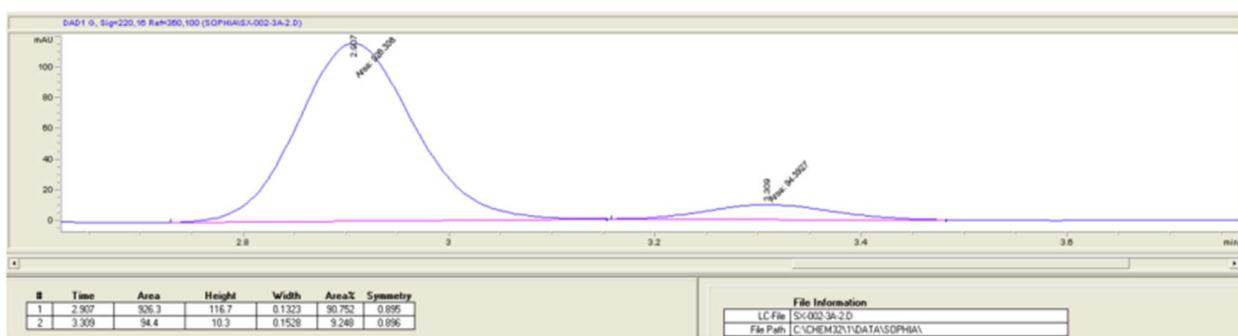


rac-3s

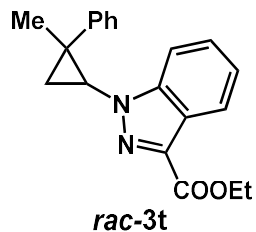
Racemic



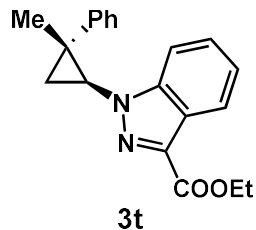
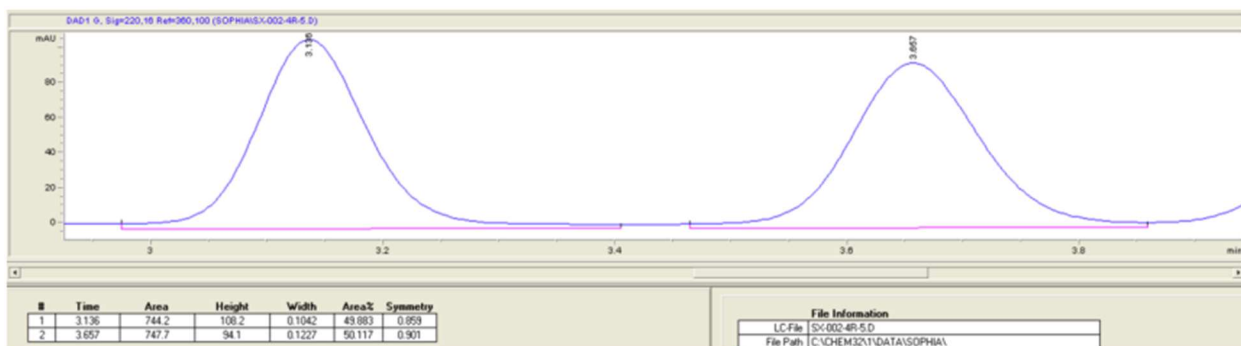
Enantioenriched



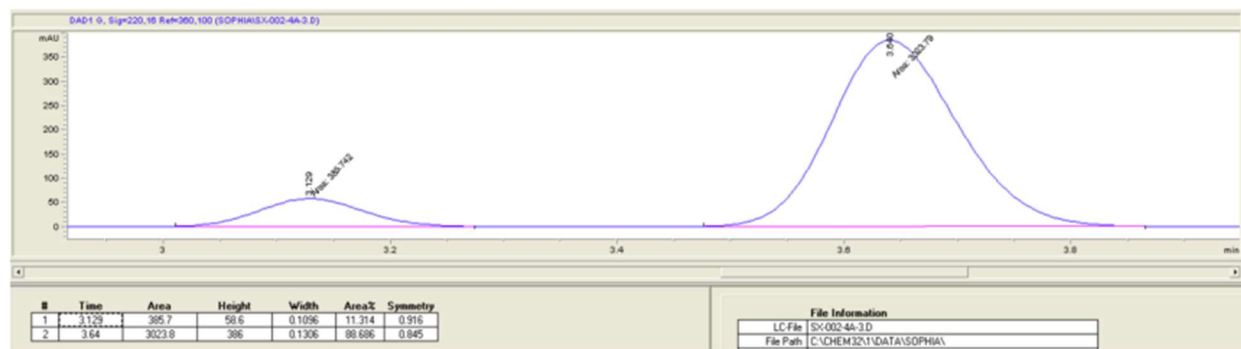
Methyl 2-((1*S*,2*R*)-2-methyl-2-phenylcyclopropyl)-2*H*-indazole-3-carboxylate (3t**)**



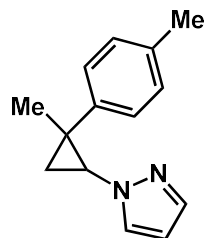
Racemic



Enantioenriched

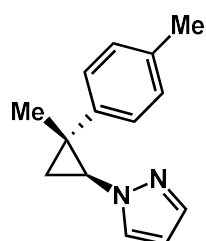
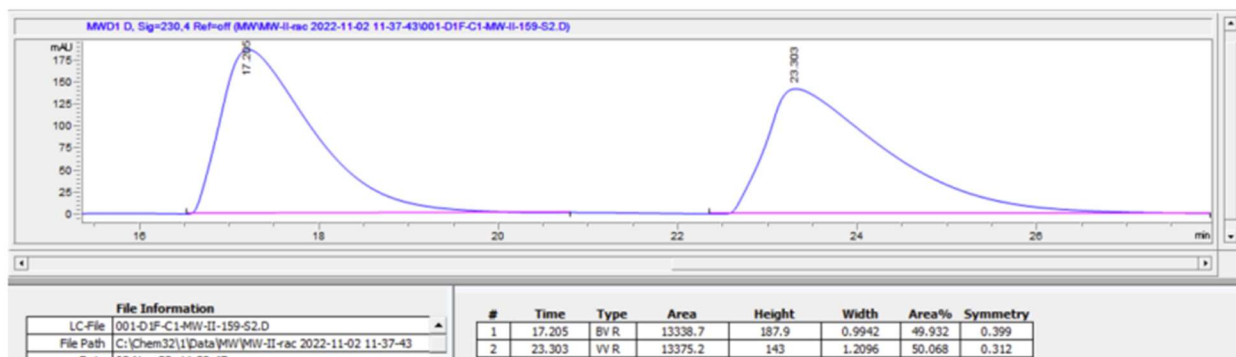


1-((1*S*,2*R*)-2-methyl-2-(*p*-tolyl)cyclopropyl)-1*H*-pyrazole (4b)



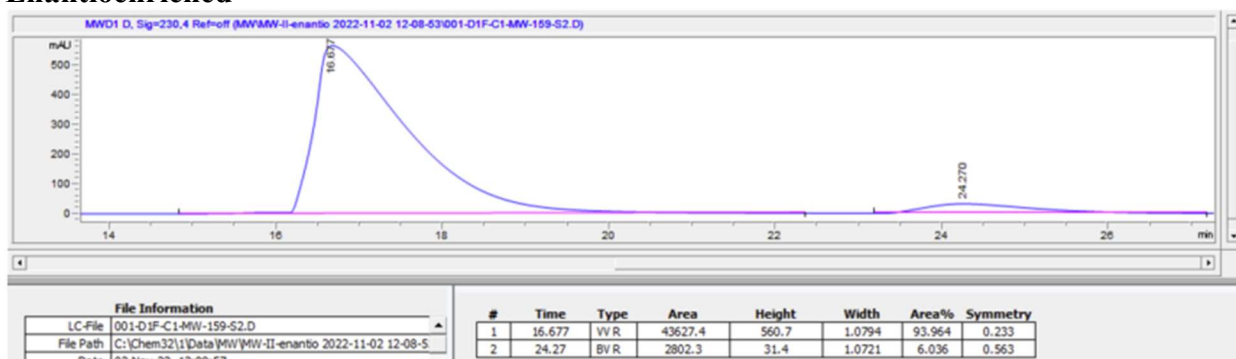
rac-4b

Racemic

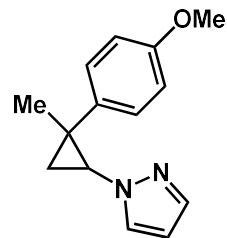


4b

Enantioenriched

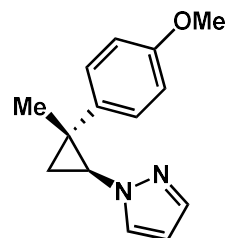
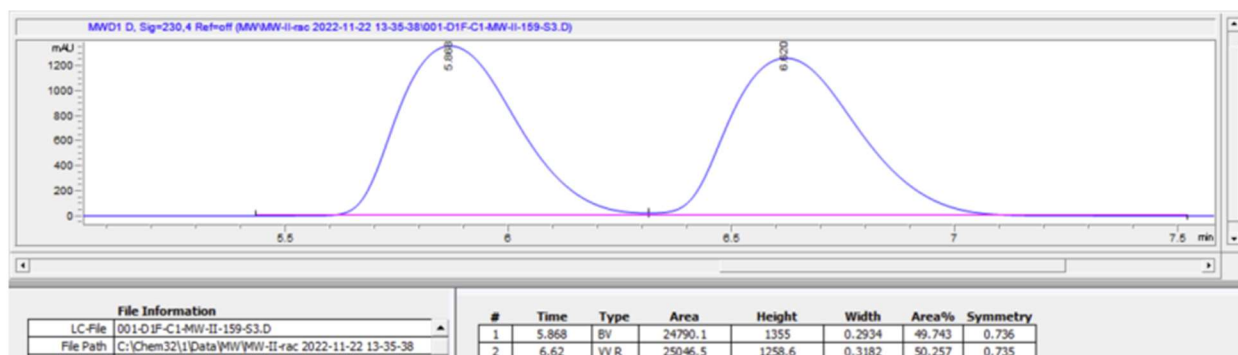


1-((1*S*,2*R*)-2-(4-methoxyphenyl)-2-methylcyclopropyl)-1*H*-pyrazole (4c)



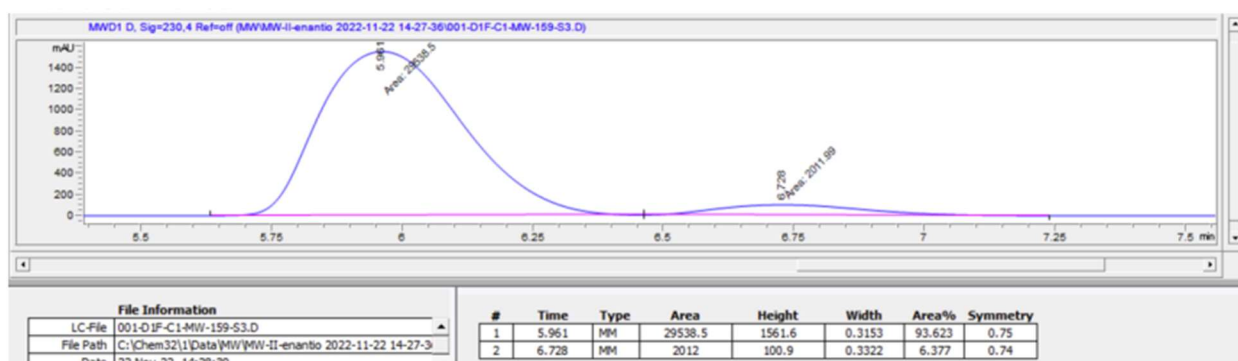
rac-4c

Racemic

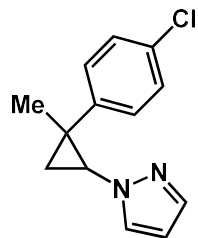


4c

Enantioenriched

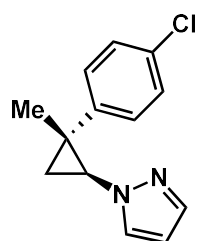
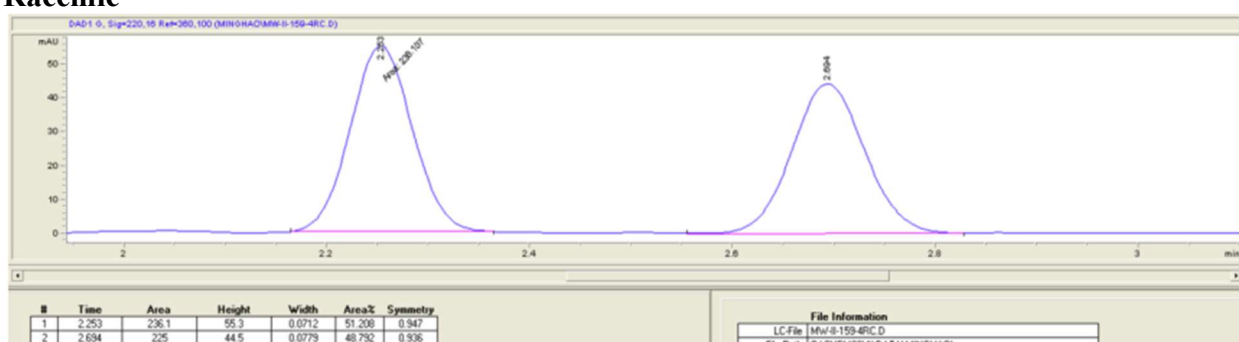


1-((1*S*,2*R*)-2-(4-chlorophenyl)-2-methylcyclopropyl)-1*H*-pyrazole (4d)



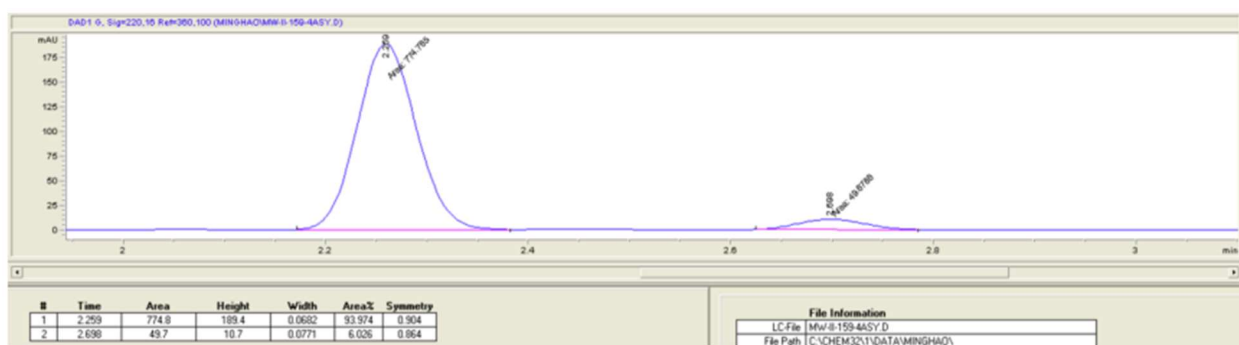
rac-4d

Racemic

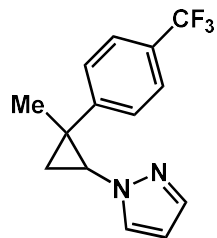


4d

Enantioenriched

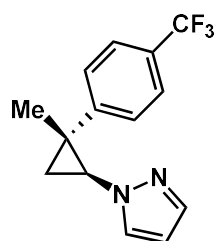
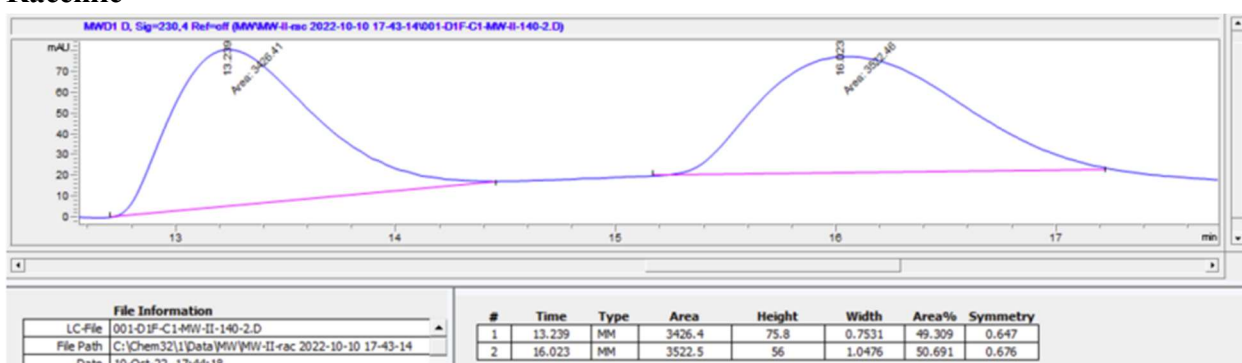


1-((1*S*,2*R*)-2-methyl-2-(4-(trifluoromethyl)phenyl)cyclopropyl)-1*H*-pyrazole (4e)



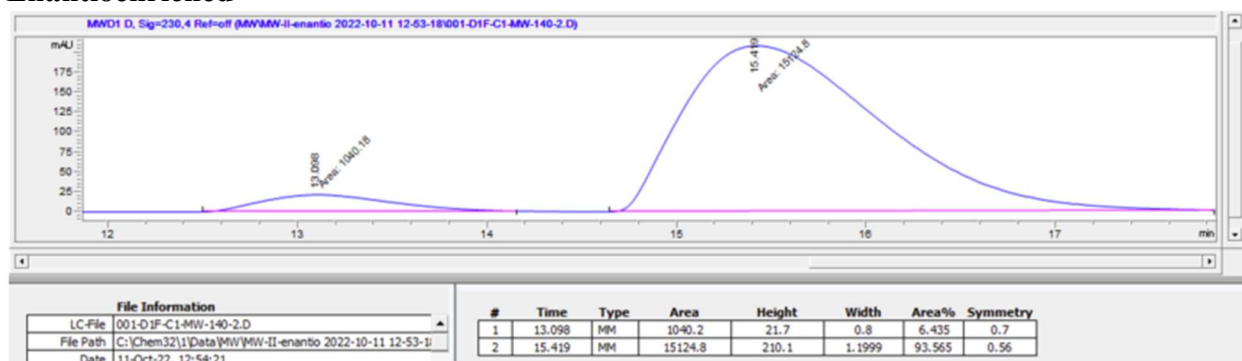
rac-4e

Racemic

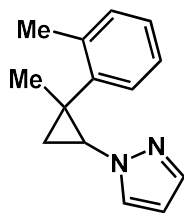


4e

Enantioenriched

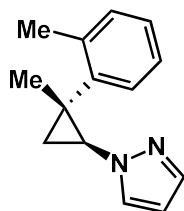
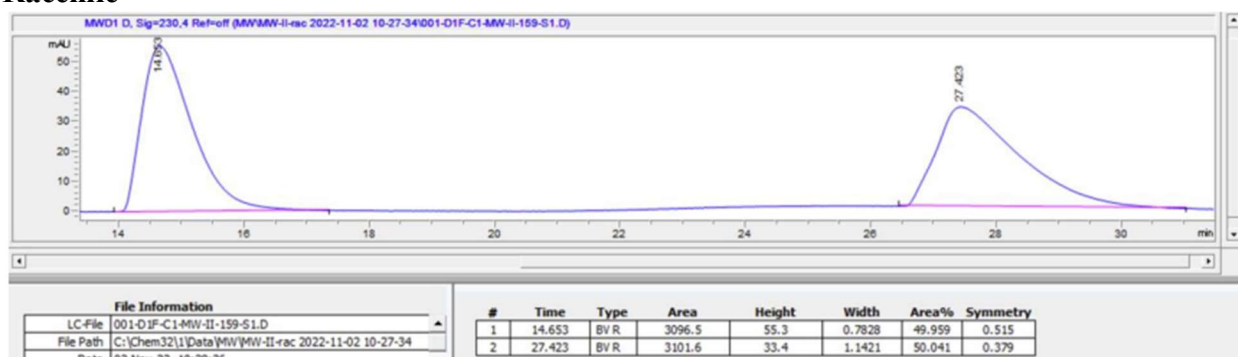


1-((1*S*,2*R*)-2-methyl-2-(*o*-tolyl)cyclopropyl)-1*H*-pyrazole (4f)



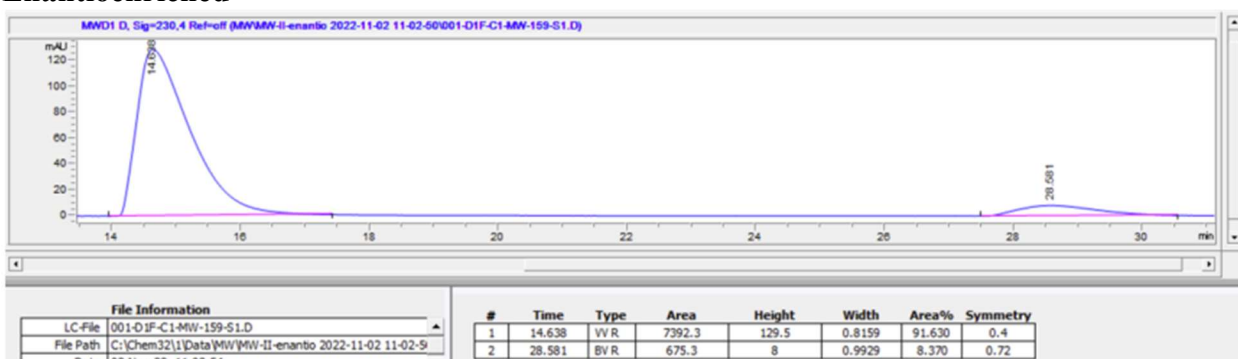
rac-4f

Racemic

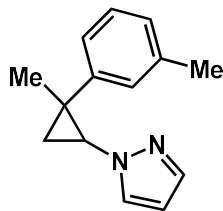


4f

Enantioenriched

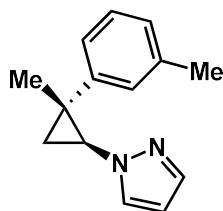
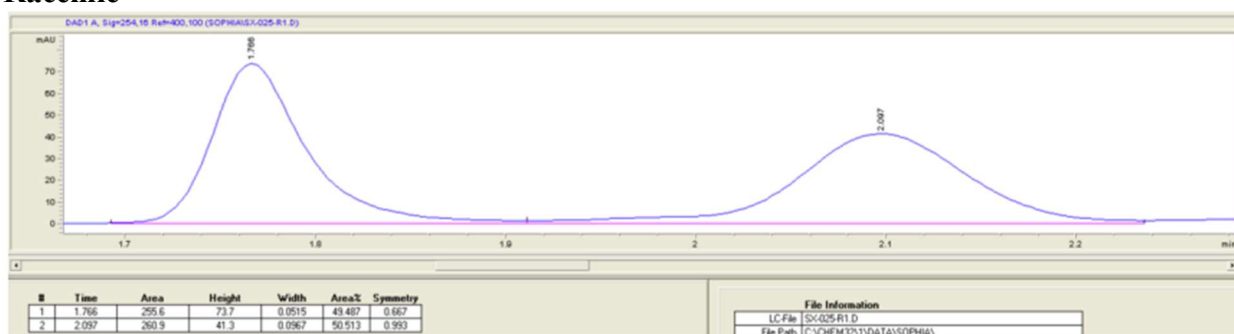


1-((1*S*,2*R*)-2-methyl-2-(*m*-tolyl)cyclopropyl)-1*H*-pyrazole (4g)



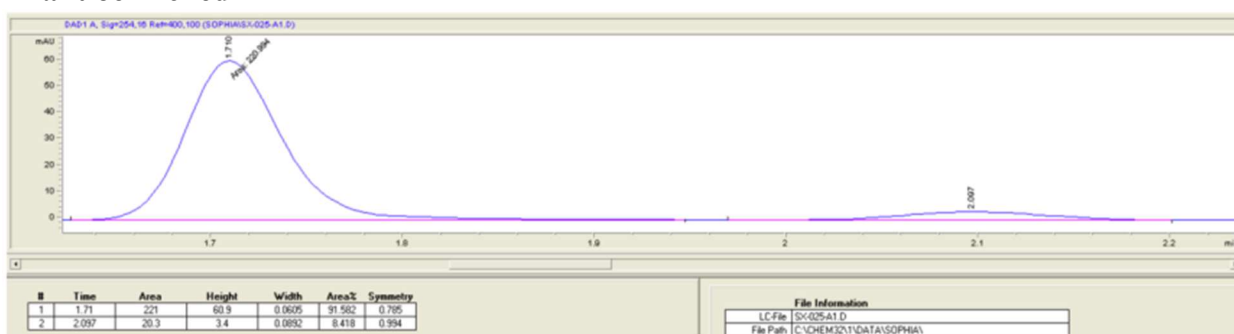
rac-4g

Racemic

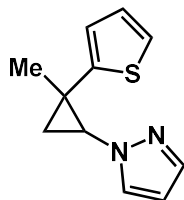


4g

Enantioenriched

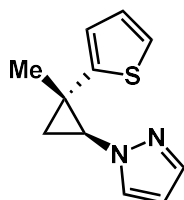
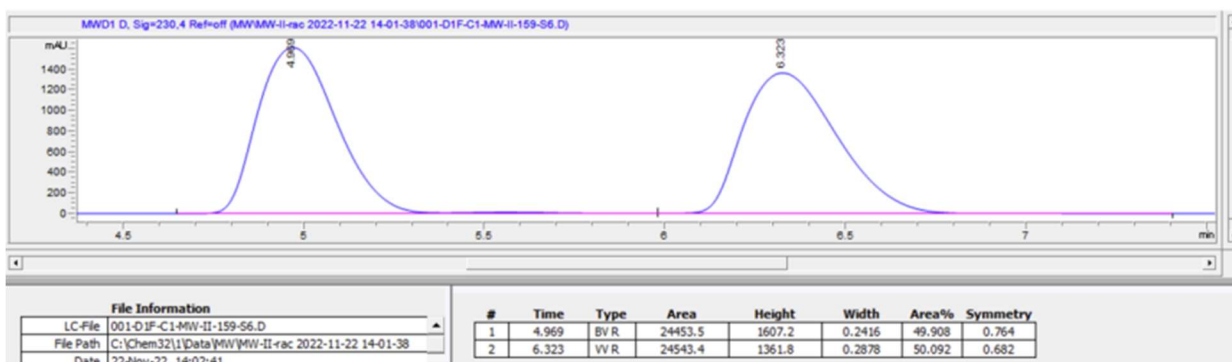


1-((1*S*,2*S*)-2-methyl-2-(thiophen-2-yl)cyclopropyl)-1*H*-pyrazole (4h)



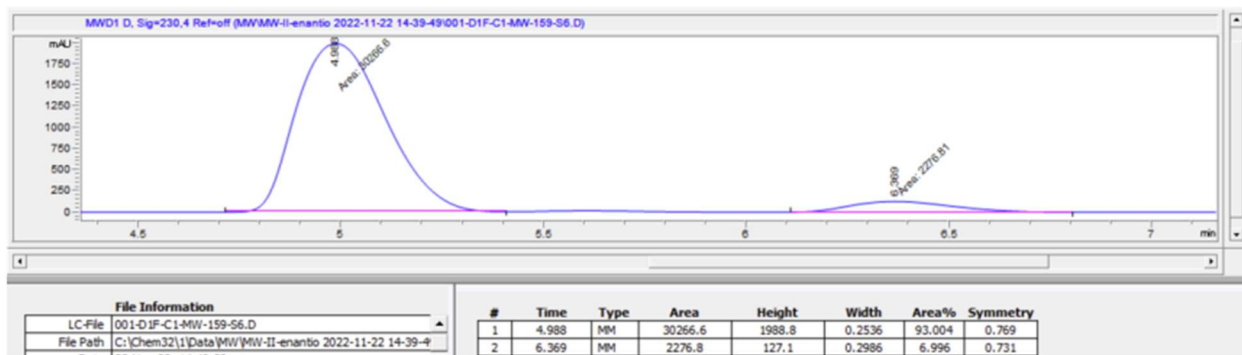
rac-4h

Racemic

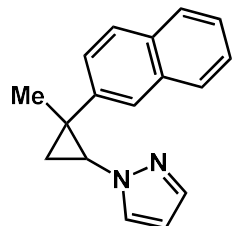


4h

Enantioenriched

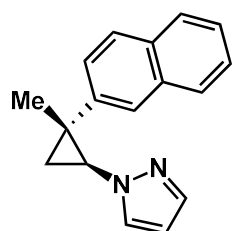
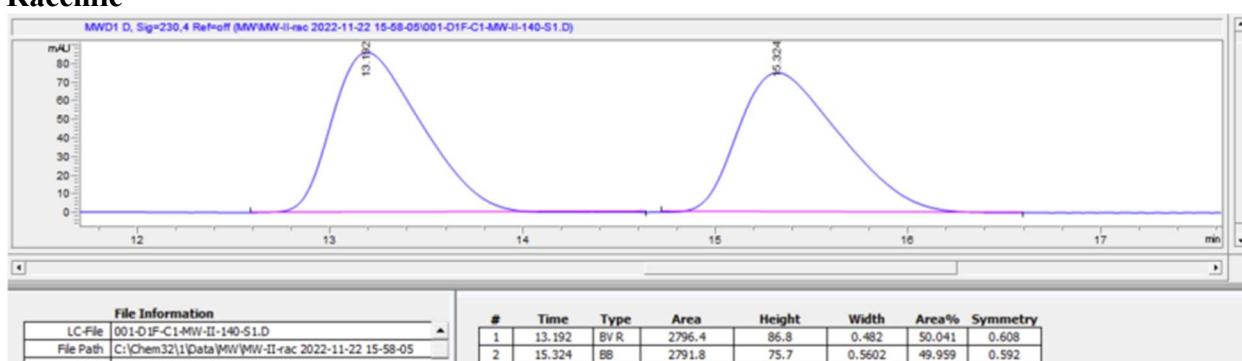


1-((1*S*,2*R*)-2-methyl-2-(naphthalen-2-yl)cyclopropyl)-1*H*-pyrazole (4i)



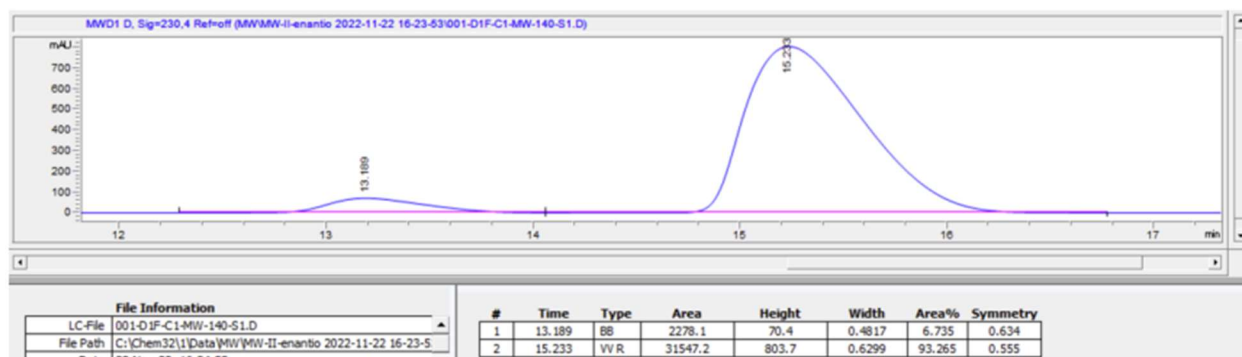
rac-4i

Racemic

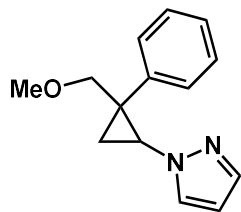


4i

Enantioenriched

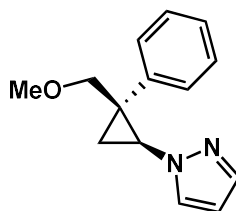
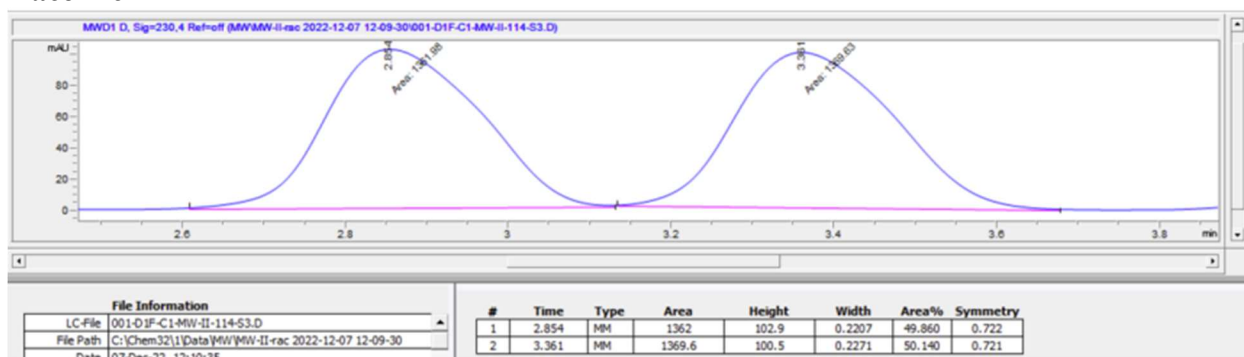


1-((1*S*,2*S*)-2-(methoxymethyl)-2-phenylcyclopropyl)-1*H*-pyrazole (4j)



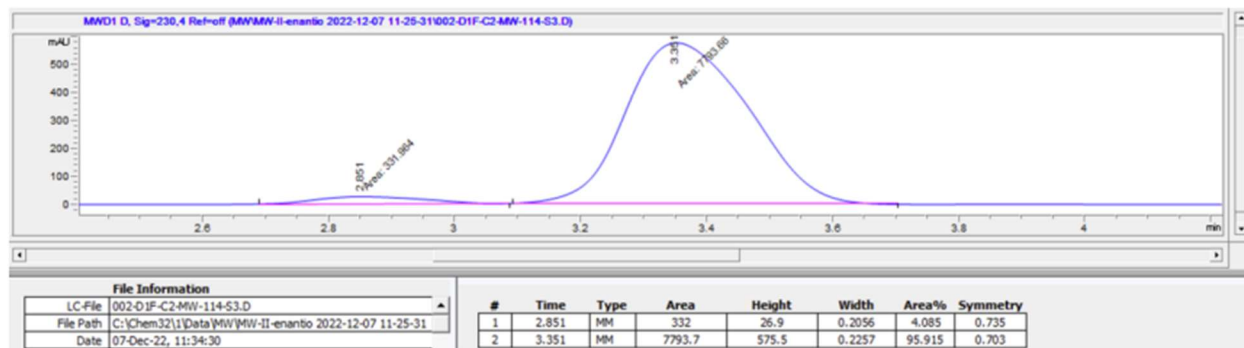
rac-4j

Racemic

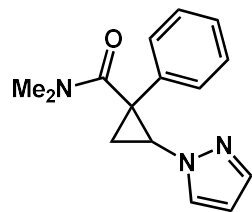


4j

Enantioenriched

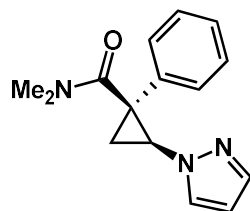
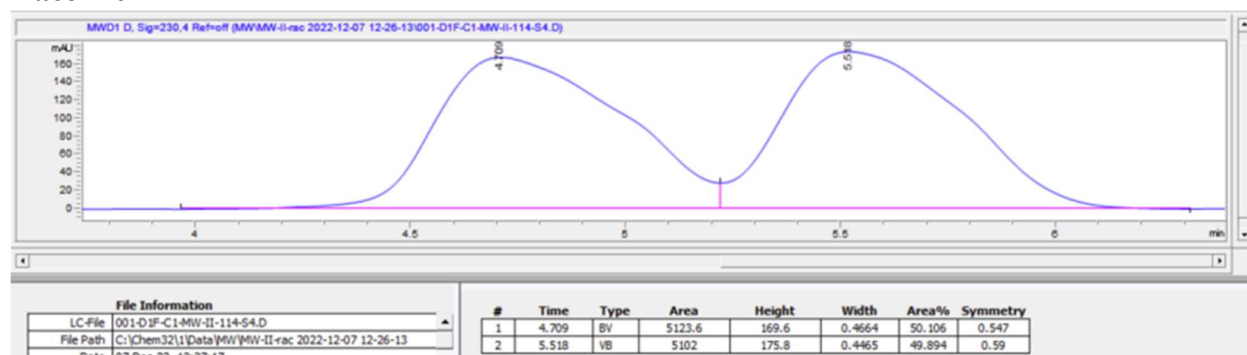


(1*S*,2*S*)-*N,N*-dimethyl-1-phenyl-2-(1*H*-pyrazol-1-yl)cyclopropane-1-carboxamide (4k)



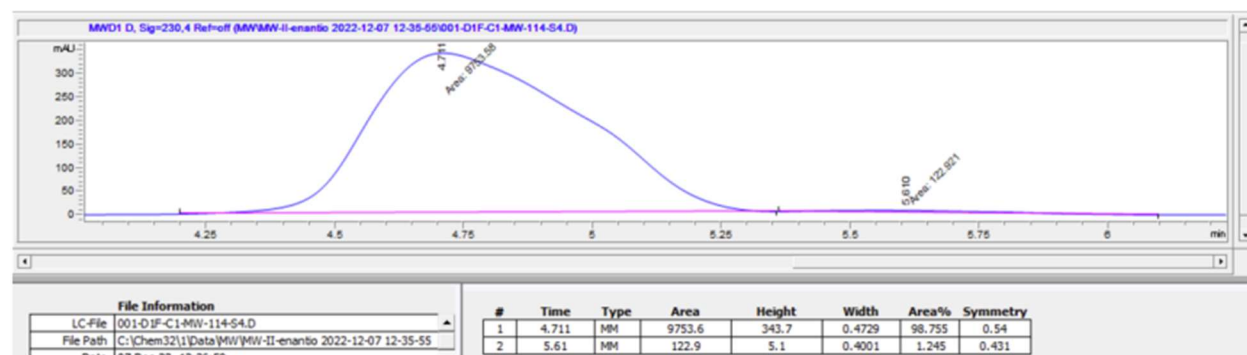
rac-4k

Racemic

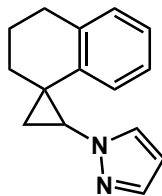


4k

Enantioenriched

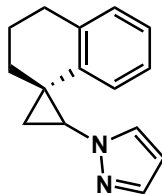
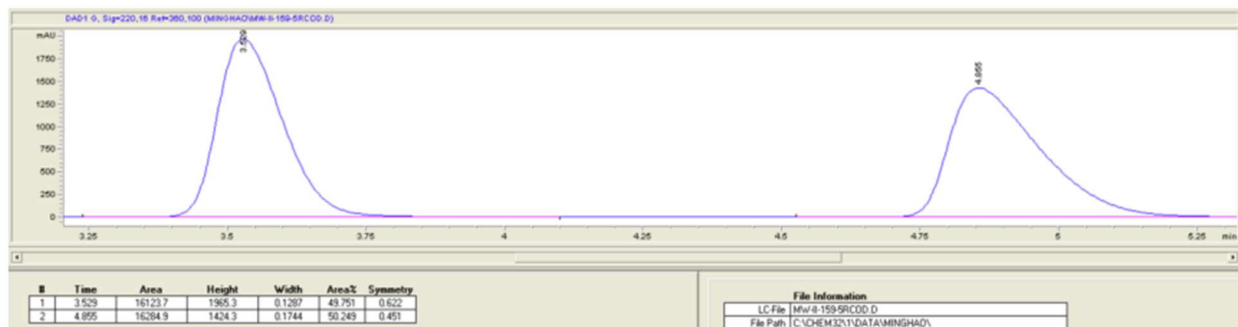


1-((1*R*,2*S*)-3',4'-dihydro-2'*H*-spiro[cyclopropane-1,1'-naphthalen]-2-yl)-1*H*-pyrazole (4l)



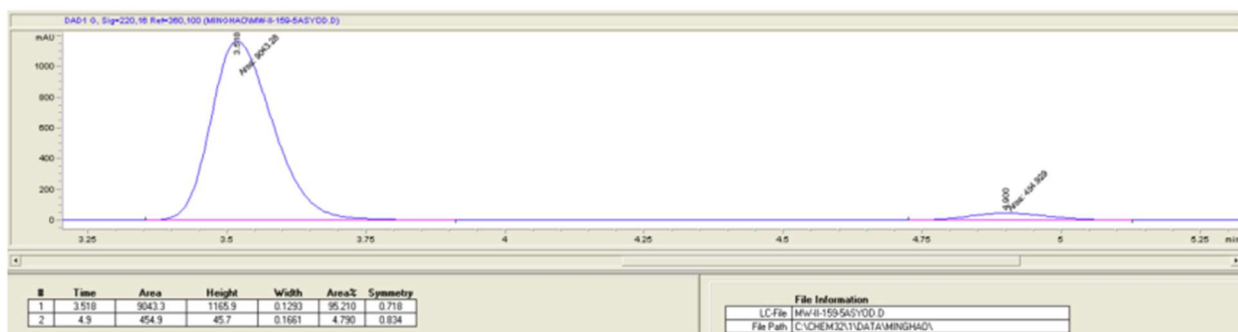
rac-4l

Racemic

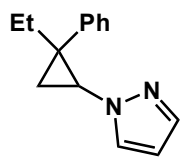


4l

Enantioenriched

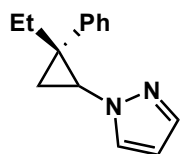
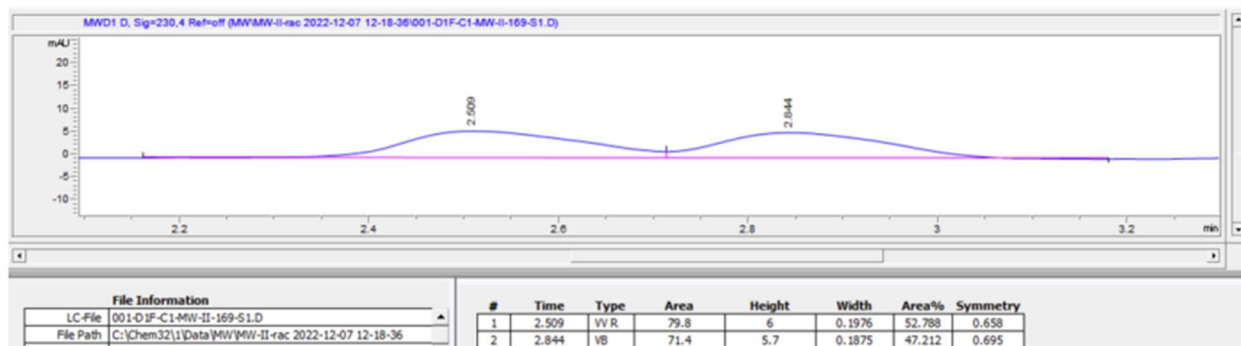


1-((1*S*,2*R*)-2-ethyl-2-phenylcyclopropyl)-1*H*-pyrazole (4m)



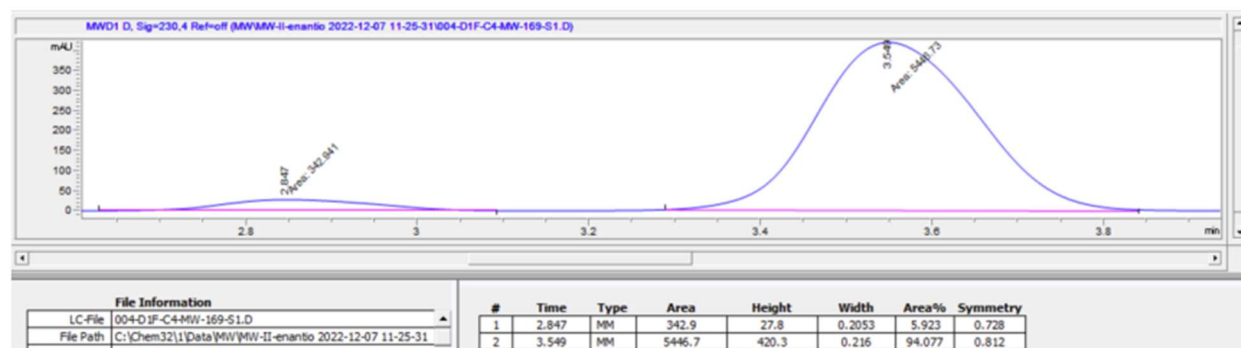
rac-4m

Racemic

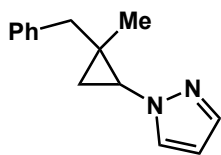


4m

Enantioenriched

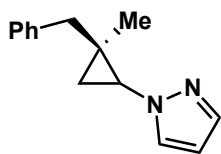
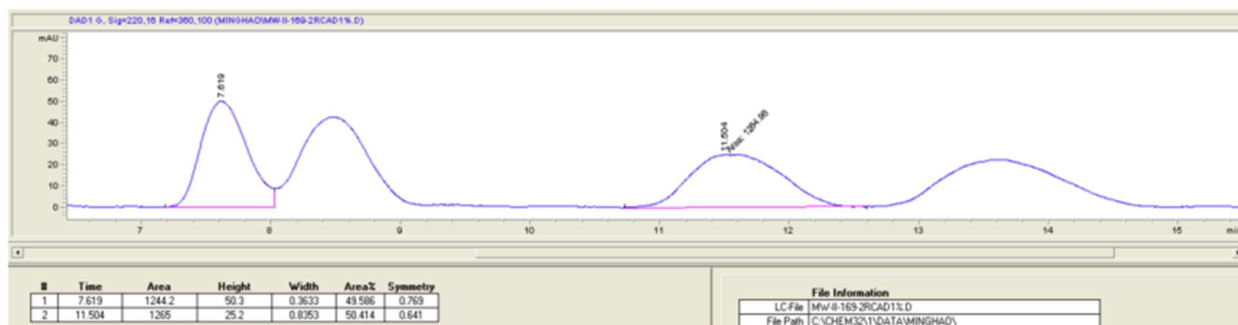


1-((1*S*,2*R*)-2-benzyl-2-methylcyclopropyl)-1*H*-pyrazole (4n)



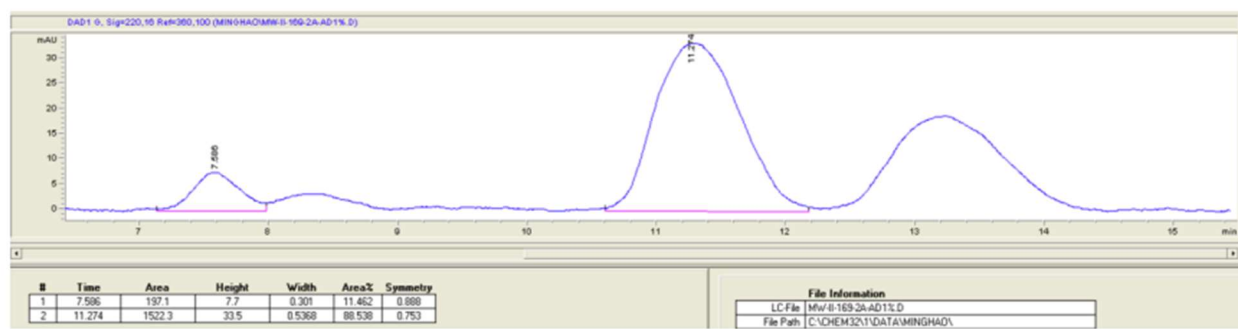
rac-4n

Racemic



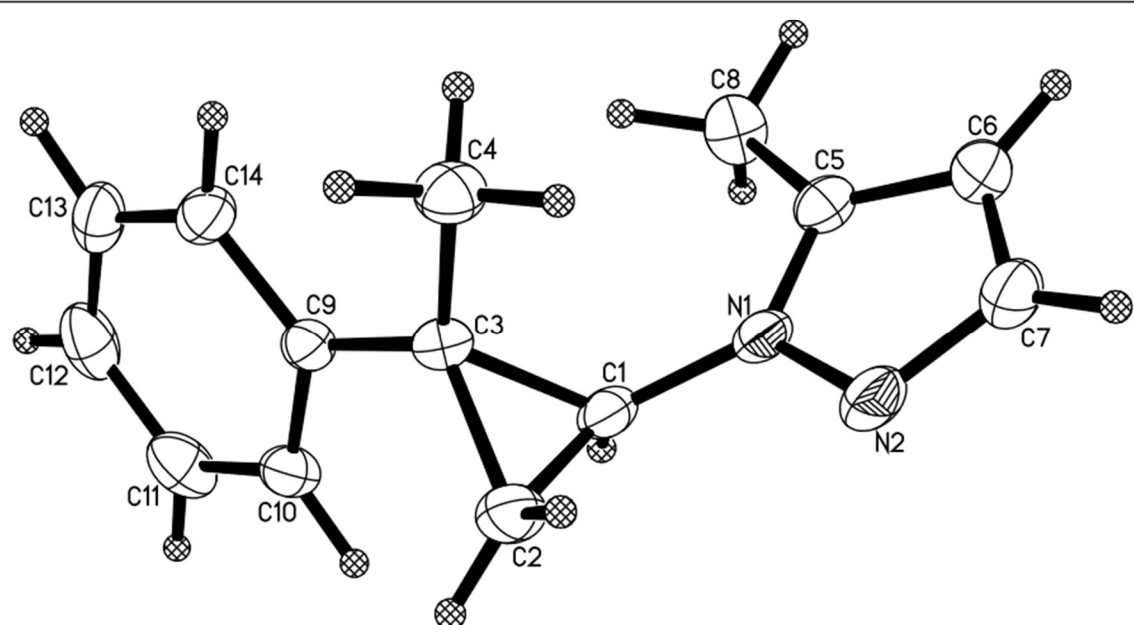
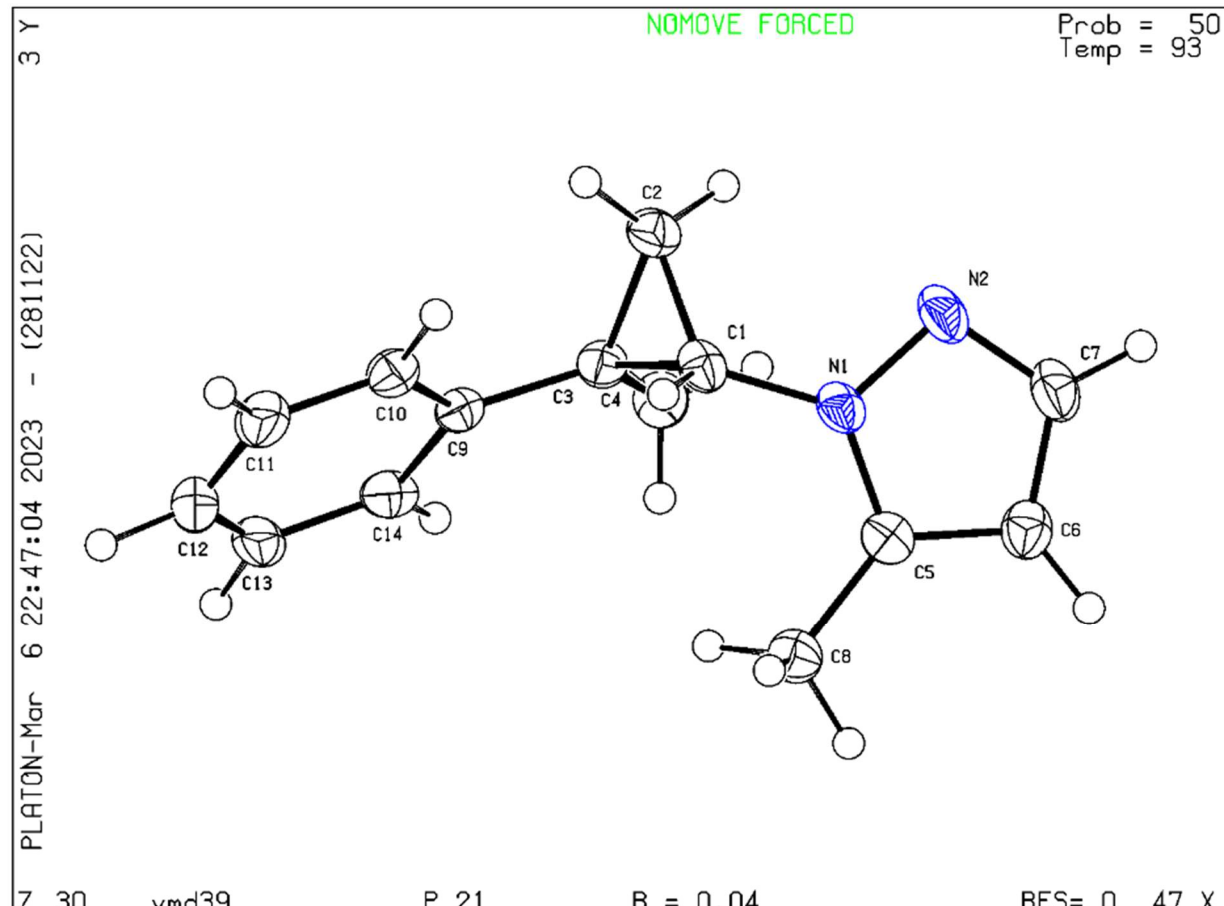
4n

Enantioenriched



APPENDIX C: X-Ray Crystallographic Data

3-methyl-1-((1*S*,2*R*)-2-methyl-2-phenylcyclopropyl)-1*H*-pyrazole (3j)



Crystal data and structure refinement for 3j

Identification code	3j	
Empirical formula	C ₁₄ H ₁₆ N ₂	
Formula weight	212.29	
Temperature	93(2) K	
Wavelength	1.54178 Å	
Crystal system	Monoclinic	
Space group	<i>P</i> 2 ₁	
Unit cell dimensions	a = 9.3916(5) Å b = 5.6428(3) Å c = 11.2883(5) Å	α = 90° β = 95.053(5)° γ = 90°
Volume	595.90(5) Å ³	
Z	2	
Density (calculated)	1.183 Mg/m ³	
Absorption coefficient	0.542 mm ⁻¹	
F(000)	228	
Crystal color	colorless	
Crystal size	0.211 x 0.175 x 0.128 mm ³	
Theta range for data collection	3.931 to 68.320°	
Index ranges	-11 ≤ <i>h</i> ≤ 11, -6 ≤ <i>k</i> ≤ 6, -10 ≤ <i>l</i> ≤ 13	
Reflections collected	7444	
Independent reflections	2170 [R(int) = 0.0458]	
Completeness to theta = 67.679°	99.8%	

Absorption correction	Semi-empirical from equivalents
Max. and min. transmission	0.8643 and 0.7427
Refinement method	Full-matrix least-squares on F^2
Data / restraints / parameters	2170 / 1 / 209
Goodness-of-fit on F^2	1.047
Final R indices [$I > 2\text{sigma}(I)$ = 2072 data]	$R_1 = 0.0414$, $wR_2 = 0.1098$
R indices (all data, 0.83 Å)	$R_1 = 0.0435$, $wR_2 = 0.1122$
Largest diff. peak and hole	0.196 and -0.194 e.Å ⁻³

**Atomic coordinates (x 10⁴) and equivalent isotropic displacement parameters (Å² x 10³) for
3j**

	x	y	z	U(equiv.)
N(1)	6884(2)	6535(4)	8522(2)	25(1)
N(2)	7389(2)	8343(5)	9246(2)	33(1)
C(1)	5423(3)	5786(5)	8477(2)	25(1)
C(2)	4294(3)	7508(6)	8758(2)	30(1)
C(3)	4342(3)	6684(5)	7480(2)	23(1)
C(4)	4887(3)	8448(5)	6629(2)	29(1)
C(5)	7918(3)	5578(5)	7901(2)	25(1)
C(6)	9153(3)	6801(6)	8239(2)	30(1)
C(7)	8769(3)	8472(6)	9065(2)	33(1)
C(8)	7621(3)	3573(5)	7060(3)	32(1)
C(9)	3257(3)	4921(5)	6985(2)	22(1)
C(10)	2607(3)	3329(5)	7721(2)	27(1)
C(11)	1637(3)	1654(6)	7251(3)	36(1)
C(12)	1293(3)	1514(6)	6031(3)	39(1)
C(13)	1915(3)	3079(6)	5295(2)	33(1)
C(14)	2880(3)	4774(5)	5765(2)	28(1)

U(equiv.) is defined as one third of the trace of the orthogonalized U^{ij} tensor.

Bond lengths [Å] and angles [°] for 3j

N(1)–C(5)	1.359(4)
N(1)–N(2)	1.366(3)
N(1)–C(1)	1.432(3)
N(2)–C(7)	1.332(4)
C(1)–C(2)	1.493(4)
C(1)–C(3)	1.534(3)
C(1)–H(1)	0.94(3)
C(2)–C(3)	1.520(3)
C(2)–H(2A)	1.00(4)
C(2)–H(2B)	1.00(4)
C(3)–C(9)	1.497(4)
C(3)–C(4)	1.504(4)
C(4)–H(4A)	1.01(4)
C(4)–H(4B)	0.97(4)
C(4)–H(4C)	1.00(4)
C(5)–C(6)	1.374(4)
C(5)–C(8)	1.488(4)
C(6)–C(7)	1.396(4)
C(6)–H(6)	0.98(4)
C(7)–H(7)	0.96(4)
C(8)–H(8A)	1.01(4)
C(8)–H(8B)	0.97(5)
C(8)–H(8C)	1.02(5)
C(9)–C(14)	1.395(3)
C(9)–C(10)	1.399(4)
C(10)–C(11)	1.386(4)
C(10)–H(10)	0.96(3)
C(11)–C(12)	1.388(5)
C(11)–H(11)	0.98(4)
C(12)–C(13)	1.378(5)
C(12)–H(12)	1.04(4)
C(13)–C(14)	1.390(4)
C(13)–H(13)	1.01(4)
C(14)–H(14)	1.01(3)
C(5)–N(1)–N(2)	112.3(2)
C(5)–N(1)–C(1)	126.2(2)
N(2)–N(1)–C(1)	121.5(2)

C(7)–N(2)–N(1)	103.9(2)
N(1)–C(1)–C(2)	119.8(2)
N(1)–C(1)–C(3)	119.9(2)
C(2)–C(1)–C(3)	60.29(17)
N(1)–C(1)–H(1)	114.6(17)
C(2)–C(1)–H(1)	116.9(17)
C(3)–C(1)–H(1)	114.7(16)
C(1)–C(2)–C(3)	61.19(17)
C(1)–C(2)–H(2A)	113.5(19)
C(3)–C(2)–H(2A)	112.4(19)
C(1)–C(2)–H(2B)	116(2)
C(3)–C(2)–H(2B)	115(2)
H(2A)–C(2)–H(2B)	123(3)
C(9)–C(3)–C(4)	117.4(2)
C(9)–C(3)–C(2)	118.8(2)
C(4)–C(3)–C(2)	116.4(2)
C(9)–C(3)–C(1)	116.1(2)
C(4)–C(3)–C(1)	116.5(2)
C(2)–C(3)–C(1)	58.52(17)
C(3)–C(4)–H(4A)	110(2)
C(3)–C(4)–H(4B)	112(2)
H(4A)–C(4)–H(4B)	109(3)
C(3)–C(4)–H(4C)	110(2)
H(4A)–C(4)–H(4C)	109(3)
H(4B)–C(4)–H(4C)	108(3)
N(1)–C(5)–C(6)	106.4(2)
N(1)–C(5)–C(8)	121.9(2)
C(6)–C(5)–C(8)	131.7(3)
C(5)–C(6)–C(7)	105.3(2)
C(5)–C(6)–H(6)	125(3)
C(7)–C(6)–H(6)	130(3)
N(2)–C(7)–C(6)	112.2(3)
N(2)–C(7)–H(7)	119(2)
C(6)–C(7)–H(7)	128(2)
C(5)–C(8)–H(8A)	112(2)
C(5)–C(8)–H(8B)	112(2)
H(8A)–C(8)–H(8B)	108(4)
C(5)–C(8)–H(8C)	109(3)
H(8A)–C(8)–H(8C)	115(3)
H(8B)–C(8)–H(8C)	100(4)

C(14)–C(9)–C(10)	117.5(2)
C(14)–C(9)–C(3)	120.9(2)
C(10)–C(9)–C(3)	121.6(2)
C(11)–C(10)–C(9)	121.1(2)
C(11)–C(10)–H(10)	117.5(18)
C(9)–C(10)–H(10)	121.3(18)
C(10)–C(11)–C(12)	120.4(3)
C(10)–C(11)–H(11)	118(2)
C(12)–C(11)–H(11)	121(2)
C(13)–C(12)–C(11)	119.2(3)
C(13)–C(12)–H(12)	123(2)
C(11)–C(12)–H(12)	117(2)
C(12)–C(13)–C(14)	120.5(3)
C(12)–C(13)–H(13)	123(2)
C(14)–C(13)–H(13)	116(2)
C(13)–C(14)–C(9)	121.2(3)
C(13)–C(14)–H(14)	120.4(17)
C(9)–C(14)–H(14)	118.4(18)

Anisotropic displacement parameters ($\text{\AA}^2 \times 10^3$) for 3j

	U ¹¹	U ²²	U ³³	U ²³	U ¹³	U ¹²
N(1)	29(1)	30(1)	16(1)	-1(1)	0(1)	-4(1)
N(2)	36(1)	42(1)	20(1)	-7(1)	1(1)	-12(1)
C(1)	30(1)	28(1)	15(1)	2(1)	-1(1)	-6(1)
C(2)	32(1)	34(2)	23(1)	-6(1)	5(1)	-4(1)
C(3)	26(1)	26(1)	19(1)	1(1)	4(1)	0(1)
C(4)	32(1)	28(1)	26(1)	4(1)	5(1)	-4(1)
C(5)	30(1)	25(1)	20(1)	3(1)	0(1)	1(1)
C(6)	27(1)	36(2)	26(1)	3(1)	0(1)	-3(1)
C(7)	34(1)	41(2)	25(1)	-3(1)	-2(1)	-11(1)
C(8)	31(1)	26(2)	38(2)	-4(1)	2(1)	1(1)
C(9)	21(1)	24(1)	21(1)	0(1)	3(1)	3(1)
C(10)	26(1)	30(1)	25(1)	0(1)	7(1)	-1(1)
C(11)	30(1)	34(2)	47(2)	-5(2)	12(1)	-6(1)
C(12)	24(1)	40(2)	53(2)	-18(2)	1(1)	-2(1)
C(13)	28(1)	40(2)	31(1)	-12(1)	-6(1)	8(1)
C(14)	30(1)	31(2)	22(1)	0(1)	1(1)	9(1)

The anisotropic displacement factor exponent takes the form: $-2\pi^2 [h^2 a^{*2} U^{11} + \dots + 2 h k a^* b^* U^{12}]$

Hydrogen coordinates ($\times 10^4$) and isotropic displacement parameters ($\text{\AA}^2 \times 10^3$) for 3j

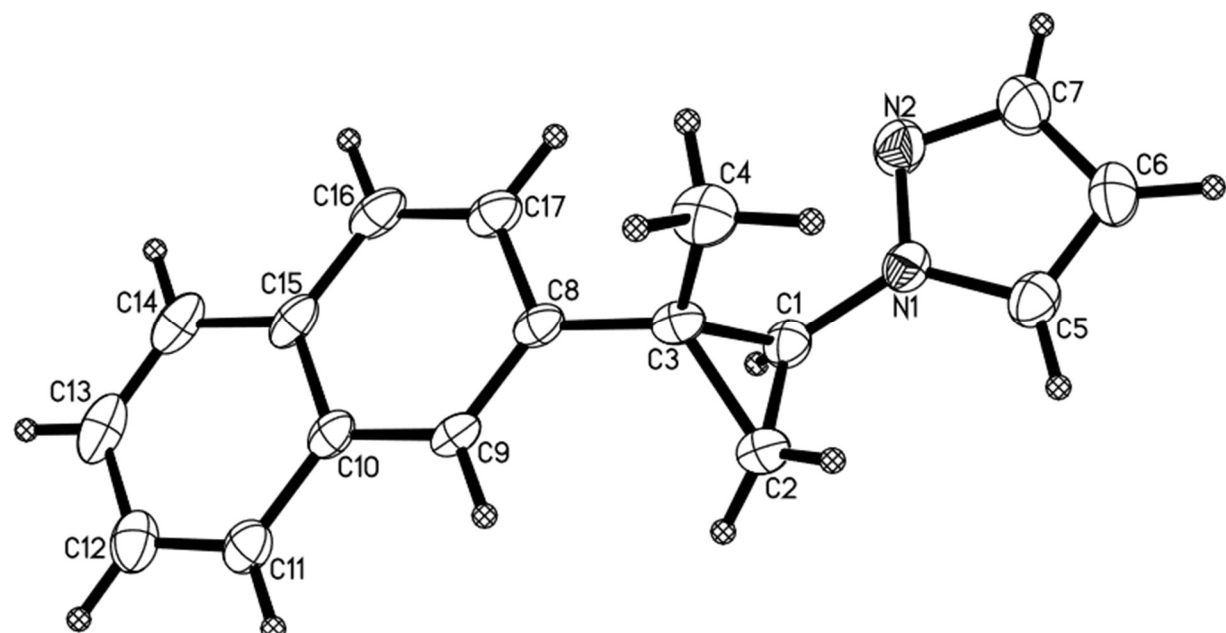
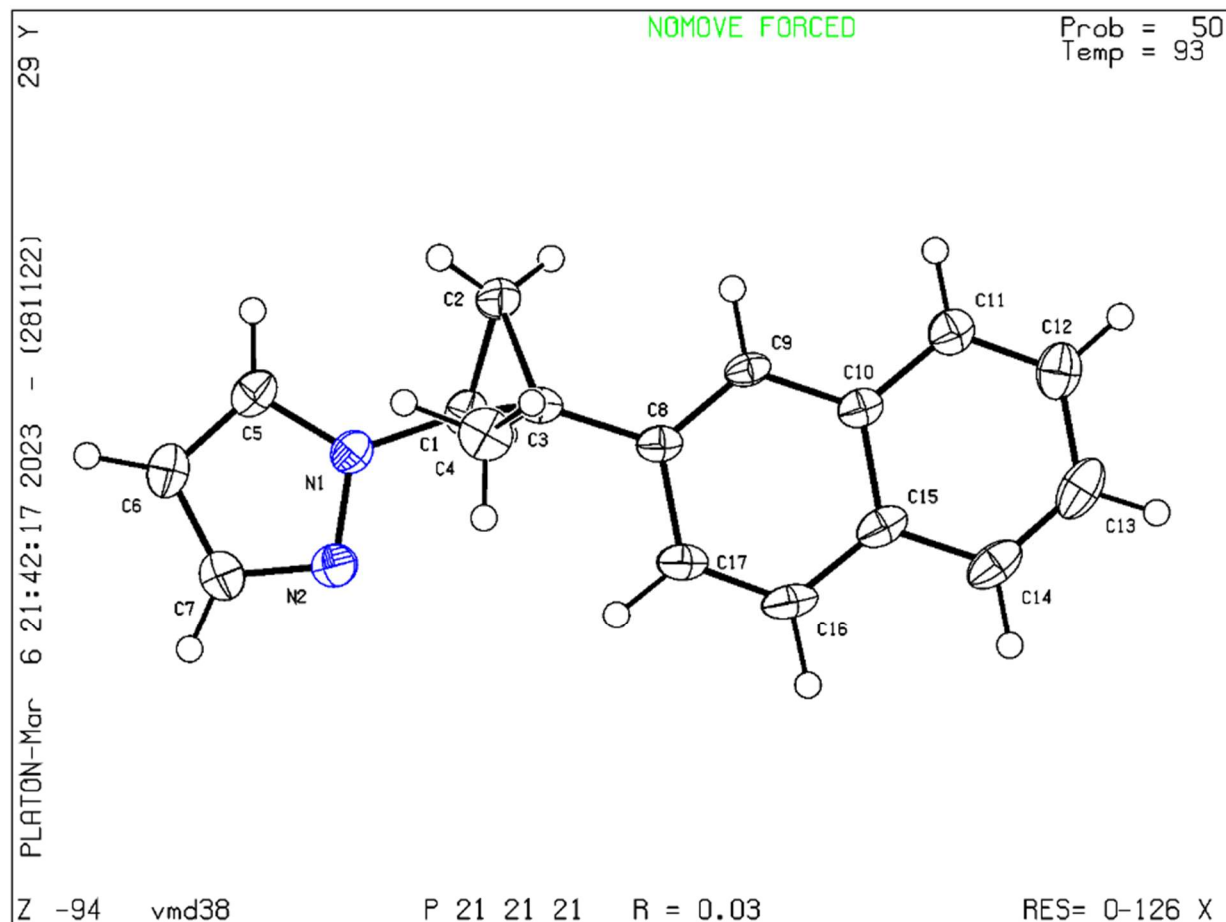
	x	y	z	U(equiv.)
H(1)	5290(30)	4200(60)	8700(20)	16(6)
H(2A)	4660(30)	9160(70)	8880(30)	31(8)
H(2B)	3490(40)	6860(70)	9180(30)	46(10)
H(4A)	4080(40)	9490(80)	6290(30)	41(9)
H(4B)	5310(40)	7660(70)	5980(30)	39(9)
H(4C)	5630(40)	9470(70)	7060(30)	37(9)
H(6)	10090(40)	6480(80)	7950(30)	50(10)
H(7)	9340(40)	9710(80)	9450(30)	37(9)
H(8A)	6700(40)	3810(80)	6540(30)	49(10)
H(8B)	7560(40)	2060(80)	7470(40)	51(11)
H(8C)	8500(50)	3290(100)	6610(40)	69(13)
H(10)	2820(30)	3350(60)	8570(30)	16(6)
H(11)	1220(40)	560(80)	7790(30)	49(11)
H(12)	640(40)	110(80)	5720(30)	51(11)
H(13)	1720(40)	3060(70)	4400(30)	41(9)
H(14)	3310(30)	5970(70)	5230(30)	27(8)

Torsion angles [$^\circ$] for 3j

C(5)–N(1)–N(2)–C(7)	-0.5(3)
C(1)–N(1)–N(2)–C(7)	178.5(2)
C(5)–N(1)–C(1)–C(2)	-153.8(2)
N(2)–N(1)–C(1)–C(2)	27.3(3)
C(5)–N(1)–C(1)–C(3)	-83.0(4)
N(2)–N(1)–C(1)–C(3)	98.1(3)
N(1)–C(1)–C(2)–C(3)	109.6(2)
C(1)–C(2)–C(3)–C(9)	104.6(3)
C(1)–C(2)–C(3)–C(4)	-106.3(3)
N(1)–C(1)–C(3)–C(9)	141.4(2)
C(2)–C(1)–C(3)–C(9)	-109.2(2)
N(1)–C(1)–C(3)–C(4)	-3.3(4)

C(2)–C(1)–C(3)–C(4)	106.0(3)
N(1)–C(1)–C(3)–C(2)	-109.4(3)
N(2)–N(1)–C(5)–C(6)	0.4(3)
C(1)–N(1)–C(5)–C(6)	-178.6(2)
N(2)–N(1)–C(5)–C(8)	179.6(2)
C(1)–N(1)–C(5)–C(8)	0.7(4)
N(1)–C(5)–C(6)–C(7)	-0.1(3)
C(8)–C(5)–C(6)–C(7)	-179.3(3)
N(1)–N(2)–C(7)–C(6)	0.4(3)
C(5)–C(6)–C(7)–N(2)	-0.2(3)
C(4)–C(3)–C(9)–C(14)	6.3(4)
C(2)–C(3)–C(9)–C(14)	155.1(2)
C(1)–C(3)–C(9)–C(14)	-138.1(2)
C(4)–C(3)–C(9)–C(10)	-175.1(2)
C(2)–C(3)–C(9)–C(10)	-26.3(4)
C(1)–C(3)–C(9)–C(10)	40.5(3)
C(14)–C(9)–C(10)–C(11)	0.7(4)
C(3)–C(9)–C(10)–C(11)	-178.0(3)
C(9)–C(10)–C(11)–C(12)	0.4(4)
C(10)–C(11)–C(12)–C(13)	-0.8(5)
C(11)–C(12)–C(13)–C(14)	0.3(4)
C(12)–C(13)–C(14)–C(9)	0.8(4)
C(10)–C(9)–C(14)–C(13)	-1.2(4)
C(3)–C(9)–C(14)–C(13)	177.5(3)

1-((1*S*,2*R*)-2-methyl-2-(naphthalen-2-yl)cyclopropyl)-1*H*-pyrazole (4i)



Crystal data and structure refinement for 4i

Identification code	4i	
Empirical formula	C ₁₇ H ₁₆ N ₂	
Formula weight	248.32	
Temperature	93(2) K	
Wavelength	1.54178 Å	
Crystal system	Orthorhombic	
Space group	P2 ₁ 2 ₁ 2 ₁	
Unit cell dimensions	a = 5.6710(2) Å b = 10.6406(4) Å c = 22.3113(9) Å	α = 90° β = 90° γ = 90°
Volume	1346.33(9) Å ³	
Z	4	
Density (calculated)	1.225 Mg/m ³	
Absorption coefficient	0.560 mm ⁻¹	
F(000)	528	
Crystal color	colorless	
Crystal size	0.145 x 0.133 x 0.087 mm ³	
Theta range for data collection	3.962 to 68.490°	
Index ranges	-6 ≤ h ≤ 6, -12 ≤ k ≤ 12, -23 ≤ l ≤ 26	
Reflections collected	13387	
Independent reflections	2472 [R(int) = 0.0419]	
Completeness to theta = 67.679°	100.0 %	

Absorption correction	Semi-empirical from equivalents
Max. and min. transmission	0.8643 and 0.7893
Refinement method	Full-matrix least-squares on F^2
Data / restraints / parameters	2472 / 0 / 237
Goodness-of-fit on F^2	1.055
Final R indices [$I > 2\sigma(I)$ = 2072 data]	$R_1 = 0.0281, wR_2 = 0.0702$
R indices (all data, 0.83 Å)	$R_1 = 0.0299, wR_2 = 0.0715$
Absolute structure parameter	-0.1(3)
Extinction coefficient	0.0043(8)
Largest diff. peak and hole	0.176 and -0.132 e.Å ⁻³

**Atomic coordinates (x 10⁴) and equivalent isotropic displacement parameters (Å² x 10³) for
4i**

	x	y	z	U(equiv.)
N(1)	6641(3)	1852(1)	3410(1)	25(1)
N(2)	4615(3)	2185(2)	3129(1)	34(1)
C(1)	7135(3)	2419(2)	3980(1)	26(1)
C(2)	9626(4)	2561(2)	4192(1)	34(1)
C(3)	8226(3)	3707(2)	4013(1)	24(1)
C(4)	8905(4)	4327(2)	3428(1)	34(1)
C(5)	7797(3)	924(2)	3120(1)	30(1)
C(6)	6493(4)	634(2)	2622(1)	36(1)
C(7)	4547(4)	1435(2)	2649(1)	39(1)
C(8)	7221(3)	4561(1)	4482(1)	23(1)
C(9)	8328(3)	4778(1)	5019(1)	22(1)
C(10)	7319(3)	5569(1)	5465(1)	23(1)
C(11)	8419(3)	5769(2)	6026(1)	28(1)
C(12)	7405(4)	6532(2)	6447(1)	34(1)
C(13)	5240(4)	7130(2)	6326(1)	38(1)

C(14)	4130(3)	6960(2)	5787(1)	34(1)
C(15)	5124(3)	6168(1)	5343(1)	26(1)
C(16)	4031(3)	5945(2)	4780(1)	30(1)
C(17)	5024(3)	5163(2)	4369(1)	28(1)

U(equiv.) is defined as one third of the trace of the orthogonalized U_{ij} tensor.

Bond lengths [\AA] and angles [$^\circ$] for 4i

N(1)–C(5)	1.350(2)
N(1)–N(2)	1.356(2)
N(1)–C(1)	1.435(2)
N(2)–C(7)	1.336(2)
C(1)–C(2)	1.497(3)
C(1)–C(3)	1.505(2)
C(1)–H(1A)	0.97(2)
C(2)–C(3)	1.508(2)
C(2)–H(2A)	0.96(2)
C(2)–H(2B)	0.98(2)
C(3)–C(8)	1.499(2)
C(3)–C(4)	1.514(2)
C(4)–H(4A)	1.01(2)
C(4)–H(4B)	0.99(2)
C(4)–H(4C)	1.04(2)
C(5)–C(6)	1.371(3)
C(5)–H(5A)	0.97(2)
C(6)–C(7)	1.396(3)
C(6)–H(6A)	0.98(2)
C(7)–H(7A)	0.95(3)
C(7)–C(9)	1.371(2)
C(8)–C(17)	1.424(2)
C(9)–C(10)	1.423(2)
C(9)–H(9A)	0.97(2)
C(10)–C(11)	1.415(2)
C(10)–C(15)	1.425(2)
C(11)–C(12)	1.368(3)
C(11)–H(11A)	0.98(2)
C(12)–C(13)	1.409(3)
C(12)–H(12A)	0.97(2)
C(13)–C(14)	1.369(3)
C(13)–H(13A)	0.96(2)

C(14)–C(15)	1.416(3)
C(14)–H(14A)	0.98(2)
C(15)–C(16)	1.421(3)
C(16)–C(17)	1.361(3)
C(16)–H(16A)	1.02(2)
C(17)–H(17A)	1.01(2)
C(5)–N(1)–N(2)	112.40(15)
C(5)–N(1)–C(1)	129.54(16)
N(2)–N(1)–C(1)	117.76(14)
C(7)–N(2)–N(1)	103.83(15)
N(1)–C(1)–C(2)	120.46(15)
N(1)–C(1)–C(3)	120.49(14)
C(2)–C(1)–C(3)	60.30(11)
N(1)–C(1)–H(1A)	113.6(11)
C(2)–C(1)–H(1A)	116.2(11)
C(3)–C(1)–H(1A)	115.8(12)
C(1)–C(2)–C(3)	60.11(11)
C(1)–C(2)–H(2A)	116.3(13)
C(3)–C(2)–H(2A)	115.9(13)
C(1)–C(2)–H(2B)	112.3(14)
C(3)–C(2)–H(2B)	117.8(14)
H(2A)–C(2)–H(2B)	120.0(19)
C(8)–C(3)–C(1)	115.51(13)
C(8)–C(3)–C(2)	120.42(14)
C(1)–C(3)–C(2)	59.59(12)
C(8)–C(3)–C(4)	115.76(14)
C(1)–C(3)–C(4)	117.29(14)
C(2)–C(3)–C(4)	116.53(16)
C(3)–C(4)–H(4A)	110.8(12)
C(3)–C(4)–H(4B)	108.5(13)
H(4A)–C(4)–H(4B)	108.0(18)
C(3)–C(4)–H(4C)	110.1(12)
H(4A)–C(4)–H(4C)	109.8(17)
H(4B)–C(4)–H(4C)	109.6(18)
N(1)–C(5)–C(6)	106.93(17)
N(1)–C(5)–H(5A)	122.1(13)
C(6)–C(5)–H(5A)	130.9(13)
C(5)–C(6)–C(7)	104.70(16)
C(5)–C(6)–H(6A)	127.3(14)

C(7)–C(6)–H(6A)	128.0(14)
N(2)–C(7)–C(6)	112.14(17)
N(2)–C(7)–H(7A)	118.9(15)
C(6)–C(7)–H(7A)	129.0(15)
C(9)–C(8)–C(17)	118.66(15)
C(9)–C(8)–C(3)	122.51(14)
C(17)–C(8)–C(3)	118.83(14)
C(8)–C(9)–C(10)	121.71(14)
C(8)–C(9)–H(9A)	118.8(10)
C(10)–C(9)–H(9A)	119.5(11)
C(11)–C(10)–C(9)	122.01(15)
C(11)–C(10)–C(15)	119.09(15)
C(9)–C(10)–C(15)	118.90(15)
C(12)–C(11)–C(10)	120.75(18)
C(12)–C(11)–H(11A)	121.3(12)
C(10)–C(11)–H(11A)	118.0(12)
C(11)–C(12)–C(13)	120.18(18)
C(11)–C(12)–H(12A)	119.0(13)
C(13)–C(12)–H(12A)	120.9(13)
C(14)–C(13)–C(12)	120.60(17)
C(14)–C(13)–H(13A)	121.6(15)
C(12)–C(13)–H(13A)	117.8(15)
C(13)–C(14)–C(15)	120.61(17)
C(13)–C(14)–H(14A)	120.2(13)
C(15)–C(14)–H(14A)	119.1(13)
C(14)–C(15)–C(16)	122.90(16)
C(14)–C(15)–C(10)	118.76(16)
C(16)–C(15)–C(10)	118.33(15)
C(17)–C(16)–C(15)	121.17(15)
C(17)–C(16)–H(16A)	122.5(12)
C(15)–C(16)–H(16A)	116.3(12)
C(16)–C(17)–C(8)	121.21(16)
C(16)–C(17)–H(17A)	121.4(13)
C(8)–C(17)–H(17A)	117.4(13)

Anisotropic displacement parameters ($\text{\AA}^2 \times 10^3$) for 4i

	U ¹¹	U ²²	U ³³	U ²³	U ¹³	U ¹²
N(1)	26(1)	22(1)	28(1)	1(1)	3(1)	0(1)
N(2)	30(1)	32(1)	42(1)	-7(1)	-6(1)	4(1)
C(1)	33(1)	21(1)	24(1)	4(1)	4(1)	2(1)
C(2)	39(1)	35(1)	29(1)	-2(1)	-8(1)	15(1)
C(3)	20(1)	24(1)	28(1)	4(1)	-2(1)	0(1)
C(4)	36(1)	31(1)	36(1)	8(1)	4(1)	-8(1)
C(5)	32(1)	28(1)	31(1)	2(1)	7(1)	4(1)
C(6)	40(1)	28(1)	32(1)	-7(1)	6(1)	2(1)
C(7)	38(1)	39(1)	38(1)	-9(1)	-7(1)	2(1)
C(8)	20(1)	16(1)	32(1)	6(1)	-2(1)	-1(1)
C(9)	17(1)	16(1)	32(1)	5(1)	0(1)	2(1)
C(10)	21(1)	15(1)	33(1)	4(1)	1(1)	-2(1)
C(11)	30(1)	21(1)	34(1)	2(1)	1(1)	-2(1)
C(12)	45(1)	23(1)	35(1)	-1(1)	6(1)	-4(1)
C(13)	46(1)	20(1)	46(1)	0(1)	20(1)	1(1)
C(14)	28(1)	20(1)	54(1)	5(1)	12(1)	1(1)
C(15)	20(1)	15(1)	45(1)	5(1)	6(1)	-2(1)
C(16)	17(1)	22(1)	53(1)	6(1)	-3(1)	2(1)
C(17)	21(1)	22(1)	41(1)	4(1)	-7(1)	0(1)

The anisotropic displacement factor exponent takes the form: $-2\pi^2 [h^2 a^{*2} U^{11} + \dots + 2 h k a^* b^* U^{12}]$

Hydrogen coordinates ($\times 10^4$) and isotropic displacement parameters ($\text{\AA}^2 \times 10^3$) for 4i

	x	y	z	U(equiv.)
H(1A)	5970(40)	2228(19)	4286(9)	26(5)
H(2A)	10840(40)	2300(20)	3917(10)	35(5)
H(2B)	9790(40)	2380(20)	4620(10)	42(6)
H(4A)	10080(40)	5030(20)	3498(9)	39(6)
H(4B)	7470(40)	4700(20)	3248(10)	41(6)
H(4C)	9620(40)	3670(20)	3136(10)	43(6)
H(5A)	9250(40)	560(20)	3276(9)	39(6)
H(6A)	6830(40)	-10(20)	2324(10)	43(6)
H(7A)	3230(50)	1490(20)	2383(11)	52(7)

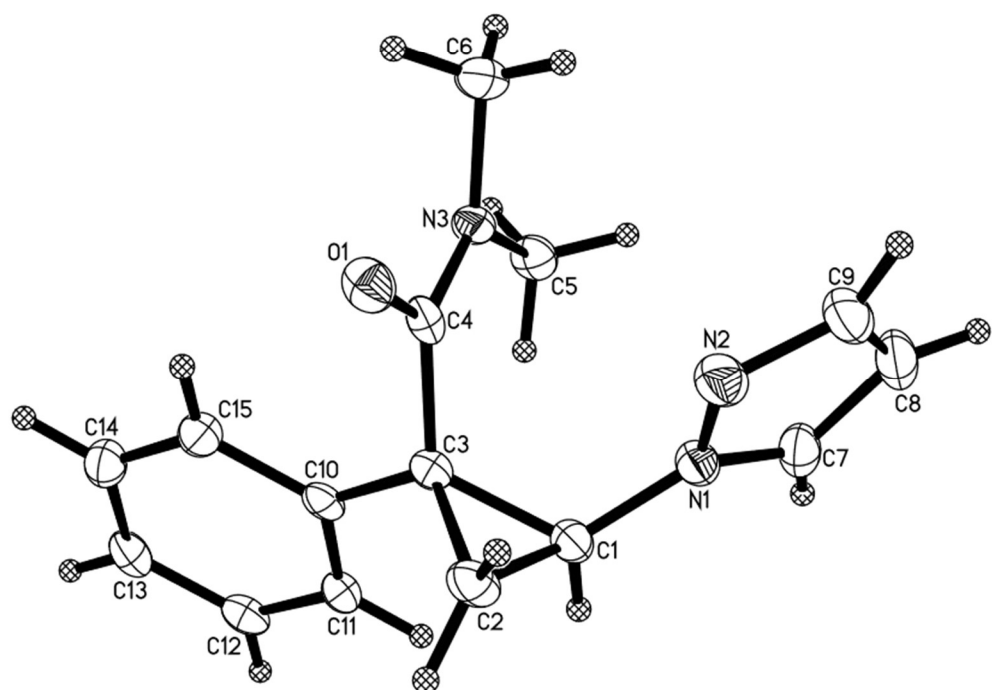
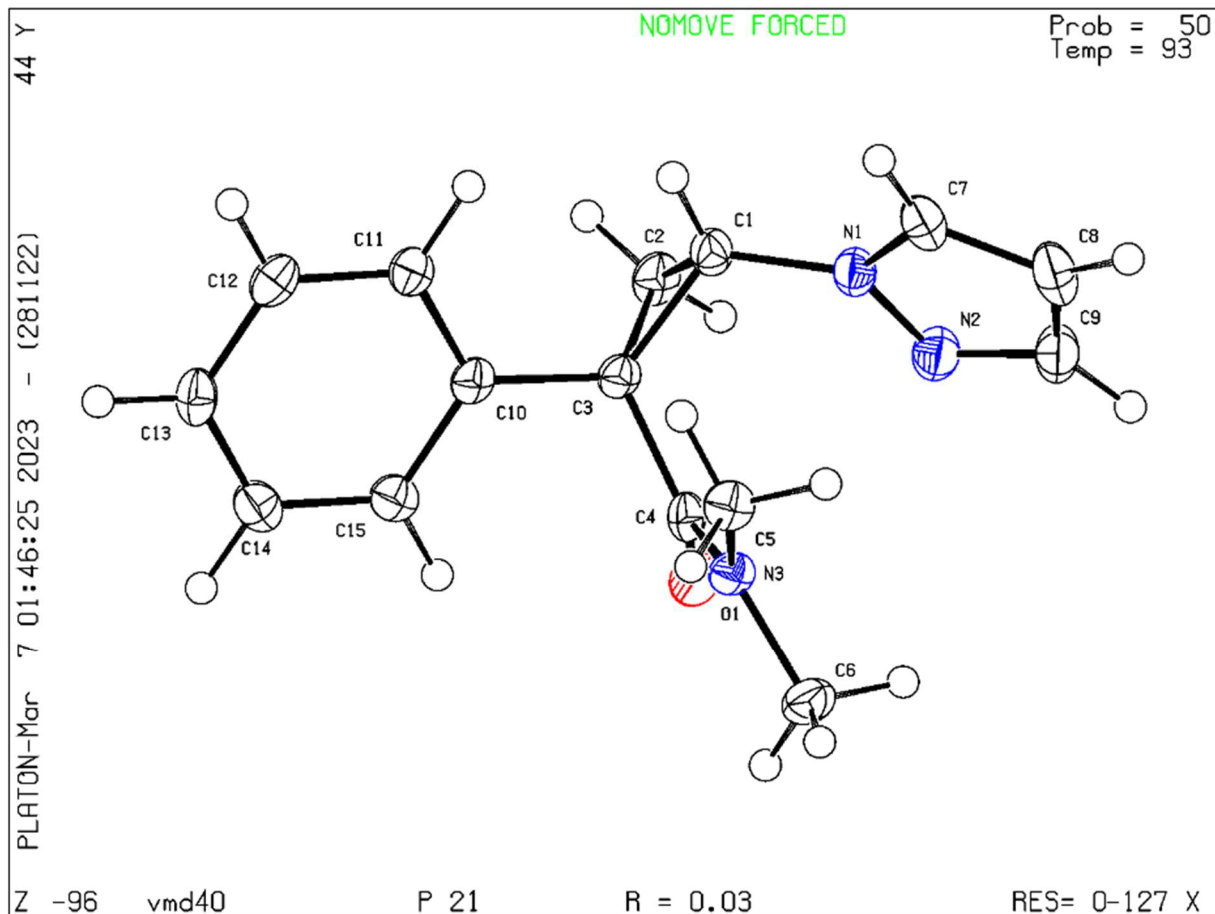
H(9A)	9850(40)	4386(18)	5093(8)	24(4)
H(11A)	9950(40)	5370(20)	6097(9)	40(6)
H(12A)	8210(40)	6660(20)	6828(10)	37(5)
H(13A)	4590(40)	7660(20)	6629(11)	46(6)
H(14A)	2610(40)	7370(20)	5707(10)	38(6)
H(16A)	2440(40)	6370(20)	4714(9)	39(6)
H(17A)	4250(40)	5000(20)	3970(10)	39(6)

Torsion angles [°] for 4i

C(5)–N(1)–N(2)–C(7)	-0.3(2)
C(1)–N(1)–N(2)–C(7)	-174.59(16)
C(5)–N(1)–C(1)–C(2)	33.3(3)
N(2)–N(1)–C(1)–C(2)	-153.54(16)
C(5)–N(1)–C(1)–C(3)	104.6(2)
N(2)–N(1)–C(1)–C(3)	-82.3(2)
N(1)–C(1)–C(2)–C(3)	110.01(17)
N(1)–C(1)–C(3)–C(8)	138.30(16)
C(2)–C(1)–C(3)–C(8)	-111.74(16)
N(1)–C(1)–C(3)–C(2)	-109.96(18)
N(1)–C(1)–C(3)–C(4)	-3.7(2)
C(2)–C(1)–C(3)–C(4)	106.25(18)
C(1)–C(2)–C(3)–C(8)	103.56(16)
C(1)–C(2)–C(3)–C(4)	-107.53(17)
N(2)–N(1)–C(5)–C(6)	0.5(2)
C(1)–N(1)–C(5)–C(6)	173.94(16)
N(1)–C(5)–C(6)–C(7)	-0.4(2)
N(1)–N(2)–C(7)–C(6)	0.0(2)
C(5)–C(6)–C(7)–N(2)	0.3(2)
C(1)–C(3)–C(8)–C(9)	101.68(17)
C(2)–C(3)–C(8)–C(9)	33.4(2)
C(4)–C(3)–C(8)–C(9)	-115.72(17)
C(1)–C(3)–C(8)–C(17)	-77.86(18)
C(2)–C(3)–C(8)–C(17)	-146.13(16)
C(4)–C(3)–C(8)–C(17)	64.7(2)
C(17)–C(8)–C(9)–C(10)	1.1(2)
C(3)–C(8)–C(9)–C(10)	-178.48(14)
C(8)–C(9)–C(10)–C(11)	178.16(15)
C(8)–C(9)–C(10)–C(15)	-1.3(2)

C(9)–C(10)–C(11)–C(12)	-179.81(15)
C(15)–C(10)–C(11)–C(12)	-0.4(2)
C(10)–C(11)–C(12)–C(13)	0.0(3)
C(11)–C(12)–C(13)–C(14)	-0.2(3)
C(12)–C(13)–C(14)–C(15)	0.7(3)
C(13)–C(14)–C(15)–C(16)	179.11(16)
C(13)–C(14)–C(15)–C(10)	-1.0(2)
C(11)–C(10)–C(15)–C(14)	0.8(2)
C(9)–C(10)–C(15)–C(14)	-179.72(14)
C(11)–C(10)–C(15)–C(16)	-179.26(14)
C(9)–C(10)–C(15)–C(16)	0.2(2)
C(14)–C(15)–C(16)–C(17)	-178.97(15)
C(10)–C(15)–C(16)–C(17)	1.1(2)
C(15)–C(16)–C(17)–C(8)	-1.4(2)
C(9)–C(8)–C(17)–C(16)	0.3(2)
C(3)–C(8)–C(17)–C(16)	179.84(15)

(1*S*,2*S*)-*N,N*-dimethyl-1-phenyl-2-(1*H*-pyrazol-1-yl)cyclopropane-1-carboxamide (4k)



Crystal data and structure refinement for 4k

Identification code	4k	
Empirical formula	C ₁₅ H ₁₇ N ₃ O	
Formula weight	255.31	
Temperature	93(2) K	
Wavelength	1.54178 Å	
Crystal system	Monoclinic	
Space group	P2 ₁	
Unit cell dimensions	a = 6.0612(2) Å b = 7.2028(2) Å c = 15.3454(5) Å	α = 90° β = 92.204(2)° γ = 90°
Volume	669.45(4) Å ³	
Z	2	
Density (calculated)	1.267 Mg/m ³	
Absorption coefficient	0.652 mm ⁻¹	
F(000)	272	
Crystal color	colorless	
Crystal size	0.253 x 0.095 x 0.035 mm ³	
Theta range for data collection	2.882 to 68.482°	
Index ranges	-6 ≤ h ≤ 7, -8 ≤ k ≤ 8, -18 ≤ l ≤ 18	
Reflections collected	9190	
Independent reflections	2434 [R(int) = 0.0470]	
Completeness to theta = 67.679°	99.9%	

Absorption correction	Semi-empirical from equivalents
Max. and min. transmission	0.8643 and 0.7411
Refinement method	Full-matrix least-squares on F^2
Data / restraints / parameters	2434 / 1 / 241
Goodness-of-fit on F^2	1.091
Final R indices [$I > 2\sigma(I)$ = 2229 data]	$R_1 = 0.0338$, $wR_2 = 0.0806$
R indices (all data, 0.83 Å)	$R_1 = 0.0383$, $wR_2 = 0.0839$
Absolute structure parameter	-0.2(2)
Extinction coefficient	0.0058(14)
Largest diff. peak and hole	0.132 and -0.140 e.Å ⁻³

**Atomic coordinates ($\times 10^4$) and equivalent isotropic displacement parameters ($\text{\AA}^2 \times 10^3$) for
4k**

	x	y	z	U(equiv.)
O(1)	3176(3)	5082(3)	7522(1)	25(1)
N(1)	8529(4)	5789(3)	8787(1)	22(1)
N(2)	6641(4)	6439(3)	9130(2)	27(1)
N(3)	5720(4)	7123(3)	7090(1)	19(1)
C(1)	8540(5)	4154(4)	8252(2)	21(1)
C(2)	6737(5)	4154(4)	8288(2)	24(1)
C(3)	6902(4)	3979(4)	7484(2)	18(1)
C(4)	5123(4)	5447(4)	7378(2)	20(1)
C(5)	7979(5)	7677(4)	6927(2)	23(1)
C(6)	4079(5)	8603(4)	7063(2)	26(1)
C(7)	10271(5)	6929(4)	8965(2)	26(1)
C(8)	9503(5)	8379(5)	9445(2)	31(1)
C(9)	7261(5)	8008(4)	9529(2)	31(1)
C(10)	7261(5)	3112(3)	6632(2)	18(1)
C(11)	9626(4)	2384(4)	6493(2)	21(1)

C(12)	10071(5)	1540(4)	5704(2)	23(1)
C(13)	8458(5)	1401(4)	5042(2)	24(1)
C(14)	6389(5)	2144(4)	5174(2)	25(1)
C(15)	5934(4)	2987(4)	5957(2)	22(1)

U(equiv.) is defined as one third of the trace of the orthogonalized U^{ij} tensor.

Bond lengths [Å] and angles [°] for 4k

O(1)–C(4)	1.238(3)
N(1)–C(7)	1.357(4)
N(1)–N(2)	1.362(3)
N(1)–C(1)	1.435(3)
N(2)–C(9)	1.332(4)
N(3)–C(4)	1.340(3)
N(3)–C(5)	1.457(3)
N(3)–C(6)	1.458(4)
C(1)–C(2)	1.481(4)
C(1)–C(3)	1.517(4)
C(1)–H(1)	0.98(3)
C(2)–C(3)	1.517(4)
C(2)–H(2A)	1.00(3)
C(2)–H(2B)	0.98(4)
C(3)–C(10)	1.512(3)
C(3)–C(4)	1.515(4)
C(5)–H(5A)	0.99(3)
C(5)–H(5B)	1.00(4)
C(5)–H(5C)	0.94(4)
C(6)–H(6A)	0.97(4)
C(6)–H(6B)	0.97(5)
C(6)–H(6C)	0.99(5)
C(7)–C(8)	1.369(4)
C(7)–H(7)	0.96(3)
C(8)–C(9)	1.396(5)
C(8)–H(8)	0.97(4)
C(9)–H(9)	0.96(3)
C(10)–C(15)	1.394(4)
C(10)–C(11)	1.395(4)
C(11)–C(12)	1.391(4)
C(11)–H(11)	1.02(3)
C(12)–C(13)	1.386(4)

C(12)–H(12)	0.96(3)
C(13)–C(14)	1.386(4)
C(13)–H(13)	1.00(3)
C(14)–C(15)	1.383(4)
C(14)–H(14)	0.99(3)
C(15)–H(15)	0.99(3)
C(7)–N(1)–N(2)	111.9(2)
C(7)–N(1)–C(1)	126.3(2)
N(2)–N(1)–C(1)	121.7(2)
C(9)–N(2)–N(1)	104.1(2)
C(4)–N(3)–C(5)	124.8(2)
C(4)–N(3)–C(6)	118.4(2)
C(5)–N(3)–C(6)	116.1(2)
N(1)–C(1)–C(2)	120.8(2)
N(1)–C(1)–C(3)	119.7(2)
C(2)–C(1)–C(3)	60.78(18)
N(1)–C(1)–H(1)	111.0(17)
C(2)–C(1)–H(1)	120.1(17)
C(3)–C(1)–H(1)	116.1(16)
C(1)–C(2)–C(3)	60.78(18)
C(1)–C(2)–H(2A)	118.5(19)
C(3)–C(2)–H(2A)	116.1(19)
C(1)–C(2)–H(2B)	118.1(19)
C(3)–C(2)–H(2B)	119.4(19)
H(2A)–C(2)–H(2B)	114(3)
C(10)–C(3)–C(4)	113.5(2)
C(10)–C(3)–C(1)	121.8(2)
C(4)–C(3)–C(1)	117.9(2)
C(10)–C(3)–C(2)	119.6(2)
C(4)–C(3)–C(2)	114.8(2)
C(1)–C(3)–C(2)	58.44(18)
O(1)–C(4)–N(3)	121.5(2)
O(1)–C(4)–C(3)	120.8(2)
N(3)–C(4)–C(3)	117.6(2)
N(3)–C(5)–H(5A)	113.4(17)
N(3)–C(5)–H(5B)	109.9(18)
H(5A)–C(5)–H(5B)	105(3)
N(3)–C(5)–H(5C)	109.3(19)
H(5A)–C(5)–H(5C)	112(3)

H(5B)–C(5)–H(5C)	107(3)
N(3)–C(6)–H(6A)	111(2)
N(3)–C(6)–H(6B)	111(3)
H(6A)–C(6)–H(6B)	112(4)
N(3)–C(6)–H(6C)	109(3)
H(6A)–C(6)–H(6C)	108(3)
H(6B)–C(6)–H(6C)	107(4)
N(1)–C(7)–C(8)	107.0(3)
N(1)–C(7)–H(7)	120(2)
C(8)–C(7)–H(7)	133(2)
C(7)–C(8)–C(9)	104.8(3)
C(7)–C(8)–H(8)	127(2)
C(9)–C(8)–H(8)	128(2)
N(2)–C(9)–C(8)	112.2(3)
N(2)–C(9)–H(9)	118(2)
C(8)–C(9)–H(9)	129(2)
C(15)–C(10)–C(11)	118.3(2)
C(15)–C(10)–C(3)	118.4(2)
C(11)–C(10)–C(3)	123.3(2)
C(12)–C(11)–C(10)	120.3(2)
C(12)–C(11)–H(11)	120.0(17)
C(10)–C(11)–H(11)	119.7(17)
C(13)–C(12)–C(11)	121.0(3)
C(13)–C(12)–H(12)	119.0(18)
C(11)–C(12)–H(12)	120.0(18)
C(14)–C(13)–C(12)	118.8(2)
C(14)–C(13)–H(13)	121.1(19)
C(12)–C(13)–H(13)	120.2(19)
C(15)–C(14)–C(13)	120.6(3)
C(15)–C(14)–H(14)	120.3(18)
C(13)–C(14)–H(14)	119.1(18)
C(14)–C(15)–C(10)	121.1(3)
C(14)–C(15)–H(15)	120.5(17)
C(10)–C(15)–H(15)	118.4(17)

Anisotropic displacement parameters ($\text{\AA}^2 \times 10^3$) for 4k

	U ¹¹	U ²²	U ³³	U ²³	U ¹³	U ¹²
O(1)	20(1)	22(1)	32(1)	-2(1)	4(1)	-3(1)
N(1)	28(1)	18(1)	19(1)	-1(1)	1(1)	0(1)
N(2)	33(1)	25(1)	24(1)	-2(1)	3(1)	3(1)
N(3)	22(1)	14(1)	23(1)	2(1)	-1(1)	-2(1)
C(1)	27(1)	17(1)	19(1)	0(1)	0(1)	0(1)
C(2)	33(2)	16(1)	23(1)	2(1)	4(1)	-1(1)
C(3)	21(1)	14(1)	21(1)	1(1)	1(1)	-1(1)
C(4)	24(1)	16(1)	20(1)	-4(1)	1(1)	-3(1)
C(5)	24(1)	19(2)	25(1)	3(1)	2(1)	-4(1)
C(6)	27(2)	19(2)	33(2)	2(1)	-2(1)	4(1)
C(7)	34(2)	24(2)	19(1)	-1(1)	-2(1)	-5(1)
C(8)	47(2)	26(2)	20(1)	-4(1)	-1(1)	-7(2)
C(9)	47(2)	24(2)	22(1)	-4(1)	2(1)	4(1)
C(10)	23(1)	11(1)	22(1)	2(1)	2(1)	-3(1)
C(11)	23(1)	15(2)	24(1)	-1(1)	0(1)	-3(1)
C(12)	26(2)	15(1)	29(1)	1(1)	6(1)	-1(1)
C(13)	32(2)	18(1)	21(1)	-3(1)	6(1)	-4(1)
C(14)	30(2)	24(2)	22(1)	0(1)	-3(1)	-3(1)
C(15)	22(1)	21(1)	23(1)	1(1)	-1(1)	-1(1)

The anisotropic displacement factor exponent takes the form: $-2\pi^2 [h^2 a^{*2} U^{11} + \dots + 2 h k a^* b^* U^{12}]$

Hydrogen coordinates ($\times 10^4$) and isotropic displacement parameters ($\text{\AA}^2 \times 10^3$) for 4k

	x	y	z	U(equiv.)
H(1)	10060(50)	3750(40)	8151(17)	15(7)
H(2A)	5460(50)	3040(50)	8670(20)	28(8)
H(2B)	7120(50)	1460(50)	8260(20)	31(9)
H(5A)	9050(50)	6650(40)	6989(18)	20(7)
H(5B)	8490(50)	8620(50)	7370(20)	35(9)
H(5C)	8020(50)	8240(50)	6370(20)	28(8)
H(6A)	2670(60)	8150(60)	6830(20)	47(10)
H(6B)	4590(80)	9660(70)	6740(30)	72(14)
H(6C)	3850(70)	9040(60)	7670(30)	65(13)

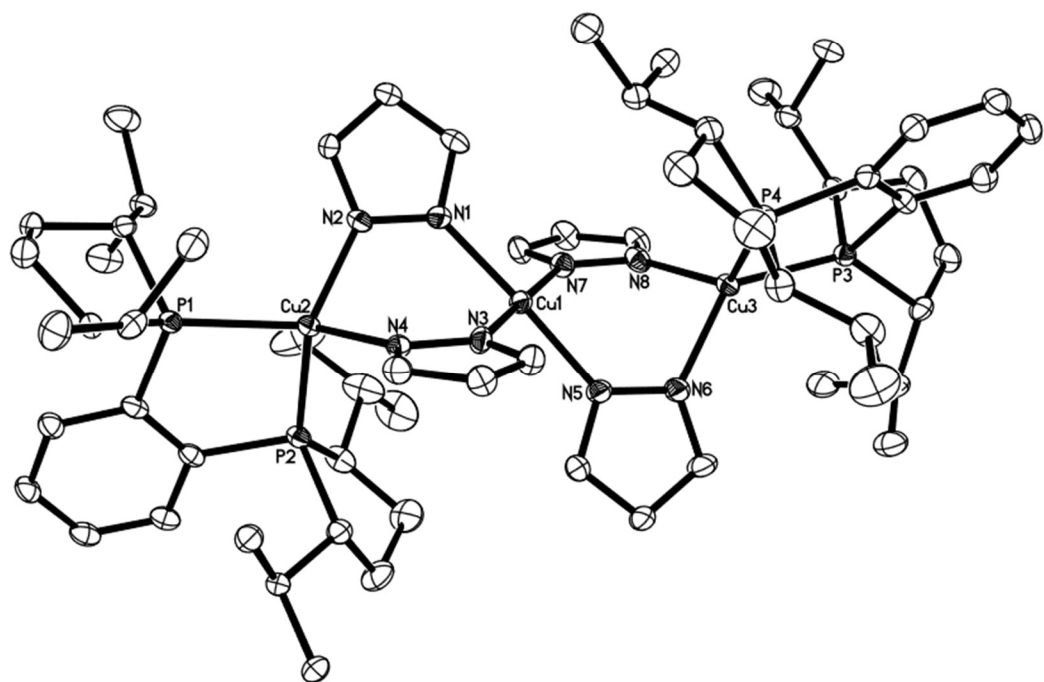
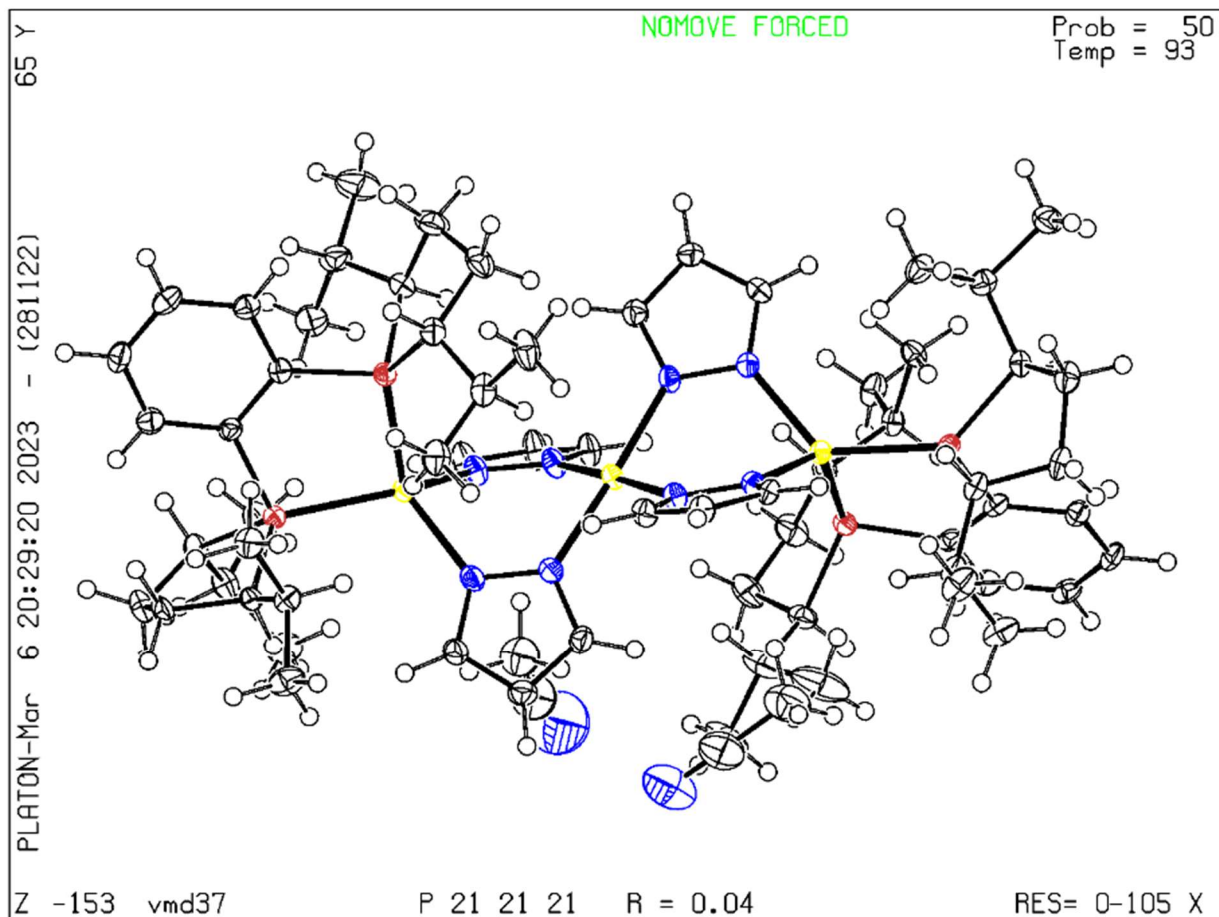
H(7)	11720(50)	6600(50)	8780(20)	31(9)
H(8)	10340(60)	9430(60)	9660(20)	36(9)
H(9)	6170(50)	8720(50)	9810(20)	37(9)
H(11)	10840(50)	2510(50)	6970(20)	26(8)
H(12)	11500(50)	1010(40)	5618(19)	23(8)
H(13)	8800(50)	780(50)	4480(20)	34(9)
H(14)	5210(50)	2000(50)	4710(20)	29(8)
H(15)	4450(50)	3490(50)	6056(19)	24(8)

Torsion angles [°] for 4k

C(7)–N(1)–N(2)–C(9)	-0.2(3)
C(1)–N(1)–N(2)–C(9)	-176.1(2)
C(7)–N(1)–C(1)–C(2)	164.0(3)
N(2)–N(1)–C(1)–C(2)	-20.6(4)
C(7)–N(1)–C(1)–C(3)	-124.3(3)
N(2)–N(1)–C(1)–C(3)	51.0(3)
N(1)–C(1)–C(2)–C(3)	109.1(3)
N(1)–C(1)–C(3)–C(10)	141.6(2)
C(2)–C(1)–C(3)–C(10)	-107.5(3)
N(1)–C(1)–C(3)–C(4)	-7.5(3)
C(2)–C(1)–C(3)–C(4)	103.4(3)
N(1)–C(1)–C(3)–C(2)	-110.8(3)
C(1)–C(2)–C(3)–C(10)	111.2(3)
C(1)–C(2)–C(3)–C(4)	-108.7(3)
C(5)–N(3)–C(4)–O(1)	178.3(3)
C(6)–N(3)–C(4)–O(1)	8.4(4)
C(5)–N(3)–C(4)–C(3)	-4.4(4)
C(6)–N(3)–C(4)–C(3)	-174.2(2)
C(10)–C(3)–C(4)–O(1)	100.1(3)
C(1)–C(3)–C(4)–O(1)	-108.3(3)
C(2)–C(3)–C(4)–O(1)	-42.4(4)
C(10)–C(3)–C(4)–N(3)	-77.3(3)
C(1)–C(3)–C(4)–N(3)	74.3(3)
C(2)–C(3)–C(4)–N(3)	140.2(2)
N(2)–N(1)–C(7)–C(8)	0.1(3)
C(1)–N(1)–C(7)–C(8)	175.8(2)
N(1)–C(7)–C(8)–C(9)	0.0(3)
N(1)–N(2)–C(9)–C(8)	0.2(3)

C(7)–C(8)–C(9)–N(2)	-0.1(3)
C(4)–C(3)–C(10)–C(15)	-30.2(3)
C(1)–C(3)–C(10)–C(15)	179.5(2)
C(2)–C(3)–C(10)–C(15)	110.3(3)
C(4)–C(3)–C(10)–C(11)	151.6(2)
C(1)–C(3)–C(10)–C(11)	1.3(4)
C(2)–C(3)–C(10)–C(11)	-67.8(3)
C(15)–C(10)–C(11)–C(12)	-0.7(4)
C(3)–C(10)–C(11)–C(12)	177.5(3)
C(10)–C(11)–C(12)–C(13)	-0.1(4)
C(11)–C(12)–C(13)–C(14)	0.9(4)
C(12)–C(13)–C(14)–C(15)	-0.9(4)
C(13)–C(14)–C(15)–C(10)	0.0(4)
C(11)–C(10)–C(15)–C(14)	0.8(4)
C(3)–C(10)–C(15)–C(14)	-177.5(3)

Copper-Trimer VI



Crystal data and structure refinement for Copper–trimer VI

Identification code	Copper–trimer VI	
Empirical formula	$C_{64}H_{100}Cu_3N_8P_4 \cdot 2(CH_3CN)$	
Formula weight	255.31	
Temperature	93(2) K	
Wavelength	0.71073 Å	
Crystal system	Orthorhombic	
Space group	$P2_12_12_1$	
Unit cell dimensions	$a = 17.1415(8)$ Å	$\alpha = 90^\circ$
	$b = 18.0336(8)$ Å	$\beta = 90$
	$c = 23.1509(10)$ Å	$\gamma = 90^\circ$
Volume	7156.5(6) Å ³	
Z	4	
Density (calculated)	1.279 Mg/m ³	
Absorption coefficient	1.019 mm ⁻¹	
F(000)	2924	
Crystal color	orange	
Crystal size	0.360 x 0.241 x 0.202 mm ³	
Theta range for data collection	1.431 to 27.876°	
Index ranges	$-22 \leq h \leq 22, -23 \leq k \leq 23, -30 \leq l \leq 30$	
Reflections collected	160910	
Independent reflections	17065 [R(int) = 0.0319]	
Completeness to theta = 25.242°	99.8%	

Absorption correction	Semi-empirical from equivalents
Max. and min. transmission	0.7463 and 0.6820
Refinement method	Full-matrix least-squares on F^2
Data / restraints / parameters	17065 / 0 / 770
Goodness-of-fit on F^2	1.151
Final R indices [$I > 2\sigma(I)$ = 16689 data]	$R_1 = 0.0398$, $wR_2 = 0.1109$
R indices (all data, 0.76 Å)	$R_1 = 0.0407$, $wR_2 = 0.1116$
Absolute structure parameter	0.026(11)
Largest diff. peak and hole	1.008 and -0.720 e.Å ⁻³

Atomic coordinates ($\times 10^4$) and equivalent isotropic displacement parameters ($\text{\AA}^2 \times 10^3$) for Copper-trimer VI

	x	y	z	U(equiv.)
Cu(1)	7693(1)	6030(1)	6559(1)	16(1)
Cu(2)	7067(1)	7825(1)	7078(1)	14(1)
Cu(3)	8294(1)	4192(1)	6127(1)	16(1)
P(1)	6828(1)	9016(1)	7316(1)	15(1)
P(2)	5857(1)	7722(1)	6693(1)	16(1)
P(3)	8815(1)	3157(1)	5708(1)	15(1)
P(4)	9139(1)	4082(1)	6880(1)	17(1)
N(1)	8277(2)	6969(2)	6446(2)	18(1)
N(2)	8088(2)	7653(2)	6663(2)	17(1)
N(3)	7431(2)	6264(2)	7381(2)	18(1)
N(4)	7233(2)	6943(2)	7607(2)	16(1)
N(5)	7047(2)	5115(2)	6639(2)	20(1)
N(6)	7215(2)	4412(2)	6466(2)	20(1)
N(7)	7996(2)	5757(2)	5758(2)	19(1)
N(8)	8213(2)	5065(2)	5576(2)	20(1)
N(9)	8351(5)	7640(5)	4284(3)	70(2)

N(10)	4846(8)	4829(8)	4924(6)	124(4)
C(1)	9005(3)	7014(3)	6220(2)	22(1)
C(2)	9297(3)	7719(3)	6291(2)	21(1)
C(3)	8701(3)	8100(2)	6567(2)	17(1)
C(4)	7475(3)	5777(3)	7816(2)	22(1)
C(5)	7306(3)	6124(3)	8336(2)	21(1)
C(6)	7163(3)	6851(3)	8178(2)	20(1)
C(7)	6315(3)	5129(3)	6850(2)	23(1)
C(8)	5984(3)	4432(3)	6807(3)	28(1)
C(9)	6576(3)	4008(3)	6573(3)	29(1)
C(10)	7946(3)	6210(3)	5292(2)	22(1)
C(11)	8125(3)	5818(3)	4800(2)	26(1)
C(12)	8290(3)	5105(3)	5000(2)	23(1)
C(13)	5836(2)	9212(3)	7035(2)	17(1)
C(14)	5476(3)	9908(3)	7116(2)	20(1)
C(15)	4723(3)	10039(3)	6913(2)	21(1)
C(16)	4321(3)	9486(3)	6631(2)	21(1)
C(17)	4661(3)	8792(3)	6554(2)	21(1)
C(18)	5422(3)	8650(3)	6754(2)	17(1)
C(19)	7524(2)	9692(2)	6991(2)	18(1)
C(20)	7374(3)	10432(3)	7290(2)	23(1)
C(21)	7281(3)	10259(3)	7940(2)	25(1)
C(22)	6802(3)	9538(2)	8022(2)	17(1)
C(23)	7622(3)	9714(3)	6328(2)	23(1)
C(24)	8374(3)	10128(3)	6171(3)	33(1)
C(25)	6925(3)	10038(3)	6009(2)	31(1)
C(26)	7058(3)	9074(3)	8549(2)	20(1)
C(27)	6994(4)	9552(3)	9103(2)	28(1)
C(28)	7872(3)	8744(3)	8489(2)	26(1)
C(29)	5515(3)	7366(3)	5979(2)	22(1)
C(30)	5170(4)	6597(3)	6128(3)	33(1)
C(31)	4697(3)	6692(3)	6677(2)	30(1)
C(32)	5193(3)	7098(3)	7123(2)	19(1)
C(33)	6157(3)	7357(4)	5515(2)	37(1)
C(34)	6476(5)	8123(5)	5413(3)	59(2)
C(35)	5854(5)	7029(5)	4949(3)	49(2)
C(36)	4725(3)	7475(3)	7611(2)	18(1)
C(37)	4129(3)	6941(3)	7874(2)	25(1)
C(38)	5266(3)	7760(3)	8091(2)	21(1)
C(39)	9551(3)	2816(3)	6227(2)	17(1)

C(40)	9960(3)	2154(3)	6145(2)	23(1)
C(41)	10552(3)	1940(3)	6521(2)	24(1)
C(42)	10749(3)	2378(3)	6986(2)	23(1)
C(43)	10332(3)	3027(3)	7082(2)	20(1)
C(44)	9742(3)	3265(3)	6712(2)	18(1)
C(45)	9351(3)	3347(3)	5024(2)	17(1)
C(46)	9623(3)	2592(3)	4795(2)	23(1)
C(47)	8929(3)	2063(3)	4859(2)	26(1)
C(48)	8430(3)	2262(3)	5402(2)	20(1)
C(49)	9952(3)	3980(3)	5016(2)	21(1)
C(50)	10089(3)	4231(3)	4392(2)	31(1)
C(51)	10731(3)	3793(3)	5309(2)	24(1)
C(52)	7549(3)	2269(3)	5261(2)	24(1)
C(53)	7292(3)	2918(3)	4886(3)	32(1)
C(54)	7082(3)	2255(3)	5822(2)	30(1)
C(55)	9842(3)	4777(3)	7193(2)	22(1)
C(56)	9510(3)	4945(3)	7799(2)	29(1)
C(57)	9187(3)	4222(4)	8053(2)	32(1)
C(58)	8679(3)	3848(3)	7598(2)	22(1)
C(59)	9941(3)	5477(3)	6824(2)	25(1)
C(60)	10266(3)	5296(3)	6232(3)	28(1)
C(61)	10470(3)	6047(3)	7126(3)	33(1)
C(62)	8507(3)	3028(3)	7722(2)	28(1)
C(63)	8159(4)	2927(4)	8326(3)	45(2)
C(64)	7954(4)	2693(3)	7283(2)	31(1)
C(65)	8478(5)	8700(5)	5049(3)	55(2)
C(66)	8401(5)	8107(5)	4618(3)	52(2)
C(67)	6282(4)	4905(4)	5231(3)	48(2)
C(68)	5529(6)	4821(5)	5016(4)	61(2)

Bond lengths [Å] and angles [°] for Copper–trimer VI

Cu(1)–N(1)	1.985(4)
Cu(1)–N(7)	1.986(4)
Cu(1)–N(5)	1.997(4)
Cu(1)–N(3)	2.001(4)
Cu(2)–N(2)	2.020(4)
Cu(2)–N(4)	2.027(4)
Cu(2)–P(1)	2.2561(13)

Cu(2)–P(2)	2.2645(12)
Cu(3)–N(8)	2.031(4)
Cu(3)–N(6)	2.048(4)
Cu(3)–P(4)	2.2751(12)
Cu(3)–P(3)	2.2844(12)
P(1)–C(13)	1.855(5)
P(1)–C(19)	1.863(5)
P(1)–C(22)	1.887(5)
P(2)–C(18)	1.837(5)
P(2)–C(29)	1.867(5)
P(2)–C(32)	1.886(5)
P(3)–C(39)	1.848(5)
P(3)–C(45)	1.862(5)
P(3)–C(48)	1.882(5)
P(4)–C(44)	1.841(5)
P(4)–C(55)	1.884(5)
P(4)–C(58)	1.890(5)
N(1)–C(1)	1.355(6)
N(1)–N(2)	1.370(5)
N(2)–C(3)	1.343(6)
N(3)–C(4)	1.339(6)
N(3)–N(4)	1.373(5)
N(4)–C(6)	1.339(6)
N(5)–C(7)	1.345(6)
N(5)–N(6)	1.360(5)
N(6)–C(9)	1.338(6)
N(7)–C(10)	1.357(6)
N(7)–N(8)	1.369(6)
N(8)–C(12)	1.342(6)
C(1)–C(2)	1.376(7)
C(2)–C(3)	1.386(6)
C(4)–C(5)	1.388(7)
C(5)–C(6)	1.382(7)
C(7)–C(8)	1.383(7)
C(8)–C(9)	1.381(7)
C(10)–C(11)	1.375(7)
C(11)–C(12)	1.396(7)
C(13)–C(18)	1.398(7)
C(13)–C(14)	1.410(6)
C(14)–C(15)	1.395(7)

C(15)–C(16)	1.376(7)
C(16)–C(17)	1.391(7)
C(17)–C(18)	1.409(6)
C(19)–C(20)	1.525(6)
C(19)–C(23)	1.546(7)
C(20)–C(21)	1.545(7)
C(21)–C(22)	1.550(6)
C(22)–C(26)	1.541(6)
C(23)–C(25)	1.520(7)
C(23)–C(24)	1.533(7)
C(26)–C(28)	1.524(7)
C(26)–C(27)	1.549(7)
C(29)–C(33)	1.537(7)
C(29)–C(30)	1.546(8)
C(30)–C(31)	1.517(8)
C(31)–C(32)	1.527(7)
C(32)–C(36)	1.543(6)
C(33)–C(34)	1.504(11)
C(33)–C(35)	1.529(8)
C(36)–C(37)	1.531(6)
C(36)–C(38)	1.535(7)
C(39)–C(40)	1.397(7)
C(39)–C(44)	1.422(6)
C(40)–C(41)	1.391(7)
C(41)–C(42)	1.378(8)
C(42)–C(43)	1.389(7)
C(43)–C(44)	1.394(6)
C(45)–C(46)	1.533(6)
C(45)–C(49)	1.538(7)
C(46)–C(47)	1.533(7)
C(47)–C(48)	1.563(7)
C(48)–C(52)	1.546(7)
C(49)–C(50)	1.531(7)
C(49)–C(51)	1.537(7)
C(52)–C(53)	1.524(8)
C(52)–C(54)	1.527(7)
C(55)–C(59)	1.534(7)
C(55)–C(56)	1.543(7)
C(56)–C(57)	1.533(8)
C(57)–C(58)	1.524(7)

C(58)–C(62)	1.535(7)
C(59)–C(60)	1.514(8)
C(59)–C(61)	1.538(7)
C(62)–C(64)	1.517(8)
C(62)–C(63)	1.531(7)
N(9)–C(66)	1.147(11)
C(65)–C(66)	1.470(11)
C(67)–C(68)	1.390(12)
C(68)–N(10)	1.190(15)
N(1)–Cu(1)–N(7)	87.56(16)
N(1)–Cu(1)–N(5)	176.06(18)
N(7)–Cu(1)–N(5)	91.57(16)
N(1)–Cu(1)–N(3)	93.33(16)
N(7)–Cu(1)–N(3)	176.85(17)
N(5)–Cu(1)–N(3)	87.74(16)
N(2)–Cu(2)–N(4)	92.59(15)
N(2)–Cu(2)–P(1)	114.82(11)
N(4)–Cu(2)–P(1)	128.68(11)
N(2)–Cu(2)–P(2)	126.42(11)
N(4)–Cu(2)–P(2)	107.58(11)
P(1)–Cu(2)–P(2)	90.44(4)
N(8)–Cu(3)–N(6)	91.67(17)
N(8)–Cu(3)–P(4)	126.32(12)
N(6)–Cu(3)–P(4)	107.33(12)
N(8)–Cu(3)–P(3)	113.14(12)
N(6)–Cu(3)–P(3)	132.38(12)
P(4)–Cu(3)–P(3)	90.29(4)
C(13)–P(1)–C(19)	108.7(2)
C(13)–P(1)–C(22)	100.8(2)
C(19)–P(1)–C(22)	92.2(2)
C(13)–P(1)–Cu(2)	105.18(16)
C(19)–P(1)–Cu(2)	114.07(15)
C(22)–P(1)–Cu(2)	133.71(15)
C(18)–P(2)–C(29)	104.7(2)
C(18)–P(2)–C(32)	105.0(2)
C(29)–P(2)–C(32)	94.2(2)
C(18)–P(2)–Cu(2)	105.50(15)
C(29)–P(2)–Cu(2)	131.61(16)
C(32)–P(2)–Cu(2)	113.16(15)

C(39)–P(3)–C(45)	106.1(2)
C(39)–P(3)–C(48)	101.4(2)
C(45)–P(3)–C(48)	90.6(2)
C(39)–P(3)–Cu(3)	105.21(15)
C(45)–P(3)–Cu(3)	113.82(15)
C(48)–P(3)–Cu(3)	136.34(16)
C(44)–P(4)–C(55)	104.8(2)
C(44)–P(4)–C(58)	104.0(2)
C(55)–P(4)–C(58)	94.3(2)
C(44)–P(4)–Cu(3)	105.42(15)
C(55)–P(4)–Cu(3)	130.12(17)
C(58)–P(4)–Cu(3)	115.34(17)
C(1)–N(1)–N(2)	107.8(4)
C(1)–N(1)–Cu(1)	124.5(3)
N(2)–N(1)–Cu(1)	126.9(3)
C(3)–N(2)–N(1)	107.1(3)
C(3)–N(2)–Cu(2)	131.6(3)
N(1)–N(2)–Cu(2)	121.2(3)
C(4)–N(3)–N(4)	108.2(4)
C(4)–N(3)–Cu(1)	124.3(3)
N(4)–N(3)–Cu(1)	127.3(3)
C(6)–N(4)–N(3)	106.7(4)
C(6)–N(4)–Cu(2)	133.0(3)
N(3)–N(4)–Cu(2)	120.2(3)
C(7)–N(5)–N(6)	108.8(4)
C(7)–N(5)–Cu(1)	122.4(3)
N(6)–N(5)–Cu(1)	128.7(3)
C(9)–N(6)–N(5)	106.3(4)
C(9)–N(6)–Cu(3)	134.7(3)
N(5)–N(6)–Cu(3)	119.0(3)
C(10)–N(7)–N(8)	108.7(4)
C(10)–N(7)–Cu(1)	125.2(3)
N(8)–N(7)–Cu(1)	125.8(3)
C(12)–N(8)–N(7)	106.5(4)
C(12)–N(8)–Cu(3)	131.3(3)
N(7)–N(8)–Cu(3)	122.1(3)
N(1)–C(1)–C(2)	110.1(4)
C(1)–C(2)–C(3)	104.2(4)
N(2)–C(3)–C(2)	110.8(4)
N(3)–C(4)–C(5)	110.2(4)

C(6)–C(5)–C(4)	103.6(4)
N(4)–C(6)–C(5)	111.3(4)
N(5)–C(7)–C(8)	109.8(4)
C(9)–C(8)–C(7)	103.3(4)
N(6)–C(9)–C(8)	111.8(4)
N(7)–C(10)–C(11)	109.6(4)
C(10)–C(11)–C(12)	104.1(4)
N(8)–C(12)–C(11)	111.1(4)
C(18)–C(13)–C(14)	119.0(4)
C(18)–C(13)–P(1)	119.4(3)
C(14)–C(13)–P(1)	121.6(4)
C(15)–C(14)–C(13)	120.7(5)
C(16)–C(15)–C(14)	120.0(4)
C(15)–C(16)–C(17)	120.3(4)
C(16)–C(17)–C(18)	120.6(5)
C(13)–C(18)–C(17)	119.4(4)
C(13)–C(18)–P(2)	119.4(3)
C(17)–C(18)–P(2)	121.1(4)
C(20)–C(19)–C(23)	116.4(4)
C(20)–C(19)–P(1)	106.4(3)
C(23)–C(19)–P(1)	119.2(3)
C(19)–C(20)–C(21)	106.4(4)
C(20)–C(21)–C(22)	110.2(4)
C(26)–C(22)–C(21)	113.8(4)
C(26)–C(22)–P(1)	114.1(3)
C(21)–C(22)–P(1)	107.4(3)
C(25)–C(23)–C(24)	111.0(4)
C(25)–C(23)–C(19)	114.0(4)
C(24)–C(23)–C(19)	109.9(4)
C(28)–C(26)–C(22)	113.6(4)
C(28)–C(26)–C(27)	111.0(4)
C(22)–C(26)–C(27)	109.5(4)
C(33)–C(29)–C(30)	114.8(5)
C(33)–C(29)–P(2)	113.4(4)
C(30)–C(29)–P(2)	103.4(3)
C(31)–C(30)–C(29)	106.9(4)
C(30)–C(31)–C(32)	108.8(4)
C(31)–C(32)–C(36)	114.6(4)
C(31)–C(32)–P(2)	105.3(3)
C(36)–C(32)–P(2)	116.0(3)

C(34)–C(33)–C(35)	110.1(6)
C(34)–C(33)–C(29)	111.1(5)
C(35)–C(33)–C(29)	111.1(5)
C(37)–C(36)–C(38)	109.0(4)
C(37)–C(36)–C(32)	111.2(4)
C(38)–C(36)–C(32)	111.2(4)
C(40)–C(39)–C(44)	118.5(4)
C(40)–C(39)–P(3)	122.6(4)
C(44)–C(39)–P(3)	118.8(3)
C(41)–C(40)–C(39)	121.3(5)
C(42)–C(41)–C(40)	120.5(5)
C(41)–C(42)–C(43)	118.9(5)
C(42)–C(43)–C(44)	122.3(5)
C(43)–C(44)–C(39)	118.5(4)
C(43)–C(44)–P(4)	121.6(4)
C(39)–C(44)–P(4)	119.5(3)
C(46)–C(45)–C(49)	116.8(4)
C(46)–C(45)–P(3)	106.4(3)
C(49)–C(45)–P(3)	118.5(3)
C(45)–C(46)–C(47)	106.5(4)
C(46)–C(47)–C(48)	111.0(4)
C(52)–C(48)–C(47)	111.5(4)
C(52)–C(48)–P(3)	114.5(3)
C(47)–C(48)–P(3)	108.0(3)
C(50)–C(49)–C(51)	110.3(4)
C(50)–C(49)–C(45)	109.5(4)
C(51)–C(49)–C(45)	114.4(4)
C(53)–C(52)–C(54)	110.3(5)
C(53)–C(52)–C(48)	114.2(4)
C(54)–C(52)–C(48)	109.3(4)
C(59)–C(55)–C(56)	112.7(4)
C(59)–C(55)–P(4)	113.8(3)
C(56)–C(55)–P(4)	104.3(3)
C(57)–C(56)–C(55)	108.3(4)
C(58)–C(57)–C(56)	108.6(4)
C(57)–C(58)–C(62)	114.0(4)
C(57)–C(58)–P(4)	105.7(4)
C(62)–C(58)–P(4)	117.3(3)
C(60)–C(59)–C(55)	111.6(4)
C(60)–C(59)–C(61)	109.7(4)

C(55)–C(59)–C(61)	111.2(5)
C(64)–C(62)–C(63)	108.7(5)
C(64)–C(62)–C(58)	112.2(4)
C(63)–C(62)–C(58)	111.1(5)
N(9)–C(66)–C(65)	178.9(10)
N(10)–C(68)–C(67)	167.2(12)

Anisotropic displacement parameters ($\text{\AA}^2 \times 10^3$) for Copper–trimer VI

	U ¹¹	U ²²	U ³³	U ²³	U ¹³	U ¹²
Cu(1)	16(1)	15(1)	17(1)	-3(1)	3(1)	-1(1)
Cu(2)	12(1)	15(1)	16(1)	0(1)	0(1)	1(1)
Cu(3)	13(1)	17(1)	16(1)	-2(1)	0(1)	1(1)
P(1)	12(1)	15(1)	18(1)	2(1)	-1(1)	1(1)
P(2)	13(1)	19(1)	16(1)	-3(1)	-1(1)	1(1)
P(3)	15(1)	16(1)	15(1)	-1(1)	1(1)	0(1)
P(4)	16(1)	17(1)	16(1)	-2(1)	-2(1)	1(1)
N(1)	16(2)	18(2)	21(2)	-2(1)	3(2)	-1(1)
N(2)	12(2)	20(2)	17(2)	-2(1)	0(1)	2(1)
N(3)	22(2)	13(2)	21(2)	-2(1)	4(2)	-1(1)
N(4)	12(2)	16(2)	19(2)	-2(1)	-2(1)	0(1)
N(5)	18(2)	18(2)	23(2)	-6(2)	6(2)	-3(2)
N(6)	18(2)	19(2)	23(2)	-5(2)	5(2)	-1(2)
N(7)	18(2)	19(2)	18(2)	-2(2)	0(2)	0(2)
N(8)	18(2)	23(2)	19(2)	-4(2)	0(2)	4(2)
N(9)	81(5)	78(5)	52(4)	-9(4)	9(4)	-25(4)
C(1)	14(2)	28(2)	23(2)	-2(2)	4(2)	4(2)
C(2)	14(2)	23(2)	25(2)	-1(2)	2(2)	1(2)
C(3)	17(2)	13(2)	21(2)	2(2)	0(2)	0(2)
C(4)	25(2)	19(2)	22(2)	-1(2)	1(2)	0(2)
C(5)	24(2)	22(2)	17(2)	2(2)	1(2)	2(2)
C(6)	20(2)	22(2)	17(2)	-4(2)	1(2)	0(2)
C(7)	21(2)	19(2)	30(3)	-5(2)	7(2)	1(2)
C(8)	22(2)	18(2)	45(3)	-9(2)	12(2)	-4(2)
C(9)	22(2)	22(2)	42(3)	-12(2)	11(2)	-9(2)
C(10)	22(2)	20(2)	24(2)	2(2)	3(2)	6(2)
C(11)	27(2)	31(3)	19(2)	2(2)	2(2)	5(2)
C(12)	23(2)	26(2)	21(2)	-4(2)	-1(2)	7(2)

C(13)	13(2)	21(2)	17(2)	6(2)	3(2)	3(2)
C(14)	19(2)	19(2)	21(2)	3(2)	2(2)	3(2)
C(15)	18(2)	19(2)	26(2)	6(2)	2(2)	7(2)
C(16)	14(2)	29(2)	21(2)	7(2)	-1(2)	3(2)
C(17)	14(2)	29(2)	21(2)	1(2)	-1(2)	1(2)
C(18)	15(2)	21(2)	15(2)	5(2)	3(2)	4(2)
C(19)	13(2)	15(2)	27(2)	4(2)	1(2)	-1(2)
C(20)	19(2)	13(2)	36(3)	2(2)	1(2)	1(2)
C(21)	24(2)	19(2)	33(3)	-2(2)	-2(2)	1(2)
C(22)	15(2)	15(2)	21(2)	-2(2)	0(2)	1(2)
C(23)	16(2)	20(2)	31(3)	4(2)	5(2)	2(2)
C(24)	23(2)	35(3)	40(3)	16(2)	8(2)	0(2)
C(25)	25(3)	38(3)	31(3)	14(2)	0(2)	2(2)
C(26)	22(2)	17(2)	22(2)	2(2)	-2(2)	-4(2)
C(27)	37(3)	25(2)	23(2)	-2(2)	-2(2)	-3(2)
C(28)	25(2)	21(2)	31(3)	2(2)	-10(2)	0(2)
C(29)	18(2)	33(3)	16(2)	-4(2)	-2(2)	4(2)
C(30)	34(3)	35(3)	31(3)	-15(2)	-3(2)	-7(2)
C(31)	31(3)	27(3)	31(3)	-7(2)	-3(2)	-12(2)
C(32)	19(2)	18(2)	20(2)	-2(2)	2(2)	-2(2)
C(33)	27(3)	63(4)	21(2)	-12(3)	-1(2)	-1(3)
C(34)	63(5)	88(6)	26(3)	-5(3)	12(3)	-42(4)
C(35)	52(4)	72(5)	23(3)	-22(3)	-1(3)	4(4)
C(36)	15(2)	16(2)	25(2)	0(2)	4(2)	0(2)
C(37)	24(2)	17(2)	34(3)	7(2)	7(2)	-2(2)
C(38)	23(2)	20(2)	19(2)	-3(2)	5(2)	-3(2)
C(39)	16(2)	20(2)	16(2)	2(2)	0(2)	4(2)
C(40)	26(2)	22(2)	21(2)	3(2)	3(2)	0(2)
C(41)	23(2)	19(2)	29(2)	4(2)	6(2)	6(2)
C(42)	17(2)	24(2)	28(2)	7(2)	-2(2)	0(2)
C(43)	20(2)	21(2)	20(2)	2(2)	-2(2)	-2(2)
C(44)	16(2)	17(2)	19(2)	0(2)	2(2)	-1(2)
C(45)	17(2)	19(2)	15(2)	-1(2)	2(2)	3(2)
C(46)	23(2)	25(2)	21(2)	-8(2)	4(2)	6(2)
C(47)	26(2)	24(2)	29(3)	-11(2)	2(2)	3(2)
C(48)	20(2)	15(2)	25(2)	-5(2)	0(2)	-4(2)
C(49)	16(2)	23(2)	23(2)	3(2)	3(2)	1(2)
C(50)	26(2)	39(3)	28(3)	11(2)	4(2)	-1(2)
C(51)	14(2)	31(3)	29(3)	0(2)	1(2)	2(2)
C(52)	20(2)	22(2)	30(2)	-8(2)	2(2)	-7(2)

C(53)	23(2)	36(3)	36(3)	1(2)	-10(2)	-5(2)
C(54)	25(2)	32(3)	35(3)	-9(2)	5(2)	-8(2)
C(55)	18(2)	21(2)	26(2)	-5(2)	-6(2)	1(2)
C(56)	28(3)	30(3)	28(3)	-13(2)	-6(2)	0(2)
C(57)	35(3)	42(3)	18(2)	-6(2)	-6(2)	1(2)
C(58)	27(2)	23(2)	17(2)	-2(2)	1(2)	2(2)
C(59)	17(2)	21(2)	36(3)	-5(2)	-5(2)	0(2)
C(60)	25(2)	22(2)	39(3)	-3(2)	0(2)	-4(2)
C(61)	25(2)	27(3)	49(3)	-16(3)	-2(2)	-2(2)
C(62)	28(3)	35(3)	21(2)	7(2)	4(2)	5(2)
C(63)	53(4)	57(4)	25(3)	7(3)	10(3)	-10(3)
C(64)	35(3)	29(3)	29(3)	3(2)	7(2)	-3(2)
C(65)	49(4)	76(6)	40(4)	-2(4)	3(3)	4(4)
C(66)	52(4)	63(5)	40(4)	2(3)	10(3)	-8(4)

The anisotropic displacement factor exponent takes the form: $-2\pi^2 [h^2 a^{*2} U^{11} + \dots + 2 h k a^* b^* U^{12}]$

Hydrogen coordinates ($\times 10^4$) and isotropic displacement parameters ($\text{\AA}^2 \times 10^3$) for

Copper-trimer VI

	x	y	z	U(equiv.)
H(1A)	9274	6617	6038	26
H(2A)	9793	7903	6178	25
H(3A)	8723	8608	6673	20
H(4A)	7602	5267	7774	26
H(5A)	7292	5913	8712	26
H(6A)	7033	7236	8442	24
H(7A)	6064	5555	7004	28
H(8A)	5473	4281	6913	34
H(9A)	6535	3492	6496	34
H(10A)	7809	6720	5304	27
H(11A)	8134	5993	4413	31
H(12A)	8438	4701	4760	28
H(14A)	5750	10291	7312	23
H(15A)	4487	10511	6968	25
H(16A)	3810	9578	6490	26
H(17A)	4376	8411	6364	26

H(19A)	8046	9532	7138	22
H(20A)	6895	10666	7136	27
H(20B)	7818	10774	7226	27
H(21A)	7012	10677	8133	30
H(21B)	7802	10201	8119	30
H(22A)	6248	9689	8090	20
H(23A)	7685	9191	6193	27
H(24A)	8467	10088	5754	49
H(24B)	8814	9910	6381	49
H(24C)	8322	10652	6277	49
H(25A)	7013	10002	5592	47
H(25B)	6860	10559	6118	47
H(25C)	6454	9760	6112	47
H(26A)	6682	8653	8588	24
H(27A)	7115	9246	9441	42
H(27B)	6462	9746	9138	42
H(27C)	7363	9966	9081	42
H(28A)	7898	8446	8135	38
H(28B)	7983	8428	8823	38
H(28C)	8257	9144	8469	38
H(29A)	5082	7692	5841	27
H(30A)	4833	6419	5809	40
H(30B)	5594	6232	6189	40
H(31A)	4540	6201	6828	36
H(31B)	4218	6981	6594	36
H(32A)	5533	6717	7311	23
H(33A)	6592	7036	5657	44
H(34A)	6851	8109	5094	88
H(34B)	6737	8299	5764	88
H(34C)	6048	8460	5315	88
H(35A)	6284	6991	4671	74
H(35B)	5446	7352	4791	74
H(35C)	5637	6535	5021	74
H(36A)	4438	7907	7444	22
H(37A)	3859	7186	8195	38
H(37B)	4398	6498	8017	38
H(37C)	3748	6797	7579	38
H(38A)	4955	8008	8389	31
H(38B)	5641	8112	7927	31
H(38C)	5547	7341	8262	31

H(40A)	9831	1845	5827	27
H(41A)	10823	1488	6455	28
H(42A)	11163	2239	7236	28
H(43A)	10454	3318	7412	24
H(45A)	8938	3508	4746	21
H(46A)	10074	2411	5020	28
H(46B)	9779	2633	4384	28
H(47A)	9123	1547	4894	32
H(47B)	8598	2092	4509	32
H(48A)	8520	1866	5697	24
H(49A)	9718	4408	5229	25
H(50A)	9587	4329	4206	47
H(50B)	10365	3840	4181	47
H(50C)	10405	4684	4391	47
H(51A)	10635	3635	5708	37
H(51B)	11067	4233	5309	37
H(51C)	10989	3391	5097	37
H(52A)	7427	1802	5045	29
H(53A)	6733	2877	4804	47
H(53B)	7584	2912	4522	47
H(53C)	7394	3385	5090	47
H(54A)	6533	2364	5740	46
H(54B)	7290	2630	6088	46
H(54C)	7124	1764	6000	46
H(55A)	10362	4534	7239	26
H(56A)	9927	5144	8052	35
H(56B)	9090	5320	7771	35
H(57A)	9622	3890	8163	38
H(57B)	8875	4330	8402	38
H(58A)	8164	4109	7607	27
H(59A)	9415	5708	6771	30
H(60A)	9904	4967	6029	43
H(60B)	10772	5050	6275	43
H(60C)	10332	5755	6011	43
H(61A)	10503	6497	6890	50
H(61B)	10993	5836	7175	50
H(61C)	10252	6170	7505	50
H(62A)	9011	2749	7705	34
H(63A)	8004	2408	8379	68
H(63B)	7701	3247	8368	68

H(63C)	8549	3060	8618	68
H(64A)	8171	2755	6894	46
H(64B)	7448	2944	7306	46
H(64C)	7886	2164	7364	46
H(65A)	7993	8988	5064	82
H(65B)	8911	9027	4942	82
H(65C)	8581	8482	5429	82
H(67A)	6637	4575	5021	73
H(67B)	6289	4779	5642	73
H(67C)	6450	5420	5180	73

Torsion angles [°] for Copper-trimer VI

C(1)–N(1)–N(2)–C(3)	-0.1(5)
Cu(1)–N(1)–N(2)–C(3)	169.8(3)
C(1)–N(1)–N(2)–Cu(2)	-177.0(3)
Cu(1)–N(1)–N(2)–Cu(2)	-7.2(5)
C(4)–N(3)–N(4)–C(6)	0.2(5)
Cu(1)–N(3)–N(4)–C(6)	-175.5(3)
C(4)–N(3)–N(4)–Cu(2)	-177.6(3)
Cu(1)–N(3)–N(4)–Cu(2)	6.7(5)
C(7)–N(5)–N(6)–C(9)	0.3(6)
Cu(1)–N(5)–N(6)–C(9)	-175.1(4)
C(7)–N(5)–N(6)–Cu(3)	-179.6(3)
Cu(1)–N(5)–N(6)–Cu(3)	5.1(6)
C(10)–N(7)–N(8)–C(12)	-0.2(5)
Cu(1)–N(7)–N(8)–C(12)	173.8(3)
C(10)–N(7)–N(8)–Cu(3)	-176.2(3)
Cu(1)–N(7)–N(8)–Cu(3)	-2.2(5)
N(2)–N(1)–C(1)–C(2)	0.5(5)
Cu(1)–N(1)–C(1)–C(2)	-169.6(3)
N(1)–C(1)–C(2)–C(3)	-0.7(6)
N(1)–N(2)–C(3)–C(2)	-0.4(5)
Cu(2)–N(2)–C(3)–C(2)	176.1(3)
C(1)–C(2)–C(3)–N(2)	0.7(5)
N(4)–N(3)–C(4)–C(5)	0.0(5)
Cu(1)–N(3)–C(4)–C(5)	175.9(3)
N(3)–C(4)–C(5)–C(6)	-0.3(6)
N(3)–N(4)–C(6)–C(5)	-0.4(5)

Cu(2)–N(4)–C(6)–C(5)	177.1(3)
C(4)–C(5)–C(6)–N(4)	0.4(6)
N(6)–N(5)–C(7)–C(8)	-1.2(6)
Cu(1)–N(5)–C(7)–C(8)	174.5(4)
N(5)–C(7)–C(8)–C(9)	1.5(7)
N(5)–N(6)–C(9)–C(8)	0.7(7)
Cu(3)–N(6)–C(9)–C(8)	-179.4(4)
C(7)–C(8)–C(9)–(6)	-1.3(7)
N(8)–N(7)–C(10)–C(11)	0.4(6)
Cu(1)–N(7)–C(10)–C(11)	-173.6(3)
N(7)–C(10)–C(11)–C(12)	-0.4(6)
N(7)–N(8)–C(12)–C(11)	-0.1(6)
Cu(3)–N(8)–C(12)–C(11)	175.4(4)
C(10)–C(11)–C(12)–N(8)	0.3(6)
C(19)–P(1)–C(13)–C(18)	123.3(4)
C(22)–P(1)–C(13)–C(18)	-140.6(4)
Cu(2)–P(1)–C(13)–C(18)	0.8(4)
C(19)–P(1)–C(13)–C(14)	-59.0(4)
C(22)–P(1)–C(13)–C(14)	37.1(4)
Cu(2)–P(1)–C(13)–C(14)	178.4(3)
C(18)–C(13)–C(14)–C(15)	-0.9(7)
P(1)–C(13)–C(14)–C(15)	-178.5(4)
C(13)–C(14)–C(15)–C(16)	0.3(7)
C(14)–C(15)–C(16)–C(17)	0.6(7)
C(15)–C(16)–C(17)–C(18)	-1.0(7)
C(14)–C(13)–C(18)–C(17)	0.6(6)
P(1)–C(13)–C(18)–C(17)	178.3(3)
C(14)–C(13)–C(18)–P(2)	-175.5(3)
P(1)–C(13)–C(18)–P(2)	2.2(5)
C(16)–C(17)–C(18)–C(13)	0.3(7)
C(16)–C(17)–C(18)–P(2)	176.3(4)
C(29)–P(2)–C(18)–C(13)	-145.7(4)
C(32)–P(2)–C(18)–C(13)	115.8(4)
Cu(2)–P(2)–C(18)–C(13)	-4.0(4)
C(29)–P(2)–C(18)–C(17)	38.3(4)
C(32)–P(2)–C(18)–C(17)	-60.2(4)
Cu(2)–P(2)–C(18)–C(17)	180.0(3)
C(13)–P(1)–C(19)–C(20)	73.9(4)
C(22)–P(1)–C(19)–C(20)	-28.3(3)
Cu(2)–P(1)–C(19)–C(20)	-169.1(3)

C(13)–P(1)–C(19)–C(23)	-60.2(4)
C(22)–P(1)–C(19)–C(23)	-162.4(4)
Cu(2)–P(1)–C(19)–C(23)	56.8(4)
C(23)–C(19)–C(20)–C(21)	178.8(4)
P(1)–C(19)–C(20)–C(21)	43.2(4)
C(19)–C(20)–C(21)–C(22)	-40.3(5)
C(20)–C(21)–C(22)–C(26)	145.9(4)
C(20)–C(21)–C(22)–P(1)	18.6(5)
C(13)–P(1)–C(22)–C(26)	129.0(3)
C(19)–P(1)–C(22)–C(26)	-121.5(3)
Cu(2)–P(1)–C(22)–C(26)	5.5(4)
C(13)–P(1)–C(22)–C(21)	-103.9(3)
C(19)–P(1)–C(22)–C(21)	5.6(3)
Cu(2)–P(1)–C(22)–C(21)	132.6(3)
C(20)–C(19)–C(23)–C(25)	-58.3(6)
P(1)–C(19)–C(23)–C(25)	71.3(5)
C(20)–C(19)–C(23)–C(24)	67.0(5)
P(1)–C(19)–C(23)–C(24)	-163.3(3)
C(21)–C(22)–C(26)–C(28)	-66.9(5)
P(1)–C(22)–C(26)–C(28)	56.7(5)
C(21)–C(22)–C(26)–C(27)	57.7(5)
P(1)–C(22)–C(26)–C(27)	-178.6(3)
C(18)–P(2)–C(29)–C(33)	106.5(4)
C(32)–P(2)–C(29)–C(33)	-146.8(4)
Cu(2)–P(2)–C(29)–C(33)	-20.5(5)
C(18)–P(2)–C(29)–C(30)	-128.5(3)
C(32)–P(2)–C(29)–C(30)	-21.8(4)
Cu(2)–P(2)–C(29)–C(30)	104.5(3)
C(33)–C(29)–C(30)–C(31)	167.2(5)
P(2)–C(29)–C(30)–C(31)	43.2(5)
C(29)–C(30)–C(31)–C(32)	-49.7(6)
C(30)–C(31)–C(32)–C(36)	159.5(5)
C(30)–C(31)–C(32)–P(2)	30.8(5)
C(18)–P(2)–C(32)–C(31)	102.0(4)
C(29)–P(2)–C(32)–C(31)	-4.4(4)
Cu(2)–P(2)–C(32)–C(31)	-143.5(3)
C(18)–P(2)–C(32)–C(36)	-25.9(4)
C(29)–P(2)–C(32)–C(36)	-132.3(4)
Cu(2)–P(2)–C(32)–C(36)	88.7(3)
C(30)–C(29)–C(33)–C(34)	-178.1(5)

P(2)–C(29)–C(33)–C(34)	-59.5(6)
C(30)–C(29)–C(33)–C(35)	59.0(7)
P(2)–C(29)–C(33)–C(35)	177.5(5)
C(31)–C(32)–C(36)–C(37)	49.1(6)
P(2)–C(32)–C(36)–C(37)	172.3(3)
C(31)–C(32)–C(36)–C(38)	170.8(4)
P(2)–C(32)–C(36)–C(38)	-66.0(5)
C(45)–P(3)–C(39)–C(40)	-64.0(4)
C(48)–P(3)–C(39)–C(40)	30.0(4)
Cu(3)–P(3)–C(39)–C(40)	175.1(4)
C(45)–P(3)–C(39)–C(44)	112.3(4)
C(48)–P(3)–C(39)–C(44)	-153.7(4)
Cu(3)–P(3)–C(39)–C(44)	-8.7(4)
C(44)–C(39)–C(40)–C(41)	-1.2(7)
P(3)–C(39)–C(40)–C(41)	175.1(4)
C(39)–C(40)–C(41)–C(42)	0.1(7)
C(40)–C(41)–C(42)–C(43)	1.7(7)
C(41)–C(42)–C(43)–C(44)	-2.6(7)
C(42)–C(43)–C(44)–C(39)	1.5(7)
C(42)–C(43)–C(44)–P(4)	174.6(4)
C(40)–C(39)–C(44)–C(43)	0.4(7)
P(3)–C(39)–C(44)–C(43)	-176.0(3)
C(40)–C(39)–C(44)–P(4)	-172.9(3)
P(3)–C(39)–C(44)–P(4)	10.8(5)
C(55)–P(4)–C(44)–C(43)	40.1(4)
C(58)–P(4)–C(44)–C(43)	-58.3(4)
Cu(3)–P(4)–C(44)–C(43)	179.9(4)
C(55)–P(4)–C(44)–C(39)	-146.9(4)
C(58)–P(4)–C(44)–C(39)	114.7(4)
Cu(3)–P(4)–C(44)–C(39)	-7.1(4)
C(39)–P(3)–C(45)–C(46)	67.3(4)
C(48)–P(3)–C(45)–C(46)	-34.8(3)
Cu(3)–P(3)–C(45)–C(46)	-177.5(3)
C(39)–P(3)–C(45)–C(49)	-66.7(4)
C(48)–P(3)–C(45)–C(49)	-168.8(4)
Cu(3)–P(3)–C(45)–C(49)	48.5(4)
C(49)–C(45)–C(46)–C(47)	179.1(4)
P(3)–C(45)–C(46)–C(47)	44.2(4)
C(45)–C(46)–C(47)–C(48)	-32.9(6)
C(46)–C(47)–C(48)–C(52)	133.8(4)

C(46)–C(47)–C(48)–P(3)	7.2(5)
C(39)–P(3)–C(48)–C(52)	144.4(4)
C(45)–P(3)–C(48)–C(52)	-109.0(4)
Cu(3)–P(3)–C(48)–C(52)	17.6(5)
C(39)–P(3)–C(48)–C(47)	-90.8(4)
C(45)–P(3)–C(48)–C(47)	15.8(4)
Cu(3)–P(3)–C(48)–C(47)	142.4(3)
C(46)–C(45)–C(49)–C(50)	71.8(5)
P(3)–C(45)–C(49)–C(50)	-158.8(4)
C(46)–C(45)–C(49)–C(51)	-52.6(6)
P(3)–C(45)–C(49)–C(51)	76.7(5)
C(47)–C(48)–C(52)–C(53)	-71.2(6)
P(3)–C(48)–C(52)–C(53)	51.7(5)
C(47)–C(48)–C(52)–C(54)	164.8(4)
P(3)–C(48)–C(52)–C(54)	-72.3(5)
C(44)–P(4)–C(55)–C(59)	115.1(4)
C(58)–P(4)–C(55)–C(59)	-139.1(4)
Cu(3)–P(4)–C(55)–C(59)	-10.4(5)
C(44)–P(4)–C(55)–C(56)	-121.7(3)
C(58)–P(4)–C(55)–C(56)	-16.0(4)
Cu(3)–P(4)–C(55)–C(56)	112.7(3)
C(59)–C(55)–C(56)–C(57)	161.8(4)
P(4)–C(55)–C(56)–C(57)	37.9(5)
C(55)–C(56)–C(57)–C(58)	-47.9(6)
C(56)–C(57)–C(58)–C(62)	163.5(4)
C(56)–C(57)–C(58)–P(4)	33.2(5)
C(44)–P(4)–C(58)–C(57)	97.0(4)
C(55)–P(4)–C(58)–C(57)	-9.5(4)
Cu(3)–P(4)–C(58)–C(57)	-148.1(3)
C(44)–P(4)–C(58)–C(62)	-31.4(4)
C(55)–P(4)–C(58)–C(62)	-137.8(4)
Cu(3)–P(4)–C(58)–C(62)	83.5(4)
C(56)–C(55)–C(59)–C(60)	-180.0(4)
P(4)–C(55)–C(59)–C(60)	-61.6(5)
C(56)–C(55)–C(59)–C(61)	57.2(5)
P(4)–C(55)–C(59)–C(61)	175.6(4)
C(57)–C(58)–C(62)–C(64)	176.0(5)
P(4)–C(58)–C(62)–C(64)	-59.7(6)
C(57)–C(58)–C(62)–C(63)	54.0(6)
P(4)–C(58)–C(62)–C(63)	178.3(4)